CSIC
CONSEJO SUPERIOR DE INVESTIGACIONES CIENTÍFICAS
Instituto de Agroquímica y Tecnología de Alimentos
Grupo de Nuevos Materiales y Nanotecnología

VNIVERSITAT DE VALÈNCIA

Universitat de València
Facultat de Farmàcia

Departament de Medicina Preventiva i Salut Pública, Ciències de l' Alimentació, Toxicología i Medicina Legal

Doctorat en Ciències de l' Alimentació
Tesis Doctoral Internacional
Valencia, 2015

DEVELOPMENT AND CHARACTERIZATION OF NOVEL NANOBIOCOMPOSITES WITH ENHANCED PROPERTIES BY VARIOUS PROCESSING METHODS OF INTEREST IN FOOD PACKAGING APPLICATIONS

DESARROLLO Y CARACTERIZACIÓN DE NUEVOS NANOBIOCOMPOSITES CON PROPIEDADES MEJORADAS MEDIANTE VARIOS MÉTODOS DE PROCESADO DE INTERÉS EN ENVASADO DE ALIMENTOS

Jesús Ambrosio Martín

Dirigida por:
Dr. Jose María Lagarón Cabello
Dra. Amparo López Rubio

CSIC
CONSEJO SUPERIOR DE INVESTIGACIONES CIENTÍFICAS
Instituto de Agroquímica y Tecnología de Alimentos
Grupo de Nuevos Materiales y Nanotecnología

VNIVERSITAT DE VALÈNCIA

Dr. José María Lagarón Cabello, investigador científico del Consejo Superior de Investigaciones Científicas (CSIC) en el Instituto de Agroquímica y Tecnología de Alimentos (IATA) y Dra. Amparo López Rubio, científica titular en el mismo instituto

CERTIFICAN: que el presente trabajo que lleva por título **DEVELOPMENT AND CHARACTERIZATION OF NOVEL NANOBIOCOMPOSITES WITH ENHANCED PROPERTIES BY VARIOUS PROCESSING METHODS OF INTEREST IN FOOD PACKAGING APPLICATIONS**, que para aspirar a grado de Doctor presenta D. Jesús Ambrosio Martín, ha sido realizado bajo su dirección en el Instituto de Agroquímica y Tecnología de Alimentos (IATA-CSIC) y reúne las condiciones adecuadas para su presentación como tesis doctoral por lo que **AUTORIZAN** al interesado a su presentación.

Y para que así conste a los efectos oportunos, expiden y firman el presente certificado en Valencia a 1 de Junio de 2015.

Fdo: Dr. José María Lagarón Fdo: Dra. Amparo López Rubio

This Thesis has been carried out in the *Institute of Agrochemistry and Food Technology* (IATA) belonging to *Spanish National Research Council* (CSIC) of Spain.

Esta Tesis ha sido desarrollada en el Instituto de Agroquímica y Tecnología de Alimentos (IATA) que pertenece al Consejo Superior de Investigaciones Científicas (CSIC) de España.

Av. Agustín Escardino, 7
46980 Paterna, Valencia, Spain
Tel: +34 963 90 0022
Fax: +34 963 63 6301
http://www.iata.csic.es/

This work has been funded by the Spanish Ministry of Economy and Competitiveness (before Ministry of Science and Innovation) through the Projects MAT2009-14533-C02-01, MAT2012-38947-C02-01 and FPI fellowship BES-2010-038203 and by the European Union's Research and Innovation funding programme *The* Seventh *Framework Programme* through the project EcoBioCap.

Este trabajo ha sido financiado por el Ministerio de Economía y Competitividad (antes Ministerio de Ciencia e Innovación) a través de los Proyectos MAT2009-14533-C02-01, MAT2012-38947-C02-01 y la beca FPI BES-2010-038203 y por el programa para la financiación de la investigación y el desarrollo tecnológico en la Unión Europea *Séptimo Programa Marco* a través del proyecto EcoBioCap

A mis padres;

José y Ana María

AGRADECIMIENTOS

Llegó la hora, parecía que este momento nunca iba a llegar, ya han pasado casi cinco años y aquí estoy con mi tesis escrita. Ha sido un tiempo de intenso trabajo, de subidas y bajadas, donde he aprendido muchísimo a nivel tanto profesional como personal teniendo la oportunidad de afrontar retos verdaderamente apasionantes que me han enriquecido en todos los sentidos así como de conocer gente maravillosa a la que me he ido encontrando por el camino. Por ello me gustaría dar las gracias a todas aquellas personas que han hecho posible que esto suceda y que yo esté aquí ahora mismo.

En primer lugar quisiera agradecer a mis directores de tesis. Gracias a Chema por apostar por mí en su momento y darme la oportunidad de trabajar en este laboratorio y aprender así muchísimo. No a todas las personas que afrontan una tesis se les da la oportunidad de enriquecerse personal y profesionalmente como en este grupo ocurre, para lo cual siempre estuvo dispuesto, y me siento afortunado por ello. Gracias a Amparo (Ampi), sin ella esto no hubiese sido posible. Gracias por estar siempre ahí cuando lo he necesitado, has sido el pilar fundamental en todo el desarrollo de mi tesis. Además, gracias por apostar por mí también en su momento. Trabajar contigo es siempre un placer. Diría muchísimas cosas positivas y llenaría páginas y páginas, pero solo voy a decir que eres la "number 1".

Agradecer también a todos mis compañeros del laboratorio 502 del IATA, aquellos que ya se fueron así como todos los que siguen. Sergio (Sergi), quien me ayudó mucho en mis inicios, Marta, que es una "crack", quien me ayudó bastante también durante todo el tiempo que coincidimos en el laboratorio, sobre todo en mi primera etapa, enseñándome todas las tareas a realizar. Antonio, una persona digna de conocer, como yo le decía, la Wikipedia personificada, el hombre que sabe de todo o casi todo (otro "crack"). Rocío con quien me reí mucho con "sus cosas". María José por su inestimable ayuda también. Lorena, a la que hice enojar alguna vez, jeje, una persona con las ideas claras y que sabe lo que quiere; buenos ratos hemos pasado y los que nos quedan. Además, Wilson, Laura, Pablo, Gloria, Marian, Celia, Sabina y Sergio. Gracias por compartir conmigo conocimientos y por esos buenos momentos que hemos tenido, todos habéis hecho que el día a día sea más fácil. Es un placer trabajar con vosotros.

Agradecer también a todos los chicos de prácticas o estancia con los que he coincidido en el laboratorio, pues todos ellos también han aportado su granito de arena a todo este trabajo, ya sea material o emocionalmente (María, Begoña, Pablo, Marisol, Alejo, Fran, Diego, Paula, y un largo etcétera).

Me gustaría agradecer también a todas las personas que trabajan en el IATA con las que de una forma u otra he tenido relación. Gracias por facilitarme las cosas y hacer que venir a trabajar sea un agrado. Hacer mención especial al personal de Administración e Informática que han estado dispuesto a ayudarme en todo momento.

Agradecer también al Dr. Luís Cabedo y a todo su grupo de la Universidad Jaume I por su disponibilidad en todo momento para ayudar en lo que fuese necesario así como al servicio de microscopía de la Universidad de Valencia también por su ayuda durante mis visitas para SEM y TEM.

Quisiera agradecer también la ayuda incondicional que recibí durante mi estancia en la Universidad de Salerno (Italia), a toda la gente que allí conocí, Giuliana, Luigi, Regina, Carlo, Loredana, Valeria, Giovanni, Umberto, Tina, Vittoria, Roberto, Andrea y Filippo. Además a todos aquellos que conocí fuera de la Universidad. Entre todos hicieron que el estar lejos de casa fuese más llevadero. Fue un placer conocerlos y trabajar con ellos.

Gracias también a todas las personas que he conocido fuera del laboratorio que han hecho que mi vida social aquí en Valencia sea un poco más llevadera, en especial a Miguel Ángel (Papu), nos conocimos de forma poco usual pero fue todo un acierto, desde un primer momento me sentí como uno más de todos vosotros, así como a Paula, una de las primeras personas que conocí y con la que congenié estupendamente. Además a Ainhoa y todos sus amigos. Con todos ellos he pasado muy buenos ratos, y espero que queden muchos más.

Por último agradecer a las personas, que no por dejarlas las últimas son menos importantes, todo lo contrario, son las personas más importantes en mi vida. En primer lugar a mis padres, a quien se lo debo todo. El esfuerzo y la constancia que tienen es de un valor incalculable. Si hoy estoy aquí es gracias a ellos y a nadie más. A pesar de lo duro de tenerlos en la distancia, han sido la principal motivación que he tenido para acabar esta etapa, esto es por y para ellos. A mi hermano, la persona con el corazón más grande que he conocido nunca. Y finalmente a Juana, qué puedo decir..., desde el minuto 1, hace ya casi 5 años, me apoyaste en esta aventura, la "aventura del conocimiento" como yo la llamo, y hoy día, a pesar de la distancia que nos separa, sigues a mi lado dándome tu apoyo. No ha sido fácil, ha sido una carrera de obstáculos ininterrumpidos que hemos ido superando. Muchas gracias por ser como eres, por aguantar este largo periodo de subidas y bajadas, sufriendo esto en tus carnes más incluso que yo mismo, pues es algo que te encontraste, no que decidiste. Para mí eso tiene un valor inconmensurable, y no mucha gente es capaz de hacerlo y aguantar como tú has aguantado. GRACIAS por todo, hemos derramado muchas gotas de sudor durante este periodo pero hemos podido con ello y ahora todo converge a lo que más deseamos, estar de una vez por todas juntos.

A tod@s vosotros y a aquellos para los que no me da la memoria;

Muchas gracias!!!

ABSTRACT

The present work aims to improve the properties of biopolyesters to be used in food packaging applications through the development of nanobiocomposites using different processing methods and incorporating different nanostructured materials within the biopolymeric matrices.

Two incorporation strategies were used. The first one was based on a pre-incorporation of nanostructured additives, also called nanoadditives, into lactic acid oligomers by *in situ* polymerization technologies (specifically polycondensation) resulting in masterbatches that were subsequently mixed with commercial polylactic acid (PLA) by melt compounding (technology widely used by the industry). Thus, bacterial cellulose nanowhiskers (BCNW) and functionalized graphene nanosheets (FGS) were incorporated by this route into PLA matrices.

It was first studied the effect on the final properties of the materials after incorporating oligomers, obtained by polycondensation of lactic acid, within commercial PLA matrix, in absence of nanoadditives. This resulted in an improvement in barrier properties but had no significant effect on mechanical properties.

The next step consisted in the introduction of nanoadditives within PLA by the aforementioned route. The purification process of the materials obtained after the pre-incorporation step was of major importance to achieve materials where the used nanoadditive reached proper dispersion and distribution in the subsequent melt mixing step. This route of incorporation led to considerable improvements in the final properties of the synthesized materials such as mechanical and barrier properties.

The second processing route consisted in the development of nanocomposites by means of High Energy Ball Milling which is a one-single step and solvent free technology. BCNW and FGS were also used as nanoadditives, although in this case, in addition to incorporation into PLA matrices, their addition into polyhydroxyalkanoates (PHAs) matrices namely a copolymer, poly (hydroxybutyrate-co-hydroxyvalerate) (PHBV), was also assessed. Again, the dispersion factor played a key role in improving the final properties of the nanocomposites. Probably due to the inherent properties of nanoadditives, better dispersion was achieved for materials with FGS by this mixing technique, which resulted in better final properties of the prepared nano-biocomposites.

Finally, degradation studies with some of the developed nanocomposites were carried out, comparing with the matrices without nano-additives. Moreover, post-processing studies for the development of food packaging applications from some of the developed materials based on thermoforming of sheets to obtain trays were also performed.

RESUMEN

El presente trabajo tiene como objetivo mejorar las propiedades de matrices biopoliméricas para su uso en aplicaciones de envasado de alimentos mediante el desarrollo de nanobiocompuestos utilizando diferentes metodologías de procesado o estrategias de incorporación de materiales nanoestructurados en el interior de las matrices biopoliméricas.

Dos estrategias de incorporación fueron empleadas. La primera de ellas estaba basada en una pre-incorporación de los aditivos nanoestructurados, también llamados nanoaditivos, en oligómeros de ácido láctico mediante tecnologías de polimerización *in situ* (específicamente policondensación), dando lugar a masterbatches que, posteriormente, se mezclaban con ácido poliláctico (PLA) comercial mediante mezclado en fundido (tecnología ampliamente utilizada industrialmente). Así, nanocristales de celulosa bacteriana (BCNW) y nanoláminas de grafeno funcionalizado (FGS) fueron incorporados mediante esta ruta en matrices de PLA.

En primer lugar se estudió el efecto en las propiedades finales de los materiales tras incorporar oligómeros obtenidos por policondensación del ácido láctico, en ausencia de aditivos, en la matriz de PLA comercial. Ello dio como resultado una mejora en las propiedades de barrera aunque no tuvo efectos significativos sobre las propiedades mecánicas.

El siguiente paso consistió en la incorporación de los nanoaditivos en el interior de PLA mediante la ruta anteriormente citada. El proceso de purificación de los materiales obtenidos tras la etapa de pre-incorporación fue de destacada importancia a la hora de conseguir materiales donde el nanoaditivo utilizado alcanzase una correcta dispersión en la posterior etapa de mezclado en fundido. Esta ruta de incorporación condujo a una mejora en la dispersión de los nanoaditivos, que se tradujo en considerables mejoras en las propiedades finales de los materiales sintetizados como propiedades de barrera y mecánicas.

La segunda ruta de incorporación consistía en el desarrollo de nanocompuestos mediante el uso de un molino de bolas de alta energía (High Energy Ball Milling), tecnología en una sola etapa y libre de disolventes. BCNW y FGS fueron también utilizados como nanoaditivos, aunque en este caso, además de incorporarlos en matrices de PLA, también se evaluó su inclusión en matrices de polihidroxialcanoatos (PHAs) concretamente en un copolímero, poli(hidroxibutirato-co-hidroxivalerato) (PHBV). De nuevo, el factor de la dispersión tuvo un papel muy relevante en la mejora de las propiedades finales de los nanocompuestos. Probablemente debido a las propiedades inherentes de los nanoaditivos, mediante esta técnica de mezclado se consiguió una mejor dispersión para los materiales con FGS, lo cual se tradujo en mejores propiedades finales de los nanobiocomposites preparados.

Por último, se llevaron a cabo estudios de degradación de algunos de los nanocompuestos desarrollados, comparándolos con las matrices sin nanoaditivos. Además, estudios de procesado para el desarrollo de aplicaciones de envasado alimentario, obteniendo bandejas a partir de algunos de los materiales desarrollados mediante técnicas de termoconformado, fueron también realizados.

RESUM

El present treball té com a objectiu millorar les propietats de matrius biopolimèriques per al seu ús en aplicacions d'envasament d'aliments mitjançant el desenvolupament de nano-biocompostos utilitzant diferents metodologies de processament o estratègies d'incorporació de materials nanoestructurats en l'interior de les matrius biopolimèriques.

Dues estratègies d'incorporació van ser emprades. La primera d'elles estava basada en una pre-incorporació dels additius nanoestructurats, també anomenats nanoadditius, en oligòmers d'àcid làctic mitjançant tecnologies de polimerització in situ (específicament policondensació), donant lloc a masterbatches que, posteriorment, es barrejaven amb àcid polilàctic (PLA) comercial mitjançant barrejat en fos (tecnologia àmpliament utilitzada industrialment). Així, mitjançant aquesta ruta es van incorporar nanocristalls de cel·lulosa bacteriana (BCNW) i nanolàmines de grafè funcionalitzat (FGS) a matrius de PLA.

En primer lloc es va estudiar l'efecte en les propietats finals dels materials després d'incorporar oligòmers obtinguts per policondensació de l'àcid làctic, en absència d'additius, en la matriu de PLA comercial. Això va donar com a resultat una millora en les propietats de barrera encara que no va tenir efectes significatius sobre les propietats mecàniques.

El següent pas va consistir en la incorporació dels nanoadditius a l'interior de PLA mitjançant la ruta anteriorment esmentada. El procés de purificació dels materials obtinguts després de l'etapa de pre-incorporació va ser de destacada importància a l'hora d'aconseguir materials on el nanoadditiu utilitzat assolís una correcta dispersió en la posterior etapa de barreja en fos. Amb independència del nanoadditiu utilitzat, es van observar grans diferències respecte als materials obtinguts mitjançant addició directa dels nanoadditius en el procés de barrejat en fos. Aquesta ruta d'incorporació va conduir a una millora en la dispersió dels nanoadditius, que es va traduir en considerables millores en les propietats finals dels materials sintetitzats com és a les propietats de barrera i mecàniques.

La segona ruta d'incorporació consistia en el desenvolupament de nanocompostos mitjançant l'ús d'un molí de boles d'alta energia (High Energy Ball Milling), tecnologia en una sola etapa i lliure de dissolvents. Com a nanoadditius es van utilitzar BCNW i FGS, encara que en aquest cas, a més d'incorporar-los en matrius de PLA, també es va avaluar la seva inclusió en matrius de polihidroxialcanoats (PHAs) concretament en un copolímer, poli (hidroxibutirat-co-hidroxivalerat) (PHBV) . De nou, el factor de la dispersió va tenir un paper molt rellevant en la millora de les propietats finals dels nanocompostos. Probablement a causa de les inherents propietats dels nanoadditius, mitjançant la tècnica de barreja utilitzada es va aconseguir una millor dispersió per als materials amb FGS, la qual cosa es va traduir en millors propietats finals dels nano-biocompostos preparats.

Finalment, es van dur a terme estudis de degradació d'alguns dels nanocompostos desenvolupats, comparant-los amb les matrius sense nanoadditius. A més, es van realitzar estudis de processament per al desenvolupament d'aplicacions d'envasament alimentari, obtenint safates a partir d'alguns dels materials desenvolupats mitjançant tècniques de termoconformat.

INDEX

I. INTRODUCTION/INTRODUCCIÓN 1

1. INTRODUCTION TO FOOD PACKAGING 3
2. FOOD PACKAGING MATERIALS 4
2.1. Biodegradable polymers 6
2.1.1. Polylactic acid (PLA) 8
2.1.1.1. Pla synthesis 9
2.1.1.1.1. Polycondensation 10
2.1.1.1.2. Azeotropic condensation polymerization 11
2.1.1.1.3. Ring opening polymerization (ROP) 11
2.1.1.2. Pla properties 12
2.1.2. Polyhydroxyalkanoates (PHAs) 14
3. NANOTECHNOLOGY: USE FOR REINFORCING BIOPOLYMERS 17
3.1. Cellulosic materials 18
3.1.1. Bacterial cellulose 19
3.2. Carbonaceous materials. Graphene 20
3.3. Strategies to incorporate nanofillers into polymeric matrices 22
3.3.1. Cellulose-based nanocomposites 23
3.3.2. Graphene-based nanocomposites 25
4. MASS TRANSPORT PROPERTIES 27
4.1. Factors influencing mass transport properties 28
4.1.1. Polymer 28
4.1.2. Polymer morphology 29
4.1.3. Nanofillers and additives 30
4.1.4. Temperature 31
4.1.5. The permeant 31
5. LEGISLATION IN THE FOOD PACKAGING FRAMEWORK. 32

1. INTRODUCCIÓN AL ENVASADO ALIMENTARIO 35
2. MATERIALES DE ENVASADO ALIMENTARIO 36

2.1. Polímeros biodegradables ... 39
2.1.1. Ácido poliláctico (PLA) ... 41
2.1.1.1. Síntesis de PLA ... 42
2.1.1.1.1. Policondensación ... 43
2.1.1.1.2. Polimerización por condensación azeotrópica ... 43
2.1.1.1.3. Polimerización por apertura de anillo (ROP) ... 44
2.1.1.2. Propiedades del PLA ... 45
2.1.2. Polihidroxialcanoatos (PHAs) ... 46
3. NANOTECNOLOGÍA: USO PARA REFORZAR BIOPOLÍMEROS. ... 50
3.1. Materiales celulósicos ... 51
3.1.1. Celulosa bacteriana ... 53
3.2. Materiales carbonáceos. Grafeno ... 54
3.3. Estrategias de incorporación de nano-refuerzos en matrices poliméricas ... 55
3.3.1. Nanocompuestos celulósicos ... 57
3.3.2. Nanocompuestos de grafeno ... 59
4. EL TRANSPORTE DE MASAS. PROPIEADES ... 61
4.1. Factores que influyen en las propiedades de transporte de masa ... 62
4.1.1. El polímero ... 62
4.1.2. Morfología de polímeros ... 64
4.1.3. Nanocargas y aditivos ... 64
4.1.4. Temperatura ... 65
4.1.5. El permeante ... 66
5. ASPECTOS LEGALES EN EL MARCO DEL ENVASADO DE ALIMENTOS ... 67

REFERENCES / REFERENCIAS ... 69

II. OBJECTIVES ... 79

1. GENERAL AND SPECIFIC OBJECTIVES ... 81

III. RESULTS AND DISCUSSION ... 83

1. GENERAL INTRODUCTION TO RESULTS ... 85

Chapter 1. An effect of lactic acid oligomers on the barrier properties of polylactide 87

Chapter 2. Melt polycondensation to improve the dispersion of bacterial cellulose into polylactide via melt compounding: Enhanced barrier and mechanical properties 109

Chapter 3. Synergistic efect of lactic acid oligomers and laminar graphene sheets on the barrier properties of polylactide nanocomposites obtained by the in situ polymerization pre-incorporaton method. 143

Chapter 4. Assessment of ball milling methodology to develop polylactide-bacterial cellulose nanowhiskers nanocomposites 165

Chapter 5. Assessment of ball milling as compounding technique to develop nanocomposites of poly (3-hydroxybutyrate-co-3-hydroxyvalerate) and bacterial cellulose nanowhiskers..181

Chapter 6. On the use of ball milling to develop PHBV-graphene nanocomposites (I) - Morophology, thermal properties and thermal stability 203

Chapter 7. On the use of ball milling to develop PHBV-graphene nanocomposites (II) - Mechanical, barrier and electrical properties 223

IV. GENERAL DISCUSSION 243

1. GENERAL DISCUSSION OF THE RESULTS 245
   1.1. Initial studies. Analyses and optimization. 245
   1.2. An effect of lactic acid oligomers on the properties of polylactide 247
   1.3. Using melt polycondensation of lactic acid as pre-incorporation method 248
   1.4. Using ball milling to synthesize polymer nanocomposites 251
   1.5. Final and complementary studies 254

V. CONCLUSIONS / CONCLUSIONES 257

VI. ANNEXES 265

Annex A. Supplementary data: Tables and Figures 267
Annex B. List of publications 277

I. Introduction / Introducción

1. INTRODUCTON TO FOOD PACKAGING

The pace of modern life as well as the increased consumer preference towards healthy foods have directly influenced our eating habits and reduced the time spent on cooking [1]. In this context, currently consumers are demanding foods which do not involve long cooking or preparation times, extended shelf-life, lower contents in preservatives or additives and, of course, food products with guaranteed quality and safety.

The evolution of these habits is also reflected in the packaging, which has traditionally been created as mere containers for food. However, today, moved by these new consumer trends, the containers have acquired another functions, from being a mere container to be an active element in food preservation, distribution and marketing, becoming what is called the 5th "P" (for "packaging") that determines the sale of the products along with the product, price, place and promotion [2].

Food products are constantly exposed to deteriorative processes by external agents such as heat, light, presence or absence of moisture, oxygen, microorganisms, insects, dirt and dust particles, gases, etc. Hence, sometimes the packaging become more important or expensive than the product they contain. Therefore, out of all the functions of packaging, which could be basically summarized as containment, protection, product information and convenience, protection and preservation of its contents are the most important. In the case of food, this function involves a delay in deterioration, thus extending the shelf-life and maintaining the quality and safety of packaged food through minimizing chemical, biochemical and microbiological alterations.

Great efforts are focused on the development of packaging technologies to ensure the freshness and safety of foods, to facilitate the preparation of ready-to-eat food and extend the products shelf-life using technologies implemented to this end, with also an attractive packaging design.

Thus, during the last decades novel functions have been added to packaging. For instance, one can find in the market ready-to-eat salads using modified atmosphere packaging or ready-to-eat meals that only require a simple microwave heating, for which the packaging is already perfectly implemented.

An ideal packaging should have good mechanical strength while being lightweight to facilitate handling throughout the distribution chain, should be cheap enough to make the product competitive and, of course, safe for the consumer.

Therefore, research in the food packaging area is directed towards the selection and development of suitable packaging materials and manufacturing methods that allow minimizing nutrient losses and providing safe and healthy food. In this context, several developments in the food packaging area have taken place, including active and intelligent packaging technologies to provide extended shelf-life and to monitor parameters related to food quality. Moreover, currently there is also a growing interest in developing technologies to minimize the environmental problems associated with the use of fossil resources for the synthesis of packaging materials as well as with the waste management generated from food packaging traditionally used. Therefore, there is a general interest in the development and use of more environmentally-friendly packaging materials.

2. FOOD PACKAGING MATERIALS

A wide variety of materials have been traditionally used for food packaging applications, such as tinplate, paper and cardboard, glass and ceramics as well as combinations thereof. However, nowadays plastic or polymeric materials and paper represent the two main materials used for food packaging. In particular, plastics or polymeric materials have a number of advantages compared to other conventional packaging materials such as versatility of processing methods and compositions as well as their cost/performance ratio. Furthermore, the use of polymers to produce food packages provides other advantages such as light weight, reduced cost and ability to be heat sealed or modified (either chemically or by mixing with other materials) in order to adapt their properties. In fact, the versatility of polymers allows obtaining a wide range of products from highly flexible structures (such as bags or wraps) to more rigid structures (bottles or caps) being able to modify their properties for different applications. The optical properties of packaging (brightness and transparency) can be also adapted to the specific requirements of each product. Transparent containers allow the consumer to see the product, thereby causing some attraction and impression, but you can also add filters or pigments to generate opaque containers and protect the products from light and radiations. Many polymers can be printed, thus being able to provide information to the consumers, to identify the brand or to add an attractive design. In addition, polymeric packaging can be produced as part of integrated processes in industrial production lines, which are formed, filled and sealed in the same line, resulting in quick and cheap processes, being also able to create unlimited sizes and shapes.

This versatility that allows the design of polymeric packaging that meet the requirements of almost every foodstuff has caused that only social and environmental issues or economic factors justify the use of non-polymeric materials, resulting in massive uses of this type of packaging materials. In fact, according to the Spanish Plastics Centre, plastics consumption for this year is estimated to be around 330 million tonnes, with the greatest contribution corresponding to the packaging field, which uses approximately 40% as shown in Figure 1, which compiles the estimated worldwide plastic consumption by 2015 segmented by world regions and the consumption during 2010 segmented by market areas.

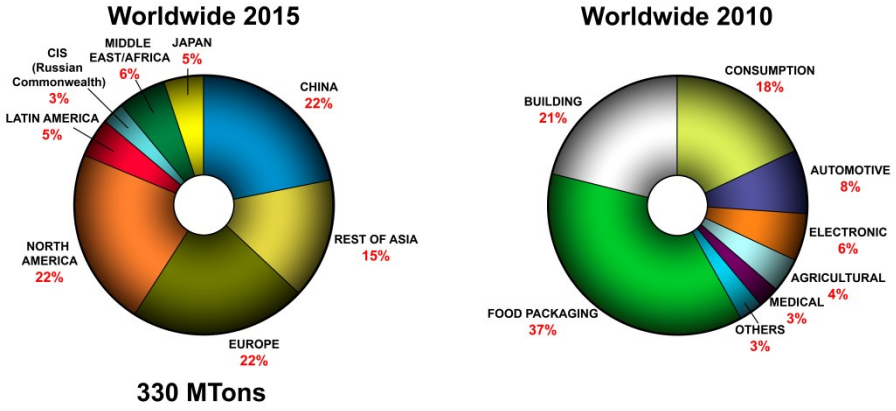

Figure 1. Estimated global consumption of plastics by 2015 and consumption by market sector in 2010 (Source: Spanish Plastics Centre - CEP)

One of the main drawbacks of plastic materials used for packaging is that they are permeable to the transport of low molecular weight compounds, thus having limited barrier properties. This causes various mass transport phenomena in what is known as a ternary system "food/package/environment", as it will be discussed below, which limits the use of polymers for certain applications where high barrier to oxygen or moisture are required, as these are determining factors in food deterioration. High barrier polymers and multilayer systems have been developed to overcome these problems. Moreover, in the last decades, an alternative to the development of high barrier material as monolayer systems consists in the development of nanocomposite materials by incorporating nanostructured additives into polymer matrices to modify its properties, as it will also be discussed below.

The other main drawback deriving from high plastics consumption is associated with environmental problems related to the slow degradation rate of most commonly used polymers, most of them being petroleum-based materials. As a result, legislation is evolving towards stricter measures to improve the efficiency of materials and reduce the impact of packaging waste on the environment (e.g. Directive 94/62/EC of the European Parliament on packaging and packaging waste). Although the stability of containers during product shelf-life is an advantage, it becomes a disadvantage because they are rarely reused or recycled, thereby generating large volumes of residues. Furthermore, reusing or recycling are not fully suitable methods to manage all packaging structures, especially in the case of food packaging materials, since they often consist of several different materials (blends of plastics or multilayer systems) to achieve optimum properties in terms of gas barrier or mechanical properties. This leads to intrinsic limitations in terms of separation efficiency prior to recycling and generates classification problems and reduced physical properties of the recycled materials [3]. Cleaning and decontamination costs of the plastic packaging are also significant due to contamination by foodstuffs. Table 1 represents the amount of food packaging materials in municipal solid waste (MSW) generated, recovered and discarded in 2011 in the United States.

As it can be observed from Table 1, the plastics waste ranks second in terms of waste generation, just after paper and cardboard, but they have the lowest level of recovery with an 8.3% of the total amount of waste generated. In addition, Figure 2 shows, in millions of tonnes, the generation and recovery of plastics in MSW between 1960 and 2011 in the United States. A great discrepancy is clearly observed between the evolution of plastic waste generation and plastic recovery during this period.

Taking in account these data and even considering the development, creation and improvement of recycling systems in many developed countries, it is thought that this environmental problem will only be overcome with the introduction of biodegradable polymers in the industry which replace, at least in part, petroleum-based plastics and that can be obtained from renewable resources [4]. Thus, the two main environmental drawbacks derived from plastic packaging could be addressed: firstly, to achieve commercial biodegradable packaging and, secondly, to develop materials for food packaging with good properties that ensures and guarantee food quality and safety using renewable resources.

Table 1. Generation, recovery and discards of materials in municipal solid wastes in 2011 (United States). (In millions of tons and percent of generation of each material) (Source: United States Environmental Protection Agency)

Material	Weight Generated	Weight Recovered	Recovery As a Percent of Generation	Weight Discarded
Paper and paperboard	70.02	45.90	65.6%	24.12
Glass	11.47	3.17	27.6%	8.30
Metals				
Steel	16.52	5.45	33.0%	11.07
Aluminium	3.47	0.72	20.7%	2.75
Other nonferreous metals	1.96	1.34	68.4%	0.62
Total metals	21.95	7.51	34.2%	14.44
Plastics	31.84	2.65	8.3%	29.19
Rubber and leather	7.49	1.31	17.5%	6.18
Textiles	13.09	2.00	15.3%	11.09
Wood	16.08	2.38	14.8%	13.70
Other materials	4.59	1.28	27.9%	3.31
Total Materials in Products	***176.53***	***66.20***	***37.5%***	***110.33***
Other Wastes				
Food Other	36.31	1.40	3.9%	34.91
Yard trimmings	33.71	19.30	57.3%	14.41
Miscellaneous inorganic wastes	3.87	Negligible	Negligible	3.87
Total Other Wastes	*73.89*	*20.70*	*28.0%*	*53.19*
TOTAL MUNICIPAL SOLID WASTE	***250.42***	***86.90***	***34.7%***	***163.52***

Negligible = Less than 5000 tons or 0.05%

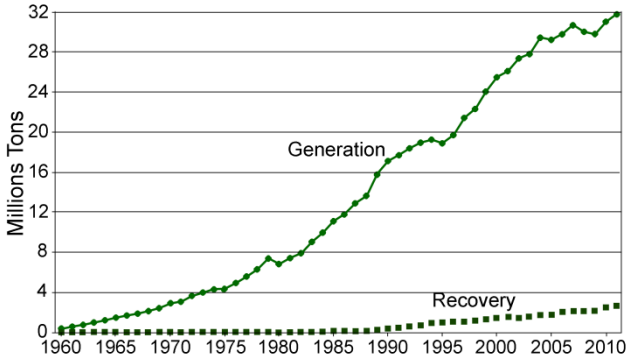

Figure 2. Plastics generation and recovery from 1960 to 2011 in US. (Source: United States Environmental Protection Agency)

2.1. Biodegradable Polymers

As previously mentioned, there is a worldwide general problem derived from waste management because of the high plastics consumption. Moreover, from the economic point of view, according to González García et al. [5], around 5% of available worldwide fossil

resources are currently employed to produce 200 million tons of plastic per year. It is estimated that there will be a demand of 2 billion tons per year by 2100 which implies a consumption of 50% of the available worldwide fossil resources. This will cause a dramatic increase in the price of plastics produced from fossil resources.

Therefore, from the food packaging point of view, great efforts should be focused in order to extend the shelf-life and improve the quality of the food while reducing the generated plastic wastes, hence minimizing their environmental impact. Consequently, there is growing interest both in academia and industry areas in the development and implementation of "bioplastics". Bioplastics, also called biopolymers include both polymers from renewable resources such as plants and microorganisms, as well as biodegradable polymers from renewable or non-renewable resources [6]. Figure 3 depicts the global production capacity of bioplastics by market segment in 2013 and the estimation by 2018. An increase in the production capacity is clearly observed, with more notorious increase in the packaging sector.

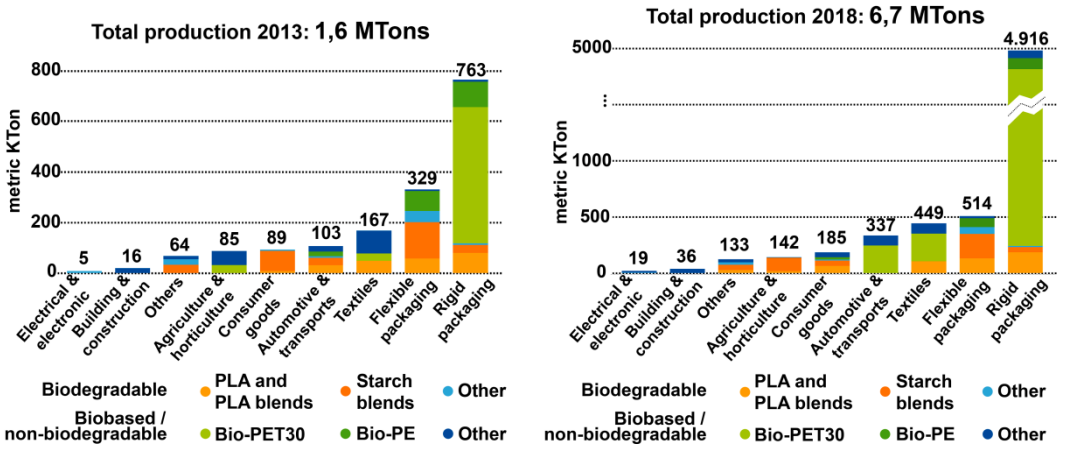

Figure 3. Global production capacity of bioplastics by 2013 and 2018 by market segment. (Source: European Bioplastics, Institute for Bioplastics and Biocomposites, Nova-Institute (2014). More information: www.bio-based.eu/markets and www.downloads.ifbb-hannover.de)

According to ASTM International, "biodegradable" is defined as capable of undergoing decomposition into carbon dioxide, methane, water, inorganic compounds or biomass in which the predominant mechanism is enzymatic action of microorganisms [7]. This type of degradation must be differentiated from other degradation processes such as photodegradation, chemical or thermal degradation. Thus, biodegradable plastics are polymeric materials in which, at least one step in the degradation process, is through metabolism in the presence of naturally occurring organisms which, under proper conditions, are able to disintegrate these materials producing non-toxic or harmful residues to the environment [8]. However, as conventional packaging, bioplastics-based packaging must meet a number of important criteria, including acting as a container of the product while maintaining its sensory quality and safety as well as providing information to consumers. However, as it will be shown later, these materials have poorer properties than those of petroleum-based plastics, thus, limiting their industrial use. The development of

technologies to improve their properties is one of the main issues in the development of bioplastic-based packaging, to which the present work is aimed.

Amongst the biodegradable materials, three main groups are generally considered [9]:

a) The first group includes polymers directly extracted from biomass such as polysaccharides (e.g. chitosan, carrageenan, starch, cellulose, etc.) and proteins (e.g. gluten, soy and zein).

b) A second group makes use of petroleum-based monomers or biomass-derived monomers but uses classical chemical routes for the chemical synthesis to obtain the final biodegradable polymer. This is the case of polycaprolactone (PCL), polyvinyl alcohol (PVOH) and their copolymers (EVOH) derived from petroleum, and polylactic acid (PLA) derived from biomass.

c) The third family makes use of polymers produced by natural or genetically-modified microorganisms, for example, polyhydroxyalkanoates (PHAs), mainly polyhydroxybutyrate (PHB) and its copolymers with hydroxyvalerate (PHBV), or bacterial cellulose.

Among the most widely studied thermoplastic polymers in recent years, some biopolyesters such as PHAs and PLA have attracted particular attention because they are commercially available, produced at industrial scale, can be processed by conventional equipment and have relatively good properties for many applications, such as biomedical or food packaging applications, for which they have already been extensively studied [10-13]. Figure 4 depicts the global production capacity of bioplastics in 2013 by material type, where the contribution of both PLA and PHAs as biodegradable polymers is shown.

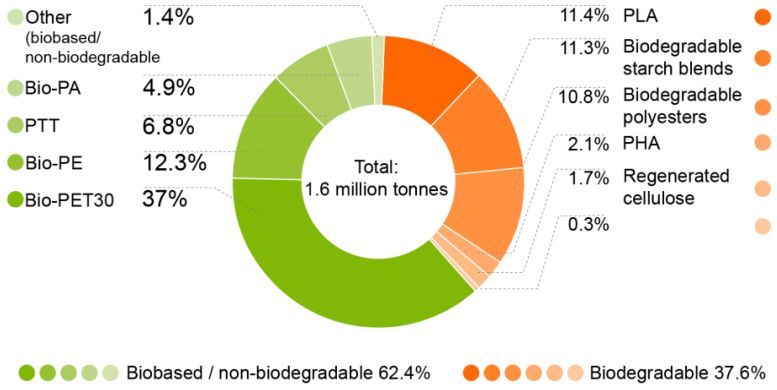

Figure 4. Global production capacity of bioplastics in 2013 by material type. (Source: European Bioplastics, Institute for Bioplastics and Biocomposites, Nova-Institute (2014). More information: www.bio-based.eu/markets and www.downloads.ifbb-hannover.de)

2.1.1. *Polylactic Acid (PLA)*

The polylactic acid, poly (lactic acid) or polylactide (PLA) is an aliphatic polyester derived from renewable resources such as corn starch, sugar beet, sugar cane, potatoes and

other biomass types, being one of the bioplastics which are in continuous commercial development nowadays [14], and the most used polymer produced from natural resources on a large scale, with around 140,000 tonnes per year [15]. Due to its versatility, PLA is being used for different applications in various areas (cf. Figure 5) such as in the biomedical area where it is one of the innovative materials used in long-term resorbable implants. Besides, its use has also increased in textile and packaging applications. It is of particular interest in packaging applications mainly due to its exceptional characteristics such as excellent transparency, good processability, mechanical properties comparable to those of polyethylene terephthalate (PET) [16] and polyethylene (PE) [17] and relatively good water barrier properties. The water vapour permeability of PLA is, for instance, much lower than that of starch [18],but still higher than that of conventional polyolefins such as high or low density polyethylene (HDPE and LDPE, respectively), polypropylene (PP) or polyethylene terephthalate (PET). However, its medium gases and vapours barrier properties and its brittleness are the most important handicaps for its use in certain applications such as food packaging [19]. PLA mechanical properties can be improved by the addition of plasticizers [20-21] but this also results in a decrease in oxygen barrier and transparency. Therefore, the main performance drawbacks of PLA are mainly associated to its low thermal resistance, excessive brittleness and insufficient barrier to oxygen and water compared to other benchmark packaging polymers like PET. Thus, it is of great industrial interest to enhance the barrier properties of this material because of its renewable and eco-friendly properties while maintaining its inherent good properties such as transparency and biodegradability [22].

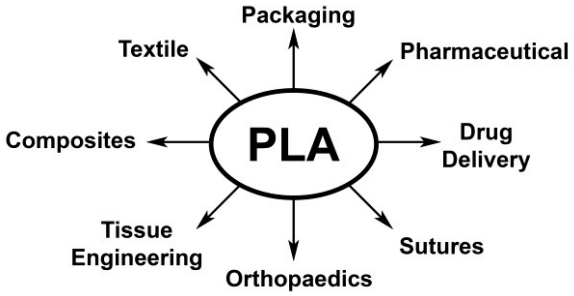

Figure 5. Different PLA applications (adapted from Gupta & Kumar [23])

2.1.1.1. PLA synthesis

The starting point for obtaining PLA is lactic acid (LA). There are two basic processes for obtaining LA based on chemical and biotechnological routes. Currently, the biotechnological route produces over 95% of global consumption of LA and consists of carbohydrate fermentation using various microorganisms. Conversely, chemical routes are used to obtain PLA from lactic acid. There are three synthesis routes which are summarized in Figure 6 [24]: Direct condensation polymerization of lactic acid also called polycondensation, the azeotropic condensation and ring opening polymerization (ROP).

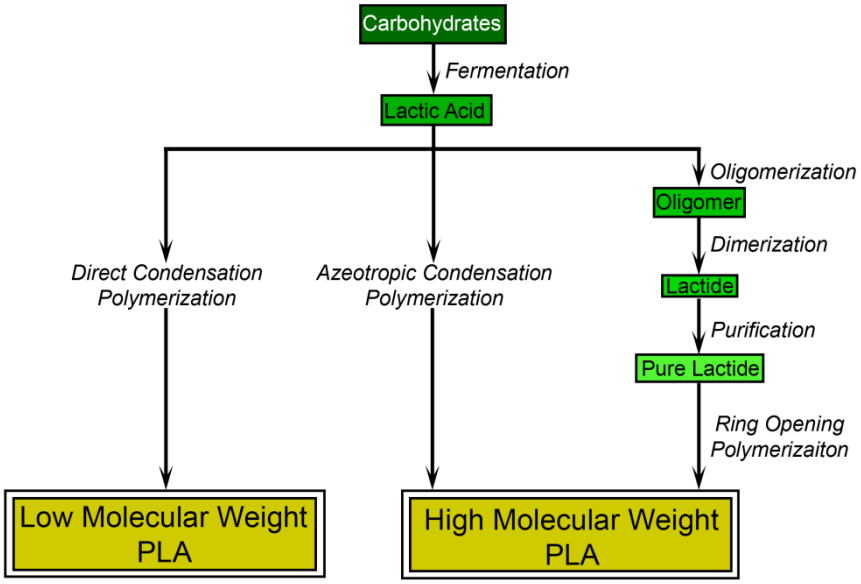

Figure 6. Synthesis of PLA by several routes (adapted from Gupta & Kumar [23])

2.1.1.1.1. Polycondensation

Condensation polymerization or polycondensation occurs through an equilibrium reaction where the initial components (monomers) are linked together by chemical reaction of their reactive groups accompanied by water molecule elimination for each monomer (lactic acid molecule) linked to the polymer chain. The reaction procedure is presented in Figure 7.

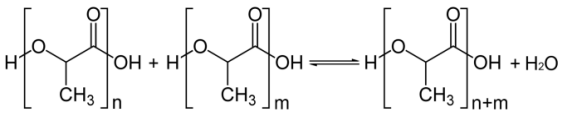

Figure 7. Polycondensation Reaction

The polycondensation process of lactic acid involves, in addition to the condensation reaction, another equilibrium reaction, the depolymerization reaction towards the formation of lactide, which is a cyclic dimer of lactic acid [25] (cf. Figure 8).

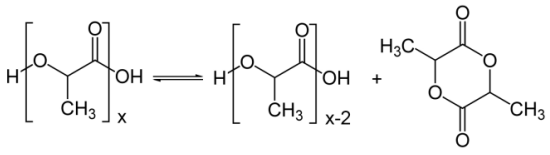

Figure 8. Depolymerization reaction of PLA with lactide formation

Although it is the simplest and cheapest process, the main drawback of this type of reaction is the low molecular weight of the obtained polymer. This is due, on one hand, to the high viscosity of the polymer in melt state which in turn complicates the extraction of water from the reaction medium in order to shift the equilibrium to the production of polymer and, on the other hand, to the undesired equilibrium reaction causing depolymerization. In fact, under typical reaction conditions, with high temperature and high vacuum to promote the dehydrative polycondensation, the evaporation of the lactide is also favoured, thus inducing the depolymerization [25]. Another drawback of this procedure is that the obtained polymer is brittle, glassy and essentially unusable for many applications unless extenders or adjuvants are incorporated to increase the molecular weight of the polymer. Moreover, increased coloring and racemization can also occur during the reaction.

2.1.1.1.2. Azeotropic condensation polymerization

The same steps as in the direct condensation of lactic acid are present in the azeotropic condensation polymerization but with the difference that in this procedure the monomer is polymerized in a solution system, where, along with the catalyst, is dehydrated using reflux under boiling conditions. This facilitates the removal of the water produced during the reaction due to a decrease in the viscosity of the medium, thus obtaining high molecular weight PLA. The choice of solvent, which should be aprotic, and more specifically its boiling temperature, represent a restriction of the polycondensation temperature that can be used. The water produced during the reaction must be removed from the solvent by using a drying agent (for example a molecular sieve). Alternatively, dry and clean solvent can be added during the reaction, although this is undesirable from the economic and environmental points of view [26, 27]. Several patents from Mitsui Toatsu Chemicals have been issued about the azeotropic dehydration of PLA. Different claims about various factors affecting the properties of the final polymer such as drying the solvent and its subsequent addition to the reaction medium, the use of various drying agents and the use of different solvents are listed, giving raise to PLA with molecular weight greater than 300,000 g mol^{-1} [28, 29, 30, 31].

Although high molecular weight polymer can be obtained through this type of polymerization without the use of extenders or adjuvants, this route has some drawbacks mainly related with the use of organic solvents as well as the considerable amounts of catalyst impurities in the final product. These residual catalysts can cause problems during subsequent processing, such as uncontrolled degradation or hydrolysis reactions or, in the case of medical applications, along with the use of solvents, toxicity and other undesirable properties [26].

2.1.1.1.3. Ring opening polymerization (ROP)

The cyclic dimers of lactic acid, i.e. lactides are used as initial monomers in the ring-opening polymerization reaction. This lactic acid dimer is obtained by thermal cracking of low molecular weight PLA (oligomers) previously obtained by polycondensation. Lactide has functional groups that are susceptible to nucleophilic or electrophilic attack by anions or cations, which act as initiators and promote the ring opening. From this opening, the

propagation of the polymer chain is carried out, thereby obtaining PLA. The reaction procedure is depicted on Figure 9.

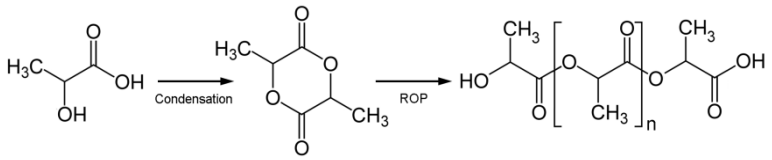

Figure 9. Ring opening polymerization (ROP) reaction

There are different reaction mechanisms and initiator types for ring-opening polymerization of lactide: cationic polymerization, anionic polymerization, coordination-insertion mechanism and enzymatic polymerization [32, 23]. Among them, the coordination-insertion mechanism has several advantages such as greater control of the molecular weight, higher degrees of polymerization, lower probability of side reactions than in the case of ionic initiators and limited racemization [32, 33]. In this mechanism, lactide plays temporarily the role of a ligand coordinated with the catalyst, typically a metal alkoxide. Although a large number of catalysts have been studied, the most widely used is bis (2-ethylhexanoate) tin (II), commonly known as tin octoate (often abbreviated $SnOct_2$) [32, 23].

This polymerization method is the best route to synthesize high molecular weight PLA. The reaction can be easily controlled, tailoring the characteristics of the resulting polymer in a more controlled way. In addition, there is a high control of the stereochemistry of the final product, which can extend its field of application. This reaction has other advantages such as the use of moderate reaction conditions, short reaction times, control of the chain length and the low existence of side reactions.

Although there is ambiguity in the literature, typically the polymer derived from lactide is referred to as polylactide and that obtained from lactic acid is referred as polylactic acid or poly (lactic acid). Both names are currently being used indistinctly in the literature and will also be used interchangeably throughout this work.

2.1.1.2. PLA properties

PLA properties largely depend of the stereochemistry of the polymer chain, which is directly related to the ratio of the starting enantiomers. Since the lactic acid can be found as two different enantiomers, D-lactic acid and L-lactic acid, the cyclic dimer production can result in four different enantiomeric forms: the D,D-lactide (called D-lactide), L,L-lactide (called L-lactide) and L,D- or D,L-lactide (called *meso*-lactide) as well as equimolar or racemic mixtures of D- and L enantiomers (referred *rac*-lactide). All of them are presented in Figure 10 [23, 24]. Sometimes, *meso*-lactide and *rac*-lactide are confused in the literature, being both commonly called D,L-lactide. Obtaining a specific dimer enantiomeric form can be controlled trough the control of the starting lactic acid and using stereoselective catalysts.

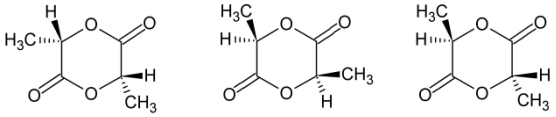

Figure 10. Different lactide enantiomers

The repeating units are added, either as lactic acid during direct condensation polymerization or as lactide during ROP. Therefore, it is possible to obtain poly (L-lactic acid), poly (D-lactic acid) from polycondensation or poly-D-lactide, poly-L-lactide, poly-D, L-lactide or racemic mixtures of poly-D-lactide and poly-L-lactide by ROP route. Stereoregularity of polymers obtained by polymerization of pure lactide enantiomers is rather obvious. However, synthesis of stereoregular PLA from racemic mixtures of L-lactide and D-lactide can be carried out by using stereoselective catalysts for the stages of initiation and propagation of ROP [27, 34]. A wide range of degradation rates, physical and mechanical properties can be obtained by varying the molecular weight and stereochemistry of the polymer chain.

Thus, while the optically pure poly (L-lactide) (PLLA) is a crystalline, hard and brittle solid, poly (D,L-lactide) (PDLLA) is amorphous and transparent [32]. Furthermore, while the PLA produced by more than 93% of L-lactic acid is a semicrystalline material, those produced from 50 to 93% of L-lactic acid are strictly amorphous. Both *meso*- and D-lactide induce spins in polymer chain architecture unlike L-lactide which possess more regular architecture [24]. Due to the crystallinity and more orderly and compact structure of the PLLA, it has better mechanical properties and lower degradation rates than PDLLA [23].

In addition to the renewable character of PLA, this polymer can be degraded under composting conditions being decomposed into water and carbon dioxide that is sent back to the atmosphere, according to the life cycle of PLA (c.f. Figure 11).

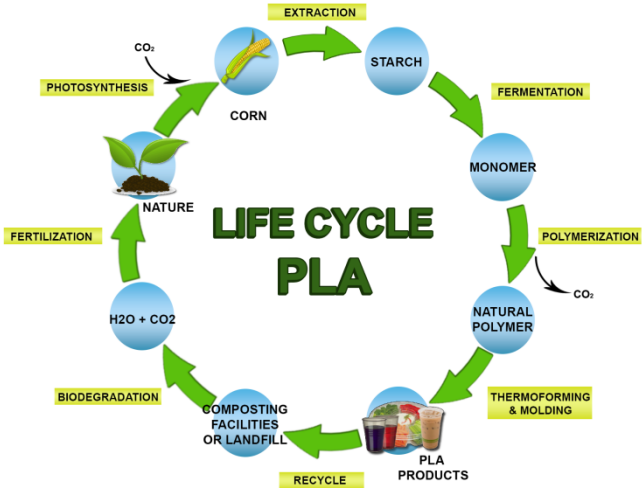

Figure 11. Lifecycle of PLA

The life cycle of PLA was studied by Vink et al. [35] and it was concluded that the most significant benefits of using PLA are reductions in the use of fossil resources and in the global

warming or greenhouse effect since, on one hand, PLA uses renewable materials and, secondly, its overall negative balance in terms of carbon dioxide emissions. This can be explained by all the carbon in the lactic acid being derived from the glucose, which is produced by plants through photosynthesis, wherein the carbon is consumed as carbon dioxide (CO_2). Therefore, all of the carbon in PLA comes from atmospheric CO_2. However, like all industrial production processes, production of PLA requires energy, which causes CO_2 emissions. Thus, considering the CO_2 absorbed by the plants during their growth to perform photosynthesis and the CO_2 released during the production and biodegradation of the PLA, an overall negative balance is reached. For example, in comparison with nylon and PET, PLA used 30-50% less fossil resources resulting in 50-70% lower CO_2 emissions. Furthermore, this study also showed that the PLA has a lower non-renewable energy content compared to a variety of common plastic materials. Therefore, PLA has a unique combination of energy, environment and sustainability which make it one of industrial products from biomass with good future prospects.

However, considerable research and development efforts are needed in order to replace fossil-derived plastics with PLA for certain applications. This is due to, as for most biodegradable polymers, an improvement of some of their properties is required, such as barrier and mechanical properties, to allow its use in applications for which the current physical-chemical behaviour is insufficient [36].

In this sense, some strategies have been developed in order to improve the properties of this material which include its use in coatings [37-39], multilayer systems [40, 41], as well as blends with other polymeric matrices derived from renewable resources such as chitosan, starch or PHB or non-renewable such as PCL, poly (vinyl acetate) (PVAc) or polyethylene glycol (PEG) [42]. In addition, in an attempt to improve PLA properties, copolymerization with other monomers and mixtures with other materials, which acted as plasticizers, have been also used [43, 44]. Nowadays, an efficient strategy widely studied to improve the properties of biopolymer matrices in general, and particularly for PLA, is based on the use of nanotechnology. The incorporation of either organic or inorganic nanostructured materials, also known as nanofillers or nanoreinforcements within polymer matrices has proven to be effective in terms of improving the final properties, being this technology also attractive for its low cost [45]. Possible solutions using nanotechnology to enhance the properties of biopolymer matrices will be further discussed.

2.1.2. *Polyhydroxyalkanoates (PHAs)*

Another alternative to the non-biodegradable polymers from fossil resources are polyhydroxyalkanoates (PHAs), which have attracted great interest due to their biodegradable, biocompatible and renewable character. PHAs are biopolyesters of hydroxylalkanoic acids synthesized intracellularly by some microorganisms as a carbon and energy storage (cf. Figure 12) [5]. More than 300 microorganisms are known to produce and accumulate PHAs [46]. Moreover, PHAs can be degraded by bacteria, fungi and algae in various ecosystems [47]. PHAs granules were first observed in 1888, but its composition was not confirmed until 1925 [11]. Ideally, PHAs may be synthesized intracellularly to represent 80% of the total mass of bacteria on dry basis.

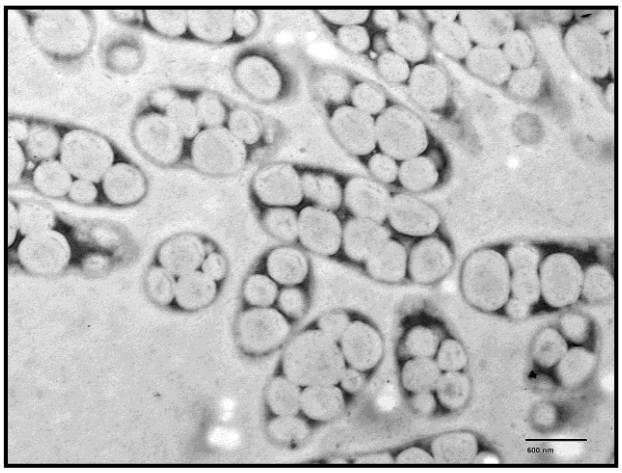

Figure 12. PHAs granules in *Ralstonia eutropha*

Regarding the monomeric structure of the PHAs, they can be classified depending on the chain length of hydroxyalkanoic acids from which they are composed. Thus, short chain (monomers 3 to 5 carbon atoms), medium chain (monomers from 6 to 12 carbon atoms) and hybrid PHAs (containing short chain and medium chain) are defined. Short chain PHAs are typically semicrystalline thermoplastic polymers with high degree of crystallinity (60-80%), melting temperature (T_m) of about 180°C and glass transition temperatures (T_g) between -5 and 20°C. In contrast, medium-chain PHAs are highly amorphous materials with T_m between 42 and 58°C and T_g between -62 and -26°C being therefore classified as elastomers [5].

Amongst this family of polymers, the homopolymer polyhydroxybutyrate (PHB) has been extensively studied, because it has similar mechanical properties to those from conventional petroleum-based polymers, relatively good thermal properties and high stiffness due to its high crystallinity degree [48]. However, while high crystallinity is useful for some applications, their rigidity limits their use in other commercial applications. Another drawback of this polymer is its low thermal stability, which makes it less useful and unstable during high temperature processing techniques such as melt blending, also limiting its industrial applicability [49].

Several strategies have been developed to solve such drawbacks, including blending with other polymers such as PVA [50], polypropylene glycol (PPG) [51] and PCL [52], or modification of the homopolymer by incorporating different types of monomers during fermentation such as hydroxyvalerate (HV) or hydroxyhexanoate (HH). The possibility of preparing various polyesters as a function of the substrate was first reported by De Smet et al. [53] who produced a polymer consisting mainly of 3-hydroxyoctanoate units after a culture grown in n-octane. The general structure of the PHAs can be seen in Figure 13. About 150 of such monomers have been identified up to date, although from a commercial point of view the poly (hydroxybutyrate-co-hydroxyvalerate) (PHBV) is presented as a better candidate than PHB due to its greater ductility and better processability [11].

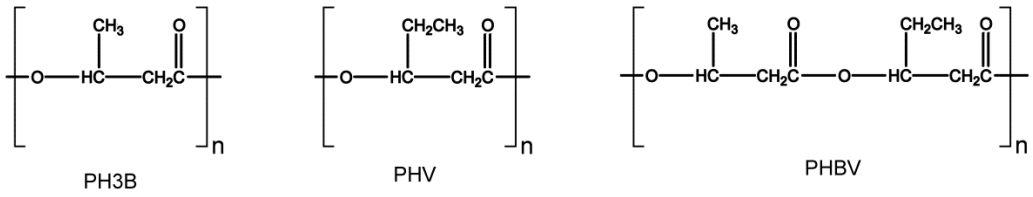

Figure 13. Structures of poly-3-hydroxybutyrate (PH3B), polyhydroxyvalerate (PHV) and polyhydroxybutyrate-co-hydroxyvalerate (PHBV)

The mechanism of bacterial synthesis of PHAs is widely known which allows the possibility of modifying the processes in order to obtain the desired product. Thus, depending on the selected microorganism and the culture conditions, homo- or copolyesters can be obtained [5, 11, 54].

PHBV has improved mechanical and thermal properties since incorporation of hydroxyvalerate reduces the crystallinity, thereby decreasing stiffness and brittleness of the material, and also reduces the melting point of the polymer without decreasing the thermal stability [48, 55]. However, it is well known that a reduction in crystallinity affects the barrier properties to low molecular weight compounds, which is a key property of materials intended to be used in food packaging applications [56, 57].

High production costs are another drawback associated with these materials because of expensive substrates for bacterial growth and sterile conditions during the process are required. Because of this, the optimization of the fermentation and extraction processes, as well as the isolation and development of more productive microbial strains which can use cheaper substrates have been studied [58]. Therefore, PHBV still has some disadvantages such as high cost, low crystallization rate, relative brittleness and low thermal stability, hindering a widespread use of this family of polymers.

In view of the foregoing information, although both biopolymer families (PLA and PHAs) represent an alternative to conventional petroleum-based polymers, they have a number of drawbacks that preclude their widespread use in food packaging applications. Hence, the modification of these materials to improve their properties through innovative technologies is an important challenge for worldwide research. Undoubtedly, the main challenge in recent times is focused on developing environmentally-friendly and economically viable biopolymers, which can be processed by conventional technologies used at industrial scale and reach similar properties to those of conventional polymers.

Various technologies have been used to this aim, including chemical modification of biopolymers, addition of plasticizers in order to improve mechanical properties, mixing with other polymer or biopolymer matrices, etc. [8]. Moreover, in the last decades many studies have been focused on the production of composite materials and, more specifically, nanocomposite materials using these biopolymeric matrices through the use of nano-reinforcements, which is an effective way to improve their properties. Therefore, the development of new polymeric-based nanocomposites, renewable and biodegradable,

commonly called new green nanocomposite materials, has good future prospect, being considered as the next generation of materials. Possible solutions related to the development of nanostructured materials and their incorporation by different technologies within polymeric matrices are discussed in the following paragraphs.

3. NANOTECHNOLOGY: USE FOR REINFORCING BIOPOLYMERS.

Polymer "composites" or composite materials are heterogeneous or hybrid materials essentially consisting of a continuous phase or polymer matrix and a discontinuous phase or fillers. Fibers, films and particles of organic and inorganic materials have been used during decades to form polymer composites with improved mechanical and thermal properties. A recent development in composite materials is nanotechnology. Nanotechnology is defined as the study, design, characterisation, production and application of structures, devices and systems by controlling shape and size at nanoscale. A material is considered "nano" when its size is between 1 and 100 nanometers in at least one dimension. Thus, incorporating materials at the nanoscale within polymer matrices leads to nanocomposites. This technology is nowadays applied in areas related to physics, chemistry and biology, among others. For many biodegradable polymers applications the use of such technologies in order to improve some properties such as gas barrier and mechanical properties is required, increasing, in this way, their competition in the current market. The combination of using biopolymers with the possibility of modifying their properties using nanotechnology allows the creation of materials that can be called *nanobiocomposites*.

It is noteworthy to mention that in order to achieve good reinforcing effect and optimal improvements in the final properties of the composite material, good interaction between the filler and the polymer matrix must be reached. This, in turn, depends on the dispersion, the chemistry of the interface, the polymer-filler affinity, filler morphology and the preparation method [59, 60]. In fact, achieving good dispersion of filler within the polymer matrix is one of the biggest problems which arise when developing new composites. It is widely known that a good interaction between both phases, i.e. polymer and filler, is achieved when good dispersion of the filler within the polymer matrix is obtained and also by reducing the size of the filler. Larger particles drastically alter and deteriorate the characteristics of the composite material but, in contrast, the trend to form reinforcement aggregates increases with decreasing particle size [61]. Therefore, changing from macro- or micro- to nanoscale leads to better performance of the nanocomposites as nanostructured materials have a higher specific area which can be used to establish interactions with the polymer matrix, although it can lead to increased nanoreinforcement agglomeration. Well dispersed nanometric additives may lead to materials with improved mechanical, thermal and barrier properties compared to the starting polymers and their conventional hybrid compounds at macro- and microscale [62, 63]. Nanocomposites, thus, represent a new alternative to conventional technologies to improve the properties of polymers. However, the use of this kind of nanostructured materials in the area of food packaging presents various issues, since nowadays there is no knowledge about the possible migration of these nanoparticles to food and their potential effects on the health of consumers.

Among the most commonly used fillers to synthesize nanocomposites are cellulose nanowhiskers (also called cellulose nanocrystals) and carbon-based compounds such as graphene. The following paragraphs describe more in detail each of them and their incorporation strategies into polymeric matrices.

3.1. Cellulosic materials

Cellulose is the most abundant natural molecule and one of the most abundant biopolymers on earth. Annually 10^{11} to 10^{12} tons of plant-derived cellulose are produced. It is the major cell-wall component of plants, being a strong natural polymer with the formula $(C_6H_{10}O_5)_n$, consisting of linear chains of several hundred to over ten thousand units of D-glucose linked by β (1 → 4) linkages. Cellulose fibers are inexpensive, widely available, environmentally-friendly, easy to recycle and require low power consumption in its production.

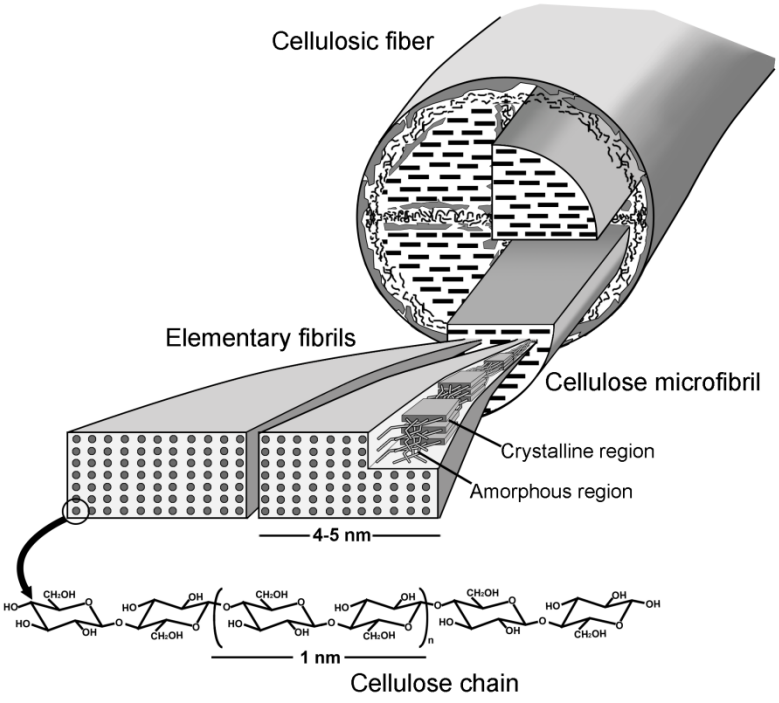

Figure 14. Internal structure of plant-derived cellulose

Figure 14 shows a schematic model of the hierarchical structure of plant-derived cellulose. Several models have been proposed to explain the internal structure of plant cellulose and, moreover, different terminology has been used to describe the cellulose structure, fact which has led to certain misunderstanding [64-66].

Cellulose microfibrils, with diameters ranging from 2 to 50 nm and lengths up to several tens of microns [65, 66], are formed by aggregation of elementary fibrils which are

composed by cellulose chains containing both ordered (crystalline) and less ordered (amorphous) regions. These crystalline regions which can be isolated by various treatments are "cellulose nanowhiskers" (CNW), also known as cellulose nanocrystals. The dimensions of these crystals depend on the origin and treatment of the samples. Each microfibril can be considered as a flexible string with cellulose crystals linked along the microfibril axis by disordered amorphous domains. Four of these cellulose microfibrils are held together by other polysaccharides, such as hemicellulose or lignin, into larger units known as cellulose fibers as observed in Figure 1. The hydroxyl groups present in the cellulose surface and their ability to form strong hydrogen bonds are closely related with the most important properties of cellulose such as hierarchical organization (crystalline vs. amorphous region) and highly cohesive nature, among others. In fact the lattice forces that are responsible for maintaining the crystalline regions are the result of stabilization by strong and complex networks of inter- and intramolecular hydrogen bonding [66].

For their application as nanofillers, cellulose elementary fibrils are usually isolated from native cellulose either by mechanical processes, producing microfibrillated cellulose (MFC) or by acid hydrolysis to obtain nanocrystalline cellulose. While MFC exhibits both amorphous and crystalline parts, nanocrystalline cellulose exhibits only crystalline regions. These nanostructured materials have excellent mechanical properties and a complete renewable and biodegradable character. Values of elastic modulus higher than 130 GPa and tensile strength close at 10 GPa have been reported for the CNW [67-69]. Furthermore, these materials have other interesting properties such as high barrier to gases and vapours, high specific area and low density [67]. All these properties, make cellulose nanoadditives a class of nanomaterial very attractive for the preparation of low cost, lightweight and with high mechanical properties nanocomposites [65].

3.1.1. *Bacterial cellulose*

In addition to plant cellulose (PC), cellulose can be synthesized by various organisms resulting in bacterial cellulose (BC). Particularly, some bacterial genera such as *Rhizobium*, *Acetobacter*, *Agrobacterium* and *Sarcina* are able to synthesize cellulose [70]. Within the *Acetobacter* genus, *Gluconacetobacter xylinus*, *Acetobacter hansenii* or *Acetobacter pasterianus* produce BC. Among them, the species *Gluconacetobacter xylinus* is considered the model microorganism for the production of BC due to its greater production capacity, giving raise to high purity cellulose with similar structure to that of plant-derived cellulose [71]}.

In a static culture medium rich in polysaccharides, this bacterial species is capable of producing a BC layer at the liquid/air interface. This highly hydrated pellicle consists of a random assembly of fibrils of less than 100 nm wide, which are composed of a bundle of nanofibrils. There are several hypotheses explaining why this type of microorganisms produce cellulose, including the fact that the cellulose layer can act as a protection barrier against external agents such as radiation, other microorganisms or heavy metals or even relating cellulose production to positioning bacteria in an optimal area, close to the culture medium but in turn where there is greater oxygen abundance [72].

Although PC and BC have the same chemical structure, they have different structural organization and different mechanical properties. BC shows an improved web-like network structure of the fibers, higher water holding capacity and higher crystallinity. A schematic model of the structure of the microfibers of PC and BC can be observed in Figure 15.

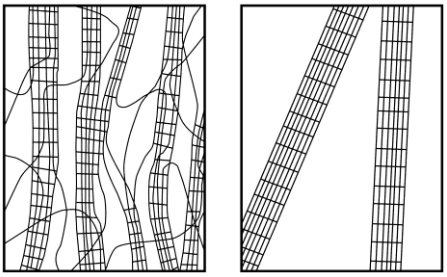

Figure 15. Schematic model of bacterial cellulose microfibrils (right) drawn in comparison with plant cellulose (left) [72]

Moreover, while PC is naturally associated with other biopolymers such as hemicellulose and lignin, which requires purification and bleaching operations to extract cellulose, BC is essentially pure [73]. Only the remaining bacteria and the culture medium absorbed into the bacterial cellulose film must be eliminated, which is achieved by washing with boiling water as well as aqueous solutions of sodium hydroxide. Due to their excellent properties, i.e. high purity, high crystallinity, high mechanical strength, low density and biocompatibility, the bacterial cellulose has become a very interesting material, with applications in biomedicine [74], in the paper industry [75] and, more recently, as a reinforcing agent in polymer matrices [76-77]. Therefore, bacterial cellulose represents an alternative to plant-derived cellulose due to its outstanding properties.

As previously commented, in order to use both PC and BC as nanofillers they are subjected to hydrolysis with strong acids such as sulfuric acid or hydrochloric acid, producing a preferential digestion of the amorphous domains of the material leaving the crystalline regions intact. Thus, nanofibrils bundles are divided, resulting in smaller molecules. This acid treatment that breaks the structure of cellulose results in crystalline nanofibers or cellulose nanocrystals (CNW). CNW morphology depends on the source of cellulose and the hydrolysis conditions. While CNW extracted from vegetables resources such as cotton or wood often have a length of 100-300 nm and a diameter range from 5 to 20 nm, those obtained from bacterial cellulose may have several microns in length and a diameter of 5- 50 nm increasing its aspect ratio (L/D) which is a critical parameter with a remarkable influence on reinforcing capacity of the nanofiller when incorporating it into a polymer matrix [78]. Regarding to the hydrolysis conditions, the acid concentration, cellulose/acid ratio and hydrolysis time and temperature are factors that determine the morphology of the CNW obtained [73].

3.2. Carbonaceous materials. Graphene

There is no doubt that the 21st century is the era of carbon nanomaterials, from graphite to carbon nanotubes and now with intense focus on graphene. Graphene belongs to a new

class of carbon nanomaterials, 2-D materials, which represent the basic structure of graphite made up entirely of conjugated sp^2 carbons arranged in a honeycomb structure.

This material has gained special attention in recent years because of its outstanding physical properties, which are significantly higher than those of any other known inorganic filler up to date, even higher than those of carbon nanotubes [79]. As a result, the graphene-based materials are expected to be used in a variety of applications including, sensors, batteries, supercapacitors, nanocomposites, solar cells, active and intelligent packaging and hydrogen storage systems [80].

There are two main routes in regard to graphene production, "bottom-up" and "top-down" routes. The first one is based on the synthesis of graphene sheets by assembling carbon atoms starting from simple molecules such as methane or ethanol. On the other hand, the top-down technique is based on graphite disintegration until graphene nanosheets are obtained. Both methods provide graphene with different properties and performance. Out of all graphene production processes, which include mechanical exfoliation, chemical vapour deposition (CVD) or epitaxial growth, among others, those based on bottom-up technique produce more perfect graphene nanosheets and with better properties but they are not suitable for large scale production [79]}. On the other hand, graphite oxidized derivatives (graphite oxide) are synthesized by submitting graphite to strong oxidizing agents prior to the graphene production in the "top-down" processes. This material is subsequently exfoliated and generates monoatomic oxidized sheets called graphene oxide. Thus, reduction of graphene oxide has attracted particular attention since it is a route by which it is possible to produce graphene sheets in both powder and colloidal dispersions with high processability. There is a wide variety of systems used as reducing agents ranging from the use of temperature to the use of various chemicals agents or even microorganisms {[79, 81]. From the chemical point of view, the presence of oxidized functional groups on the surface of graphene oxide, make this route especially interesting as these groups provide reactive sites for chemical modification using the surface chemistry of carbon [80]. Furthermore, it is the optimum route in terms of performance and costs, being the graphene obtained through this route demanded by different industrial sectors such as coatings, paints/inks, transparent conductive layers, applications related to biology and energy storage [81].

This material has evolved rapidly due to extensive studies that have been carried out. The main reason behind the fast-paced development of graphene research is due to its unique properties [81], presenting not only excellent mechanical, electrical and thermal properties, but also excellent barrier properties to gases and vapours, due to the fact that the defect-free graphene sheets are impermeable to low molecular weight compounds [82]. It has been observed that this type of laminar structured materials are highly effective in improving the barrier properties of various polymeric matrices [82-84], which makes the graphene an excellent nanoreinforcement for polymers and biopolymers matrices [85]. Improved mechanical, barrier and/or electrical properties have been demonstrated in several studies in which graphene has been used as reinforcement in different polymer matrices such as PVA [86], PE [87], polystyrene (PS) [88], PLA [89] and PHBV [55] among others.

3.3. Strategies to incorporate nanofillers into polymeric matrices

There are three main routes for the development of polymeric nanocomposites, regardless of the nanofiller used: solution mixing, *in situ* polymerization and melt mixing [59, 82].

Solution mixing is one of the most widely studied methods for the incorporation of nanofillers. This methodology is mostly based on dispersing the nanostructured reinforcements in a solvent in which the polymer is soluble. The final dispersion of nanofillers depends on the interacting forces between the nanoparticles themselves and their interactions with the solvent or polymer solution. After the dissolution/dispersion step, the solvent is evaporated or the mixture is precipitated thus obtaining the polymer loaded with the nanoadditive. Although good results in terms of dispersion of nanomaterial within the polymer matrix are obtained through this approach, it requires large amounts of solvent which makes it a non-environmentally-friendly technology with difficult extrapolation to the industrial scale.

The second method is by *in situ* polymerization. In this technique, the monomer is used as a medium to pre-disperse the nanofiller and, subsequently, the system is submitted to polymerization conditions. Compared to other methods to prepare nanocomposites, the use of *in situ* polymerization offers several advantages such as uniform dispersion of nanofillers, minimizing aggregation, or generation of strong interactions between the matrix and the nanoreinforcement, increasing, in this way, the compatibility between both phases. However, during the polymerization process, the viscosity tends to increase, thereby reducing the processability of the nanocomposites. Moreover, many of these reactions must be carried out in presence of solvents, thus entailing drawbacks associated with their use [90]. In such cases, although the use of solvents is much lower than in the solution mixing method, considerable amounts are still necessary to carry out the incorporation of nanofillers [91]. On the other hand, large amounts of reagents are required to carry out the reaction, thus reducing its applicability [92, 93]. The polymerization can be initiated by heat, using an initiator or using catalysts. Sometimes, the system may be induced in order to use the reactive groups in the nanofiller surface as initiators of the polymerization reaction, generating covalent bonds between the polymer and the nanofiller ("grafting from"). On the contrary, it is also possible to generate a covalent bond between the polymer chain, once already synthesized, and nanofiller ("grafting to") [59, 94].

Finally, the melt mixing route involves the mixing of nanofillers with thermoplastic polymers in melt state under high shear forces. The use of elevated temperatures necessary to achieve a homogeneous mixture can cause degradation of the nanofiller, which in turn may cause a degradation of the polymer chains. However, this is a method that does not require the use of solvents, simple and economical, being, therefore, widely used for the synthesis of polymeric nanocomposites. This route is also considered one of the most attractive for commercial development of these nanocomposites materials since it is one of the most widespread industrially.

Apart from the above-mentioned techniques, a novel strategy that has recently emerged for the development of polymer-based nanocomposites is the "ball-milling" technique. This technique is considered as a new method of synthesis of composites and nanocomposites and is based on high energy milling (HEBM for its acronym High Energy Ball Milling) capable

of producing mechano-chemical changes in materials. The ball milling technique involves mixing the polymer and the nanofillers in a ball mill using the energy released during the ball impacts. The effectiveness of mechano-chemical character of this technique has been previously confirmed by the appearance of covalent bonds between the polymer matrix and nanofiller after being processed by ball-milling [95]. Moreover, it is a solvent-free technology and is presented as an efficient alternative to produce novel high performance composite materials since during the grinding an intimate mixing between the polymer and the reinforcing material are promoted [96, 97]. Its efficiency has been widely demonstrated in the development of nanoclays- and nanostructured carbonaceous materials-based nanocomposites [95, 96, 98-101]. Additionally, this technology has also been used for the development of nanocomposites where there was a low compatibility between the nano-reinforcement and matrix in order to overcome the lack of affinity between both components [100].

3.3.1. *Cellulose-based nanocomposites*

CNW have outstanding properties that make them very attractive for their use in nanocomposite materials. However, the hydrophilic nature of the CNW makes them incompatible with most organic solvents and thermoplastic polymer matrices, mainly of hydrophobic nature, which complicates their use as nanoreinforcements. Additionally, these materials also exhibit a strong tendency to self-association due to strong hydrogen bonds that occur between cellulose molecules when this material is subjected to drying processes [102]. As a result, the incorporation of highly dispersed CNW within polymeric matrices, which is essential for achieving good properties in the final nanocomposite, is not an easy task. When a good dispersion of the cellulose nanocrystals into polymeric matrices is achieved, a percolation network among the nanoreinforcements throughout the polymer matrix is obtained resulting in exceptional reinforcing effects, even at low nanofiller contents [103].

Traditionally, the solution mixing has been the most widely used route for the preparation of cellulose nanocrystals-based nanocomposites. This method generally requires a solvent exchange prior to the use of cellulose, which involves successive centrifugation steps [104], without ensuring good dispersion of the nanocrystals into the matrix due to the difficulty in dispersing these hydrophilic materials into organic solvents [105]. For this reason, several studies have focused on finding strategies to improve both the dispersion and compatibility of CNW with hydrophobic systems, such as the use of a suitable solvent [106], the use of surfactants [107, 108] or by chemical surface modification of cellulose nanofillers [104, 109-111], thereby obtaining improved properties. However, as previously stated, this approach requires the use of large amounts of organic solvents which are toxic and expensive, also being an impractical and inappropriate from an industrial application point of view.

Several studies have reported on the incorporation of cellulose within non-renewable polymeric matrices using the *in situ* polymerization route [112-114]. However, there is scarce literature reporting on the incorporation of this type of nano-reinforcement into biopolymer matrices by this route. The surface hydroxyl groups of cellulose can act as

initiators of the polymerization reaction resulting in a grafting of the polymer chains on the nanocellulose surface. Nanocomposites of PLA and CNW have been obtained by this route, using the surface hydroxyl groups of cellulose as initiators of the polymer chain being grafted onto the reinforcement surface [115]. However, in this case, the length of the polymer chains developed from the initiator points on the cellulose surface resulted in a moderate molecular weight polymer. This treatment, as it will be discussed below, can be used as cellulose pre-incorporation step giving rise to a starting material which subsequently diluted in the molten state, improve the final CNW dispersion into polymer matrices. By controlling the hydroxyl groups available on the cellulose surface, it is possible to obtain larger polymer chains grafted on its surface. Thus, by partial acetylation of the hydroxyl groups present on the cellulose surface nanocomposites of PLA and CNW with high molecular weight have been obtained, thus not requiring further steps to achieve good properties of the polymer [103]. In any case, although this strategy uses less organic solvents than those required in the solution mixing route, significant amounts were also required.

As stated above, the melt blending technique is the most widespread route at industrial level. However, few studies reporting on the incorporation of cellulose into polymer matrices by this route have been reported in the literature. Again, the main drawback is based on the hydrophilicity of the cellulose making it poorly compatible with most polymer matrices which are mainly of hydrophobic nature, as well as on the strong interactions, via hydrogen bonding, occurring between cellulose nanocrystals when submitting them to drying processes. This results in weak interactions between the matrix and cellulose which complicate the dispersion and induce to agglomeration. For example, Jiang et al. [106] observed low compatibility between CNW and melt PHBV, complicating the dispersion of cellulose leading to weak interactions between matrix and filler. They observed that, even with the use of a compatibilizer, such as PEG, CNW agglomerates formed during freeze-drying could not be broken and, thus, they were not well dispersed through this technology. Recently, different strategies to improve the compatibility between cellulose and naturally hydrophobic matrices by melt mixing have been reported. Among these strategies, one of the most widely used is the surface chemical modification of cellulose by reaction of hydroxyl groups with different chemical agents, leading to improvements in the dispersion within polymeric matrices. For instance, the surface silanization of cellulose led to improved dispersion in PLA [116]. However, although the surface modification of cellulose seems to be a good strategy to improve its compatibility with both hydrophobic matrices and organic solvents, it has been demonstrated that an excess of surface modification may lead to detrimental effects on the structure and properties of CNW [117-119] and also it may cause various problems associated with CNW biodegradability, economy and migration process in nanocomposites materials used in food packaging. In recent years, other mechanisms have been developed to improve the compatibility of cellulosic nano-reinforcement with polymeric matrices. They are mainly based on the development of an initial nanocomposite with high nano-reinforcement concentration (known as "masterbatch"), which is subsequently diluted with the polymer in melt state. This initial masterbatch may be developed using different technologies such as solution mixing, electrospinning or *in situ* polymerization, achieving through the latter methodology grafted polymer chains on the cellulose surface. Using these strategies, improved dispersion of the CNW into polymer matrices such as PLA [76, 77, 115, 120, 121] or PCL [122] have been obtained.

In addition to the above strategies, in order to obtain a good dispersion of the cellulose nanocrystals into polymer matrices by melt mixing, it should be noted that, as previously demonstrated, these nanoreinforcements should be used partially hydrated instead of dried or freeze-dried [123]. As already mentioned, strong hydrogen bonds between the cellulose chains are generated during the drying processes, causing the self-association and making it very difficult to re-disperse them. In this line, an improved dispersion of cellulose nanofillers into PLA prepared by extrusion, using a plasticizer as an adjuvant and feeding cellulose in liquid medium has been recently reported [17].

3.3.2. *Graphene-based nanocomposites*

As previously commented, the best known and used procedures for the development of polymeric nanocomposites are solution mixing, *in situ* polymerization and melt mixing {[82, 91, 124]. The first two routes are the most widely used ones to prepare graphene-based polymeric nanocomposites mainly due to dispersion issues, since good results have been obtained using these methodologies [91]. For example, Kim et al. dispersed graphene into polyurethane (PU) by solution mixing, *in situ* polymerization and melt mixing [125]. Incorporation by solution mixing and by *in situ* polymerization resulted in better dispersion of graphene than that obtained by melt mixing. Moreover, graphene and its derivatives have been incorporated by solution mixing into polymer and biopolymer matrices such as PVA [86, 126, 127], PE [128], PS [88], PLA [89, 129] and PHBV [55, 130], among others. Similarly, graphene has also been incorporated by *in situ* polymerization into different polymer matrices such as polyamide-6 (PA6) [131], PE [132] and PLA [133]. However the use of *in situ* polymerization require monomer units and lots of reagents for the polymerization procedure, and this results in less applicable for the case of naturally existing polymers [92, 93]. Furthermore, to use solution mixing as strategy to incorporate graphene or graphene derivatives into polymer matrices, the common suitable solvents are water, acetone, chloroform, tetrahydrofuran, dimethylformamide and toluene, which cause the weak forces to stack the graphene layers together [92]. However, as previously mentioned, this method to develop nanocomposites requires large amounts of solvents, also leading to a critical issue related to the elimination of the solvents in the obtained materials through this route [92].

Conversely, melt mixing is the most attractive methodology for the development of polymer nanocomposites, as stated above, since it does not require the use of reagents neither solvents, it is a simple and industrially scalable, being, therefore of greater economic and environmental viability [79, 124]. However, using melt blending to obtain graphene nanocomposite generally results in a poorer dispersion than that obtained by the other routes. Nevertheless, melt mixing technique can be used as a post-treatment technique after a first incorporation of the filler into polymer matrices at high concentration, similar to that previously discussed for the case of CNW. Different studies have been reported using this strategy of incorporation [91, 134-136], where a initial step prior to melt mixing process was required to achieve good dispersion of graphene and/or graphene derivatives into the polymer matrix.

In addition to pre-incorporation strategies, graphene-based nanocomposites were also synthesized by ball milling since this high energy milling route induces delamination of

multilayered graphitic structures improving the final properties of the material [101]. Another advantage of this technology is that it does not require solvents and it is performed in one step. As previously reported, covalent bonds between polystyrene and graphene nanosheets were obtained using ball milling, thus demonstrating the mechano-chemical character of this technique [95]. Graphene incorporation into polyphenylene sulfide (PPS) by ball milling led to improvements in mechanical, electrical and barrier properties [137]. However this technology had not been used for the development of biopolymeric-based nanocomposites, work that has been developed during this thesis.

To summarize, it seems that the pre-incorporation of the nanofillers, either CNW or graphenes, using different technologies prior to melt mixing with polymer matrices is a good strategy to improve the final dispersion of these nanofillers, with special interest on the CNW as it increases its compatibility with non-polar hydrophobic matrices. However, while this strategy has proved efficient to improve the final properties of the materials, their use in biopolymer matrices was not extensively studied, especially when graphene or bacterial cellulose nanowhiskers (BCNW) were used as nanofillers, although a significant number of studies have been published in recent years, mostly on CNW incorporation into biopolymers. However, in many cases the effect that the incorporation of these nanofillers had on barrier properties of the obtained nanobiocomposites had not been extensively studied or reported and, as stated above, the barrier properties of the materials play an important role for food packaging applications.

Therefore, studies aimed at improving biopolymer matrices properties by incorporating nanofillers such as BCNW or graphenes using innovative, efficient technologies used at industrial scale which, in turn, ensure proper nanofiller dispersion into polymer matrices should be carried out. In addition, evaluation of the effect of the nanofiller incorporation on the final properties, especially on the barrier properties, should also be performed. This could result in biodegradable and renewable materials that can compete with more advantage in order to be used in food packaging applications.

Additionally, the development of technologies that involve a reduction of the organic solvents used during the nanofillers incorporation within polymeric matrices would be of interest because of the drawbacks associated with their use, being of particular interest in food packaging applications. It is worth to mention that for most of the studies detailed above, where nanofillers pre-incorporation prior to melt mixing was established as a good strategy reaching good nanoadditive dispersion, considerable amounts of organic solvents were required in this pre-incorporation step in order to disperse the nanoadditive. On the other hand, water is one of the best systems for incorporating graphene as nanofiller and it is the most appropriate medium to prepare CNW-based nanocomposites since CNW aqueous suspensions are much more stable than those in organic solvents. Therefore, incorporation or pre-incorporation methods compatible with aqueous media could be, in principle, more suitable in order to incorporate these nanofillers into polymeric matrices. The use of aqueous suspensions of cellulose has some advantages such as avoiding cellulose self-association, its high stability in this solvent and avoiding the necessity of additional treatments such as solvent exchange. Furthermore, development and optimization of systems incorporating these types of nanoreinforcements through free-solvent strategies where high yields in terms of dispersion can be achieved would also be interesting from an industrial point of view. All these aspects have been addressed throughout this thesis.

4. MASS TRANSPORT PROPERTIES

The transport of low molecular weight molecules through polymeric films is known as permeation. The driving force for the mass transport is the concentration gradient between the two environments separated by the polymeric film. The low molecular weight substances that pass through the film are known as permeant and the phenomenon is generally characterized by the permeability coefficient (P). The permeability mechanism involves several stages such as the ingress of the permeant into the polymer by an initial sorption process on the side of high concentration, its diffusion through the polymer and its desorption on the side of low concentration (cf. Figure 16). As a result, the permeability depends firstly on the initial solubility of the permeant molecules in the polymer matrix and, secondly, on its diffusion through the film. Therefore, in order to act on the permeability coefficient of any material the solubility and/or diffusion coefficients through the polymer matrix should be modified.

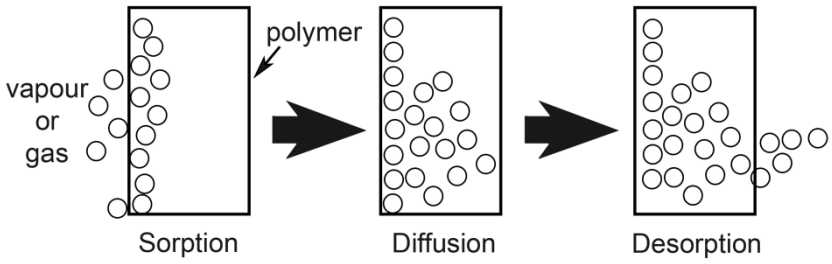

Figure 16. Permeability mechanism

Excess of moisture, oxygen and organic compounds can easily cause food spoilage affecting the product quality and shelf-life [109]. Chemical reactions, sensory or morphological changes in water sensitive products are just a few examples of the negative effects that mass transfer can cause. Furthermore, loss of food constituents, such as aroma losses or absorption of components from food by packaging materials, which are called sorption processes, can also cause dramatic changes in product quality.

Different mass transport phenomena can be observed in Figure 17 that can occur in the food/package/environment system. Thus, another transport phenomenon that can occur is the migration of elements from the packaging into the food, which is considered as a negative problem because many substances represent a danger to human health and/or modify the food composition thereby causing organoleptic changes and even lead to possible toxic effects [109]. Compounds that normally migrate from food packaging include residual monomers, processing additives and molecules that have been absorbed by the container during its previous use or during the recycling process. Therefore, migration has become a phenomenon of great importance in the development and implementation of laws for food packaging in many countries such as the European Regulation EU 1935/2004 on materials and articles intended to come into contact with food [138].

Nevertheless, the migration process can be used as controlled release agent of substances to the food, which are intentionally added to the packaging with the aim of being

released into the product in a controlled manner. This is used by the so-called active packaging.

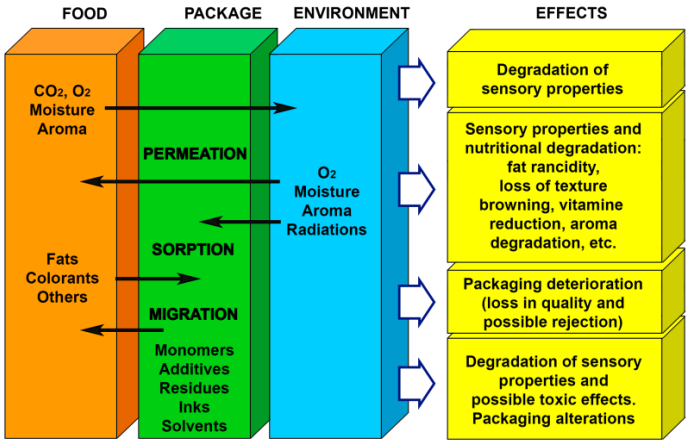

Figure 17. Mass transport phenomena and its effects on food products

4.1. Factors influencing mass transport properties

4.1.1. *Polymer*

The composition and chemical structure of the polymers is the basic and main defining factor determining barrier properties in polymeric materials, being related to a large extent, to the differences in the permeability of each type of polymer. Thus, by varying the chemistry of the macromolecule, often by just adjusting the pendant group along the polymer chain, a significant variation in barrier properties of up to six orders of magnitude can be achieved. As an example, the PP, where the pendant group along the polymer chain is the methyl group ($-CH_3$), has an oxygen permeability 15000 times higher than the PVOH, where the pendant group is the hydroxyl group (-OH) [139]. The following table shows some oxygen and water vapour permeability values of different polymers both conventional and biodegradable polymers.

Table 2. Water vapour and oxygen permeability of different polymers (adapted from Lagarón et al. [139]).

Material	P water (x 10^{18}) Kg m m^{-2} s Pa	P oxygen (x 10^{21}) m^3 m m^{-2} s Pa	
		0 % RH	80 % RH
EVOH	17000	0.77	91
PET	2300	135	
PP	726	6750	
LDPE	1200	21500	
PLA	12600	2250	2209
PHBV	6900	1590	3010
PCL	26600	4380	7850

It is considered that the transport of low molecular weight substances is carried out only through the amorphous phase of semicrystalline polymers, where intermolecular interactions are mainly produced by secondary forces such as Van der Waals forces or hydrogen bonding. Therefore, the chemical structure of the polymer influences intermolecular interactions, increasing or decreasing them, thus playing a determining role in the transport of low molecular weight compounds through the polymer. For example polymers with strongly self-interacting chemical groups, as polar groups (OH or CN), usually have low values of oxygen permeability at low relative humidity conditions, while polymers with apolar groups have poorer barrier properties. Furthermore, the chemical nature of the polymers also defines the affinity between a potential permeant and the polymer matrix. Low solubility of a permeant molecule in the polymer matrix due to low chemical affinity will result in low permeability.

There are two parameters closely related to the barrier properties of polymeric materials. On the one hand, the cohesive energy, which is a measure of the internal energy of a substance related to the strength of interaction between molecules and to the interaction changes that occur when different chemicals groups are added to the polymer chain. On the other hand, the free volume provides information related to the microcavities present in polymeric materials, which are used by the permeant molecules to diffuse through the polymer matrix. This parameter is also strongly related to the chemical nature of polymers since more voluminous groups leave larger free volume in the polymer material. In addition, the free volume is also related to the thermal history, glass transition temperature (T_g), crystallinity, etc.

Thus, for high barrier efficiency of polymers to vapour and gases, high cohesion energy as well as low free volume are required.

4.1.2. *Polymer morphology*

Many polymeric materials used for food packaging applications have a semicrystalline nature, and therefore they are heterogeneous materials from a structural point of view. In these cases, the polymers contain both a fraction of chain segments constituing highly packed and conformatinally ordered three-dimensional structures (polymer crystalline fraction) and another fraction in an amorphous state without conformational regularity and lateral order. As it is widely known polymer crystals are impermeable to the transport of most low molecular weigh substances. Then, it can be said that the polymer matrix is considered an amorphous structure filled with impermeable crystals. The size, orientation and shape of the crystals affects transport properties through the matrix. As the crystalline fraction increases, the crystals constrain the movement of the non-crystalline fraction, reducing their mobility, which becomes lower than the mobility in the amorphous regions not surrounded by crystals or the mobility of totally amorphous polymers [140]. A schematic model of these types of materials is depicted in Figure 18. In fact, it is widely known that an increase in the crystalline fraction of semicrystalline polymers is related to improved barrier properties mainly due to the tortuosity associated with the presence of crystalline domains [141-144].

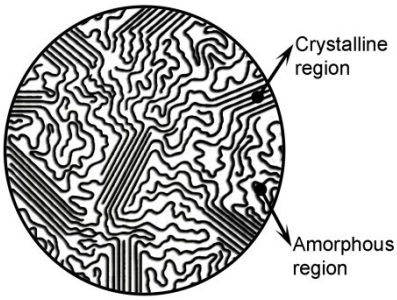

Figure 18. Semicrystalline polymers morphology

The crystalline fraction is affected by the thermal history of the polymer, i.e. it can be modified depending on the thermal processing conditions which can be optimized in order to improve the barrier properties of the polymeric material.

4.1.3. *Nanofillers and additives*

The incorporation of additives and nanofillers within polymeric matrices can have an effect on the barrier properties. This effect depends, among other things, on the nature of the nanofiller, degree of adhesion and compatibility with the polymer. The addition of impermeable nanofillers to polymer matrices usually leads, among other changes, to a decrease in the diffusion coefficient, which is due to the increased tortuosity of the pathway required for the permeant to pass through the polymer [145], as shown in Figure 19.

In the case of laminar structured nanofillers, in order to achieve an optimum improvement of the barrier properties of the material, in addition to a good dispersion, it is considered that they must be oriented perpendicularly to the direction of transport. Furthermore, the introduction of such fillers within the amorphous region, generally may lead to similar effects to that obtained by the presence of crystals, i.e. reduced chain mobility.

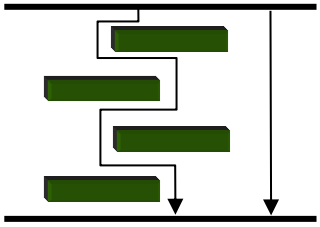

Figure 19. Tortuosity effect imposed to the transport of low molecular weight components by addition of nanofillers.

However, when the nanofillers are of hydrophilic nature, the amount of absorbed water and other polar compounds increase, thus impacting on the transport properties of certain permeants. On the other hand, when the affinity between the polymer and the reinforcement is not good, an increase of the free volume of the resulting material will take place. In both cases a reduction in the barrier properties of the polymer occurs.

4.1.4. *Temperature*

It is well known that temperature affects many properties of polymers. Changes in the barrier properties induced by temperature have an exponential character since the diffusion and solubility coefficients, which are the two main parameters affecting the permeability, exponentially increase with temperature according to Arrhenius law (equation 1) and Van't Hoff's law (equation 2) respectively, since both the activation energy (E_D) or the solution enthalpy (ΔH_S) are always positive values.

$$D = D_0 \exp\left(\frac{-E_D}{RT}\right) \quad \text{Equation 1}$$

$$S = S_0 \exp\left(\frac{-\Delta H_S}{RT}\right) \quad \text{Equation 2}$$

This phenomenon is related to the increased mobility of the polymer chains at higher temperatures, which reduces the necessary energy of permeant molecules to jump from one position to another, also leading to an increase in the free volume of the polymer.

Temperature also affects the physical state of the polymer, directly affecting the transport properties. In a molten polymer, the crystalline regions disappear and transport takes place throughout the whole matrix, which behaves like a liquid. In this case, the whole volume of the polymer is available for the permeant molecules, increasing their solubility. Furthermore, the crystals blocking effect disappears, reducing the tortuosity and making easier the diffusion, as the polymer chains are in constant motion, thus facilitating the mobility of permeant molecules.

Changes associated with the glass transition, i.e. with the transition of the polymer from glassy to rubbery state occur as a result of relaxation or increased mobility of chain segments in the amorphous phase of the polymer. Above the glass transition temperature, the amorphous phase of the polymer is in the rubbery state, and below this temperature is in the glassy state. In the rubbery state, the relaxation times are shorter and, after absorption of the permeant molecules, a new steady state is reached faster. As a result, the diffusion is faster when the polymer is in this state.

4.1.5. *The permeant*

The characteristics of the permeant molecules, such as molecular size, shape and chemical nature, affect their transport properties. Increasing molecular size of the permeant molecules reduces their diffusion coefficients and solubility, mainly due to steric reasons. Regarding the shapes of the permeant molecules, flattened or elongated molecules diffuse faster through the polymer than spherical molecules with the same molecular volume [146].

Compatibility between the permeant and the polymer matrix also affects their transport properties. If the affinity between the permeant and the polymer is very high, it can sometimes cause plasticization of the polymer. In this case, the permeant sorption leads to a

decrease in the association of adjacent polymer chains in the amorphous region, i.e., initial hydrogen bonds and Van der Waals forces are replaced by polymer-sorbate interactions, increasing chain mobility and free volume, reducing the T_g and increasing the diffusion and solubility coefficients of the permeants.

Packaged foods are complex systems where the packaging material is in direct contact with different permeant molecules. In these cases two situations where transport properties can be affected occur:

a) The transport properties of one permeant are often affected by the presence of other permeants since they compete for the gaps within the polymeric matrix to diffuse through.

b) Some permeant molecules, once absorbed, act as co-solvents for the rest of permeants. For example, water is the main constituent of many foodstuffs and frequently acts as co-solvent. In hydrophilic polymers such as EVOH copolymers, water-induced plasticization at high humidity levels has been reported to increase the permeability to hydrophobic and apolar compounds such as limonene and oxygen, therefore negatively affecting the barrier properties of the material [147, 148].

5. LEGISLATION IN THE FOOD PACKAGING FRAMEWORK.

According to the Spanish Agency for Consumer Affairs, Food Safety and Nutrition (AECOSAN), materials and articles in contact with food include those that are:

- Intended to come into contact with food,
- already in contact with food and intended for this purpose,
- those which may reasonably be expected to be brought into contact with food or to transfer their constituents to food under normal or foreseeable conditions of use.

When we refer to these materials, we mean: adhesives, ceramics, cork, rubbers, glass, ion-exchange resins, metals and alloys, paper and board, plastics, printing inks, regenerated cellulose, silicones, textiles, varnishes and coatings, waxes, wood and active and intelligent materials and articles.

Materials in contact with food are regulated throughout the European Union by Regulation (EU) No 1935/2004, of 27 October 2004, of the European Parliament and of the Council, on materials and articles intended to come into contact with food and repealing Directives 80/590/EEC and 89/109/EEC, in order to guarantee that all materials used in the Community comply with the same quality requirements [138].

All the materials and articles intended to come into contact with foods must be manufactured in accordance with Good Manufacturing Practice, listed in Commission Regulation (EU) No 2023/2006, of 22 December 2006, on good manufacturing practice for materials and articles intended to come into contact with food [149], so that, in normal and foreseeable conditions of use, these do not transfer their constituents to food in quantities which may:

- Represent a risk for human health
- Provoke an unacceptable modification to the composition of food, or
- Provoke a change in the organoleptic characteristics thereof.

Apart from these two regulations, for some materials there is specific harmonised legislation which, based on Regulation 1935/2004, defines the special requirements of the same. Among the materials regulated by specific provisions, plastics materials are regulated by Commission Regulation (EU) No 10/2011 [150].

All plastic materials which are marketed in the European Union should comply, in addition to the specific regulations (Regulation (EU) No 10/2011), with that established in the Framework Regulation (EU) No 1935/2004 which lists the general requirements to be met by materials and articles intended to come into contact with food.

Only authorised substances may be used in the manufacture of plastic layers of materials and plastic articles. These substances are included in a positive community list, established in Annex I of Regulation (EU) No 10/2011 and consisting of: monomers or starting substances, additives (excluding colorants), production aids (except solvents) and macromolecules obtained from microbial fermentation.

Plastic materials and articles must not release their constituents to the food in quantities higher than those established. Therefore, specific migration limits are established for certain substances, and global migration limits, together with migration tests to verify the compliance of the material.

A new Commission Regulation (EU) No 2015/174 [151] has been recently published amending and correcting Regulation (EU) No 10/2011 on plastic materials and articles intended to come into contact with food. In this new Commission Regulation new substances that have a positive opinion from the European Food Safety Authority (EFSA) have been included along with the amendment and correction of restrictions for certain substances already present in the Regulation Annex.

Annex I to Commission Regulation (EU) No 10/2011 (2) establishes as approved materials to come into contact with food lactic acid as monomer (substance number 99) as well as PHBV (substance number 744).

Commission Regulation (EU) No 10/2011 includes the information related to new technologies containing engineered substances with particle sizes that exhibit chemical and physical properties that significantly differ from those at a larger scale, for example, nanoparticles. These different properties may lead to different toxicological properties and, therefore, materials containing nanoparticles should be assessed on a case-by-case basis by the Authority in regards to their risk until more information is known about such new technology. Therefore, it should be made clear that authorisations which are based on the risk assessment of the conventional particle size of a substance do not cover engineered nanoparticles. In fact, a guide has been developed by the EFSA for evaluation of the potential risks arising from food applications of nanoscience and nanotechnology [152].

Therefore, although graphite and cellulose are listed as materials allowed to come into contact with food (substances numbers 521 and 553 respectively), their nanostructured derivatives should be evaluated by the competent authority before they come into contact with food.

1. INTRODUCCIÓN AL ENVASADO ALIMENTARIO

El ritmo de vida actual así como la preocupación por alimentarnos de forma sana han influido en los últimos años de forma directa en nuestros hábitos alimentarios y en el tiempo que se dedica en los hogares a cocinar [1]. En este contexto, los consumidores actualmente demandan alimentos cuyo tiempo de cocinado o preparación sea el menor posible, con un incremento en la vida útil y, por supuesto, con calidad y seguridad garantizada, así como con menos conservantes o aditivos.

La evolución en dichos hábitos se ve también reflejada en los envases, los cuales han sido tradicionalmente creados como meros contenedores para los alimentos. Sin embargo, hoy día, movidos por estas nuevas tendencias de consumo, los envases han adquirido otra serie de funciones, pasando de ser un mero continente a ser un elemento activo en la conservación, distribución y el marketing de los alimentos, convirtiéndose en lo que se denomina la 5ª "P" (del inglés "packaging") que determina la venta de los productos, junto con el producto en sí (Product), precio (Price), lugar de venta (Place) y oferta (Promotion) [2].

Los alimentos están constantemente sometidos al ataque de agentes externos como el calor, la luz, la presencia o ausencia de humedad, oxígeno, microorganismos, insectos, suciedad y partículas de polvo, emisiones gaseosas, etc. Todos estos factores provocan el deterioro de los alimentos. De ahí que en ocasiones, los envases sean considerados mucho más importantes o costosos que el propio producto que contienen. Por ello, de entre todas las funciones de los envases, que se podrían resumir de manera básica en: contener, proteger, comunicar y/o informar, y conveniencia de uso, destacan por su importancia la protección y conservación de su contenido frente al ataque estos agentes. Esta función engloba entre otras cosas el retraso del deterioro, la extensión de vida útil y el mantenimiento de la calidad y la seguridad de los alimentos envasados mediante el mantenimiento de unas condiciones que minimicen las alteraciones químicas, bioquímicas y microbiológicas.

Grandes esfuerzos están focalizados en el desarrollo de tecnologías de envasado que garanticen la frescura de los alimentos y su seguridad, que faciliten la preparación de alimentos listos para su consumo, así como aumenten el tiempo de vida útil de los productos mediante el uso de tecnologías implementadas a tal fin, teniendo además un diseño que resulte atractivo.

Así, durante las últimas décadas se han añadido a los envases funciones más novedosas. Encontramos en el mercado ensaladas listas para consumir mediante el uso de atmósferas modificadas o platos precocinados que sólo requieren un calentamiento en el microondas, para lo cual el envase ya viene perfectamente preparado.

Un envase ideal además debe tener una buena resistencia mecánica y a la vez ser ligero para facilitar su manejo a lo largo de la cadena de distribución, debe ser suficientemente barato para conseguir un producto competitivo y, por supuesto, seguro para el consumidor.

Por lo tanto, la investigación en el área de envasado alimentario está dirigida hacia la selección y desarrollo de materiales de envasado y métodos adecuados de fabricación que permitan reducir al mínimo las pérdidas de nutrientes y proporcionar alimentos seguros y

saludables. En este marco, distintos desarrollos se han llevado a cabo, englobando tecnologías de envases activos e inteligentes que proporcionan un aumento de la vida útil y monitorizan parámetros relacionados con la calidad de los alimentos. Además, en la actualidad hay también un creciente interés en el desarrollo de tecnologías orientadas a minimizar los problemas medioambientales relacionados con el uso de recursos fósiles para la síntesis de materiales de envasado así como con la gestión de los residuos generados a partir de los envases de alimentos tradicionalmente utilizados. Por ello hay un interés general en el desarrollo y uso de materiales para envasado más respetuosos con el medio ambiente.

2. MATERIALES DE ENVASADO ALIMETARIO

Existe una amplia variedad de materiales tradicionalmente utilizados en la tecnología de envasado de alimentos, como metales, papel y cartón, cristal y cerámica así como sus combinaciones. Sin embargo, hoy día los plásticos o materiales poliméricos y el papel representan los dos materiales principales en envasado alimentario. En particular los plásticos o materiales poliméricos presentan una serie de ventajas respecto al resto de materiales de envasado como la versatilidad de sus métodos de procesado y composiciones, así como su relación calidad/precio. Además, el uso de polímeros para producir envases de alimentos presenta otras ventajas tales como su ligereza, coste y su capacidad para ser termosellados o modificados (bien químicamente o mediante mezclas con otros materiales) con el fin de adaptar sus propiedades. De hecho, la versatilidad de los polímeros permite la obtención de una amplia gama de productos, desde estructuras muy flexibles (como bolsas o envoltorios) hasta estructuras más rígidas (botellas o tapones) pudiéndose modificar sus propiedades para diferentes aplicaciones. Las propiedades ópticas de los envases (brillo y transparencia) también se pueden adaptar a las necesidades específicas de cada producto. Los envases transparentes permiten que el consumidor pueda ver el producto, provocando ello cierta atracción e impresión, aunque también se pueden añadir filtros o pigmentos para generar envases opacos y proteger el producto de la luz, o de algunas radiaciones. Muchos polímeros se pueden imprimir, lo que hace posible su uso como un medio de información al consumidor, para identificar la marca o para agregar un diseño atractivo. Además, los envases poliméricos pueden ser producidos como parte de procesos integrados en las líneas de producción industrial, donde son formados, llenados y cerrados en la misma línea de producción, haciendo el proceso rápido y barato, pudiéndose también crear en un número ilimitado de tamaños y formas.

Esta versatilidad que permite el diseño de envases poliméricos que se ajusten a los requerimientos de casi todo tipo de alimentos, ha provocado que sólo aspectos sociales y medioambientales o bien factores económicos justifiquen el uso de envases no poliméricos, siendo por tanto el uso de este tipo de envases y embalajes extremadamente elevado. De hecho, según datos del Centro Español de Plásticos, el consumo de plásticos se estima en 330 millones de toneladas para el presente año, con una mayor contribución en el sector del envase y embalaje, al que se destinará aproximadamente el 40%, como puede observarse en la Figura 1 donde se muestra el consumo mundial de plásticos estimado para el año 2015 segmentado por áreas así como el consumo en 2010 segmentado por mercados.

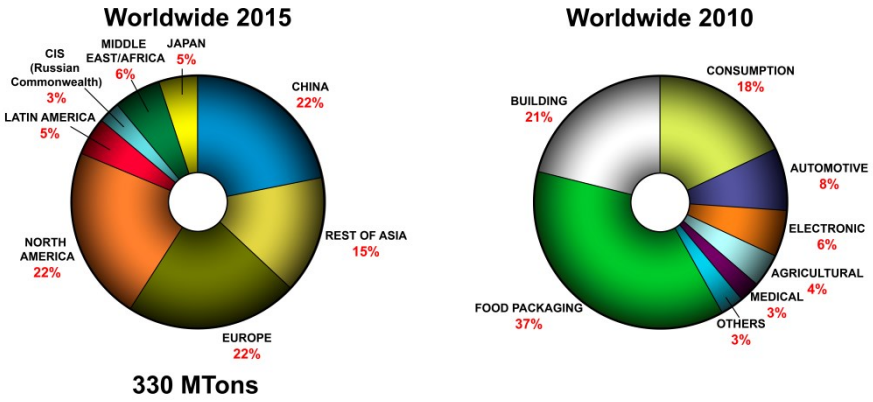

Figura 1. Estimación del consumo global de plásticos para el año 2015 y consumo por sectores en el año 2010 (Fuente: Centro Español de Plásticos - CEP)

Uno de los principales inconvenientes de los materiales plásticos utilizados para envasado de alimentos es que son permeables al transporte de compuestos de bajo peso molecular, teniendo por tanto unas propiedades barreras limitadas. Esto provoca diferentes fenómenos de transporte de masa en lo que se conoce como sistema ternario "alimento/envase/entorno", como se verá posteriormente, lo cual limita el uso de los polímeros para ciertas aplicaciones en las que se requiere una elevada barrera a oxígeno o humedad, factores que son determinantes en el deterioro de los alimentos. Para resolver esos problemas polímeros de alta barrera así como sistemas multicapas se han desarrollado. Además, en las últimas décadas, una alternativa al desarrollo de materiales de alta barrera en sistemas monocapa la representa el desarrollo de materiales nanocompuestos mediante la incorporación de aditivos nanoestructurados en matrices poliméricas para modificar sus propiedades, tal y como se discutirá posteriormente.

El otro gran inconveniente, que deriva del consumo tan elevado de materiales plásticos, es el daño medioambiental asociado a la lenta degradación de los polímeros más comúnmente utilizados, siendo la mayoría de ellos materiales derivados del petróleo. Debido a ello, la legislación impone medidas cada vez más estrictas para mejorar la eficiencia de los materiales y reducir el impacto de los residuos de envases sobre el medio ambiente (por ejemplo la Directiva 94/62/CE del Parlamento Europeo relativa a los envases y residuos de envases). Aunque la estabilidad de los envases durante la vida útil del producto es una ventaja, se convierte en una desventaja debido a que raramente son reutilizados o reciclados, generando de esta forma grandes volúmenes de residuos. Además, la reutilización o el reciclaje no son métodos totalmente adecuados para gestionar todos los envases, especialmente los materiales de envasado de alimentos, ya que con frecuencia están formados por varios materiales diferentes (bien mezclas de plásticos o sistemas multicapas) para lograr unas propiedades óptimas en términos de barrera a gases o propiedades mecánicas. Ello da lugar a una de las limitaciones intrínsecas en la eficiencia de la separación previa al reciclaje, generando problemas de clasificación así como pérdidas en las propiedades físicas finales de los materiales reciclados [3]. Costes significativos también son destinados a la limpieza y descontaminación de los envases plásticos debido a la contaminación de los productos alimenticios en ellos. La Tabla 1 representa la cantidad de

materiales de envasado de alimentos en residuos sólidos urbanos generados, recuperados y desechados en el año 2011 en Estados Unidos.

Tabla 1. Generación, recuperación y desecho de materiales en Residuos Sólidos Urbanos en 2011 (EE.UU.). (En millones de toneladas y porcentajes de generación de cada material) (Fuente: United States Environmental Protection Agency)

Material	Weight Generated	Weight Recovered	Recovery As a Percent of Generation	Weight Discarded
Paper and paperboard	70.02	45.90	65.6%	24.12
Glass	11.47	3.17	27.6%	8.30
Metals				
Steel	16.52	5.45	33.0%	11.07
Aluminium	3.47	0.72	20.7%	2.75
Other nonferreous metals	1.96	1.34	68.4%	0.62
Total metals	21.95	7.51	34.2%	14.44
Plastics	31.84	2.65	8.3%	29.19
Rubber and leather	7.49	1.31	17.5%	6.18
Textiles	13.09	2.00	15.3%	11.09
Wood	16.08	2.38	14.8%	13.70
Other materials	4.59	1.28	27.9%	3.31
Total Materials in Products	***176.53***	***66.20***	***37.5%***	***110.33***
Other Wastes				
Food Other	36.31	1.40	3.9%	34.91
Yard trimmings	33.71	19.30	57.3%	14.41
Miscellaneous inorganic wastes	3.87	Negligible	Negligible	3.87
Total Other Wastes	*73.89*	*20.70*	*28.0%*	*53.19*
TOTAL MUNICIPAL SOLID WASTE	***250.42***	***86.90***	***34.7%***	***163.52***

Negligible = Less than 5000 tons or 0.05%

Como puede observarse, los residuos plásticos ocupan el segundo lugar en cuanto a generación de residuos, por detrás del papel y cartón, pero tienen el nivel más bajo de recuperación con un 8.3% de la cantidad total de residuo generada. Además la Figura 2 representa, en millones de toneladas, la generación y recuperación de plásticos en residuos sólidos urbanos entre 1960 y 2011 en Estados Unidos. Existe claramente una gran descompensación entre la evolución de los residuos de materiales plásticos generados y su recuperación durante dicho periodo.

Con todo ello, y aun con el desarrollo, creación y mejora de sistemas de reciclaje en muchos de los países desarrollados, se piensa que la solución de este problema medioambiental solo llegará con la introducción en la industria de polímeros biodegradables que sustituyan al menos parcialmente a los plásticos derivados del petróleo y que además, puedan obtenerse de fuentes renovables [4]. Con ello se abordarían los dos principales inconvenientes que generan los envases plásticos hacia el medioambiente: por un lado conseguir envases biodegradables comerciales y por otro el conseguir mediante recursos renovables desarrollar materiales para envasado de alimentos con buenas propiedades que aseguren y garanticen, entre otras cosas, la calidad y seguridad de los alimentos.

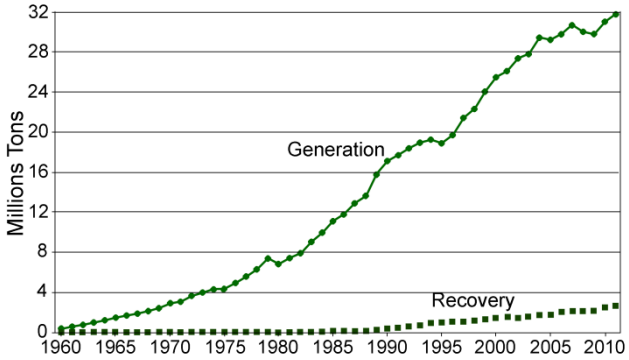

Figura 2. Generación y recuperación de materiales plásticos entre 1960 y 2011 en EE.UU. (Fuente: United Status Environmental Protection Agency)

2.1. Polímeros Biodegradables

Tal y como ya se ha comentado, existe una problemática general a nivel mundial derivada de la gestión de residuos a causa del elevado consumo de plásticos. Además, desde el punto de vista económico, según González García et al. [5], actualmente se destina un 5% del petróleo disponible mundialmente para fabricar 200 millones de toneladas de plásticos al año. Se estima que para el 2100 habrá una demanda de 2000 millones de toneladas al año lo que supone un gasto del 50% del petróleo mundial. Ello provocará un incremento drástico en el precio de los plásticos producidos a partir de recursos fósiles.

Así, desde el punto de vista del envasado de alimentos, grandes esfuerzos han de ser focalizados a la hora de extender la vida útil y mejorar la calidad de los alimentos mientras se reducen los residuos plásticos que se generan y por tanto su impacto ambiental. Debido a ello hay un creciente interés tanto a nivel de investigación como en el ámbito industrial en el desarrollo y aplicación de "bioplásticos". Los bioplásticos, también llamados biopolímeros, engloban tanto polímeros procedentes de recursos renovables, como plantas y microorganismos, así como polímeros biodegradables procedentes o no de recursos renovables [6]. En la Figura 3 puede observarse la capacidad de producción de bioplásticos a nivel mundial segmentada por mercados para el año 2013 y su estimación para el año 2018. Se observa claramente un crecimiento de la capacidad de producción con un incremento más notable en el sector del envasado.

Según ASTM D996-04 el término "biodegradable" se define como capaz de descomponerse en dióxido de carbono, metano, agua, compuestos inorgánicos o biomasa donde el mecanismo predominante es la acción enzimática de microorganismos [7]. Este tipo de degradación debe ser diferenciada de otros procesos de degradación como la fotodegradación o la degradación química o térmica. Así polímeros biodegradables son aquellos materiales poliméricos en los que al menos una etapa en su proceso de degradación es a través del metabolismo en presencia de organismos naturales, los cuales en condiciones apropiadas son capaces de desintegrarlos produciendo residuos no tóxicos ni perjudiciales para el medioambiente [8]. Sin embargo, como los envases convencionales, los envases a base de bioplásticos deben cumplir una serie de criterios importantes, incluyendo envasado

y protección del alimento manteniendo su calidad sensorial y su seguridad así como ofrecer información al consumidor. No obstante, como se indicará más adelante, estos materiales tienen peores propiedades que los materiales producidos por vía petroquímica limitando su uso industrial. El desarrollo de tecnologías que permitan mejorar esas propiedades es uno de los temas principales en el desarrollo de envases a base de bioplásticos, hacia lo cual el presente trabajo está orientado.

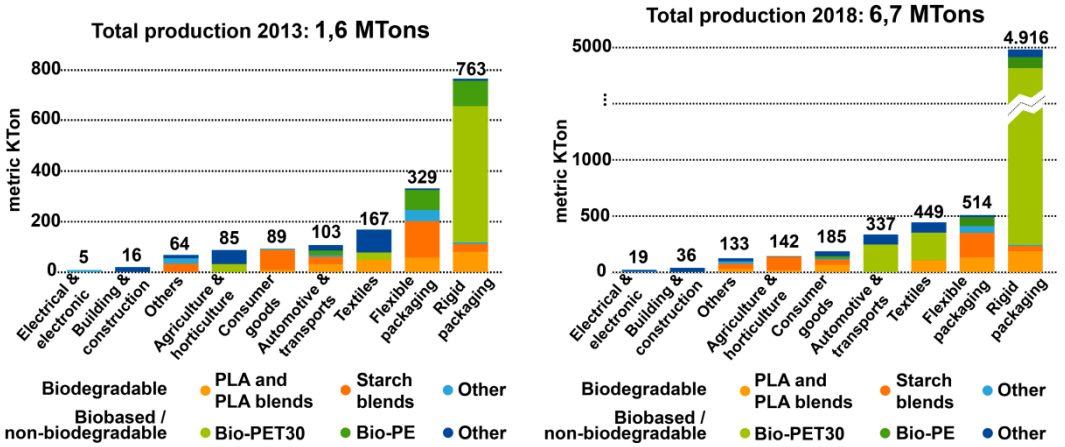

Figura 3. Capacidad de producción de bioplásticos a nivel mundial para los años 2013 y 2018 (Fuente: European Bioplastics, Institute for Bioplastics and Biocomposites, Nova-Institute (2014). Más información: www.bio-based.eu/markets and www.downloads.ifbb-hannover.de)

Entre los materiales biodegradables, se suelen considerar tres grupos principales [9]:

a) El primer grupo incluye polímeros extraídos directamente de la biomasa, como los polisacáridos (quitosano, carragenatos, almidón, celulosa, etc.) y las proteínas (como el gluten, la soja, la gelatina y la zeína).

b) Una segunda familia hace uso de monómeros derivados del petróleo o bien derivados de la biomasa pero utilizan las rutas clásicas de síntesis química para obtener el polímero biodegradable final. Este es el caso de la policaprolactona (PCL), el alcohol polivinílico (PVOH o PVA) y su copolímeros (EVOH), como derivados del petróleo, y del ácido poliláctico (PLA), como derivado de la biomasa.

c) La tercera familia hace uso de polímeros producidos por microorganismos naturales o genéticamente modificados como, por ejemplo, los polihidroxialcanoatos (PHAs), principalmente polihidroxibutirato (PHB) y sus copolímeros con hidroxivalerato (PHBV), o la celulosa bacteriana.

De entre los biopolímeros termoplásticos más ampliamente estudiados en los últimos años, algunos biopoliésteres como los PHAs y el PLA han suscitado especial interés debido a que estos materiales están comercialmente disponibles, produciéndose a escala industrial, se pueden procesar mediante equipos convencionales y presentan unas propiedades relativamente buenas para un gran número de aplicaciones, tales como aplicaciones biomédicas o para envasado de alimentos, para las cuales ya han sido ampliamente estudiados [10-13]. La Figura 4 representa la capacidad de producción de bioplásticos a nivel mundial para el año 2013 en función del tipo de material. Se puede observar la contribución tanto del PLA como de los PHAs como polímeros biodegradables.

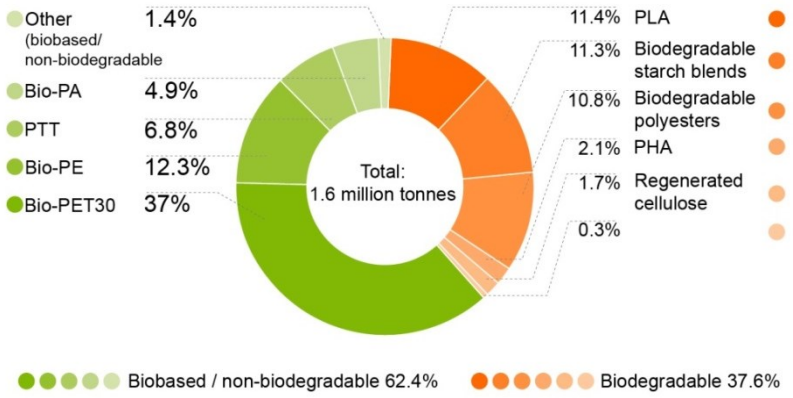

Figura 4. Capacidad de producción de bioplásticos a nivel mundial para el año 2013 en función del tipo de material (Fuente: European Bioplastics, Institute for Bioplastics and Biocomposites, Nova-Institute (2014). Más información: www.bio-based.eu/markets and www.downloads.ifbb-hannover.de)

2.1.1. *Ácido Poliláctico (PLA)*

El ácido poliláctico, poli (ácido láctico) o polilactida (PLA) es un poliéster alifático procedente de recursos renovables tales como el almidón de maíz, el azúcar de remolacha, el azúcar de caña, las patatas y otros tipos de biomasa, siendo uno de los bioplásticos que están en continuo desarrollo comercial hoy día [14], siendo el polímero procedente de recursos naturales más utilizado y producido a gran escala, con alrededor de 140.000 toneladas por año [15]. Debido a su versatilidad, el PLA está encontrando aplicaciones en diversas áreas (ver Figura 5) como en el área biomédica donde es uno de los materiales innovadores utilizados en implantes reabsorbibles de larga duración. Además su uso también ha aumentado en aplicaciones de la industria textil y del envasado. Principalmente en esta última esta despertando mucho interés por sus excepcionales características como su excelente transparencia, buena procesabilidad, sus propiedades mecánicas, comparables a las del polietilentereftalato (PET) [16] y al polietileno (PE) [17] y a su relativamente buena barrera al agua. La permeabilidad al vapor de agua del PLA es, por ejemplo, mucho más baja que la del almidón [18], pero sigue siendo mayor que la de poliolefinas convencionales como el polietileno (PE) de alta y baja densidad (HDPE y LDPE), el polipropileno (PP) o el polietilentereftalato (PET). Sin embargo, presenta baja barrera a gases así como elevada fragilidad, lo cual presenta un obstáculo para su uso en determinadas aplicaciones como envasado de alimentos [19]. Sus propiedades mecánicas se pueden mejorar mediante adición de plastificantes [20, 21] pero éstos también conducen a una disminución de la barrera a oxígeno y de la transparencia. Por lo tanto, los principales inconvenientes de este biopolímero se asocian a una baja resistencia térmica, excesiva fragilidad y una insuficiente barrera al oxígeno y al agua en comparación con otros polímeros de referencia para el envasado de alimentos como el PET. Es, por tanto, de gran interés industrial mejorar las propiedades barreras de este material debido a sus características renovables y sostenible con el medio ambiente, manteniendo sus propiedades intrínsecamente buenas, como la transparencia y la biodegradabilidad [22].

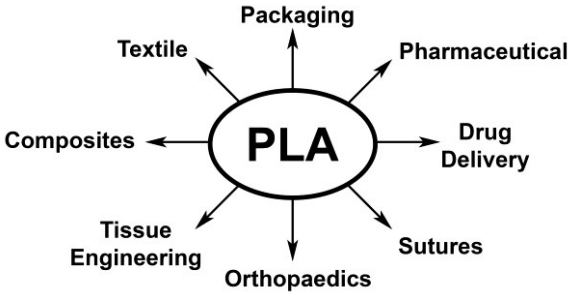

Figura 5. Aplicaciones del PLA (adaptada de Gupta & Kumar [23])

2.1.1.1. Síntesis de PLA

El punto de partida para la obtención del PLA es el ácido láctico (LA). Existen dos procesos básicos de obtención de LA basados en rutas químicas o biotecnológicas. Actualmente, la ruta biotecnológica produce más del 95% del consumo mundial de LA y consiste en la fermentación de carbohidratos usando diversos microorganismos. Por el contrario, para la obtención de PLA a partir de ácido láctico, se emplean rutas químicas. Existen tres de rutas de síntesis estando resumidas en la Figura 6 [24]: la polimerización por condensación directa del ácido láctico también llamada policondensación, la condensación azeotrópica y la polimerización por apertura de anillo (ROP de sus siglas en inglés Ring-Opening Polimerization).

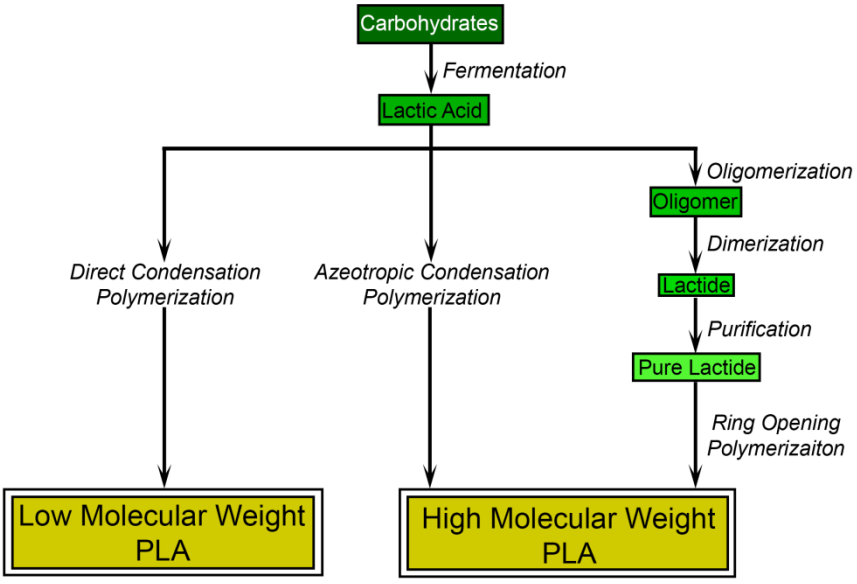

Figura 6. Varias rutas de síntesis de PLA (adaptada de Gupta & Kumar [23])

2.1.1.1.1. Policondensación

La polimerización por condensación o policondensación se da a través de una reacción de equilibrio donde los componentes iniciales (monómeros) se unen entre sí mediante reacción química de sus grupos reactivos con el desprendimiento de una molécula de agua por cada monómero (molécula de ácido láctico) añadido a la cadena. El procedimiento está esquematizado en la Figura 7.

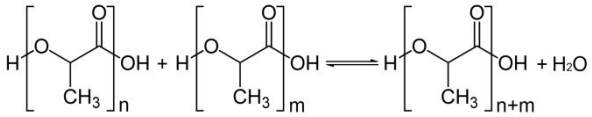

Figura 7. Reacción de condensación

El proceso de policondensación del ácido láctico involucra, además de la propia reacción de condensación, otra reacción en equilibrio, la reacción de depolimerización hacia la formación de la lactida, que es un dímero cíclico del ácido láctico [25] (ver figura 8).

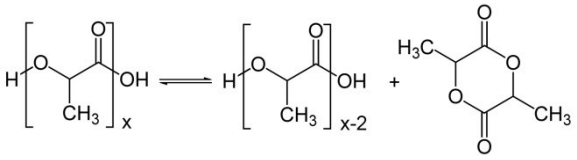

Figura 8. Reacción de depolimerización del PLA con formación de lactida

Aunque es el procedimiento más simple y barato de todos, el principal inconveniente de este tipo de reacción es el bajo peso molecular del polímero obtenido. Ello se debe, por un lado, a la elevada viscosidad del polímero fundido que a su vez dificulta la extracción del agua desde el medio de reacción para así poder desplazar el equilibrio hacia la producción de polímero, y por otro, a la reacción de equilibrio no deseada que provoca la depolimerización. De hecho, bajo condiciones típicas de reacción a elevada temperatura y elevado vacío para promover la policondensación deshidratativa, la evaporación de la lactida también es favorecida lo cual induce a la depolimerización [25]. Otro de los inconvenientes de este procedimiento es que el polímero obtenido es frágil, vidrioso y básicamente es inutilizable para muchas aplicaciones a no ser que se utilicen agentes extensores o coadyuvantes para incrementar el peso molecular del polímero. Además, durante la reacción puede aparecer un aumento de la coloración así como racemización.

2.1.1.1.2. Polimerización por condensación azeotrópica

En la condensación azeotrópica están presentes las mismas etapas que en la condensación directa del ácido láctico aunque con la diferencia que en este procedimiento el monómero es polimerizado en disolución, donde junto con el catalizador son deshidratados utilizando reflujo a alta ebullición. Ello facilita la extracción del agua producida durante la reacción debido a una disminución de la viscosidad del medio, obteniéndose de esa forma un

PLA de mayor peso molecular. La elección del disolvente, el cual debe ser aprótico y, más concretamente, su temperatura de ebullición, representan una restricción sobre la temperatura de policondensación que puede ser usada. El agua producida durante la reacción debe ser eliminada del disolvente mediante el uso de un agente desecante (un tamiz molecular por ejemplo). De forma alternativa se puede añadir disolvente limpio y seco durante la reacción aunque es indeseable desde los puntos de vista económico y medioambiental [26, 27]. Varias patentes procedentes de Mitsui Toatsu Chemicals se han desarrollado acerca de la deshidratación azeotrópica de PLA. Diferentes alegaciones sobre diversos factores que afectan a las propiedades del polímero final como el secado del disolvente y su posterior adición al medio de reacción, la utilización de diferentes agentes desecantes así como la utilización de diferentes disolventes aparecen en ellas, llegándose a obtener PLA con un peso molecular superior a 300.000 g mol^{-1} [28, 29, 30, 31].

Aunque a través de este tipo de polimerización se puede obtener polímero de alto peso molecular sin emplear agentes extensores o coadyuvantes, esta ruta de obtención tiene ciertos inconvenientes como el uso de disolventes orgánicos así como considerables cantidades de impurezas de catalizador en el producto final. Este catalizador residual puede causar problemas durante el posterior procesado, como reacciones de degradación o hidrólisis incontroladas o, en el caso de aplicaciones médicas, junto con el uso de disolventes, toxicidad y otras propiedades no deseadas [26].

2.1.1.1.3. Polimerización por apertura de anillo (ROP)

En la polimerización por apertura de anillo se utiliza como monómero el dímero cíclico del ácido láctico, la lactida. Este dímero del ácido láctico es obtenido por craqueo térmico de PLA de bajo peso molecular (oligómeros) obtenido previamente mediante policondensación. La lactida posee grupos funcionales que son susceptibles al ataque nucleofílico o electrofílico por parte de aniones o cationes, los cuales actuarán como iniciadores y propiciarán la apertura del anillo. A partir de dicha apertura se genera la propagación de la cadena polimérica obteniéndose así el PLA. El proceso de reacción está reflejado en la Figura 9

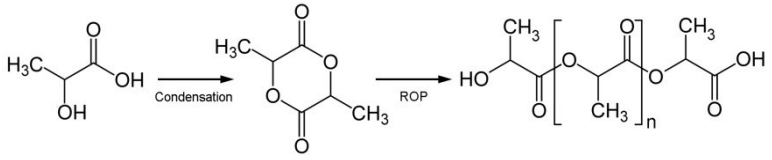

Figura 9. Reacción por apertura de anillo (ROP)

Existen diferentes mecanismos de reacción y tipos de iniciadores para la polimerización por apertura de anillo de la lactida: polimerización catiónica, polimerización aniónica, mecanismo de coordinación-inserción y polimerización enzimática [32, 23]. Entre ellos, el mecanismo de coordinación-inserción presenta un mayor número de ventajas como el control del peso molecular, la obtención de mayores grados de polimerización, la menor probabilidad de reacciones laterales que en el caso de iniciadores iónicos y la limitada racemización [32, 33]. En este mecanismo, la lactida actúa temporalmente como un ligando

de coordinación con el catalizador, normalmente un alcóxido metálico. Aunque un gran número de catalizadores han sido estudiados, el más utilizado para este tipo de reacción es el bis(2-etilhexanoato) de estaño (II), comúnmente conocido como octoato de estaño (usualmente abreviado SnOct2) [32, 23].

Este método de polimerización es la mejor ruta para la síntesis de PLA de alto peso molecular. La reacción se puede controlar fácilmente, pudiendo variar así las características del polímero resultante de una manera más controlada. Además existe un alto control sobre la estereoquímica del producto final, lo que permite ampliar su campo de aplicación. Esta reacción presenta otras ventajas como el empleo de condiciones de reacción moderadas, bajos tiempos de reacción, control de la longitud de cadena y la baja existencia de reacciones laterales.

Aunque en la literatura existe ambigüedad, normalmente el polímero obtenido a partir de la lactida se denomina polilactida y el obtenido del ácido láctico, ácido poliláctico o poli(ácido láctico). A lo largo de este trabajo se utilizarán ambos nombres indistintamente.

2.1.1.2. Propiedades del PLA

Las propiedades del PLA dependen en gran medida de la estereoquímica de la cadena polimérica, la cual está relacionada directamente con la relación entre los enantiómeros de partida. Ya que el ácido láctico se puede encontrar en forma de dos enantiómeros diferentes, D-ácido láctico y L-ácido láctico, la producción del dímero cíclico puede resultar en cuatro formas potenciales: la D,D-lactida (denominada D-lactida), L,L-Lactida (denominada L-lactida) y L,D- o D,L-lactida (denominada *meso*-lactida) así como mezclas racémicas o equimolares de los enantiomeros D- y L- (denominada *rac*-lactida). Todas ellas están mostradas en la Figura 10 [23, 24]. En la literatura, en ocasiones, se confunde *meso*-lactida y *rac*-latida, denominadas ambas comúnmente D,L-lactida. Controlando el ácido láctico de partida así como con el uso de catalizadores estereoselectivos se puede controlar la obtención de una u otra forma enantiomérica del dímero.

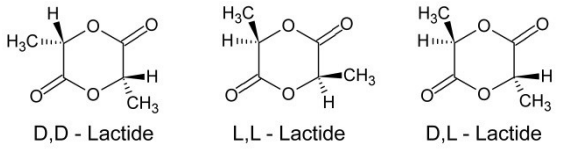

Figura 10. Distintos enantiómeros de la lactida.

Las unidades de repetición son añadidas, ya sea como ácido láctico durante la polimerización por condensación o como lactida durante ROP. Así es posible obtener poli(L-ácido láctico), poli(D-ácido láctico) a partir de policondensación o bien poli-D-lactida, poli-L-lactida, poli-D,L-lactida o mezclas racémicas de poli-D-lactida y poli-L-lactida mediante la ruta de ROP. La obtención de polímeros estereo-regulares a partir de enantiómeros de lactida puros es bastante obvia. Sin embargo, mediante el uso de catalizadores

estereoselectivos para las etapas de iniciación y propagación de ROP, se pueden sintetizar PLA estereo-regular a partir de mezclas racémicas de L-lactida y D-lactida [27, 34]. Un amplio abanico de velocidades de degradación, propiedades físicas y mecánicas se pueden obtener variando el peso molecular así como la estereoquímica de la cadena polimérica.

Así, mientras el poli(L-lactida) (PLLA) ópticamente puro es un sólido cristalino, duro y frágil, el poli(D,L-lactida) (PDLLA) es amorfo y transparente [32]. Además, mientras que el PLA producido por más de un 93% de ácido L-láctico es un material semicristalino, el procedente de entre un 50 y un 93% de ácido L-láctico es estrictamente amorfo. Tanto meso- como D-lactida inducen giros en la arquitectura de la cadena de polímero a diferencia de la L-lactida que tiene una arquitectura más regular [24]. Debido a la cristalinidad y a la estructura más ordenada y compacta del PLLA, éste tiene mejores propiedades mecánicas que el PDLLA así como una velocidad de degradación más baja [23].

Además del carácter renovable del PLA, este polímero se puede degradar bajo condiciones de compostaje descomponiéndose en agua y dióxido de carbono que es enviado hacia la atmósfera, de donde partía originalmente, de acuerdo al ciclo de vida del PLA (figura 11).

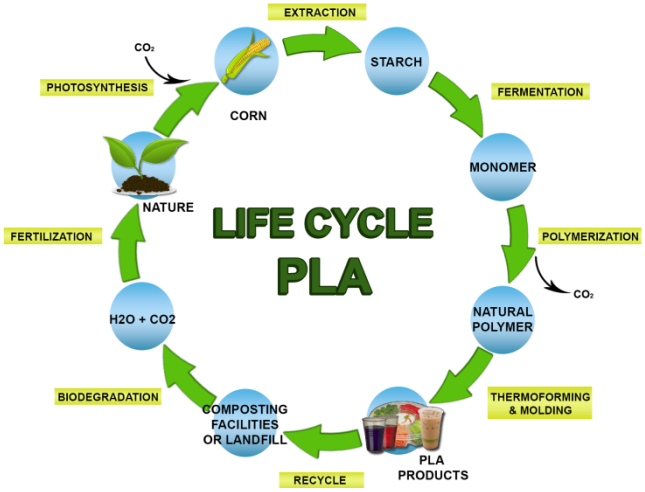

Figure 11. Ciclo de vida del PLA

En un estudio del ciclo de vida del PLA realizado por Vink et al. [35] se concluyó que entre los beneficios más notables del PLA están las reducciones tanto en el uso de combustibles fósiles como del calentamiento global o efecto invernadero ya que, por un lado, usa materiales renovables y, por otro, su balance global en cuanto a emisiones de dióxido de carbono a la atmósfera es negativo. Ello es así debido a que todo el carbono en el ácido láctico proviene de la glucosa, la cual es producida por las plantas mediante fotosíntesis, donde el carbono se consume como dióxido de carbono (CO_2) atmosférico. Por lo tanto, todo el carbono del PLA procede del CO_2 atmosférico. Sin embargo, como todo proceso de producción industrial, la producción de PLA requiere energía, lo que causa emisiones de CO_2. Así, teniendo en cuenta el CO_2 absorbido por las plantas durante su crecimiento para la realización de la fotosíntesis y el CO_2 emitido durante la producción y biodegradación del PLA se alcanza un balance global negativo. Por ejemplo, en comparación con el PET y el

nylon, el PLA utiliza un 30-50% menos de recursos fósiles que se traduce en un 50-70% menos de emisiones de CO_2. Además este estudio también mostró que el PLA tiene un contenido energético no renovable menor en comparación con una gran variedad de materiales plásticos comunes. Por lo tanto, el PLA posee una combinación única de energía, medio ambiente y sostenibilidad lo que le hacen ser uno de los productos industriales procedentes de la biomasa con más perspectiva de futuro.

Sin embargo, para que la sustitución a gran escala de los plásticos basados en combustibles fósiles por el PLA tenga lugar, se necesita un considerable esfuerzo en investigación. Ello es debido a que, como para la mayoría de los polímeros biodegradables, se requiere una mejora de algunas de sus propiedades, como las propiedades de barrera y mecánicas para que pueda utilizarse en aplicaciones para las que actualmente su comportamiento físico-químico es insuficiente [36].

En este sentido, se han desarrollado algunas estrategias para mejorar las propiedades de este material que incluyen su uso en recubrimientos [37-39], sistemas multicapas [40, 41], así como mezclas con otros matrices poliméricas procedentes de recursos renovables como quitosano, almidón o PHB o no renovables como PCL, poli (vinil acetato) (PVAc) o polietilenglicol (PEG) [42]. Además la copolimerización con otros monómeros, así como mezclas con otros agentes químicos que actúan como plastificantes son otras de las estrategias usadas para tal fin [43, 44]. Otra de las rutas más ampliamente estudiadas hoy día para intentar mejorar las propiedades de las matrices biopoliméricas, y las del PLA en concreto, se basa en el uso de la nanotecnología. La incorporación de materiales nanoestructurados, también conocidos como nanocargas nano-refuerzos o nanofillers, de origen orgánico o inorgánico en el interior de matrices poliméricas ha demostrado ser efectiva en cuanto a la mejora de las propiedades de dichos materiales, siendo esta tecnología además atractiva por su bajo coste [45]. Las posibles soluciones mediante el uso de nanotecnologías para mejorar las propiedades de las matrices biopoliméricas se discuten más adelante.

2.1.2. *Polihidroxialcanoatos (PHAs)*

Otra alternativa a los polímeros procedentes de recursos fósiles no biodegradables son los polihidroxialcanoatos (PHAs), los cuales han suscitado gran interés debido a su carácter biodegradable, biocompatible y renovable. Los PHAs son biopoliésteres de ácidos hidroxialcanoicos sintetizados intracelularmente por algunos microorganismos como reserva de carbono y energía (ver FIGURA 12) [5]. Más de 300 microorganismos son conocidos que producen y acumulan PHAs [46]. Además pueden ser degradados por diferentes bacterias, hongos y algas en varios ecosistemas [47]. Estos gránulos fueron observados por primera vez en 1888, aunque hasta 1925 no fue confirmada su composición [11]. En condiciones ideales, los PHAs pueden formarse intracelularmente hasta representar un 80% de la masa total de la bacteria en base seca.

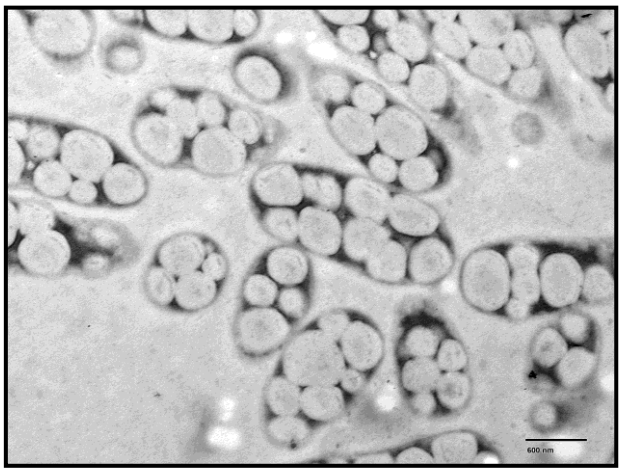

Figura 12. Gránulos de PHAs en *Ralstonia eutropha*

En cuanto a la estructura monomérica de los PHAs se pueden clasificar en función de la longitud de la cadena de los ácidos hidroxialcanoicos de los que están constituidos. Así, se definen PHAs de cadena corta (monómeros de 3 a 5 átomos de carbono), de cadena media (monómeros de 6 a 12 átomos de carbono) e híbridos (contienen cadena corta y cadena media). Los PHAs de cadena corta son típicamente polímeros termoplásticos semicristalinos con elevado grado de cristalinidad (60-80%), temperaturas de fusión (T_m) alrededor de 180°C y temperaturas de transición vítrea (T_g) entre -5 y 20°C. Por el contrario, los de cadena media son altamente amorfos y con T_m entre 42 y 58°C y T_g entre -62 y -26°C clasificándose, por tanto, como elastómeros [5].

Esta familia de polímeros comprende principalmente el homopolímero, polihidroxibutirato (PHB) el cual ha sido extensamente estudiado ya que presenta propiedades mecánicas similares a las de los polímeros convencionales procedentes del petróleo, como el PP y PE, relativamente buenas propiedades térmicas y elevada rigidez debido a su elevado grado de cristalinidad [48]. Sin embargo, aunque una elevada cristalinidad es útil para algunas aplicaciones, su rigidez limita su uso en otras aplicaciones comerciales. Otro inconveniente de este polímero es su baja estabilidad térmica, lo que lo hace poco útil e inestable durante técnicas de procesado a elevada temperatura como el mezclado en fundido, limitando también su aplicabilidad ya que este tipo de procesado es uno de los más extendidos industrialmente [49].

Varias estrategias se han desarrollado para solucionar tales inconvenientes, incluyendo mezclado con otros polímeros, tales como PVA [50], polipropilenglicol (PPG) [51] y PCL [52] o modificación del homopolímero mediante la incorporación de diferentes tipos de monómeros durante la fermentación como hidroxivalerato (HV) o hidroxihexanoato (HH). La posibilidad de obtener varios poliésteres en función del sustrato fue reportada por primera vez por De Smet et al. [53] quien produjo un polímero que consistía en unidades de poli (3-hidroxioctanoato) tras un cultivo realizado en n-octano. La estructura general de los PHAs puede verse en la Figura 13. Alrededor de 150 monómeros de este tipo han sido identificados hasta la fecha, aunque desde un punto de vista comercial, el copolímero con HV,

poly(hidroxibutirato-co-hidroxivalerato) (PHBV), se presenta como un mejor candidato que el PHB debido a su mayor ductilidad y, en principio, mejor procesabilidad [11].

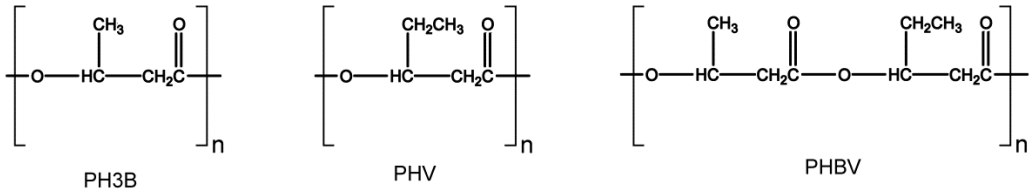

Figura 13. Estructura del poli-3-hidroxibutirato (PH3B), polihidroxivalerato (PHV) y polihidroxibutirato-co-hidroxivalerato.

El mecanismo de la síntesis bacteriana de PHAs es ampliamente conocido pudiéndose modificar los procesos para obtener el producto deseado. Así, dependiendo del microorganismo seleccionado y de las condiciones del cultivo, homo- o copoliésteres pueden obtenerse [5, 11, 54].

El PHBV posee propiedades mecánicas y térmicas mejoradas ya que la incorporación de hidroxivalerato reduce la cristalinidad, disminuyendo por tanto la rigidez y la fragilidad del material así como también reduce el punto de fusión del polímero sin que decrezca la estabilidad térmica [48, 55]. Sin embargo, es ampliamente conocido que una reducción en cristalinidad afecta a las propiedades barrera a compuestos de bajo peso molecular, siendo dicha propiedad crucial para materiales con intención de ser utilizados en aplicaciones de envasado alimentario [56, 57].

Un inconveniente asociado a este tipo de materiales es su elevado coste de producción ya que se necesitan sustratos caros para el crecimiento bacteriano así como unas condiciones estériles durante el procesado. Debido a ello se están optimizando los procesos de fermentación y extracción, así como aislando y desarrollando cepas microbianas más productivas y que puedan utilizar sustratos más baratos [58] Por todo ello, el PHBV todavía presenta alguna serie de inconvenientes como los elevados costes, baja velocidad de cristalización, relativa fragilidad y baja estabilidad térmica, que impiden un uso más generalizado de esta familia de polímeros.

Por todo lo expuesto anteriormente, aunque ambas familias de biopolímeros (PLA y PHAs) representan una alternativa a los polímeros convencionales procedentes del petróleo, presentan una serie de inconvenientes para poder ser usados en aplicaciones de envasado alimentario. De ahí que la modificación de los mismos para mejorar sus propiedades a través de tecnologías innovadoras es un reto importante para la investigación a nivel mundial. Sin duda, el principal desafío en los últimos tiempos está focalizado en el desarrollo de biopolímeros sostenibles con el medio ambiente, que sean económicamente viables, puedan ser procesados por las tecnologías convencionales a escala industrial y que alcancen propiedades similares a las de los polímeros convencionales.

Varias tecnologías se han usado para este fin, incluyendo modificación química de los biopolímeros, adición de plastificantes para mejorar sus propiedades mecánicas, mezclas con otras matrices poliméricas o biopoliméricas, etc [8]. Además, en las últimas décadas muchos estudios han sido focalizados en la obtención de materiales compuestos, y más específicamente, de materiales nanocompuestos usando estas matrices biopoliméricas mediante el uso de nano-refuerzos, siendo una manera eficaz de mejorar sus propiedades. Por lo tanto, el desarrollo de nuevos nanocompuestos de base polimérica, renovables y biodegradables, llamados comúnmente nanocompuestos ecológicos (new green nanocomposite materials), son compuestos con un futuro asegurado, siendo considerados como la próxima generación de materiales. Posibles soluciones relacionadas con el desarrollo de materiales nanoestructurados así como su incorporación mediante diferentes tecnologías dentro de matrices poliméricas se abordan en los párrafos siguientes.

3. NANOTECNOLOGÍA: USO PARA REFORZAR BIOPOLÍMEROS.

Los "composites" o materiales compuestos son materiales heterogéneos o híbridos que consisten fundamentalmente en una fase continua o matriz polimérica y una fase discontinua, relleno o cargas (fillers). Fibras, láminas, y partículas, de materiales orgánicos e inorgánicos se han utilizado durante décadas para formar compuestos de polímeros con propiedades mecánicas y térmicas mejoradas. Un avance reciente en materiales compuestos es la nanotecnología. La nanotecnología se define como el estudio, diseño, síntesis, manipulación y aplicación de materiales, aparatos y sistemas a través del control de la materia a nanoescala. Un material se considera "nano" cuando su tamaño se encuentra entre 1 y 100 nanómetros en, al menos, una de sus dimensiones. Así, la incorporación de materiales a nanoescala en el interior de matrices poliméricas da lugar a nanocompuestos. Esta tecnología tiene hoy día aplicación en áreas relacionadas con la física, la química y la biología, entre otras. Para muchas de las aplicaciones de polímeros biodegradables se requiere el uso de estas tecnologías con el objetivo de mejorar algunas de sus propiedades, como las propiedades de barrera a gases y sus propiedades mecánicas, aumentando, de este modo, su competencia en el mercado actual. La combinación del uso de biopolímeros con la posibilidad de modificar sus propiedades mediante el uso de la nanotecnología permite la creación de materiales que pueden ser denominados *nanobiocompuestos*.

Es destacable mencionar que para alcanzar un buen efecto reforzante así como óptimas mejoras en las propiedades finales del material compuesto, una buena interacción entre el relleno y la matriz polimérica se debe alcanzar. Ello a su vez dependerá de la dispersión, la química de la interfase, la afinidad polímero-relleno, la morfología del relleno y el método de preparación [59, 60]. De hecho, el alcanzar una buena dispersión de relleno en el interior de la matriz polimérica es uno de los mayores problemas que se encuentran cuando se desarrollan nuevos materiales compuestos. Es ampliamente conocido que una buena interacción entre ambas fases es lograda cuando existe una buena dispersión del relleno en la matriz de polímero, así como a través de la reducción del tamaño del relleno. Las partículas más grandes alteran drásticamente y, por lo general, deterioran las características de los materiales compuestos aunque por otro lado la tendencia a formar agregados del refuerzo añadido aumenta conforme disminuye el tamaño de partícula [61]. Así, el pasar de macro- o micro- a nanoescala conduce a un mejor rendimiento de los materiales

nanocompuestos, ya que los materiales nanoestructurados poseen una mayor área específica con la que poder establecer interacciones con la matriz polimérica, aunque puede conducir a mayor aglomeración del nano-refuerzo. Aditivos de tamaño nanométrico bien dispersos pueden conducir a materiales con mejores propiedades mecánicas, térmicas y de barrera en comparación con los polímeros de partida así como con sus compuestos híbridos convencionales a macro- y microescala [62, 63]. Los nanocompuestos, por tanto, representan una nueva alternativa a las tecnologías convencionales para mejorar las propiedades de los polímeros. Sin embargo, el uso de este tipo de materiales nanoestructurados en el área del envasado de alimentos presenta diversas cuestiones, ya que hoy día no existe conocimiento sobre la posible migración de dichas nanopartículas a los alimentos y sus potenciales efectos sobre la salud del consumidor.

Entre los tipos de cargas/refuerzos más comúnmente usados en la síntesis de nanocompuestos están las nanoagujas de celulosa (también llamadas "nanowhiskers" y "nanocristales") y los compuestos basados en carbono como el grafeno. En los párrafos siguientes se describen con más detalle cada uno de ellos así como sus estrategias de incorporación en matrices poliméricas.

3.1. Materiales celulósicos

La celulosa es la molécula natural de mayor abundancia y uno de los biopolímeros más abundantes en la Tierra. Anualmente se producen 10^{11} a 10^{12} toneladas a partir de fuentes de origen vegetal. Es el mayor componente de la pared celular de las plantas, siendo un polímero natural muy fuerte con la fórmula $(C_6H_{10}O_5)_n$, que consiste en una cadena lineal de varios cientos hasta más de diez mil unidades de D-Glucosa enlazadas por enlaces $\beta(1\rightarrow4)$. Las fibras de celulosa son de bajo coste, ampliamente disponibles, ecológicos, de fácil reciclaje y requieren bajo consumo de energía en su producción.

La Figura 14 presenta un modelo esquemático de la estructura jerárquica de la celulosa de origen vegetal. Varios modelos han sido propuestos para explicar la estructura interna de la celulosa vegetal. Debido a ello diferente terminología ha sido usada para describir la estructura de la celulosa con lo que conduce a cierta confusión [64-66].

Microfibras de celulosa, con diámetros entre 2 y 50 nm y longitudes que pueden alcanzar varias decenas de micras [65, 66], son formadas a partir de agregados de fibras elementales, las cuales están formadas a su vez por cadenas de celulosa, conteniendo regiones donde las moléculas se encuentran ordenadas (región cristalina) y otras donde las cadenas están totalmente desordenadas (región amorfa). Esas regiones cristalinas, las cuales pueden ser aisladas mediante diferentes tratamientos son los "nanowhiskers" de celulosa (CNW de sus siglas en inglés) también conocidos como nanocristales o nanoagujas de celulosa. Las dimensiones de estos cristales dependen del origen y del tratamiento de la muestra. Cada microfibra de celulosa puede ser considerada como una cuerda flexible con cristales de celulosa unidos a lo largo del eje de la microfibra mediante dominios amorfos. En la Figura 1 puede observarse como cuatro de esas microfibras de celulosa están unidas mediante otros polisacáridos, como hemicelulosa o lignina, formando unidades más grandes conocidas como fibras de celulosa. Los grupos hidroxilos presentes en la superficie de la celulosa y su habilidad de formar fuertes enlaces de hidrógeno están estrechamente

relacionados con las propiedades más importantes de la celulosa como su organización jerárquica (regiones cristalinas y amorfas) y su alta cohesión, entre otras. De hecho, las fuerzas reticulares responsables de mantener las regiones cristalinas compuestas por paquetes de cadenas de celulosa son básicamente el resultado de la estabilización mediante una red fuerte y compleja de enlaces de hidrógeno inter- e intramoleculares [66].

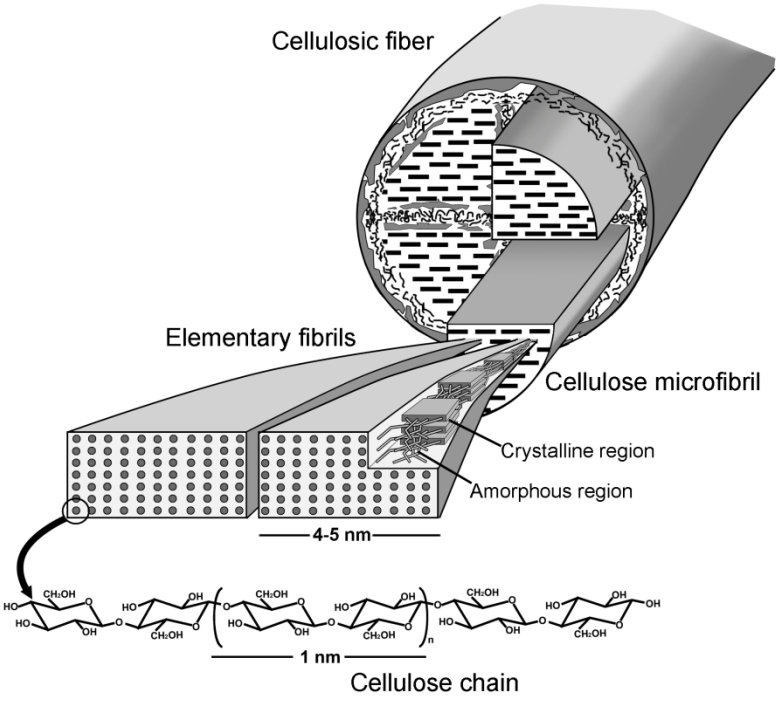

Figure 14. Estructura interna de la celulosa de origen vegetal

Para su aplicación como nano-refuerzo, las fibras elementales de celulosa son normalmente aisladas mediante procesos mecánicos, produciendo así celulosa microfibrilar (MFC de sus siglas en inglés) o bien mediante hidrólisis ácida para la obtención de nanocristales de celulosa. Mientras que MFC contiene tanto regiones cristalinas como amorfas, la celulosa nanocristalina solo está compuesta de fracciones cristalinas. Estos materiales nanoestructurados presentan excelentes propiedades mecánicas así como un completo carácter renovable y biodegradable. Valores de módulo elástico superiores a 130 GPa y de resistencia mecánica cercanos a los 10 GPa han sido reportados para los CNW [67-69]. Además, estos materiales presentan otras propiedades interesantes como elevada barrera a gases y vapores, elevada área específica y baja densidad [67]. Todo esto hace que los nanoaditivos de celulosa sean una clase de nanomaterial muy atractivo para la elaboración de nanocompuestos de bajo coste, ligeros y de elevadas propiedades mecánicas [65].

3.1.1. *Celulosa bacteriana*

Además de la celulosa vegetal, la celulosa puede ser sintetizada por diversos microorganismos dando lugar a lo que se conoce como celulosa bacteriana (BC). En particular, algunos géneros de bacterias como *Rhizobium*, *Acetobacter*, *Agrobacterium* y *Sarcina* son capaces de sintetizarla [70]. Dentro del género de las acetobacterias, especies como *Gluconacetobacter xylinus, Acetobacter hansenii* o *Acetobacter pasterianus* la producen. Entre ellas la especie *Gluconacetobacter xylinus* el organismo modelo para la producción de BC. Ello es debido a que es la especie de mayor capacidad productora, dando un producto de alta pureza y de estructura similar a la de origen vegetal [71].

En un medio de cultivo estático rico en polisacáridos, esta especie bacteriana es capaz de producir una capa de BC en la interfase líquido/aire. Esta película altamente hidratada consiste en un conjunto aleatorio de fibrillas de menos de 100 nm de ancho, que se componen a su vez de un conjunto de nanofibrillas. Existen varias hipótesis que intentan explicar porqué este tipo de microorganismos producen celulosa las cuales incluyen el hecho de que las capas de celulosa puedan actuar como barrera de protección contra agentes externos como radiaciones, otros microorganismos o metales pesados o incluso relacionan la producción de celulosa para posicionar a la bacteria en una posición óptima, cercana al medio de cultivo pero a su vez donde existe mayor abundancia de oxígeno [72].

Aunque la celulosa de origen vegetal (PC) y BC tienen la misma estructura química, tienen diferente organización estructural y diferentes propiedades mecánicas. BC muestra una mejor estructura de la red de fibras, mayor capacidad de retención de agua y una mayor cristalinidad. En la figura 15 puede observarse un modelo esquemático de la estructura de las microfibras de PC y BC.

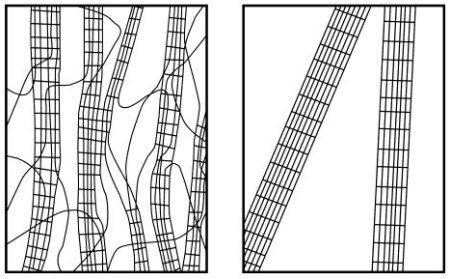

Figure 15. Modelo esquemático de microfibras de celulosa bacteriana (derecha) en comparación con celulosa vegetal (izquierda) [72]

Por otra parte, mientras que la PC está naturalmente asociada con otros tipos de biopolímeros como hemicelulosa y lignina, lo que requiere operaciones de purificación y blanqueamiento para extraer la celulosa del conjunto, la BC es prácticamente pura [73]. Solo las bacterias remanentes y el medio de cultivo absorbido en la película de celulosa deben ser eliminados, lo cual se consigue con lavados con agua hirviendo así como con disoluciones acuosas de hidróxido de sodio. Debido a sus excelentes propiedades, es decir, alta pureza, alta cristalinidad, alta resistencia mecánica, baja densidad y biocompatibilidad, la celulosa bacteriana se ha convertido en un material muy interesante, con aplicaciones en biomedicina [74], en la industria del papel [75] y, más recientemente, como agente de refuerzo de

matrices poliméricas [76, 77]. Por lo tanto, la celulosa bacteriana debido al gran conjunto de propiedades y ventajas que posee destaca como fuente alternativa a la celulosa de origen vegetal.

Como se ha dicho, para su aplicación como nanocargas tanto PC como BC son sometidas a hidrólisis con ácidos fuertes como el ácido sulfúrico o ácido clorhídrico, que producen una digestión preferencial de los dominios amorfos del material dejando las regiones cristalinas intactas. Así se dividen los conjuntos de nanofibrillas, dando lugar a moléculas de inferior tamaño. Este tratamiento ácido que rompe la estructura de la celulosa, resulta en nanofibras cristalinas o nanocristales (CNW o CNC de sus siglas en inglés). La morfología de los CNW depende de la fuente de celulosa y las condiciones de hidrólisis. Mientras los CNW extraídos de recursos vegetales como el algodón o la madera suelen tener una longitud de 100-300 nm y un diámetro de 5-20 nm, los obtenidos a partir de celulosa bacteriana pueden tener varias micras de longitud y un diámetro de 5-50 nm incrementando así su relación de aspecto (L/D) el cual es un parámetro crítico con remarcable influencia en la capacidad de refuerzo de las nanocargas cuando se incorporan en el interior de matrices poliméricas [78]. En cuanto a las condiciones de hidrólisis, la concentración de ácido, la proporción de celulosa/ácido, temperatura y tiempo de hidrólisis, son factores que determinan la morfología de los CNW [73].

3.2. Materiales carbonáceos. Grafeno

No hay duda de que el siglo XXI es la era de los nanomateriales a base de carbono, desde el grafito a los nanotubos de carbono y, recientemente, con una focalización más intensa sobre el grafeno. El grafeno pertenece a una nueva clase de nanomateriales a base de carbono en 2D. Representa la estructura elemental del grafito estando compuesto por una lámina monoatómica de carbono con hibridación sp^2 con conformación hexagonal.

Este material ha ganado especial atención en los últimos años debido a sus remarcadas propiedades físicas, las cuales son significativamente superiores a las de cualquier otro material de relleno inorgánico conocido hasta la fecha, incluso a las de los nanotubos de carbono [79]. Debido a ello, los materiales a base de grafeno se espera que puedan ser utilizados en una gran variedad de aplicaciones incluyendo, sensores, baterías, supercondensadores, materiales nanocompuestos, celdas solares, envasado activo e inteligente y sistemas de almacenamiento de hidrógeno [80].

En cuanto a la producción de grafeno, dos son las rutas principales utilizadas. La ruta “bottom-up” y la ruta “top-down”. La primera de ellas se basa en la síntesis de láminas de grafeno mediante el ensamblamiento de átomos de carbono partiendo de moléculas simples como metano o etanol. Por otro lado, la técnica top-down se basa en disgregar el grafito hasta obtener nanoláminas de grafeno. Ambos métodos proporcionan grafeno con diferentes propiedades y rendimientos. De entre todos los procesos de producción de grafeno, que incluyen entre otros, exfoliación mecánica, deposición química de vapor (CVD de sus siglas en inglés Chemical Vapour Deposition) o crecimiento epitaxial, aquellos basados en la técnica bottom-up producen nanoláminas de grafeno más perfectas y de mayores propiedades aunque no son apropiados para producción a gran escala [79]. Por otro lado, en los procesos “top-down” derivados oxidados del grafito (óxido de grafito) son sintetizados previamente

mediante el tratamiento del grafito con agentes oxidantes fuertes. Este material es posteriormente exfoliado generándose láminas monoatómicas oxidadas denominadas óxido de grafeno. Así, la reducción del óxido de grafeno ha suscitado especial interés ya que es una ruta a través de la cual es posible producir láminas de grafeno tanto en polvo como en dispersiones coloidales con elevada procesabilidad. Existe una amplia variedad de sistemas utilizados como agentes reductores que van desde el empleo de temperatura hasta la utilización de diversos agentes químicos o incluso microorganismos [79, 81]. Desde el punto de vista químico, la presencia de grupos funcionales oxidados en la superficie del óxido de grafeno, hacen esta ruta especialmente interesante ya que estos grupos proporcionan zonas reactivas para la modificación química mediante el uso de la química de superficie del carbono [80]. Además, se trata de la ruta de obtención óptima en cuanto a rendimiento y costes, siendo el grafeno obtenido mediante esta vía demandado por distintos sectores como recubrimientos, pinturas/tintas, capas conductoras transparentes, aplicaciones relacionadas con la biología y almacenamiento de energía [81].

Debido a los extensivos estudios llevados a cabo, este material ha evolucionado rápidamente. La principal razón del interés suscitado por el material y que ha impulsado estos rápidos avances está basada en sus propiedades únicas [81], presentando, no sólo unas excelentes propiedades mecánicas, eléctricas y térmicas, sino también unas excelentes propiedades de barrera a gases y vapores, debidas al hecho de que las láminas de grafeno libres de defectos son impermeables a compuestos de bajo peso molecular [82]. Se ha observado la estructura laminar de este tipo de materiales son altamente efectivos en la mejora de las propiedades barrera de distintas matrices poliméricas [82-84], lo cual hace que los grafenos constituyan un excelente nano-refuerzo para matrices de polímeros y biopolímeros [85]. La mejora de las propiedades mecánicas, de barrera y/o eléctricas ha sido demostrada en diversos trabajos en los que el grafeno se ha utilizado como refuerzo de matrices como PVA [86], PE [87], poliestireno (PS) [88], PLA [89] y PHBV [55] entre otros.

3.3. Estrategias de incorporación de nano-refuerzos en matrices poliméricas

Existen tres rutas ampliamente utilizadas para el desarrollo de nanocompuestos, independientemente del nanorrelleno utilizado: mezclado en disolución, polimerización *in situ* y mezclado en fundido [59, 82].

El mezclado en disolución es uno de los métodos más ampliamente estudiados para la incorporación de nanocargas. Esta metodología se basa fundamentalmente en dispersar refuerzos nanoestructurados en un disolvente en el cual el polímero es soluble. La dispersión final de las nanocargas dependerá de las fuerzas que interactúan entre las propias nanopartículas y de sus interacciones con el disolvente o disolución polimérica. Tras la fase de disolución/dispersión, el disolvente es evaporado o bien la mezcla es precipitada obteniéndose así el polímero cargado con el nanoaditivo. Esta metodología, aunque da buenos resultados en cuanto a la dispersión del nanomaterial en el interior de la matriz de polímero, precisa de grandes cantidades de disolventes lo que la convierten en una tecnología poco respetuosa con el medio ambiente así como no extrapolable a escala industrial.

El segundo método es mediante polimerización *in situ*. En esta técnica, el monómero es usado como un medio donde se pre-dispersa la nanocarga para posteriormente someter el sistema a condiciones de polimerización. En comparación con otros métodos de obtención de nanocompuestos, la obtención mediante polimerización *in situ* ofrece varias ventajas como por ejemplo la dispersión uniforme de las nanocargas, minimizando la agregación, o la generación de fuertes interacciones entre la matriz y el nano-refuerzo, incrementando así la compatibilidad entre ambas fases. Durante el proceso de polimerización, sin embargo, la viscosidad suele aumentar, lo cual reduce la procesabilidad de los nanocompuestos. Además, muchas de estas reacciones deben ser llevadas a cabo en presencia de disolventes, conllevando por tanto los inconvenientes asociados al uso de los mismos [90]. En esos casos, aunque el uso de disolventes es mucho menor que en el método de mezclado en disolución, aún siguen siendo necesario cantidades considerables para llevar a cabo la incorporación de las nanocargas [91]. Por otro lado, se requieren grandes cantidades de reactivo para llevar a cabo la reacción, reduciéndose así su aplicabilidad [92, 93]. La polimerización puede ser iniciada mediante calor, mediante el uso de un iniciador o mediante el uso de catalizadores. En ocasiones, se puede inducir al sistema para que la grupos reactivos en la propia superficie de las nanocargas ejerzan de iniciadores de la reacción de polimerización, apareciendo un enlace covalente entre el polímero y la nanocarga (a esta ruta se le denomina "grafting from"). Por el contrario es posible también generar un enlace covalente entre la cadena polimérica, una vez ya sintetizada y la nanocarga (a esta ruta se le denomina "grafting to") [59, 94].

Por último está el mezclado en fundido donde las nanocargas son mezcladas con polímeros termoplásticos en estado fundido bajo elevadas fuerzas de cizalla. El uso de elevadas temperaturas necesarias para alcanzar una mezcla homogénea puede ocasionar degradación de la nanocarga, la cual a su vez puede originar una degradación en cadena del polímero. Sin embargo, debido a que es un método que no requiere el uso de disolventes, es simple y económico, esta tecnología ha sido ampliamente utilizada para la síntesis de nanocompuestos poliméricos. Esta ruta es además considerada como una de las más atractivas para el desarrollo comercial de dichos materiales ya que es una de las más extendidas industrialmente.

Además de lo anterior, una estrategia novedosa que ha surgido en las últimas décadas y está siendo explorada para el desarrollo de nanocompuestos de base polimérica, es la técnica de "ball-milling". Esta técnica es considerada como un nuevo método de síntesis de materiales compuestos o nanocompuestos y se basa en la molienda de alta energía (HEBM de sus siglas en inglés High Energy Ball Milling) capaz de producir cambios mecano-químicos en los materiales. Esta técnica consiste en el mezclado del polímero y las nanocargas en un molino de bolas aprovechando la energía liberada durante el choque de las mismas. La efectividad del carácter mecano-químico de esta técnica ha sido corroborada previamente mediante la aparición de enlaces covalentes entre la matriz polimérica y la nanocarga tras ser procesados mediante "ball-milling" [95]. Es una tecnología libre de disolventes y se presenta como una alternativa eficiente para producir materiales compuestos novedosos con elevado rendimiento ya que durante la molienda se induce un mezclado íntimo entre el polímero y el material de refuerzo [96, 97]. Su eficiencia ha sido ampliamente demostrada en el desarrollo de nanocompuestos a base de nanoarcillas y materiales carbonáceos nanoestructurados [95, 96, 98-101]. Además, esta tecnología ha sido también utilizada para el desarrollo de nanocompuestos donde había una baja compatibilidad entre el nano-

refuerzo y la matriz con el objetivo de superar la carencia de afinidad entre ambos componentes [100].

3.3.1. *Nanocompuestos celulósicos*

Como se ha comentado anteriormente, los CNW presentan una serie de propiedades que los hacen bastante atractivos para su uso en materiales nanocompuestos. Sin embargo, la naturaleza hidrofílica de los mismos, los hace incompatibles con la mayoría de disolventes orgánicos así como con matrices poliméricas termoplásticas, fundamentalmente de naturaleza hidrofóbica, lo cual complica su uso como nano-refuerzo. Adicionalmente, estos materiales también presentan una fuerte tendencia a la auto-asociación debido a los fuertes enlaces de hidrógenos que se producen entre las moléculas cuando son sometidas a procesos de secado [102]. Debido a ello, la incorporación de CNW altamente dispersos en el interior de matrices poliméricas, requisito indispensable para alcanzar unas buenas propiedades en el material nanocompuesto final, no es tarea sencilla. Como se ha reportado anteriormente, cuando se consigue una buena dispersión de los nanocristales de celulosa en matrices poliméricas, la formación de una red de percolación donde exista contacto entre los nano-refuerzos añadidos a lo largo de toda la matriz polimérica resulta en excepcionales efectos de refuerzo, incluso a bajos contenidos de la nanocarga [103].

Tradicionalmente, el mezclado en disolución ha sido la ruta más extendida para la preparación de nanocompuestos a base de nanocristales de celulosa. Esta metodología, en general, requiere un cambio de disolvente previo al uso de la celulosa lo cual implica sucesivos pasos de centrifugación [104], no garantizando una buena dispersión de los nanocristales en la matriz debido a la dificultad de dispersar bien esos materiales hidrofílicos en disolventes orgánicos [105]. Por esta razón, diversos trabajos se han centrado en buscar estrategias para mejorar tanto la dispersión como la compatibilidad con sistemas hidrofóbicos, tales como el uso de un disolvente adecuado [106], el uso de surfactantes [107, 108] o mediante la modificación química de la superficie de la celulosa [104, 109-111], obteniendo con ello mejores propiedades. A pesar de ello, como se ha dicho anteriormente, esta metodología precisa del uso de grandes cantidades de disolventes orgánicos que son tóxicos y caros, siendo además una técnica no apropiada y poco práctica desde un punto de vista de aplicación industrial.

Existen trabajos donde la incorporación de celulosa en el interior de matrices poliméricas procedentes de recursos no renovables se ha llevado a cabo mediante la ruta de polimerización *in situ* [112-114]. Sin embargo, existe escasa literatura acerca de la incorporación de este tipo de nano-refuerzo en matrices de biopolímeros mediante esta vía. Los grupos hidroxilos en la superficie de la celulosa pueden ejercer de iniciadores de la reacción de polimerización facilitando el injerto de la cadena polimérica en la superficie de la celulosa. Nanocompuestos de PLA y CNW se han obtenido por esta vía, utilizando los grupos hidroxilos de la superficie de la celulosa como iniciadores de la cadena polimérica, injertándose así la cadena de polímero en la superficie del refuerzo [115]. Sin embargo, en este caso, hubo un bajo control de la cadena de polímero que se desarrolla a partir del punto de iniciación en la superficie de la celulosa, obteniendo un polímero de un peso molecular moderado. Este tratamiento, como se verá más adelante, puede ser utilizado como paso de

pre-incorporación de la celulosa dando lugar a un material inicial que, diluido posteriormente en estado fundido, mejora la dispersión final de los CNW en matrices poliméricas. Mediante el control de los grupos hidroxilos disponibles en la superficie de la celulosa, es posible obtener cadenas de polímero de mayor tamaño injertadas en su superficie. Así mediante la acetilación parcial de los grupos hidroxilos presentes en la superficie de la celulosa se han obtenido nanocompuestos de PLA y nanocristales de celulosa con cadenas de polímero de elevado peso molecular no precisando de etapas posteriores para alcanzar buenas propiedades del polímero [103]. En cualquier caso, aunque para el desarrollo de esta estrategia menos disolventes orgánicos son necesarios que en la metodología de mezclado en disolución, también se precisa de su uso en cantidades significativamente altas.

Como se ha dicho anteriormente, la técnica de mezclado en fundido es la ruta más ampliamente extendida a nivel industrial. Sin embargo, existen pocos estudios que reporten la incorporación de celulosa en matrices poliméricas mediante esta ruta. De nuevo, el principal inconveniente encontrado está basado en la hidrofilicidad de la celulosa que la hace poco compatible con la mayoría de las matrices poliméricas fundamentalmente de naturaleza hidrofóbica, así como en las fuertes interacciones, vía puentes de hidrógeno, que aparecen entre los propios nanocristales de celulosa cuando se someten a procesos de secado. Ello resulta en interacciones débiles entre la matriz y la celulosa que complican la dispersión e inducen a la aglomeración de la misma. Por ejemplo, Jiang et al. [106] observaron una baja compatibilidad entre CNW y PHBV en estado fundido, lo que complicó la dispersión de la celulosa dando lugar a interacciones débiles entre matriz y relleno. Ellos observaron que, incluso con el uso de un compatibilizante como el PEG, los aglomerados de celulosa formados durante el liofilizado de la misma no pudieron disgregarse y, por lo tanto, no se dispersaron bien mediante esta tecnología. Recientemente, se han reportado estudios usando diferentes estrategias para la mejora de la compatibilización de la celulosa con matrices de naturaleza hidrofóbica mediante mezclado en fundido. Una de las estrategias más empleadas es la modificación química de la superficie de la celulosa mediante reacción de los grupos hidroxilos con diferentes agentes químicos, lo que conduce a mejoras en la dispersión de la misma en el interior de matrices poliméricas. Por ejemplo, la silanización superficial de la celulosa condujo a una mejora de la dispersión de la misma en PLA [116]. A pesar de ello, aunque la modificación en superficie de la celulosa parece ser una buena estrategia para su compatibilización tanto con matrices hidrofóbicas como con disolventes orgánicos se ha demostrado que un exceso de modificación en superficie puede provocar efectos prejudiciales en la estructura y propiedades de los CNW [117-119], así como podría conllevar diferentes problemas asociados a su biodegradabilidad, a la economía del proceso y a la migración en materiales nanocompuestos utilizados en envasado alimentario. En los últimos años se han desarrollado otros mecanismos para la mejora de la compatibilidad de los nano-refuerzos celulósicos con las matrices poliméricas. Ellos se basan fundamentalmente en el desarrollo de un material nanocompuesto inicial con elevada concentración del nano-refuerzo (lo que se conoce como “masterbatch”), el cual se diluye posteriormente en estado fundido con el polímero. Este masterbatch inicial puede ser desarrollado utilizando diferentes tecnologías como mezclado en disolución, electroestirado (o “electrospinning”) o polimerización *in situ*, consiguiendo a través de esta última metodología injertar cadenas de polímero en la superficie de la celulosa. Utilizando estas estrategias se ha conseguido mejorar la dispersión de CNW en matrices como el PLA [76, 77, 115, 120, 121] o el PCL [122].

Además de las estrategias mencionadas, con el fin de obtener una buena dispersión de los nanocristales de celulosa en las matrices poliméricas por mezclado en fundido, conviene resaltar que, tal y como se ha demostrado previamente, éstos nano-refuerzos deben ser utilizados parcialmente hidratados en lugar de liofilizados o secados [123]. Como ya se ha comentado, durante los procesos de secado se establecen fuertes enlaces de hidrógeno entre las cadenas de celulosa, causando la autoasociación de las mismas y dificultando en gran medida su redispersión. En esta línea, recientemente se ha reportado una mejora de la dispersión de nano-refuerzos de celulosa en el interior de PLA preparados por extrusión, utilizando un plastificante como coadyuvante y alimentando la celulosa en medio líquido [17].

3.3.2. *Nanocompuestos de grafeno*

Ha sido previamente comentado que los procedimientos más conocidos y utilizados para el desarrollo de nanocompuestos poliméricos son mezclado en disolución, polimerización *in situ* y mezclado en fundido [82, 91, 124]. Los dos primeros constituyen las rutas más utilizadas para preparar nanocompuestos poliméricos basados en grafeno, fundamentalmente debido a cuestiones de dispersión, ya que se han obtenido buenos resultados mediante esas metodologías [91]. Por ejemplo, Kim et al. dispersaron grafeno dentro de poliuretano (PU) mediante mezclado en disolución, polimerización *in situ* y mezclado en fundido [125]. La incorporación mediante mezclado en disolución así como mediante polimerización *in situ* resultó en mejor dispersión del grafeno que mediante mezclado en fundido. Además, mediante mezclado en disolución, el grafeno y sus derivados han sido incorporados a matrices poliméricas y biopoliméricas como PVA [86, 126, 127], PE [128], PS [88], PLA [89, 129] y PHBV [55, 130], entre otros. De igual forma, mediante polimerización *in situ* también se han incorporado grafenos en diferentes matrices como poliamida-6 (PA6) [131], PE [132] y PLA [133]. Sin embargo el uso de polimerización *in situ* requiere unidades de monómeros así como gran cantidad de reactivos necesarios para llevar a cabo la reacción, lo cual resulta en menor aplicabilidad para los polímeros existentes en la naturaleza [92, 93]. Por otro lado, para el uso del mezclado en disolución como estrategia para incorporar grafenos o sus derivados en el interior de matrices de polímeros, los disolventes comunes más adecuados son agua, acetona, cloroformo, tetrahidrofurano, dimetil formamida y tolueno, en los cuales se establecen menos fuerzas entre las láminas de grafeno evitando su apilamiento [92]. Sin embargo, como ya se ha mencionado previamente, este método de desarrollo de nanocompuestos requiere grandes cantidades de disolventes, siendo además la eliminación del disolvente un aspecto crítico en los materiales obtenidos por esta vía [92].

Por el contrario, el mezclado en fundido, es la metodología más atractiva para el desarrollo de nanocompuestos poliméricos, como se ha dicho anteriormente, ya que no precisa del uso de reactivos ni de disolventes, es una técnica simple y escalable industrialmente, siendo por tanto de mayor viabilidad económica y medioambiental [79, 124]. Sin embargo, generalmente el uso del mezclado en fundido para la obtención de nanocompuestos de grafeno resulta en una dispersión inferior a la obtenida mediante otras rutas. A pesar de ello, el mezclado en fundido puede ser utilizado como técnica de post-tratamiento después de una primera incorporación del filler en las matrices poliméricas a

elevada concentración, similar a lo comentado anteriormente para el caso de los CNW. Diferentes trabajos se han reportado utilizando esta estrategia de incorporación [91, 134-136], donde una etapa previa al mezclado en fundido fue precisa para alcanzar una buena dispersión del grafeno, o sus derivados, en la matriz de polímero.

Además de las estrategias de pre-incorporación, nanocomposites basados en grafeno han sido también sintetizados por ball milling ya que esta ruta de molienda de elevada energía induce la delaminación del estructuras de grafito en multicapas mejorando las propiedades finales del material [101]. Otra ventaja de esta tecnología es que no requiere disolventes y que se realiza en un solo paso. Tal y como se ha reportado previamente, enlaces covalentes entre poliestireno y nanoláminas de grafeno se obtuvieron usando ball milling, demostrando de esta forma el carácter mecano-químico de esta técnica [95]. La incorporación de grafeno en el interior de sulfuro de polifenileno (PPS) mediante ball milling condujo a mejoras de las propiedades mecánicas, eléctricas y de barrera [137]. A pesar de ello esta tecnología no había sido usada para el desarrollo de nanocompuestos de matrices biopoliméricas, trabajo que se ha desarrollado durante la presente tesis doctoral.

Resumiendo, parece ser que la pre-incorporación de las nanocargas, ya sean CNW o grafenos, mediante el uso de distintas tecnologías previo al mezclado en fundido con matrices poliméricas es una buena estrategia para mejorar la dispersión final de esas nanocargas, con especial interés en los CNW ya que incrementa su compatibilidad con matrices hidrofóbicas no polares. Sin embargo, aunque esta estrategia ha demostrado ser eficiente para mejorar las propiedades finales de los materiales, su uso en matrices biopoliméricas no ha sido extensamente estudiado, especialmente cuando grafenos o nanocristales de celulosa bacteriana (BCNW) son usados como nanocargas, aunque un elevado número de estudios se han publicado en los últimos años, en su mayoría sobre el la incorporación de CNW en biopolímeros. A pesar de ello, en muchos casos el efecto que la incorporación de las nanocargas tiene sobre las propiedades barreras de los nanobiocompuestos obtenidos no ha sido ampliamente estudiado o reportado y, como ya se ha dicho anteriormente, las propiedades barreras juega un papel muy importante en aquellos materiales que van a ser utilizados en aplicaciones de envasado de alimentos.

Por tanto, estudios orientados hacia la mejora de propiedades de matrices biopoliméricas mediante la incorporación de nanoaditivos como BCNW o grafenos utilizando tecnologías novedosas, eficientes y utilizadas a nivel industrial, y que garanticen una correcta dispersión de los nanoaditivos en matrices poliméricas deben ser llevados acabo. Además, la evaluación del efecto de la incorporación de los nanoaditivos sobre las propiedades finales, especialmente las propiedades barreras, debe ser también realizada. Con ello se podrían obtener materiales biodegradables y de origen renovable que puedan competir con mayor ventaja a la hora de ser utilizados en aplicaciones de envasado de alimentos.

Adicionalmente, el desarrollo de tecnologías que involucren una reducción en el uso de disolventes orgánicos durante la incorporación de las nanocargas en el interior de matrices poliméricas sería de interés debido a los inconvenientes asociados a su uso, siendo además de especial importancia en aplicaciones de envasado alimentario. Es importante destacar que para la mayoría de los estudios detallados anteriormente, donde una pre-incorporación de las nanocargas previa al mezclado en fundido se establecía como una buena estrategia alcanzándose buena dispersión del nanoaditivo, en el propio proceso de pre-incorporación se requerían considerables cantidades de disolventes orgánicos para dispersar dicho

nanoaditivo. Por otro lado, el agua es uno de los medios más adecuados para la incorporación de grafenos como nanocargas y además es el medio idóneo para preparar nanocompuestos de CNW, ya que las suspensiones acuosas de CNW son mucho más estables que suspensiones en disolventes orgánicos. Por tanto, métodos de incorporación o pre-incorporación compatibles con medios acuosos podrían resultar, en principio, más idóneos a la hora de incorporar tales nanocargas en el interior de polímeros. El uso de suspensiones acuosas de celulosa tiene varias ventajas: evitar la auto-asociación de la misma, mayor estabilidad de la celulosa en este disolvente y evitar la necesidad de tratamientos adicionales como intercambios de disolventes. Además, el desarrollo y optimización de sistemas de incorporación de estos tipos de nano-refuerzos mediante estrategias libres de disolventes, donde se consigan elevados rendimientos en cuanto a dispersión, serían también interesantes desde un punto de vista industrial. Todos estos aspectos han sido abordados en la presente tesis doctoral.

4. EL TRANSPORTE DE MASA. PROPIEDADES

El transporte de moléculas de bajo peso molecular a través de películas o films poliméricos se conoce como permeación. La fuerza impulsora para el transporte de masa es el gradiente de concentraciones entre los dos ambientes separados por dichos materiales. La sustancia de bajo peso molecular que atraviesa el film se conoce como permeante y el fenómeno se caracteriza generalmente por el coeficiente de permeabilidad (P). El mecanismo de permeabilidad implica varias etapas como la entrada del permeante en el polímero mediante un proceso de absorción inicial en el lado de elevada concentración, su difusión a través del polímero y su desorción final en el lado de baja concentración del compuesto (ver Figura 16). Con todo ello, la permeabilidad depende, en primera medida, de la solubilidad inicial de las moléculas permeantes en el polímero y, posteriormente, de su difusión a través del mismo. Por lo tanto, para poder actuar sobre el coeficiente de permeabilidad de cualquier material, habrá que modificar el coeficiente de solubilidad y/o el coeficiente de difusión a través de la matriz polimérica.

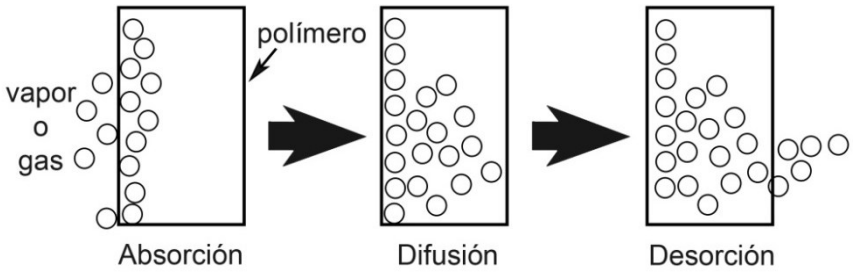

Figura 16. Mecanismo de la permeabilidad

Excesos de humedad, compuestos orgánicos y oxígeno pueden causar fácilmente su deterioro de los alimentos afectando a la calidad del producto y a su vida útil [109]. Reacciones químicas, cambios sensoriales o cambios morfológicos en los productos sensibles al agua son sólo algunos ejemplos de los efectos negativos que puede causar la transferencia de masa. Además, la pérdida de componentes de los alimentos, como pérdida de aromas, o la

absorción de componentes del alimento por parte de los materiales del envase, proceso denominado sorción, también puede causar cambios drásticos en la calidad de los productos.

En la Figura 17 puede observarse los diferentes fenómenos de transporte de masas que pueden tener lugar en los sistemas alimento / envase / entorno. Así, otro fenómeno de transporte que puede tener lugar es la migración de elementos del envase hacia el alimento, la cual es considerada como un problema negativo porque muchas sustancias representan peligro hacia la salud o modifican la composición de los alimentos provocando por tanto cambios organolépticos e incluso derivar en problemas de toxicidad de los alimentos [109]. Los compuestos que normalmente migran en envases alimentarios incluyen monómeros residuales, aditivos de procesado y moléculas que han sido absorbidas por el envase durante su uso previo o durante el proceso de reciclado.. Por ello, la migración se ha convertido en un fenómeno de elevada importancia en cuanto al desarrollo y aplicación de leyes para el envasado de alimentos en muchos países como el Reglamento Europeo EU 1935/2004 sobre los materiales y objetos destinados a entrar en contacto con alimentos [138].

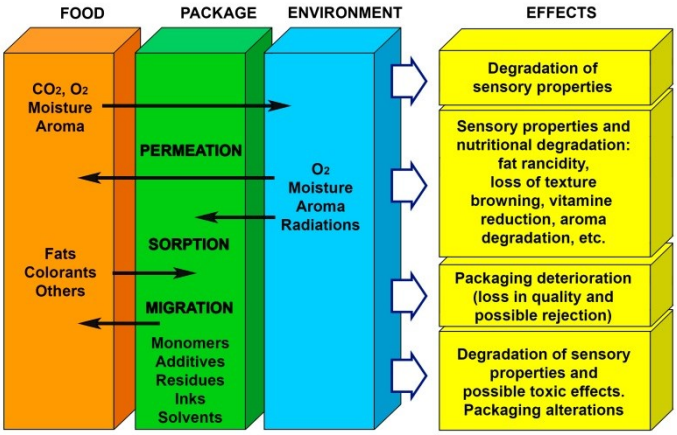

Figura 17. Mecanismos de transporte de masa y sus efectos en productos alimenticios

Aún así, el proceso de migración puede ser usado como agente de liberación controlada de sustancias hacia el alimento, las cuales se añaden intencionadamente al envase con el objetivo de que posteriormente sean liberadas hacia el producto de manera controlada. De ello hacen uso los denominados envases activos.

4.1. Factores que influyen en las propiedades de transporte de masa

4.1.1. *El polímero*

La composición y estructura química de los polímeros es el factor principal en la definición de sus propiedades de barrera y está relacionado, en gran medida, con las diferencias en la permeabilidad de cada tipo de polímero. Así, variando la química del

polímero, a menudo ajustando el grupo "colgante" a lo largo de la cadena polimérica, una variación significativa en las propiedades barrera de hasta seis órdenes de magnitud puede obtenerse. Como ejemplo, el PP, donde el grupo "colgante" de la cadena principal es el grupo metilo ($-CH_3$), tienen una permeabilidad al oxígeno 15000 veces superior que el PVOH, donde el grupo "colgante" es el grupo hidroxilo (–OH) [139]. En la siguiente tabla se muestran a modo de ejemplo algunos de los valores de permeabilidad al oxígeno y al vapor de agua de diferentes polímeros tanto convencionales como biodegradables.

Tabla 2. Valores de permeabilidad al agua y al oxígeno de diferentes polímeros (adaptada de Lagarón et al. [139]).

Material	P water (x 10^{18}) Kg m m^{-2} s Pa	P oxygen (x 10^{21}) m^3 m m^{-2} s Pa	
		0 % RH	80 % RH
EVOH	17000	0.77	91
PET	2300	135	
PP	726	6750	
LDPE	1200	21500	
PLA	12600	2250	2209
PHBV	6900	1590	3010
PCL	26600	4380	7850

Se considera que el transporte de sustancias de bajo peso molecular se lleva a cabo únicamente a través de la fase amorfa de los polímeros semicristalinos, donde las interacciones intermoleculares son producidas principalmente por fuerzas secundarias, como fuerzas de Van der Waals o puentes de hidrógeno. Por lo tanto, la naturaleza de estos grupos presentes en la estructura química influye en las interacciones intermoleculares, aumentándolas o disminuyéndolas, jugando un papel determinante en el transporte de compuestos de bajo peso molecular a través del polímero. Por ejemplo polímeros con grupos químicos de interacción fuerte como grupos polares (OH o CN), suelen tener valores de permeabilidad al oxígeno bajas en condiciones de baja humedad relativa, mientras que polímeros con grupos apolares tiene propiedades barreras más pobres. Además, la naturaleza química de los polímeros define la afinidad entre las potenciales moléculas permeantes y la matriz polimérica. Una baja solubilidad de la molécula permeante en la matriz polimérica debido a baja afinidad química dará como resultado una permeabilidad baja.

Existen dos parámetros estrechamente relacionados con las propiedades barreras de los materiales poliméricos. Por un lado la energía de cohesión, que es una medida de la energía interna de una sustancia relacionada con la fuerza de la interacción entre las moléculas y con los cambios en esas interacciones que tienen lugar cuando diferentes grupos químicos se añaden a la cadena polimérica. Por otro lado el volumen libre da información acerca de las microcavidades presentes en los materiales poliméricos, las cuales son usadas por las moléculas permeantes para difundir a través de la matriz. Este parámetro también está fuertemente relacionado con la naturaleza química de los polímeros ya que grupos más voluminosos dejan un mayor volumen libre en el material polimérico. Además, el volumen libre también está relacionado con la historia térmica, la temperatura de transición vítrea (T_g), cristalinidad, etc.

Así, para una elevada eficiencia de los polímeros en barrera a gases y vapores, elevada energía de cohesión así como bajo volumen libre son necesarios.

4.1.2. *Morfología de polímeros*

Muchos materiales poliméricos usados en aplicaciones de envasado de alimentos tienen naturaleza semicristalina, y por tanto, son materiales heterogéneos desde un punto de vista estructural. En estos casos, los polímeros contienen una fracción con segmentos de cadenas poliméricas altamente ordenados formando estructuras en tres dimensiones (fracción cristalina del polímero) así como otras fracciones en estado amorfo sin ningún orden. Es ampliamente conocido que los cristales en las matrices poliméricas son impermeables al transporte de la mayoría de compuestos de bajo peso molecular. Así, se puede decir que la matriz polimérica se considera como una estructura amorfa llena de cristales impermeables. El tamaño, la orientación y forma de los cristales afecta al transporte a través de la matriz. A medida que aumenta la fracción cristalina, los cristales constriñen el movimiento de la fracción no cristalina, reduciendo su movilidad, que llega a ser menor que en las regiones amorfas no rodeadas de cristales o que en polímeros totalmente amorfos [140]. En la Figura 18 puede observarse un modelo esquemático de estos tipos de materiales. De hecho, es ampliamente conocido que un incremento en la fracción cristalina de polímeros semicristalinos está relacionada con una mejora en las propiedades de barrera debido principalmente a la tortuosidad asociada a la presencia de dominios cristalinos [141-144].

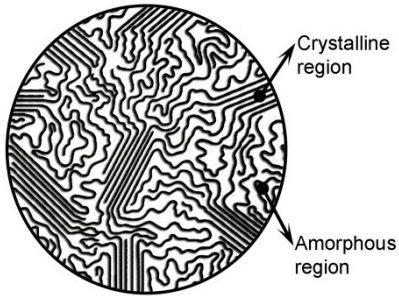

Figura 18. Morfología de polímeros semicristalinos

La fracción cristalina se ve afectada por la historia térmica del polímero, es decir, puede ser modificada según las condiciones de procesado térmico, el cual puede ser optimizado para mejorar las propiedades barreras del material polimérico.

4.1.3. *Nanocargas y aditivos*

La adición de nanocargas y aditivos en el interior de matrices poliméricas pueden tener un efecto sobre las propiedades de barrera. Ese efecto depende, entre otras cosas, de la naturaleza de la carga, su grado de adhesión y la compatibilidad con el polímero. La adición de nanocargas impermeables a matrices poliméricas, por lo general conduce, entre otros cambios, a una disminución en el coeficiente de difusión, que es debida al aumento en la tortuosidad del camino a seguir por las moléculas permeantes para pasar a través el polímero [145], como puede observarse en la Figura 19.

En el caso de nanocargas laminares, para conseguir una mejora óptima de las propiedades barrera del material, además de una buena dispersión, se considera que las mismas deben estar orientadas perpendicularmente a la dirección de transporte. Además, la introducción de este tipo de cargas dentro de la región amorfa, por lo general, puede conducir a efectos similares a la presencia de cristales, es decir, la reducción de la movilidad de las cadenas.

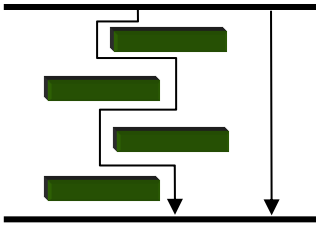

Figura 19. Efecto de tortuosidad sobre el transporte de compuestos de bajo peso molecular mediante la adición de nanocargas.

Sin embargo, cuando las nanocargas son de naturaleza hidrofílica aumenta la cantidad de agua y de otros compuestos polares absorbidos, lo cual tendrá también un efecto en las propiedades de transporte de ciertos permeantes. Por otro lado, cuando la afinidad entre el polímero y los refuerzos no es buena, aumenta el volumen libre del material resultante. En ambos casos tiene lugar una reducción en las propiedades de barrera del polímero.

4.1.4. *Temperatura*

Es bien sabido que la temperatura afecta a muchas de las propiedades de los polímeros. Los cambios en las propiedades barrera inducidos por la temperatura son de carácter exponencial, ya que los coeficientes de difusión y solubilidad, que son los dos fenómenos principales que afectan a la permeabilidad, aumentan exponencialmente con la temperatura de acuerdo con le ley de Arrhenius (ecuación 1) y la ley de Van´t Hoff, (ecuación 2) respectivamente, ya que tanto la energía de activación (E_D) o la entalpía de disolución (ΔH_S) son siempre valores positivos.

$$D = D_0 \exp\left(\frac{-E_D}{RT}\right) \quad \text{Ecuación 1}$$

$$S = S_0 \exp\left(\frac{-\Delta H_S}{RT}\right) \quad \text{Ecuación 2}$$

Este fenómeno está relacionado con la mayor movilidad de las cadenas de polímero a temperaturas más altas, lo cual reduce la energía necesaria de las moléculas permeantes para saltar de una posición a otra, conduciendo además a un aumento en el volumen libre del polímero.

La temperatura también afecta al estado físico de los polímeros, afectando ello directamente a las propiedades de transporte. En el polímero fundido, las regiones cristalinas desaparecen y el transporte se lleva a cabo a través de toda la matriz, que se comporta como un líquido. En este caso, todo el volumen de polímero está disponible para las moléculas permeantes, las cuales aumentan su solubilidad. Además, el efecto de bloqueo de los cristales desaparece, lo que reduce la tortuosidad y hace más fácil la difusión, y las cadenas de polímeros están en constante movimiento, lo que facilita los saltos de las moléculas permeantes.

Los cambios asociados con la transición vítrea, es decir, con el paso del polímero de estado vítreo a estado gomoso, se producen como resultado de la relajación o el aumento de la movilidad de los segmentos de la cadena en la fase amorfa del polímero. Por encima de la temperatura de transición vítrea la fase amorfa del polímero está en estado gomoso, por debajo de esta temperatura se encuentra en el estado vítreo. En el estado gomoso, los tiempos de relajación son más cortos y, después de la absorción de las moléculas permeantes, un nuevo estado de equilibrio se alcanza más rápidamente. Como resultado, la difusión es más rápida cuando el polímero se encuentra en este estado.

4.1.5. *El permeante*

Las características de las moléculas permeantes, tales como el tamaño molecular, la forma y la naturaleza química, afectan a sus propiedades de transporte. El aumento del tamaño molecular de las moléculas permeantes, reduce sus coeficientes de difusión y solubilidad, principalmente por causas debidas a impedimento estérico. En cuanto a las formas de las moléculas permeantes, las moléculas planas o alargadas difundirán más rápido a través del polímero que las esféricas con el mismo volumen molecular [146].

La compatibilidad entre el permeante y la matriz polimérica también afecta a sus propiedades de transporte. Si la afinidad entre el permeante y el polímero es muy alta, a veces puede causar la plastificación del polímero. En este caso, la absorción conduce a una disminución en la asociación entre las cadenas poliméricas adyacentes en la región amorfa, es decir, los enlaces de hidrógeno y las fuerzas de van der Waals iniciales son reemplazados por interacciones polímeros-sorbatos, aumentando la movilidad de la cadena y el volumen libre, reduciendo la T_g y aumentando los coeficientes de difusión y de solubilidad de los permeantes.

Los alimentos envasados son sistemas complejos donde el material de envase está en contacto directo con diferentes moléculas permeantes. En estos casos se dan dos situaciones donde las propiedades de transporte pueden ser afectadas:

a) Las propiedades de transporte de un permeante se ve a menudo afectada por la presencia del resto debido a que compiten por los espacios libres en la matriz polimérica para poder difundir a través de ella.

b) Algunas moléculas permeantes, una vez absorbidas, actúan de co-solventes para el resto. Por ejemplo, el agua es el principal componente de muchos alimentos y también con frecuencia actúa de co-solvente. En polímeros hidrofílicos como los copolímeros de EVOH, la plastificación inducida por el agua a altos niveles de

humedad aumenta la permeabilidad a compuestos hidrofóbicos y apolares como el limoneno y el oxígeno afectando, por tanto, negativamente a las propiedades barrera del material [147, 148].

5. LEGISLACIÓN EN EL MARCO DEL ENVASADO DE ALIMENTOS.

Según la Agencia Española de Consumo, Seguridad Alimentaria y Nutrición (AECOSAN), los materiales y objetos en contacto con alimentos son todos aquellos que estén:

- Destinados a entrar en contacto con alimentos,
- Ya en contacto con alimentos y estén destinados a tal efecto,
- De los que quepa esperar razonablemente que entrarán en contacto con alimentos o que transferirán sus componentes a los alimentos en condiciones normales o previsibles de empleo.

Cuando nos referimos a estos materiales hablamos de: adhesivos, cerámica, corcho, caucho, vidrio, resinas de intercambio iónico, metales y aleaciones, papel y cartón, plásticos, tintas de imprenta, celulosa regenerada, siliconas, productos textiles, barnices y revestimientos, ceras, madera y materiales y objetos activos e inteligentes.

Los materiales en contacto con alimentos están regulados en toda la Unión Europea por el Reglamento EU 1935/2004, de 27 de octubre de 2004, del Parlamento Europeo y del Consejo, sobre los materiales y objetos destinados a entrar en contacto con alimentos y por el que se derogan las Directivas 80/590/CEE y 89/109/CEE, de manera que se garantiza que todos los materiales que se ponen en el territorio comunitario cumplen los mismos requisitos de calidad [138].

Todos los materiales y objetos destinados a entrar en contacto con alimentos deben fabricarse de conformidad con las Buenas Prácticas de Fabricación, recogidas en el Reglamento EU 2023/2006, de 22 de diciembre de 2006, de la Comisión, sobre buenas prácticas de fabricación de materiales y objetos destinados a entrar en contacto con alimentos [149], para que, en las condiciones normales o previsibles de empleo, no transfieran sus componentes a los alimentos en cantidades que puedan:

- Representar un peligro para la salud humana,
- Provocar una modificación inaceptable de la composición de los alimentos, o
- Provocar una alteración de las características organolépticas de éstos.

Aparte de la existencia de estos dos reglamentos, algunos materiales disponen de legislación armonizada específica que, tomando como base el Reglamento EU 1935/2004, define los requisitos especiales de los mismos. Entre los materiales regulados por disposiciones específicas, los materiales plásticos están regulados por el Reglamento EU 10/2011 [150].

Todos los materiales plásticos que se comercialicen en la Unión Europea deberán de ser conformes, además de con su normativa específica (Reglamento EU 10/2011), con lo

dispuesto en el Reglamento EU 1935/2004 que recoge los requisitos generales a cumplir por los materiales y objetos destinados a entrar en contacto con los alimentos.

En la fabricación de capas plásticas de materiales y objetos plásticos únicamente pueden utilizarse sustancias autorizadas. Estas sustancias se incluyen en una lista comunitaria positiva, que se establece en el anexo I del Reglamento EU 10/2011 y que está formada por: monómeros o sustancias de partida, aditivos (se excluyen los colorantes), auxiliares para la producción (excepto los disolventes) y macromoléculas obtenidas por fermentación microbiana.

Los materiales y objetos plásticos no deben ceder sus constituyentes a los alimentos en cantidades superiores a las establecidas. Para ello, se establecen límites de migración específica, para determinadas sustancias, y límites de migración global, así como los ensayos de migración para demostrar la conformidad del material.

Recientemente se ha publicado un nuevo Reglamento EU 2015/174 [151], por el que se modifica y corrige el Reglamento EU 10/2011, sobre materiales y objetos plásticos destinados a entrar en contacto con alimentos. En este nuevo Reglamento se recoge la inclusión de nuevas sustancias que cuentan con una opinión positiva por parte de la Autoridad Europea de Seguridad Alimentaria (EFSA de sus siglas en inglés European Food Safety Authority), así como la modificación y corrección de restricciones para ciertas sustancias ya presentes en el anexo del Reglamento.

En el anexo I del Reglamento EU 10/2011 aparecen como materiales aprobados para contacto alimentario el ácido láctico como monómero (sustancia número 99), así como el PHBV (sustancia número 744).

En la propia Regulación EU 10/2011 aparece que las nuevas tecnologías permiten obtener sustancias en partículas que, por su tamaño, muestran propiedades químicas y físicas netamente diferentes de las observadas a gran escala, como es el caso de las nanopartículas. Estas diferentes propiedades pueden implicar propiedades toxicológicas distintas, por lo cual la Autoridad competente debe evaluar caso por caso el riesgo que estas sustancias presentan, a la espera de que se conozca más información sobre esas nuevas tecnologías. Por tanto, debe quedar claro que las autorizaciones basadas en la evaluación de riesgos de las sustancias en partículas de tamaños convencionales no incluyen las nanopartículas fabricadas. De hecho, ha sido elaborada una guía por parte de la EFSA para la evaluación de los riesgos potenciales derivados de las aplicaciones de la nanociencia y la nanotecnología a los alimentos [152].

Por lo tanto, aunque el grafito y la celulosa aparezcan en la lista como materiales para estar en contacto con alimentos (sustancias número 521 y 553 respectivamente), sus derivados nanoestructurados deberían de ser evaluados por la Autoridad competente antes de poder ser puestos en contacto con alimentos.

REFERENCES / REFERENCIAS

[1] Monsivais P, Aggarwal A, Drewnowski A. (2014) Time spent on home food preparation and indicators of healthy eating. American Journal of Preventive Medicine 47(6):796-802.

[2] Nickels WG, Jolson MA. (1976) PACKAGING - THE FIFTH ″P″ IN THE MARKETING MIX? SAM Adv Manage J 41(1):13-21.

[3] Luijsterburg B, Goossens H. (2014) Assessment of plastic packaging waste: Material origin, methods, properties. Resources, Conservation and Recycling 85:88-97.

[4] Gross RA, Kalra B. (2002) Biodegradable polymers for the environment. Science 297(5582):803-807.

[5] González García Y, Meza Contsrerass JC, González Reynoso O, Córdova López JA. (2013) Synthesis and degradation of polyhydroxyalkanoates: Plastic microbial. Revista Internacional de Contaminacion Ambiental 29(1):77-115.

[6] Song J, Kay M, Coles R. Bioplastics. Food and Beverage Packaging Technology: Second Edition2011. p. 295-319.

[7] ASTM International, W. C., PA (2010) ASTM Standard D996-10a, 2010, "Standard Terminology of Packaging and Distribution Environments" DOI: 10.1520/D0996-10A

[8] Soulestin J, Prashantha K, Lacrampe MF, Krawczak P. Bioplastics Based Nanocomposites for Packaging Applications. Handbook of Bioplastics and Biocomposites Engineering Applications: John Wiley & Sons, Inc.; 2011. p. 76-119.

[9] Petersen K, Væggemose Nielsen P, Bertelsen G, Lawther M, Olsen MB, Nilsson NH, et al. (1999) Potential of biobased materials for food packaging. Trends in Food Science and Technology 10(2):52-68.

[10] Roy I, Philip S. Polyhydroxyalkanoates: A new generation of biotechnologically produced biodegradable polymers. Biodegradable Materials: Production, Properties and Applications2011. p. 173-215.

[11] Plackett D, Siró I. Polyhydroxyalkanoates (PHAs) for food packaging. In: Lagarón J-M, editor. Multifunctional and Nanoreinforced Polymers for Food Packaging: Woodhead Publishing; 2011. p. 498-526.

[12] Lagarón JM. Polylactic acid (PLA) nanocomposites for food packaging applications. In: Lagarón J-M, editor. Multifunctional and Nanoreinforced Polymers for Food Packaging: Woodhead Publishing; 2011. p. 485-497.

[13] P. Pawar R, U. Tekale S, U. Shisodia S, T. Totre J, J. Domb A. (2014) Biomedical Applications of Poly(Lactic Acid). Recent Patents on Regenerative Medicine 4(1):40-51.

[14] Madhavan Nampoothiri K, Nair NR, John RP. (2010) An overview of the recent developments in polylactide (PLA) research. Bioresource Technology 101(22):8493-8501.

[15] Jayaramudu J, Reddy GSM, Varaprasad K, Sadiku ER, Ray SS, Rajulu AV. (2013) Structure and properties of poly (lactic acid)/Sterculia urens uniaxial fabric biocomposites. Carbohydrate Polymers 94(2):822-828.

[16] Auras R, Harte B, Selke S. (2004) Effect of water on the oxygen barrier properties of poly(ethylene terephthalate) and polylactide films. Journal of Applied Polymer Science 92(3):1790-1803.

[17] Herrera N, Mathew AP, Oksman K. (2015) Plasticized polylactic acid/cellulose

nanocomposites prepared using melt-extrusion and liquid feeding: Mechanical, thermal and optical properties. Composites Science and Technology 106:149-155.

[18] Petersen K, Nielsen PV, Olsen MB. (2001) Physical and mechanical properties of biobased materials - Starch, polylactate and polyhydroxybutyrate. Starch/Staerke 53(8):356-361.

[19] Siracusa V, Rocculi P, Romani S, Rosa MD. (2008) Biodegradable polymers for food packaging: a review. Trends in Food Science and Technology 19(12):634-643.

[20] Simoes CL, Viana JC, Cunha AM. (2009) Mechanical properties of poly(ε-caprolactone) and poly(lactic acid) blends. Journal of Applied Polymer Science 112(1):345-352.

[21] Courgneau C, Domenek S, Lebossé R, Guinault A, Avérous L, Ducruet V. (2012) Effect of crystallization on barrier properties of formulated polylactide. Polymer International 61(2):180-189.

[22] Sanchez-Garcia MD, Lagaron JM. (2010) On the use of plant cellulose nanowhiskers to enhance the barrier properties of polylactic acid. Cellulose 17(5):987-1004.

[23] Gupta AP, Kumar V. (2007) New emerging trends in synthetic biodegradable polymers - Polylactide: A critique. European Polymer Journal 43(10):4053-4074.

[24] Auras R, Harte B, Selke S. (2004) An overview of polylactides as packaging materials. Macromolecular Bioscience 4(9):835-864.

[25] Moon SI, Lee CW, Miyamoto M, Kimura Y. (2000) Melt polycondensation of L-lactic acid with Sn(II) catalysts activated by various proton acids: A direct manufacturing route to high molecular weight poly(L-lactic acid). Journal of Polymer Science, Part A: Polymer Chemistry 38(9):1673-1679.

[26] Garlotta D. (2001) A literature review of poly(lactic acid). Journal of Polymers and the Environment 9(2):63-84.

[27] Södergård A, Stolt M. Industrial Production of High Molecular Weight Poly(Lactic Acid). Poly(Lactic Acid): John Wiley & Sons, Inc.; 2010. p. 27-41.

[28] Enomoto K, Ajioka M, Yamaguchi A. Polyhydroxycarboxylic acid and preparation process thereof. Google Patents; 1994.

[29] Kashima T, Kameoka T, Higuchi C, Ajioka M, Yamaguchi A. Aliphatic polyester and preparation process thereof. Google Patents; 1995.

[30] Ichikawa F, Kobayashi M, Ohta M, Yoshida Y, Obuchi S, Itoh H. Process for preparing polyhydroxycarboxylic acid. Google Patents; 1995.

[31] Ohta M, Obuchi S, Yoshida Y. Dehydrating polycondensation of lactic acid. Google Patents; 1995.

[32] Kricheldorf HR. (2001) Syntheses and application of polylactides. Chemosphere 43(1):49-54.

[33] Hile DD, Pishko MV. (1999) Ring-opening precipitation polymerization of poly(D,L-lactide-co-glycolide) in supercritical carbon dioxide. Macromolecular Rapid Communications 20(10):511-514.

[34] Slomkowski S, Penczek S, Duda A. (2014) Polylactides-an overview. Polymers for Advanced Technologies 25(5):436-447.

[35] Vink ETH, Rábago KR, Glassner DA, Gruber PR. (2003) Applications of life cycle assessment to NatureWorks™ polylactide (PLA) production. Polymer Degradation and Stability 80(3):403-419.

[36] Braun B, Dorgan JR, Knauss DM. (2006) Reactively compatibilized cellulosic polylactide microcomposites. Journal of Polymers and the Environment 14(1):49-58.

[37] Kim HK, Kim SJ, Lee HS, Choi JH, Jeong CM, Sung MH, et al. (2012) Mechanical and barrier properties of poly(lactic acid) films coated by nanoclay-ink composition. Journal of Applied Polymer Science 127(5):3823-3829.

[38] Park SH, Lee HS, Choi JH, Jeong CM, Sung MH, Park HJ. (2012) Improvements in barrier properties of poly(lactic acid) films coated with chitosan or chitosan/clay nanocomposite. Journal of Applied Polymer Science 125(SUPPL. 1):E675-E680.

[39] Svagan AJ, Åkesson A, Cárdenas M, Bulut S, Knudsen JC, Risbo J, et al. (2012) Transparent films based on PLA and montmorillonite with tunable oxygen barrier properties. Biomacromolecules 13(2):397-405.

[40] Martucci JF, Ruseckaite RA. (2010) Three-layer sheets based on gelatin and poly(lactic acid), part 1: Preparation and properties. Journal of Applied Polymer Science 118(5):3102-3110.

[41] Busolo MA, Torres-Giner S, Laaron JM. Enhancing the gas barrier properties of polylactic acid by means of electrospun ultrathin zein fibers. 2009. p. 2763-2767.

[42] Razavi SM, Dadbin S, Frounchi M. (2012) Oxygen-barrier properties of poly(lactic acid)/poly(vinyl acetate-co-vinyl alcohol) blends as biodegradable films. Journal of Applied Polymer Science 125(SUPPL. 2):E20-E26.

[43] Perego G, Cella GD. Mechanical Properties. Poly(Lactic Acid): John Wiley & Sons, Inc.; 2010. p. 141-153.

[44] Almenar E, Auras R. Permeation, Sorption, and Diffusion in Poly(Lactic Acid). Poly(Lactic Acid): John Wiley & Sons, Inc.; 2010. p. 155-179.

[45] Siracusa V. (2012) Food packaging permeability behaviour: A report. International Journal of Polymer Science 2012.

[46] Lee SY, Choi JI, Wong HH. (1999) Recent advances in polyhydroxyalkanoate production by bacterial fermentation: Mini-review. International Journal of Biological Macromolecules 25(1-3):31-36.

[47] Gonzalez-Lopez J, Pozo C, Martinez-Toledo MV, Rodelas B, Salmeron V. (1996) Production of Polyhydroxyalkanoates by Azotobacter chroococcum H23 in Wastewater from Olive Oil Mills (Alpechin). International Biodeterioration and Biodegradation 38(3-4):271-276.

[48] Martínez-Sanz M, Villano M, Oliveira C, Albuquerque MGE, Majone M, Reis M, et al. (2014) Characterization of polyhydroxyalkanoates synthesized from microbial mixed cultures and of their nanobiocomposites with bacterial cellulose nanowhiskers. New Biotechnology 31(4):364-376.

[49] Pardo-Ibáñez P, Lopez-Rubio A, Martínez-Sanz M, Cabedo L, Lagaron JM. (2014) Keratin-polyhydroxyalkanoate melt-compounded composites with improved barrier properties of interest in food packaging applications. Journal of Applied Polymer Science 131(4).

[50] Yoshie N, Azuma Y, Sakurai M, Inoue Y. (1995) Crystallization and compatibility of poly(vinyl alcohol)/poly(3-hydroxybutyrate) blends: influence of blend composition and tacticity of poly(vinyl alcohol). Journal of Applied Polymer Science 56(1):17-24.

[51] Roa JPB, De O. Patrício PS, Oréfice RL, Lago RM. (2013) Improvement of the thermal properties of poly(3-hydroxybutyrate) (PHB) by low molecular weight polypropylene glycol (LMWPPG) addition. Journal of Applied Polymer Science 128(5):3019-3025.

[52] Hinüber C, Häussler L, Vogel R, Brünig H, Heinrich G, Werner C. (2011) Hollow fibers made from a poly(3-hydroxybutyrate)/poly-ε-caprolactone blend. Express Polymer Letters 5(7):643-652.

[53] de Smet MJ, Eggink G, Witholt B, Kingma J, Wynberg H. (1983) Characterization of intracellular inclusions formed by Pseudomonas oleovorans during growth on octane. Journal of Bacteriology 154(2):870-878.

[54] Gumel AM, Annuar MSM, Chisti Y. (2013) Recent Advances in the Production, Recovery and Applications of Polyhydroxyalkanoates. Journal of Polymers and the Environment 21(2):580-605.

[55] Sridhar V, Lee I, Chun HH, Park H. (2013) Graphene reinforced biodegradable poly(3-hydroxybutyrate-co-4-hydroxybutyrate) nano-composites. Express Polymer Letters 7(4):320-328.

[56] Guinault A, Sollogoub C, Domenek S, Grandmontagne A, Ducruet V. (2010) Influence of crystallinity on gas barrier and mechanical properties of pla food packaging films. International Journal of Material Forming 3(SUPPL. 1):603-606.

[57] Drieskens M, Peeters R, Mullens J, Franco D, Iemstra PJ, Hristova-Bogaerds DG. (2009) Structure versus properties relationship of poly(lactic acid). I. effect of crystallinity on barrier properties. Journal of Polymer Science, Part B: Polymer Physics 47(22):2247-2258.

[58] Khanna S, Srivastava AK. (2005) A simple structured mathematical model for biopolymer (PHB) production. Biotechnology Progress 21(3):830-838.

[59] Raquez JM, Habibi Y, Murariu M, Dubois P. (2013) Polylactide (PLA)-based nanocomposites. Progress in Polymer Science 38(10-11):1504-1542.

[60] Ramanathan T, Abdala AA, Stankovich S, Dikin DA, Herrera-Alonso M, Piner RD, et al. (2008) Functionalized graphene sheets for polymer nanocomposites. Nature Nanotechnology 3(6):327-331.

[61] Móczó J, Pukánszky B. (2008) Polymer micro and nanocomposites: Structure, interactions, properties. Journal of Industrial and Engineering Chemistry 14(5):535-563.

[62] Sorrentino A, Gorrasi G, Vittoria V. (2007) Potential perspectives of bio-nanocomposites for food packaging applications. Trends in Food Science & Technology 18(2):84-95.

[63] Arora A, Padua GW. (2010) Review: Nanocomposites in food packaging. Journal of Food Science 75(1):R43-R49.

[64] Pereira Ramos L. (2003) The chemistry involved in the steam treatment of lignocellulosic materials. Quimica Nova 26(6):863-871.

[65] Azizi Samir MAS, Alloin F, Dufresne A. (2005) Review of recent research into cellulosic whiskers, their properties and their application in nanocomposite field. Biomacromolecules 6(2):612-626.

[66] Lavoine N, Desloges I, Dufresne A, Bras J. (2012) Microfibrillated cellulose – Its barrier properties and applications in cellulosic materials: A review. Carbohydrate Polymers 90(2):735-764.

[67] Marta M-S, Amparo L-R, JoséMaría L. Cellulose Nanowhiskers: Properties and Applications as Nanofillers in Nanocomposites with Interest in Food Biopackaging Applications. Ecosustainable Polymer Nanomaterials for Food Packaging: CRC Press; 2013. p. 195-220.

[68] Habibi Y, Lucia LA, Rojas OJ. (2010) Cellulose nanocrystals: Chemistry, self-assembly, and applications. Chemical Reviews (Washington, DC, United States) 110(6):3479-3500.

[69] Mariano M, El Kissi N, Dufresne A. (2014) Cellulose nanocrystals and related nanocomposites: Review of some properties and challenges. Journal of Polymer Science, Part B: Polymer Physics 52(12):791-806.

[70] Shoda M, Sugano Y. (2005) Recent advances in bacterial cellulose production. Biotechnology and Bioprocess Engineering 10(1):1-8.

[71] PACHECO JLCY, Suri Martinez; ZENTELLA, Martha Contreras; MARVÁN, Edgardo Escamilla. Celulosa Bacteriana en Gluconacetobacter xylinum: Biosíntesis y Aplicaciones. Revista Especializada en Ciencias Químico-Biológicas2004. p. 18-25.

[72] Iguchi M, Yamanaka S, Budhiono A. (2000) Bacterial cellulose - a masterpiece of nature's arts. Journal of Materials Science 35(2):261-270.

[73] Martínez-Sanz M, Lopez-Rubio A, Lagaron JM. (2011) Optimization of the nanofabrication by acid hydrolysis of bacterial cellulose nanowhiskers. Carbohydrate Polymers 85(1):228-236.

[74] Ping W, Yi S, Yuanyuan J, Jingtong Z, Zongliang W, Yanyan C, et al. Study on the feasibility of bacterial cellulose as tissue engineering scaffold. 2009. p. 147-150.

[75] Yousefi H, Faezipour M, Hedjazi S, Mousavi MM, Azusa Y, Heidari AH. (2013) Comparative study of paper and nanopaper properties prepared from bacterial cellulose nanofibers and fibers/ground cellulose nanofibers of canola straw. Industrial Crops and Products 43(1):732-737.

[76] Martínez-Sanz M, Lopez-Rubio A, Lagaron JM. (2012) Optimization of the dispersion of unmodified bacterial cellulose nanowhiskers into polylactide via melt compounding to significantly enhance barrier and mechanical properties. Biomacromolecules 13(11):3887-3899.

[77] Ambrosio-Martín J, Fabra MJ, Lopez-Rubio A, Lagaron JM. (2015) Melt polycondensation to improve the dispersion of bacterial cellulose into polylactide via melt compounding: enhanced barrier and mechanical properties. Cellulose 22(2):1201-1226.

[78] Eichhorn SJ, Dufresne A, Aranguren M, Marcovich NE, Capadona JR, Rowan SJ, et al. (2010) Review: Current international research into cellulose nanofibres and nanocomposites. Journal of Materials Science 45(1):1-33.

[79] Mittal V. (2014) Functional polymer nanocomposites with graphene: A review. Macromolecular Materials and Engineering 299(8):906-931.

[80] Marques PAAP, Gonçalves G, Cruz S, Almeida N, Singh MK, Grácio J, et al. Functionalized Graphene Nanocomposites. In: Hassim A, editor. Advances in Nanocomposite Technology: InTech Rijeka Croatia; 2011. p. 247-273.

[81] Chua CK, Pumera M. (2014) Chemical reduction of graphene oxide: A synthetic chemistry viewpoint. Chemical Society Reviews 43(1):291-312.

[82] Yoo BM, Shin HJ, Yoon HW, Park HB. (2014) Graphene and graphene oxide and their uses in barrier polymers. Journal of Applied Polymer Science 131(1).

[83] Kim H, Abdala AA, MacOsko CW. (2010) Graphene/polymer nanocomposites. Macromolecules 43(16):6515-6530.

[84] Huang HD, Ren PG, Xu JZ, Xu L, Zhong GJ, Hsiao BS, et al. (2014) Improved barrier properties of poly(lactic acid) with randomly dispersed graphene oxide nanosheets. Journal of Membrane Science 464:110-118.

[85] Verdejo R, Bernal MM, Romasanta LJ, Lopez-Manchado MA. (2011) Graphene

filled polymer nanocomposites. Journal of Materials Chemistry 21(10):3301-3310.

[86] Wang J, Wang X, Xu C, Zhang M, Shang X. (2011) Preparation of graphene/poly(vinyl alcohol) nanocomposites with enhanced mechanical properties and water resistance. Polymer International 60(5):816-822.

[87] El Achaby M, Qaiss A. (2013) Processing and properties of polyethylene reinforced by graphene nanosheets and carbon nanotubes. Materials and Design 44:81-89.

[88] Stankovich S, Dikin DA, Dommett GHB, Kohlhaas KM, Zimney EJ, Stach EA, et al. (2006) Graphene-based composite materials. Nature 442(7100):282-286.

[89] Pinto AM, Cabral J, Tanaka DAP, Mendes AM, Magalhães FD. (2013) Effect of incorporation of graphene oxide and graphene nanoplatelets on mechanical and gas permeability properties of poly(lactic acid) films. Polymer International 62(1):33-40.

[90] Du J, Cheng HM. (2012) The fabrication, properties, and uses of graphene/polymer composites. Macromolecular Chemistry and Physics 213(10-11):1060-1077.

[91] Bao C, Song L, Xing W, Yuan B, Wilkie CA, Huang J, et al. (2012) Preparation of graphene by pressurized oxidation and multiplex reduction and its polymer nanocomposites by masterbatch-based melt blending. Journal of Materials Chemistry 22(13):6088-6096.

[92] Norazlina H, Kamal Y. (2015) Graphene modifications in polylactic acid nanocomposites: a review. Polymer Bulletin (Berlin).

[93] Sadasivuni KK, Ponnamma D, Thomas S, Grohens Y. (2014) Evolution from graphite to graphene elastomer composites. Progress in Polymer Science 39(4):749-780.

[94] Carlmark A, Larsson E, Malmström E. (2012) Grafting of cellulose by ring-opening polymerisation – A review. European Polymer Journal 48(10):1646-1659.

[95] Wu H, Zhao W, Hu H, Chen G. (2011) One-step in situ ball milling synthesis of polymer-functionalized graphene nanocomposites. Journal of Materials Chemistry 21(24):8626-8632.

[96] Gorrasi G, Sarno M, Di Bartolomeo A, Sannino D, Ciambelli P, Vittoria V. (2007) Incorporation of carbon nanotubes into polyethylene by high energy ball milling: Morphology and physical properties. Journal of Polymer Science, Part B: Polymer Physics 45(5):597-606.

[97] Shaw WJD. Current understanding of mechanically alloyed polymers. Switzerland: Trans Tech Publication 1998. p. 19-30.

[98] Gorrasi G, Di Lieto R, Patimo G, De Pasquale S, Sorrentino A. (2011) Structure-property relationships on uniaxially oriented carbon nanotube/polyethylene composites. Polymer 52(4):1124-1132.

[99] Vertuccio L, Gorrasi G, Sorrentino A, Vittoria V. (2009) Nano clay reinforced PCL/starch blends obtained by high energy ball milling. Carbohydrate Polymers 75(1):172-179.

[100] Perrin-Sarazin F, Sepehr M, Bouaricha S, Denault J. (2009) Potential of ball milling to improve clay dispersion in nanocomposites. Polymer Engineering and Science 49(4):651-665.

[101] Wu H, Zhao W, Chen G. (2012) One-pot in situ ball milling preparation of polymer/graphene nanocomposites. Journal of Applied Polymer Science 125(5):3899-3903.

[102] Hossain KMZ, Ahmed I, Parsons AJ, Scotchford CA, Walker GS, Thielemans W, et al. (2011) Physico-chemical and mechanical properties of nanocomposites prepared using cellulose nanowhiskers and poly(lactic acid). Journal of Materials Science:1-12.

[103] Braun B, Dorgan JR, Hollingsworth LO. (2012) Supra-molecular ecobionanocomposites based on polylactide and cellulosic nanowhiskers: synthesis and properties. Biomacromolecules 13(7):2013-2019.

[104] Yu HY, Qin ZY, Yan CF, Yao JM. (2014) Green nanocomposites based on functionalized cellulose nanocrystals: A study on the relationship between interfacial interaction and property enhancement. ACS Sustainable Chemistry and Engineering 2(4):875-886.

[105] Martínez-Sanz M, Vicente AA, Gontard N, Lopez-Rubio A, Lagaron JM. (2014) On the extraction of cellulose nanowhiskers from food by-products and their comparative reinforcing effect on a polyhydroxybutyrate-co-valerate polymer. Cellulose.

[106] Jiang L, Morelius E, Zhang J, Wolcott M, Holbery J. (2008) Study of the poly(3-hydroxybutyrate-co-3-hydroxyvalerate)/cellulose nanowhisker composites prepared by solution casting and melt processing. Journal of Composite Materials 42(24):2629-2645.

[107] Petersson L, Kvien I, Oksman K. (2007) Structure and thermal properties of poly(lactic acid)/cellulose whiskers nanocomposite materials. Composites Science and Technology 67(11-12):2535-2544.

[108] Fortunati E, Peltzer M, Armentano I, Torre L, Jiménez A, Kenny JM. (2012) Effects of modified cellulose nanocrystals on the barrier and migration properties of PLA nano-biocomposites. Carbohydrate Polymers 90(2):948-956.

[109] Yu H, Yan C, Yao J. (2014) Fully biodegradable food packaging materials based on functionalized cellulose nanocrystals/poly(3-hydroxybutyrate-co-3-hydroxyvalerate) nanocomposites. RSC Advances 4(104):59792-59802.

[110] Follain N, Belbekhouche S, Bras J, Siqueira G, Marais S, Dufresne A. (2013) Water transport properties of bio-nanocomposites reinforced by Luffa cylindrica cellulose nanocrystals. Journal of Membrane Science 427:218-229.

[111] Habibi Y, Goffin AL, Schiltz N, Duquesne E, Dubois P, Dufresne A. (2008) Bionanocomposites based on poly(ε-caprolactone)-grafted cellulose nanocrystals by ring-opening polymerization. Journal of Materials Chemistry 18(41):5002-5010.

[112] Liu DY, Sui GX, Bhattacharyya D. (2014) Synthesis and characterisation of nanocellulose-based polyaniline conducting films. Composites Science and Technology 99:31-36.

[113] Silva MJ, Sanches AO, Medeiros ES, Mattoso LHC, McMahan CM, Malmonge JA. (2014) Nanocomposites of natural rubber and polyaniline-modified cellulose nanofibrils. Journal of Thermal Analysis and Calorimetry 117(1):387-392.

[114] Saralegi A, Gonzalez ML, Valea A, Eceiza A, Corcuera MA. (2014) The role of cellulose nanocrystals in the improvement of the shape-memory properties of castor oil-based segmented thermoplastic polyurethanes. Composites Science and Technology 92:27-33.

[115] Goffin AL, Raquez JM, Duquesne E, Siqueira G, Habibi Y, Dufresne A, et al. (2011) From interfacial ring-opening polymerization to melt processing of cellulose nanowhisker-filled polylactide-based nanocomposites. Biomacromolecules 12(7):2456-2465.

[116] Raquez JM, Murena Y, Goffin AL, Habibi Y, Ruelle B, DeBuyl F, et al. (2012) Surface-modification of cellulose nanowhiskers and their use as nanoreinforcers into polylactide: A sustainably-integrated approach.

Composites Science and Technology 72(5):544-549.

[117] Martínez-Sanz M, Abdelwahab MA, Lopez-Rubio A, Lagaron JM, Chiellini E, Williams TG, et al. (2013) Incorporation of poly(glycidylmethacrylate) grafted bacterial cellulose nanowhiskers in poly(lactic acid) nanocomposites: Improved barrier and mechanical properties. European Polymer Journal 49(8):2062-2072.

[118] Ifuku S, Nogi M, Abe K, Handa K, Nakatsubo F, Yano H. (2007) Surface modification of bacterial cellulose nanofibers for property enhancement of optically transparent composites: Dependence on acetyl-group DS. Biomacromolecules 8(6):1973-1978.

[119] Andresen M, Johansson LS, Tanem BS, Stenius P. (2006) Properties and characterization of hydrophobized microfibrillated cellulose. Cellulose 13(6):665-677.

[120] Arias A, Heuzey MC, Huneault MA, Ausias G, Bendahou A. (2014) Enhanced dispersion of cellulose nanocrystals in melt-processed polylactide-based nanocomposites. Cellulose.

[121] Martínez-Sanz M, Lopez-Rubio A, Lagaron JM. (2013) Nanocomposites of ethylene vinyl alcohol copolymer with thermally resistant cellulose nanowhiskers by melt compounding (I): Morphology and thermal properties. Journal of Applied Polymer Science 128(5):2666-2678.

[122] Goffin AL, Raquez JM, Duquesne E, Siqueira G, Habibi Y, Dufresne A, et al. (2011) Poly(ε-caprolactone) based nanocomposites reinforced by surface-grafted cellulose nanowhiskers via extrusion processing: Morphology, rheology, and thermo-mechanical properties. Polymer 52(7):1532-1538.

[123] Martínez-Sanz M, Olsson RT, Lopez-Rubio A, Lagaron JM. (2011) Development of electrospun EVOH fibres reinforced with bacterial cellulose nanowhiskers. Part I: Characterization and method optimization. Cellulose 18(2):335-347.

[124] Kim H, Kobayashi S, Abdurrahim MA, Zhang MJ, Khusainova A, Hillmyer MA, et al. (2011) Graphene/polyethylene nanocomposites: Effect of polyethylene functionalization and blending methods. Polymer 52(8):1837-1846.

[125] Kim H, Miura Y, MacOsko CW. (2010) Graphene/polyurethane nanocomposites for improved gas barrier and electrical conductivity. Chemistry of Materials 22(11):3441-3450.

[126] Zhao X, Zhang Q, Chen D, Lu P. (2010) Enhanced mechanical properties of graphene-based polyvinyl alcohol composites. Macromolecules 43(5):2357-2363.

[127] Salavagione HJ, Martínez G, Gómez MA. (2009) Synthesis of poly(vinyl alcohol)/reduced graphite oxide nanocomposites with improved thermal and electrical properties. Journal of Materials Chemistry 19(28):5027-5032.

[128] Kuila T, Bose S, Mishra AK, Khanra P, Kim NH, Lee JH. (2012) Effect of functionalized graphene on the physical properties of linear low density polyethylene nanocomposites. Polymer Testing 31(1):31-38.

[129] Shen Y, Jing T, Ren W, Zhang J, Jiang ZG, Yu ZZ, et al. (2012) Chemical and thermal reduction of graphene oxide and its electrically conductive polylactic acid nanocomposites. Composites Science and Technology 72(12):1430-1435.

[130] Wang BJ, Zhang YJ, Zhang JQ, Gou QT, Wang ZB, Chen P, et al. (2013) Crystallization behavior, thermal and mechanical properties of PHBV/graphene nanosheet composites. Chinese Journal of

Polymer Science (English Edition) 31(4):670-678.

[131] Ding P, Su S, Song N, Tang S, Liu Y, Shi L. (2014) Highly thermal conductive composites with polyamide-6 covalently-grafted graphene by an in situ polymerization and thermal reduction process. Carbon 66:576-584.

[132] De C. Fim F, Basso NRS, Graebin AP, Azambuja DS, Galland GB. (2013) Thermal, electrical, and mechanical properties of polyethylene-graphene nanocomposites obtained by in situ polymerization. Journal of Applied Polymer Science 128(5):2630-2637.

[133] Yang JH, Lin SH, Lee YD. (2012) Preparation and characterization of poly(l-lactide)-graphene composites using the in situ ring-opening polymerization of PLLA with graphene as the initiator. Journal of Materials Chemistry 22(21):10805-10815.

[134] Song P, Cao Z, Cai Y, Zhao L, Fang Z, Fu S. (2011) Fabrication of exfoliated graphene-based polypropylene nanocomposites with enhanced mechanical and thermal properties. Polymer 52(18):4001-4010.

[135] Song P, Liu L, Fu S, Yu Y, Jin C, Wu Q, et al. (2013) Striking multiple synergies created by combining reduced graphene oxides and carbon nanotubes for polymer nanocomposites. Nanotechnology 24(12).

[136] Chaudhry AU, Mittal V. (2013) High-density polyethylene nanocomposites using masterbatches of chlorinated polyethylene/graphene oxide. Polymer Engineering and Science 53(1):78-88.

[137] Jiang X, Drzal LT. (2012) Exploring the potential of exfoliated graphene nanoplatelets as the conductive filler in polymeric nanocomposites for bipolar plates. Journal of Power Sources 218:297-306.

[138] Reglamento (CE) nº 1935/2004 del Parlamento Europeo y del Consejo, de 27 de octubre de 2004, sobre los materiales y objetos destinados a entrar en contacto con alimentos.

[139] Lagarón JM. Multifunctional and nanoreinforced polymers for food packaging. In: Lagarón J-M, editor. Multifunctional and Nanoreinforced Polymers for Food Packaging: Woodhead Publishing; 2011. p. 1-28.

[140] Hedenqvist M, Angelstok A, Edsberg L, Larssont PT, Gedde UW. (1996) Diffusion of small-molecule penetrants in polyethylene: Free volume and morphology. Polymer 37(14):2887-2902.

[141] Colomines G, Ducruet V, Courgneau Ć, Guinault A, Domenek S. (2010) Barrier properties of poly(lactic acid) and its morphological changes induced by aroma compound sorption. Polymer International 59(6):818-826.

[142] Kanehashi S, Kusakabe A, Sato S, Nagai K. (2010) Analysis of permeability; solubility and diffusivity of carbon dioxide; oxygen; and nitrogen in crystalline and liquid crystalline polymers. Journal of Membrane Science 365(1-2):40-51.

[143] Tsuji H, Okino R, Daimon H, Fujie K. (2006) Water vapor permeability of poly(lactide)s: Effects of molecular characteristics and crystallinity. Journal of Applied Polymer Science 99(5):2245-2252.

[144] Komatsuka T, Kusakabe A, Nagai K. (2008) Characterization and gas transport properties of poly(lactic acid) blend membranes. Desalination 234(1-3):212-220.

[145] Sanchez-Garcia MD, Gimenez E, Lagaron JM. (2008) Morphology and barrier properties of solvent cast composites of thermoplastic biopolymers and purified cellulose fibers. Carbohydrate Polymers 71(2):235-244.

[146] Berens AR, Hopfenberg HB. (1982) Diffusion of organic vapors at low concentrations in glassy PVC, polystyrene, and PMMA. Journal of Membrane Science 10(2-3):283-303.

[147] Mokwena KK, Tang J. (2012) Ethylene Vinyl Alcohol: A Review of Barrier Properties for Packaging Shelf Stable Foods. Critical Reviews in Food Science and Nutrition 52(7):640-650.

[148] Zhang Z, Britt IJ, Tung MA. (2001) Permeation of oxygen and water vapor through EVOH films as influenced by relative humidity. Journal of Applied Polymer Science 82(8):1866-1872.

[149] Commission Regulation (EU) Nº 2023/2006 of 22 December 2006 on good manufacturing practice for materials and articles intended to come into contact with food.

[150] Commission Regulation (EU) Nº 10/2011 of 14 January 2011 on plastic materials and articles intended to come into contact with food.

[151] Commission Regulation (EU) Nº 2015/174 of 5 February 2015 amending and correcting Regulation (EU) No 10/2011 on plastic materials and articles intended to come into contact with food

[152] EFSA Scientific Committee. Guidance on the risk assessment of the application of nanoscience and nanotechnologies in the food and feed chain. European Food Safety Authority. EFSA, 2011

II. Objectives

1. GENERAL AND SPECIFIC OBJECTIVES

As discussed in the introduction section, the incorporation of highly dispersed nanofillers into polymer matrices is known to be an interesting strategy to improve the properties of these materials. As a result, polymer nanocomposites based on cellulose nanowhiskers and graphene nanosheets have been extensively studied and developed. Although poor dispersion of the nanofillers is generally obtained by direct melt blending technology, this is the most industrially meaningful route to incorporate these nanofillers into polymeric matrices. However, although different strategies has been developed to incorporate these nanofillers, i.e. cellulose nanowhiskers (CNW) or graphene nanosheets, into biopolymeric matrices by melt blending, not many studies have been reported using functionalized graphene nanosheets (FGS) or bacterial cellulose nanowhiskers (BCNW). Hence, it is of interest to study and assess innovative strategies to develop novel nanobiocomposites with BCNW or FGS which could lead to good nanofiller dispersion and distribution in order to enhance the properties of commercial biopolyesters currently assessed or used in food packaging applications. Additionally, it would be of interest to develop novel strategies which avoid or at least reduce the significant use of organic solvents during the synthesis of biopolymer nanocomposites. In this context, the main objective of this work was the following:

Development of biopolymer nanocomposites (nanobiocomposites) containing bacterial cellulose nanowhiskers or functionalized graphene nanosheets with improved properties, of interest in food packaging applications, through novels strategies compatible with widely used industrial processing technologies.

To this aim, several steps were carried out. Although plant-derived cellulose has been used to improve the properties of biopolymers matrices, the use of bacterial cellulose seems to be more attractive due to their inherent properties. Hence, the first step consisted in the **development of bacterial cellulose nanowhiskers (BCNW)** which could be incorporated into biopolymer matrices in the subsequent steps.

The next step was focused on **developing a strategy that allows the incorporation of nanofillers within PLA**. To this end, an *in situ* polycondensation reaction of lactic acid was proposed. This reaction had the advantage of being able to be carried out in aqueous medium since the initial monomers were a highly concentrated lactic acid aqueous solution and, therefore, fully compatible with aqueous suspensions of BCNW and graphene nanosheets. Thus, prior to the incorporation of nanofillers, an initial step was **the study and optimization of the PLA synthesis through a polycondensation reaction**. The study of the miscibility of the so-obtained PLA with high molecular weight commercial PLA in melt state and the effect of its incorporation on the different properties was also part of this specific objective.

The third objective consisted in the **addition of BCNW into PLA** through *in situ* polycondensation reaction, starting from mixtures of aqueous solutions of lactic acid and BCNW, comparing the use of BCNW either in aqueous suspension or freeze-dried. In this case, materials to be used as masterbatches in the next stage were obtained. **Purification of**

these materials was a further aim within this objective, in order to achieve materials which would allow proper dispersion of nanoreinforcements into high molecular weight PLA by melt blending.

The next step was the **development of nanocomposites based on PLA and BCNW by melt mixing** using the masterbatches synthesized in the previous step. A comparison with the materials obtained through direct addition of BCNW in the melt mixing step, either in aqueous suspensions or freeze-dried, was a further objective.

Based on the optimization performed for incorporation of BCNW using this technology, the next step was **the incorporation of graphene nanosheets into PLA by melt mixing** using the masterbatches obtained through melt polycondensation of lactic acid in the presence of graphene nanosheets. Functionalized graphene nanosheets (FGS) were used since from the chemical point of view the presence of functional sites could favor interactions with the matrix. Similarly, part of this objective was comparing the materials obtained in this way with those in which graphene nanosheets were directly incorporated in the melt mixing step.

Finally, the last objective was aimed at **incorporating the nanofillers through a novel strategy involving a single-step by means of the "ball-milling" technique**. Again, the challenge was to achieve a good dispersion of the nanofillers into the biopolymeric matrices using dry materials. Thus, nanocomposites of PLA with BCNW and PHBV with either BCNW or FGS were developed and the obtained dispersion of the nanofillers and the final properties of the so-obtained materials were investigated.

In order to complete this thesis work, a study of the **effect of these nanoreinforcements on the biodegradability** of the developed nanobiocomposites and also a **thermoforming study to make trays** of one of the polymer nanocomposites developed were also carried out.

III. Results and Discussion

1. GENERAL INTRODUCTION TO RESULTS

As mentioned above, the present work attempted to propose several strategies to improve the properties of biopolyesters-based nanocomposites in order to expand their fields of application in food packaging. Melt blending is the most widespread polymer processing technology at industrial scale and, thus, strategies to optimize the performance of biopolymer-based nanocomposites which are compatible with this processing method are required. However, the production of composite or nanocomposite systems through this route has a major drawback associated with the poor dispersion generally observed, which is mainly associated to the incompatibility between the nanofillers and the biopolymers and the inherent dry agglomeration of the nanofillers. Although different strategies has been developed to incorporate different nanofillers into biopolymeric matrices by melt blending attempting to overcome this main drawback, it is a necessity to study and develop novel and more efficient strategies to create novel nanobiocomposites that guarantee good dispersion and distribution of the nanofillers into the biopolymeric matrices which can lead to improvements in the final properties of the developed materials. Moreover, the development of strategies which reduce or eliminate the use of organic solvents during the synthesis of nanobiocomposites should also be of relevance.

Therefore, in an attempt to use melt blending as a strategy to incorporate nanofillers such as bacterial cellulose nanowhiskers (BCNW) and functionalized graphene sheets (FGS) into biopolymer matrices a two-steps process has been developed. An *in situ* polymerization reaction has been used as pre-incorporation strategy. To this aim, the polycondensation of lactic acid in the presence of nanofillers was carried out. Lactic acid was initially in a concentrated aqueous solution, which is fully compatible with both aqueous suspensions of BCNW and FGS. Moreover, this reaction was performed in aqueous medium, without the necessity of organic solvents. Therefore, masterbatches of lactic acid oligomers (OLLA) (low molecular weight PLA) containing BCNW or FGS were synthesized. Subsequently, these masterbatches were melt blended with high molecular weight commercial PLA. PLA was chosen as biopolymer matrix due to its excellent properties as well as being one of the most industrially developed biopolymers with future prospects.

Initially, with the aim to optimize the *in situ* polymerization methodology and in order to determine the amount of OLLA that could be incorporated into the commercial PLA through melt mixing, the polymerization reaction was carried out only with lactic acid (i.e. without nanofiller). The description of this work and characterization of the so-obtained PLA films containing different amounts of OLLA are compiled in **Chapter 1**. Thereafter, the incorporation of BCNW into OLLA by melt polycondensation producing an initial masterbatch and its subsequent melt mixing with high molecular weight PLA is described in **Chapter 2**. The evolution of the properties with the BNCW content was studied as well as the synergistic effect of the optimum concentration of BCNW obtained in terms of improved properties with the amount of oligomers optimized in Chapter 1. Furthermore, a comparison of the pre-incorporation method with a direct melt mixing of BCNW with PLA was also performed.

Although a slight decrease was observed in the mechanical properties for the sample where the synergistic study was performed, the best results in terms of barrier properties were observed in this case. Hence, maintaining such conditions, i.e. with the optimized

amount of OLLA observed in Chapter 1, graphene nanosheets were introduced using the same strategy in order to use other nanofiller with interesting potential to improve mechanical and barrier properties as well as to provide to the obtained materials additional functionalities such as electrical conductivity. Thus graphene-based masterbatches were produced with OLLA by melt polycondensation and subsequently melt blended with commercial PLA. The results of this study are gathered in **Chapter 3**. Similarly, a comparison of the so-obtained materials with those obtained by direct melt mixing without pre-incorporation step was performed.

On the other hand, the use of ball milling as a one-step and solvent free method to incorporate the nanofillers (BCNW and FGS) into PLA and PHBV matrices has been proposed. In this case, in addition to PLA as biopolymer matrix, PHBV was chosen because it is also one of the biopolymer with good future prospects but also requires certain property implementation to expand its field of application and compete in the current market with petroleum-based polymers commonly used in food packaging.

Chapter 4 shows the results obtained by incorporating BCNW within PLA using the ball milling technology. The morphology, thermal stability, mechanical and barrier properties were studied. In addition the effect of BCNW on the crystallization process of the biopolymer matrix was also studied.

A similar study, but in this case using PHBV as biopolymer matrix, was developed using the ball milling and similar processing conditions. The results obtained are compiled in **Chapter 5**.

Finally, graphene nanosheets were incorporated into PHBV using ball milling. In this case, in addition to all the properties studied in the previous chapters when BCNW were added through ball milling, i.e. morphology, thermal stability, thermal, mechanical and barrier properties as well as the effects of the nanofiller on the crystallization process, degradation studies including thermal degradation and biodegradation were carried out in order to assess the effect of graphene nanosheets on these degradation processes. Thus, while **Chapter 6** describes the morphology, thermal characteristics, thermal stability and effect of graphene in the crystallization process of the developed materials, in **Chapter 7** the results about crystalline structure and the dynamo-mechanical, electrical, barrier and biodisintegration properties are presented.

Furthermore, as complementary results to the different chapters, various characterizations and previous studies are compiled in the **Annexes** section, which can be helpful for a better understanding of the results shown in each chapter.

Chapter 1

AN EFFECT OF LACTIC ACID OLIGOMERS ON THE BARRIER PROPERTIES OF POLYLACTIDE

J. Ambrosio-Martín, M. J. Fabra, A. Lopez-Rubio and J. M. Lagaron

Journal of Material Science 2014, 49, 2975-2986

Novel Materials and Nanotechnology Group, IATA, CSIC, Av. Agustín Escardino 7, 46980 Paterna (Valencia), Spain.

ABSTRACT

Oligomers of lactic acid (LA) at different concentrations were melt-mixed with a polymeric matrix of high molecular weight polylactide (PLA) to improve their barrier properties. Purified and unpurified LA oligomers, obtained by a melt polycondensation reaction, were blended with PLA in order to study how the purification process affected the final film properties. In all the developed blend compositions, significant improvements in the permeability to both water and oxygen were observed in comparison with pure PLA, achieving permeability reductions of up to 54 %. This behaviour was ascribed to an antiplasticization phenomenon of the barrier properties related to the occupancy of the so-called Langmuir-free volume sites by the oligomer molecules. The results also showed that the permeability of these materials was greatly influenced by the presence of moisture, especially in the blends with unpurified oligomers. This behaviour was mainly ascribed to the higher content of the hydroxyl groups present in the latter materials, which led to an observable water sorption and hence to an increase in free volume for permeation.

Keywords: Lactic acid, Oligomers, Barrier properties, Blends, Polylactide, Polymerization.

1. INTRODUCTION

Biopolymer materials are attracting a great interest to counteract the environmental drawbacks related to the extremely slow degradation rate of many commonly used petroleum-based polymers and also to explore alternatives to petroleum to constitute polymer-based materials [1, 2].

Polylactides (PLA) are one of the most widely studied thermoplastic sustainable biopolymers family for monolayer and multilayer packaging applications. It derives from different sources, such as corn starch, tapioca products or sugarcanes, and can be obtained through different polymerization processes, such as polycondensation or ring opening polymerization. At the same time, it is one of the most interesting families of biodegradable materials because it has become commercially available, being produced on an industrial scale by several companies around the world [3] and presenting an interesting balance of properties. In the food packaging field, PLA has particular interest due to its excellent transparency and relatively good water resistance. Plasticizers can be added to PLA to reduce its relatively high stiffness, although they lead to a decrease in the oxygen barrier and also in transparency [4, 5]. Therefore, the main performance drawbacks of PLA are mainly associated to its low thermal resistance, excessive brittleness and insufficient barrier to oxygen and water compared to other benchmark packaging polymers like polyethylene terephthalate (PET) [6]. It is, thus, of great interest to enhance the properties of this material because of its degradable, renewable and eco-friendly properties while maintaining its inherent good properties such as transparency and biodegradability [7].

In order to overcome the low barrier properties of PLA, many studies concerning mass transfer phenomena have been done. These studies primarily focused on the development of PLA composites and nanocomposites using organic or inorganic nanofillers like cellulose nanowhiskers, anhydrite (calcium sulphate) or nanoclays [6, 8– 13] and on the use of PLA in coating systems [14–16] or multilayer systems [17, 18].

Another strategy commonly used to improve PLA barrier properties has been blending the biopolymer with other polymers. Both petroleum-based polymers such as PCL and polyvinyl acetate (PVAc), and polymers from renewable resources such as chitosan, starch or polyhydroxybutyrate (PHB) have been blended with PLA to improve its properties [19].

One of the main factors that directly influence the barrier properties of polymers is the existing free volume, which is an intrinsic property of the polymeric matrix and relates to the existing voids for transport phenomena between entangled polymer chains. The sorption and diffusion of low molecular weight molecules in polymers greatly depend on the available free volume, in a way that, generally, both mass transport processes increase with increasing free volume [20].

The relationship between free volume and mass transport properties in polymers and polymer nanocomposite materials has been studied by several authors. Generally, the introduction of many low molecular weight diluents into glassy polymers tends to increase the elongation at break and reduce the elastic modulus, process that is often referred to as plasticization, directly related to the mechanical properties. It has

also been reported that the incorporation of some of these low molecular weight diluents into different polymer matrices can lead to improved barrier properties. This phenomenon has been termed as an antiplasticization effect, in clear reference to the barrier properties, and has been ascribed to a reduction in the polymer-free volume. In this context, it has been demonstrated that transport properties can be improved by means of the addition of certain low molecular weight molecules [21–25].

Addition of low molecular weight particles to polymers can also alter the crystallization rate. For instance, an increase in the crystallization rate of PLA matrices has been reported by adding 3-hydroxybutyrate oligomers (OHB) of different molecular weights to PLA [26]. Moreover, the increase in crystallinity of biopolyesters has been related to improved barrier properties to water vapour and gases [27– 30]. Sanchez-García and Lagaron [6] have reported that by nanofabrication of some fillers, it is possible to obtain high levels of crystallinity, yielding a more efficient barrier effect in PLA nanocomposites. Thus, it can be generally stated that increasing crystallinity will also have a positive effect on barrier properties.

Recent work has additionally demonstrated that by using some modified lactic acid (LA) oligomers, the mechanical properties of PLA can be effectively improved in terms of ductility, by a plasticization effect mainly caused by an increase in the free volume of the matrix and, consequently, in the mobility of macromolecular segments [31]. In this case, PLA plasticization led to a decrease in barrier properties. The oligomers used in the mentioned study were designed either to have the final carboxyl or hydroxyl groups free, or one of them blocked by esterification or both esterified with alcohol or acids [32]. In any case, the physico-chemical characteristics of these oligomers were seen to lead to a plasticization effect in the PLA matrix.

In the current study, low molecular weight oligomers of LA were synthesized and blended with a commercial PLA matrix in order to improve the biopolymer barrier properties. Such oligomers were chosen due to the large compatibility that they are expected to have with the PLA polymer. The oligomers were obtained by a polycondensation method. A preliminary study was carried out to determine the optimum amount of oligomers that induced the highest performance in barrier properties, while keeping the film-forming ability. Both purified and unpurified oligomers were used, showing the effect of the purification step on their properties and also in the barrier properties of the final blends with PLA.

2. MATERIALS AND METHODS

2.1. Materials

The semicrystalline poly(L-lactic acid) (PLA) used was a film extrusion grade with a number average molecular weight (M_n) of 130,000 g mol^{-1} and a weight average molecular weight (M_w) of 150,000 g mol^{-1} manufactured by NatureWorks (USA). LA was supplied as a 90 wt.% aqueous solution by Across Organics (Belgium).

2.2. Lactic acid oligomerization

Lactic acid oligomers were obtained after dehydration of the aqueous LA solution at 150 °C and atmospheric pressure for 2 h. Then, a pressure of 100 mmHg was applied for 2 h, followed by a final pressure of 30 mmHg for 4 h obtaining a viscous liquid of oligo(L-lactic acid) (OLLA). Part of the

product was used without further purification which, from now on, will be referred to as ''direct oligomer'' (OLLA-D), and the rest was ground into powder and washed with diethyl ether, which will be referred to ''purified oligomer'' (OLLA-P).

2.3 Preparation of blends

Neat PLA as well as blends of PLA with OLLA-P (PLA-OLLA-P) at weight ratios of 3, 5, 10, 20, 25, 30, and 40 wt.% were melt-mixed in a Brabender Plastograph internal mixer for 2 min at 162 °C and 100 rpm. Furthermore, a blend of PLA with OLLA-D (PLA-OLLA-D) in a weight ratio of 25 wt.% was melt-mixed in the same conditions specified above. The obtained products were allowed to cool at room temperature, and they were subsequently compression-moulded into films using a hot-plate hydraulic press (165 °C and 2 MPa for 2 min). The so-obtained films had a thickness of about 100 lm as measured with a Mitutoyo micrometer by averaging four measurements on each sample.

2.4. Molecular weight determination by dilute solution viscosity

Viscosity measurements were performed in $CHCl_3$ at 25 °C in a Ubbelohde viscometer type 525 with capillary 13/Ic (SI Analytics, Germany) following the adapted method of Kiremitci-Gumusderelioglu and Deniz [33] and the standard ASTM D4603, which uses the Solomon–Ciuta equation to calculate the intrinsic viscosity. Then, the molecular weight of the oligomer was calculated through the Mark–Houwink equation (Eq. 1) which relates intrinsic viscosity [η] with the viscosity average molecular weight (M_v):

$$[\eta] = K \cdot M_v^a \quad (1)$$

The value of the equation parameters for PLA in chloroform at 25 °C are: a =0.64 and K =6.06 x 10^{-4}dl g^{-1} [34].

2.5. Differential Scanning Calorimetry (DSC)

Thermal properties of the different materials were studied by DSC using a Perkin-Elmer DSC 7 calorimeter on typically 3 mg of dry material at a heating rate of 10 °C min^{-1} from 0 to 160 °C in a nitrogen atmosphere using a refrigerating cooling accessory (Intracooler 2 from Perkin-Elmer). The first and second melting endotherms, after controlled crystallization at 5 °C min^{-1} from the melt, were analysed. Calibration was performed using an indium sample, and the slope of the thermal scans was corrected by subtracting similar scans of an empty pan. All tests were carried out at least in duplicate.

The degree of crystallinity (%) of PLA was estimated using the ratio between the melting enthalpy of the studied material and the enthalpy of a perfect PLA crystal i.e. $X_c(\%) = \Delta H_f/\Delta H^o_f$; where ΔH_f is the enthalpy of fusion of the studied specimen and ΔH^o_f is the melting enthalpy of a totally crystalline material. The ΔH^o_f used for this equation was 93 J g^{-1} for PLA [6].

2.6. Thermogravimetric Analysis (TGA)

Thermogravimetric (TG) curves were recorded using a thermobalance Setaram Setsys 16/18 (Setaram Instrumentation). Samples were heated from 25 to 500 °C at a heating rate of 10 °C min^{-1} under nitrogen atmosphere. Derivative thermogravimetric curves (DTG) express the weight loss rate as a function of temperature.

2.7. Attenuated Total Reflectance (ATR) FT-IR analysis

ATR-FTIR spectra of PLA and the blends with the two different oligomers were recorded in a controlled chamber at 24 °C and 40% RH using a Bruker FT-IR Tensor 37 equipment (Rheinstetten, Germany) coupled with the ATR accessory GoldenGate of Specac Ltd. (Orpington, UK) in the 4000–600 cm^{-1} range. The spectra were taken at 4 cm^{-1} resolution by averaging 20 scans.

2.8. Water permeability

Direct permeability to water was determined from the slope of weight loss versus time curves at 24 °C. The films were sandwiched between the aluminium top (open O-ring) and bottom (deposit for the permeant) parts of a specifically designed permeability cell with screws containing deionized water as the permeant. A Viton rubber O-ring was placed between the film and the top part of the cell to enhance sealability. The cells were placed inside a desiccator at 0 % RH, and the water weight loss through a film area of 0.001 m2 was monitored and plotted as a function of time. In order to estimate the permeability values of the films, only the linear part of the weight loss data was used to ensure sample steady-state conditions. Cells with aluminium films were used as control samples to estimate solvent loss through the sealing. Water weight loss was calculated as the total cell weight loss minus the loss through the sealing. Tests were done in duplicate

2.9. Oxygen transmission rate

The oxygen permeability coefficient was derived from oxygen transmission rate (OTR) measurements recorded using an Oxtran 100 equipment (Modern Control Inc., Minneapolis, MN, US). Experiments were carried out at 24 °C and at two relative humidity conditions (0 and 80 % RH). 80 % RH was generated by a built-in gas bubbler and was checked with a hygrometer placed at the exit of the detector. The samples were purged with nitrogen for a minimum of 20 h in the humidity equilibrated samples, prior to exposure to an oxygen flow of 10 ml min^{-1}. A 5 cm^2 sample area was measured by using an in-house developed mask. The measurements were done in duplicate.

2.10. Mechanical properties

Tensile tests were carried out at 24 °C and 50 % RH on an Instron 4400 Universal Tester. Pre-conditioned dumb-bell shaped specimens with initial gauge length of 25 mm and 5 mm in width were die-stamped from the films in the machine direction according to ASTM D638. The thickness of all specimens was approximately 100 lm. A fixed crosshead rate of 10 mm min^{-1} was used in all cases, and results were taken as the average of, at least, three tests.

2.11. Statistical analysis

Results were analyzed by multifactor analysis of variance (ANOVA) using Statgraphics Centurion 15.1 software (Statpoint Technologies, INC, Warrenton, VA, USA). Fisher's least significant difference (LSD) was used at the 95% confidence level.

3. RESULTS AND DISCUSSION

3.1. Preparation and characterization of the lactic acid oligomers

In the present study, lactic acid oligomers (OLLA) were synthesized according to the direct melt polycondensation method of LA reported by Moon et al. [35] who divided the melt

polycondensation process in two steps, an oligomerization step followed by a subsequent polycondensation step. In this work, only the first step was performed to obtain the oligomers and no catalyst was needed to carry out the reaction. The viscosity average molecular weight obtained for the direct oligomer (OLLA-D) just after the first step of the polycondensation reaction was M_v=640 g mol^{-1}, which is in accordance with the number average molecular weight for the oligomer M_n=570 g mol^{-1} reported by Moon et al. [35]. Part of the so-obtained material was washed with diethyl ether in order to remove unreacted monomers and very short chain oligomers, resulting in a purified oligomer (OLLA-P) with a viscosity average molecular weight of M_v=1355 g mol^{-1}.

Both the direct (OLLA-D) and purified (OLLA-P) oligomers were characterized by FTIR spectroscopy. Figure 1 shows the complete ATR-FTIR spectra and a zoom of the spectral range from 740 to 900 cm^{-1} and from 890 to 980 cm^{-1} of the initial LA, OLLA-D, OLLA-P and pure PLA showing that, after oligomerization by melt polycondensation of LA, the generated oligomers had a similar molecular structure than that of PLA, suggesting that the chemical bonding required for PLA synthesis was effectively generated. The polymerization reaction was mainly characterized by increased intensity of the bands at 1460, 1390 and especially 875 and 760 cm^{-1}, which appear in the FTIR spectra with numbers of (1), (2), (7) and (9), and are characteristic of the $\delta_{as}(CH_3)$, $\delta_s(CH_3)$, ν(C–COO) and δ(C=O) bonds, respectively. At the same time, the intensity at 1135 and 826 cm^{-1}, attributed to $r(CH_3)$ and ν(C-COOH) vibration [(5) and (8) in the spectrum, respectively] decreased [36,37]. A small shift of the band at 826 cm^{-1} characteristic of lactic acid was also observed in the oligomer spectra, as a consequence of chain extension during the oligomerization reaction (cf. magnified spectra from 740 to 900 cm^{-1} in Figure 1). Moreover, different bands attributed to ester groups (i.e. ν(COC) bonds), at 1210, 1180, and 1090 cm^{-1} [(3), (4) and (6), respectively] appeared after the oligomerization reaction. The C=O stretching

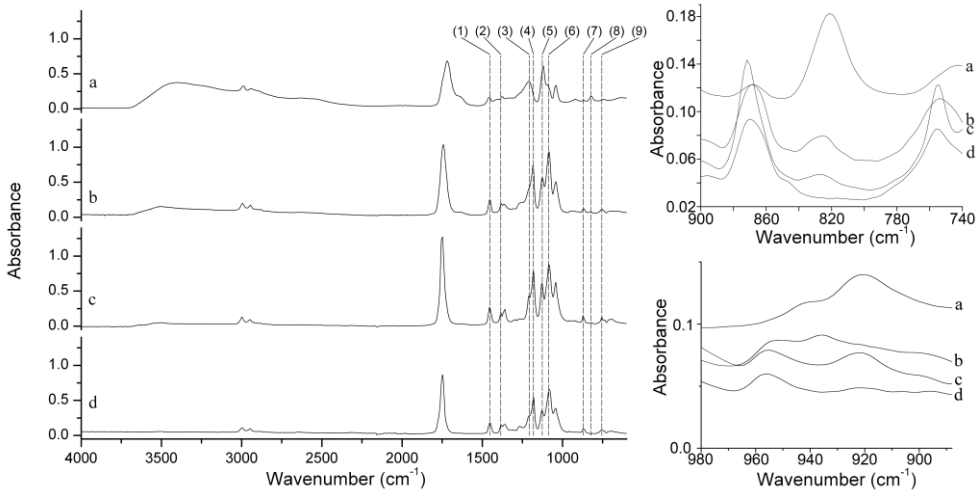

Figure 1. ATR-FTIR spectra of lactic acid (a), oligomer without purification (b), purified oligomer (c), and pure PLA (d). Dashed lines point out the main spectral bands used to follow the polymerization reaction. The numbers 1-9 correspond to the characteristics bands which change after polymerization reaction, and they are related with δ_{as}(CH3), δ_s(CH3), ν(COC), ν(COC), r(CH3), ν(COC), ν(C-COO), ν(C-COOH) and δ(C=O) vibrations, respectively.

band of lactic acid, which is characteristic of the acid groups from monomers, was centred around 1720 cm^{-1} and it appeared as a relatively broad band. When the oligomers were formed, this carbonyl stretching band corresponded to aliphatic esters, thus, appeared as a more intense band between 1740 and 1750 cm^{-1} [38]. The polycondensation system of LA involves two different equilibrium reactions: a dehydration reaction needed for esterification and a ring-chain equilibrium involving the depolymerization of PLLA into L-lactide (cyclic dimer of lactic acid) [35], which displays a characteristic band at ~1770 cm^{-1} related to cyclic dilactone C=O valence vibration [39]. Thus, before the purification step, OLLA, LA unreacted monomers and L-lactide were present in the material, being the main impurities when PLA is produced by step-growth polymerization [40]. A broader band centred at 1750 cm^{-1} was seen for OLLA-D, due to the contribution of these impurities. Furthermore, in the spectrum from lactic acid, and partially overlapped with the C=O stretching band, the characteristic band of water, at 1640 cm^{-1} was apparent, while it significantly decreased in the OLLA-D spectrum and almost disappeared in the OLLA-P spectrum, since the first step in the oligomerization process consisted of the dehydration of lactic acid. However, the spectra of OLLA-D and OLLA-P showed a typical absorption band at ~3500 cm^{-1}, attributed to hydroxyl groups, which did not appear in the PLA spectrum. This result could be explained by both the shorter chain length of the oligomers, resulting in more hydroxyl terminal groups, and by the presence of unreacted lactic acid in the final products. In the direct oligomer spectrum, the band attributed to hydroxyl groups appeared more intense, as during the purification step the unreacted monomers and the very short chain oligomers were removed, thus decreasing the hydroxyl terminal groups present.

Moreover, the PLA spectral bands around 921 cm^{-1} and 908 cm^{-1} are related to the presence of α and β-crystals, respectively [41,42], while the band at 955 cm^{-1} has been assigned to the PLA amorphous fraction [41,43,44]. From the magnified spectra in Figure 1 it was observed that while contributions of both amorphous and crystalline fractions were apparent for the purified oligomer, only the band related to the amorphous fraction was observed for OLLA-D. This indicates that after removing impurities such as unreacted monomers, very short chain oligomers and L-lactide through the purification process, the oligomer was able to crystallize. In fact, in the OLLA-D spectra another band at 935 cm^{-1} appears which is assigned to the COO ring breathing mode in L-lactide [39,45], confirming, firstly, the presence of this compound in the unpurified material, and secondly, the effectiveness of the purification treatment, since this band did not appear in OLLA-P spectrum. In order to qualitatively follow the oligomerization reaction process, the ratio between the intensity of bands at 760 cm^{-1} (ascribed to C=O bonds from oligomers) and at 826 cm^{-1} (ascribed to C-COOH vibration from lactic acid) (A_{760}/A_{826}) was calculated, showing that the presence of carboxyl groups in OLLA-D was greater than in OLLA-P ($A_{760}/A_{826OLLA\text{-}D}$=2.54 vs. $A_{760}/A_{826OLLA\text{-}P}$= 6.69), thus confirming that the purification step eliminated most of the unreacted monomers and, hence, contributed to a decrease in the number of carboxyl terminal groups. For the pure PLA, the band at 826 cm^{-1} disappeared, indicating that in the fully polymerized material there was no contribution of carboxyl groups, which were involved in the polycondensation reaction to form ester bonds.

Finally, it is worth mentioning that the purification step of the oligomer also resulted in more defined spectral bands than in the OLLA-D spectrum, thus further confirming the effectiveness of the treatment.

The thermal properties of the direct and purified oligomers were also analysed. From Figure 2, it can be observed that, while the unpurified oligomer was a totally amorphous material, the purified one showed a double melting peak, suggesting that after purification the oligomer was able to crystallize. This is in accordance with the previous observations by FTIR, where no signal associated with the crystalline fraction was observed for the OLLA-D. Furthermore, a significant increase in the glass transition temperature (T_g) of the OLLA-P (T_g=27.70 °C), compared to OLLA-D (T_g=13.77 °C) was also noticed. This is the result of the higher molecular weight attained in the purified material and also by the presence of crystals, which are thought to impose constraints to the chain mobility in the amorphous phase.

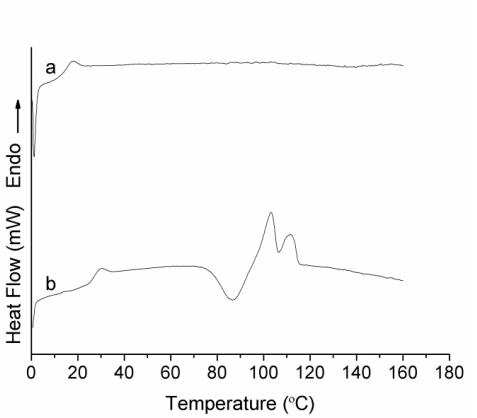

Figure 2. DSC second heating run curves of OLLA-D (*a*) and OLLA-P (*b*)

3.2. Optimization of the PLA/OLLA ratio for improving barrier properties

Initially, different ratios of oligomer/biopolyester were studied to find the optimum composition, in terms of maximum permeability improvement, while maintaining the ability of the blend to retain a film structure after compression molding. To this end, only the purified oligomer was used and different PLA-OLLA-P blends containing from 3 wt.% to 40 wt.% OLLA-P were developed and characterized. Specifically, the film morphology of the blends and the oxygen permeability measured at 80% RH was evaluated for the different specimens. Table 1 compiles the results for the various blends developed.

This preliminary study showed that the maximum oligomer content to develop blends with good film-forming ability was 30 wt.%. Above this content, it seems that the percentage of low M_w chains was probably too high to allow the necessary chain entanglements for the development of a continuous solid film. From Table 1 it can also be seen that, in terms of oxygen barrier properties, the greatest improvement was obtained for the blend PLA-OLLA-P with

Table 1. Oxygen permeability coefficients for PLA films and for their blends films with oligomer

	P oxygen (80% RH)·10^{18} ($m^3 m\ m^{-2} s^{-1} Pa^{-1}$)	Reduction in oxygen permeability (%)	Film-forming capacity
PLA	1.748 ± 0.104^{a}	-	Yes
PLA + 3 % OLLA-P	1.778 ± 0.070^{a}	-	Yes
PLA + 5 % OLLA-P	1.547 ± 0.064^{b}	11	Yes
PLA + 10 % OLLA-P	1.430 ± 0.022^{bc}	18	Yes
PLA + 20 % OLLA-P	1.408 ± 0.015^{bc}	19	Yes
PLA + 25 % OLLA-P	1.358 ± 0.017^{c}	22	Yes
PLA + 30 % OLLA-P	1.730 ± 0.091^{a}	1	Yes
PLA + 40 % OLLA-P	-	-	No

a-c: different superscripts within the same column indicates significant differences among samples ($p<0.05$)

25 wt.% of OLLA-P content. In fact, although the material with an oligomer content of 30 wt.% was capable of structuring a continuous film, its visual appearance was not good and a substantial deterioration, in terms of handling, was noticed, in comparison with the pure high M_w PLA film.

3.3. Characterization of the optimized PLA-OLLA blends

3.3.1. Optical properties

Both OLLA-D and OLLA-P were blended with high M_w PLA at the optimized composition (i.e. PLA-OLLA 25 wt.%). In order to ascertain if the addition of this amount of oligomer affected the optical appearance of the PLA films, both, contact transparency and transparency against a background pictures were taken (cf. Figure 3). These pictures showed that the addition of both direct and purified oligomers to the PLA matrix did not significantly affect its optical properties.

3.3.2. Thermal properties and thermal stability of the blends

Tables 2 and 3 show the thermal characteristics of the samples determined from the DSC first and second heating runs, respectively. From these tables, it can be observed that when the oligomers were added to the high M_w PLA matrix, double melting peaks appeared. Some authors have ascribed the double melting behaviour to the melt-recrystallization model [46] suggesting that small and imperfect crystals are able to evolve during the DSC heating scan into more stable crystals through a melt-recrystallization mechanism. This model can be used when there is a crystal size distribution of a single phase material. In this case, the obtained polymer was composed of two different crystalline species that were coexisting in the final material, which have been referred to as α and β crystals by some authors [47].

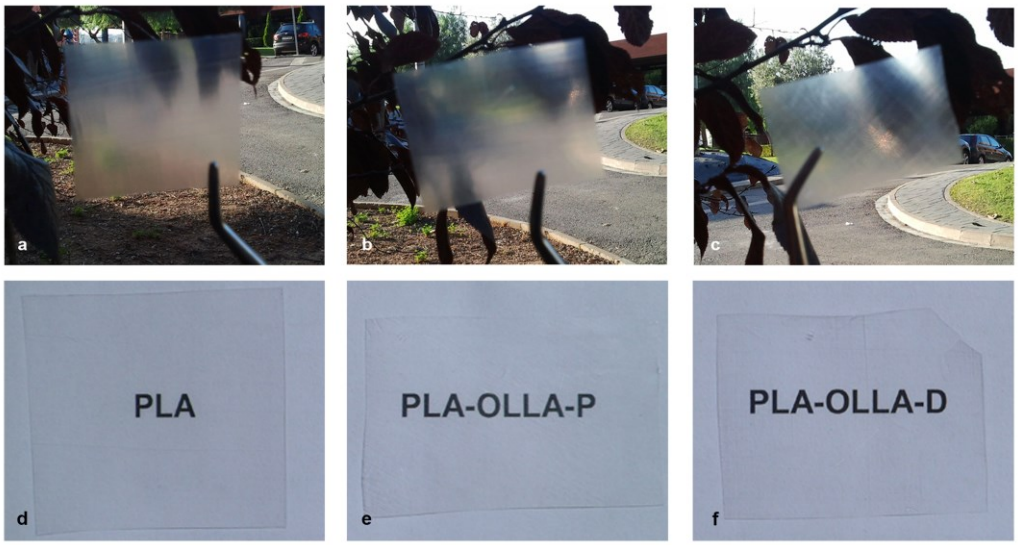

Figure 3. Photographs of ~100μm thickness films showing their transparency against a background and contact transparency, respectively, for PLA (a, d), PLA-OLLA-P (b, e) and PLA-OLLA-D (c, f)

Table 2. DSC maximum of melting (T_m), glass transition temperature (T_g), melting enthalpy (ΔH_m), cold crystallization temperature (T_{cc}) and degree of crystallinity (X_c) of PLA and its blends with LA oligomers during the first heating run

	T_g(°C)	T_{m1} (°C)	T_{m2} (°C)	T_{cc} (°C)	ΔH_m(J g^{-1})	%X_c
PLA	59.4 ± 3.2^a	-	148.6 ± 0.6^a	113.4 ± 0.2^a	6.6 ± 0.1^a	7.1^a
PLA+OLLA-P	48.0 ± 0.4^b	137.9 ± 1.3^a	149.4 ± 1.4^a	99.9 ± 1.5^b	4.4 ± 0.7^b	4.7^b
PLA+OLLA-D	36.3 ± 2.9^c	133.9 ± 5.1^a	145.1 ± 0.8^b	96.9 ± 3.5^b	3.8 ± 0.8^b	4.1^b

a-c: different superscripts within the same column indicates significant differences among samples (p<0.05)

Table 3. DSC maximum of melting (T_m), glass transition temperature (T_g), melting enthalpy (ΔH_m) and cold crystallization temperature (T_{cc}) of PLA and its blends with LA oligomers during the second heating run

	T_g(°C)	T_{m1} (°C)	T_{m2} (°C)	T_{cc} (°C)	ΔH_m(J g^{-1})
PLA	58.8 ± 1.3^a	-	148.9 ± 0.8^a	117.5 ± 0.0^a	6.6 ± 1.8^a
PLA+OLLA-P	50.7 ± 0.4^b	138.6 ± 1.0^a	148.9 ±1.3^a	104.0 ± 0.7^b	3.5 ± 0.7^{ab}
PLA +OLLA-D	39.9 ± 2.6^c	134.9 ± 2.8^a	145.3 ±1.1^b	103.7 ± 2.4^b	2.8 ± 0.1^b

a-c: different superscripts within the same column indicates significant differences among samples (p<0.05)

As a consequence, in this case, the double melting peaks could be attributed to the melting at lower temperature of less ordered or smaller crystals, followed by the melting of more perfect or bigger crystals. Yet another hypothesis arises from the work of Zhang et al. [48], who observed that, when the crystallization temperature of PLLA was below 120 °C, a modification of the α crystal form occurred, which was named α' (disordered α), corresponding to smaller spherulites. Thus, the double melting peak behaviour could be attributed either to a melt-recrystallization process [46] or to the coexistence of two different crystal size populations [47,48]. It should be noticed that in the blend containing the purified oligomer (i.e. PLA-OLLA-P), the melting temperature which corresponds to the higher temperature melting peak was the same as in the pure polymeric sample, thus suggesting that similar crystallites were formed in both materials. However, the addition of this purified oligomer to the PLA matrix hindered crystallization to some extent and, as a result, lower melting enthalpies were observed for the blends with oligomers. On the other hand, addition of the directly obtained oligomer (i.e. PLA-OLLA-D) resulted in a decrease in both melting peaks in comparison with PLA-OLLA-P. Therefore, in addition to reducing the degree of crystallinity to the some extent as previously observed for the PLA-OLLA-P, the addition of PLA-OLLA-D impaired proper chain packing, resulting in smaller or more defective crystals. Figure 4 displays the DSC curves during the second heating run for the pure PLA and for the blends with the purified and unpurified oligomers showing that, in the latter, broader melting peaks were observed, pointing out to the formation of more heterogeneous crystallites, probably due to the presence of impurities.

It is important to highlight that a single glass transition temperature was observed for the blends, thus, indicating a good miscibility between both components, as

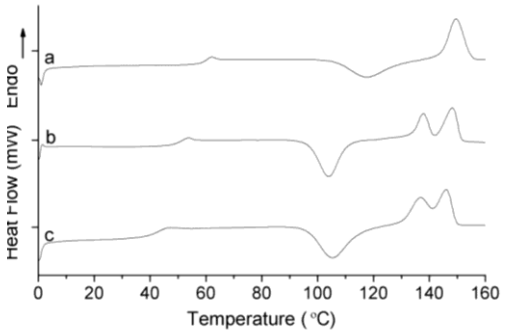

Figure 4. DSC second heating run curves of PLA (*a*), PLA-OLLA-P blends (*b*) and PLA-OLLA-D blends (*c*)

expected. Addition of the oligomers resulted in a T_g decrease, although less pronounced than that obtained in a recent work incorporating similar amounts of other commercial lactic acid oligomers [31]. The difference is mainly due to the different physical properties of the used oligomers. While T_g of the oligomers used by Burgos et al. [31] was -40.4 °C, the T_g values of the unpurified and purified oligomer used in this study were 13.8 °C and 27.7 °C respectively. This T_g decrease associated with enhanced long-range mobility fits the Fox equation for miscible blends [49]:

$$1/T_g = w_1/T_{g1} + w_2/T_{g2} \quad (2)$$

where "w" is the weight fraction of the blend constituents and T_{gi} are the T_g values of the pure components. According to this equation, the T_g values for the blends with OLLA-P and OLLA-D would be 46.2 °C and 32.5 °C, respectively, values which are very close to the ones obtained through DSC (cf. Table 2). Consequently, the oligomer-containing materials would change from the glassy to rubbery state at a lower temperature according to the overall decrease in molecular weight, since longer polymer chains require more energy to activate molecular mobility [50]. The greater decrease in T_g of PLA-OLLA-D could be attributed to the presence of impurities as previously explained.

Regarding the cold crystallization process of PLA, while the cold crystallization temperature of neat PLA occurred at about 117 °C in the second heating run, a sharp exothermic peak at ~104 °C was observed in the blends with oligomers (cf. Figure 4), which could be ascribed to a nucleating effect of the shorter polymer chains, as suggested by a previous study [51]. Moreover, narrower crystalli-zation peaks have been related to more homogeneous crystallites, indicating that enhanced crystallization occurs in the material when the crystallization peak narrows [52,53]. Comparing both blends, more heterogeneous crystals were obtained in the case of PLA-OLLA-D, as deduced from the broader melting and crystallization peaks.

Thermal degradation of PLA and their blends with oligomers was also studied by TGA. Figure 5 shows the weight loss and the first derivative curve from the different specimens and Table 4 gathers the decomposition temperature (calculated from the peak maximum of the first derivative), onset and endset degradation temperatures and the residue (%) at 410 °C for PLA and its blends with direct and purified LA oligomers. From this table, it can be stated that the addition of oligomer to the PLA matrix did not significantly affect the degradation temperature. However, from the first derivative curve, a lower onset of degradation was seen for the materials containing oligomers, which showed a shoulder before the main degradation peak (cf. Figure 5). Hence, the presence of two different species was also apparent in the blend materials, as expected, indicating that the short chain oligomers degraded at lower temperatures. This effect was more pronounced when the direct oligomer was added, as the presence of impurities provoked a greater decrease in the onset temperature. These results contrast with those obtained in a previous work, in which addition of 25 wt.% of LA oligomers to a PLA matrix caused a significant decrease in the

Table 4 TGA decomposition temperature, degradation onset and endset temperatures and % residue at 410 °C of PLA and its blends with direct (OLLA-D) and purified (OLLA-P) oligomer.

	T_d (°C)	T_{Onset} (°C)	T_{Endset} (°C)	Residue (%) at 410 °C
PLA	332.5	268.7	355.4	4.2
PLA-OLLA-P	332.1	256.2	353.3	1.0
PLA -OLLA-D	330.9	221.4	354.8	2.3

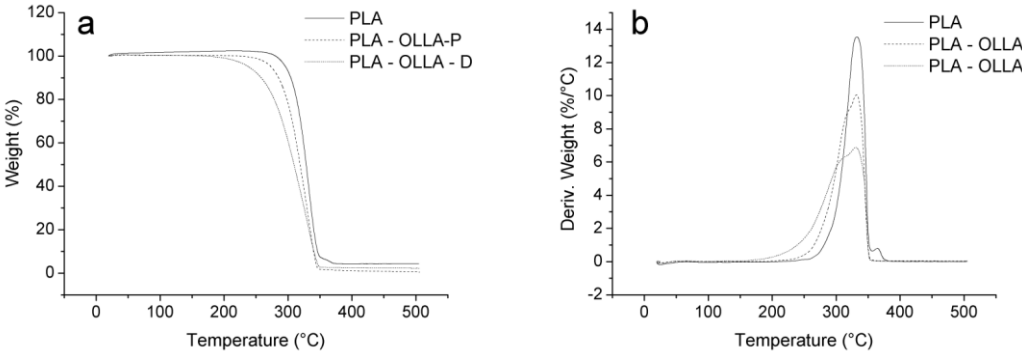

Figure 5. TG (*a*) and DTG (*b*) curves of pure PLA and its blends with direct (OLLA-D) and purified (OLLA-P) oligomer

maximum degradation temperature and a greater shift of the onset degradation temperature [31] , even if compared with the blend containing direct oligomer used in the present work. It could be mainly due to the above mentioned differences between the used oligomers.

3.3.3. Mechanical properties

The mechanical properties of the pure PLA film and of the blend films with oligomers are compiled in Table 5.

When OLLA-P was added to the PLA matrix, no significant effects on the mechanical properties of PLA were observed since tensile strength and elastic modulus remained almost constant. Although, there was a slight decrease in elongation at break, it was not significantly different, as shown by statistical analysis. Similar behaviour was previously reported by Ishihara et al. [54] when oligo (D-lactic acid) (ODLA), also obtained by the polycondensation method, was mixed with poly (L-lactic acid).

In contrast, OLLA-D addition into PLA matrices resulted in a significant decrease in the elastic modulus and tensile strength but no significant differences were observed in elongation at break, indicating that, though PLA-OLLA-D films were mechanically plasticized, they were not more stretchable.

Table 5. Mechanical properties of PLA and their blends with direct (OLLA-D) and purified (OLLA-P) oligomer.

	E modulus (MPa)	Tensile Strength (MPa)	ε_b (%)
PLA	1971.7 ± 39.0^a	45.5 ± 2.1^a	5.2 ± 3.0^a
PLA-OLLA-P	1983.3 ± 25.0^a	42.4 ± 3.7^{ab}	2.5 ± 0.2^a
PLA-OLLA-D	1321.8 ± 70.1^b	42.5 ± 1.6^b	4.4 ± 0.0^a

a-b: different superscripts within the same column indicates significant differences among samples ($p<0.05$)

This is closely related with the above-mentioned significant decrease in T_g values when OLLA-D was added to the polymer matrix, being a characteristic feature of plasticized systems [55]. Changes in mechanical properties are closely related with T_g variations. A progressive decrease of elastic modulus and tensile strength was observed as the T_g of the materials approaches the test temperature, normally room temperature [31, 56]. In this context, the addition of OLLA-D decreased the T_g value of PLA matrices near to room temperature, favoring the formation of more elastic films, although they were not more deformable, since no significant changes in elongation at break values were observed. On the contrary, the addition of OLLA-P did not modify tensile properties of PLA films probably due to the fact that the T_g value did not decreased as much.

3.3.4. Barrier properties

Oxygen permeability coefficients at two different relative humidities (0% and 80%) as well as water permeability coefficients were measured for PLA, PLA-OLLA-D and PLA-OLLA-P films (Tables 6 and 7 respectively). Interestingly, the oxygen and water permeability of PLA significantly decreased with the addition of LA oligomers, which confirms the antiplasticization effect on barrier that this low molecular weight compounds had on the PLA matrix since plasticization if often associated to deterioration in barrier properties [31,55]. More specifically, reductions in the oxygen permeability measured at 0% RH of ca. 47 and 54% were obtained for PLA-OLLA-P and PLA-OLLA-D films, respectively. Furthermore, even at high relative humidity (80%) reductions in the oxygen permeability values of ca. 22 and 7% for PLA-OLLA-P and PLA-OLLA-D films, respectively, were observed. Finally, the water permeability coefficient was reduced by 25 and 21% for PLA-OLLA-P and PLA-OLLA-D films, respectively. This effect is believed to be caused by a reduction in free volume of the matrix. Several works have demonstrated reductions in gas permeability associated with a fractional free volume blockage phenomenon in polymers leading to the antiplasticization effect [57,58]. Byun et al. [56] reported that PLA blended with poly ethylene glycol (PEG) had lower oxygen permeability than pure PLA. Contrary to the results here, although PEG acted as a mechanical plasticizer increasing elongation at break and reducing brittleness by decreasing T_g, an improvement in oxygen permeability was also seen. In that case, fractional free volume size played a crucial role in explaining the gas barrier, and a linear correlation between this parameter and the oxygen permeability was seen [56]. Several other research works have shown the relevant role of fractional free volume for explaining the barrier properties of polymer blends and composites [59][60].

A previous work reported that the specific volume of polymer blends can be either above or below the specific volume of the pure polymer at room temperature [57]. If the additive has a much higher free volume than the polymer, an increase of the free volume take place and preferential pathways are created for the transport of the low molecular weight molecules passing through, which seems to be the case in the materials developed by Burgos et al. [31]. On the other hand, if the additive free volume is not much higher or even lower than that of the polymer, which is thought to be the case in the present work, a reduction in free volume would take place [21]. Therefore, based on the free volume approach the reduction in T_g implies a densification of the material and hence, a reduction in the free volume. According to the dual mode model of sorption in polymers, two types of occupancy exist. Occupancy of unrelaxed (non equilibrium) volume region, known as Langmuir region, and occupancy of densely packed (equilibrium) region, known as Henry region.

Therefore, as described by Lee et al. [21], it appears that the short-chain oligomers would preferentially fill in the Langmuir sorption sites (the non equilibrium regions), since these “holes” can accommodate low molecular weight compounds without the need to dilate the matrix and do not increase the total free volume, as occurs when Henry regions are filled. This effect was even more pronounced when unreacted monomers and very short-chain oligomers (unpurified oligomer) were present in the film (PLA-OLLA-D) which occupied a greater free volume fraction.

Table 6. Oxygen permeability coefficients for PLA films and for their blend films with oligomers

	P oxygen (0% RH) ($m^3m\ m^{-2}s^{-1}Pa^{-1}$)	Reduction in oxygen permeability (%)	P oxygen (80% RH) ($m^3m\ m^{-2}s^{-1}Pa^{-1}$)	Reduction in oxygen permeability (%)
PLA	$2.017 \pm 0.083\ e^{-18\ a}$		$1.748 \pm 0.104\ e^{-18\ a}$	
PLA-OLLA-P	$1.064 \pm 0.163\ e^{-18\ b}$	47	$1.358 \pm 0.017\ e^{-18\ b}$	22
PLA-OLLA-D	$0.919 \pm 0.008\ e^{-18\ b}$	54	$1.626 \pm 0.172\ e^{-18\ ab}$	7

a-b: different superscripts within the same column indicates significant differences among samples ($p<0.05$)

Table 7 Water permeability coefficients for PLA films and for their blend films with oligomers.

	P water ($Kg\ m\ m^{-2}s^{-1}Pa^{-1}$)	Reduction in water permeability (%)
PLA	$1.669 \pm 0.053e^{-14\ a}$	
PLA-OLLA-P	$1.249 \pm 0.060e^{-14\ b}$	25
PLA-OLLA-D	$1.311 \pm 0.103e^{-14\ b}$	21

a-b: different superscripts within the same column indicates significant differences among samples ($p<0.05$)

The improvement in barrier properties was seen to greatly depend on the presence of water in the environment, as water molecules penetrate into the polymer matrix and can not only form an ordinary polymer-diluent solution, but also adsorb on hydrophilic sites [61]. Thus, the best results in oxygen permeability were found in the absence of water. PLA has two hydrophilic end groups, an alcohol initiating end group and a carboxylic acid terminating end group. As mentioned before, when the LA oligomers were added to the PLA matrix, more hydroxyl and carboxyl groups were present in the final material. Recent studies have demonstrated that these terminal groups significantly affect water sorption [62, 63]. Thus, these reactive end groups are capable of sorbing water, counteracting the antiplasticization of the material and leading to preferential pathways used for the oxygen molecules to pass through the films [56].

The transport properties of the blends with unpurified oligomer were more affected in the presence of water, since this material also had the hydroxyl groups of unreacted LA and very short chain oligomers which could retain larger amounts of water. In fact, while the reduction in oxygen permeability measured at 0% RH was greater for PLA-OLLA-D than PLA-OLLA-P, when the oxygen permeability was measured at 80% RH the material with the purified oligomer showed the best performance.

Likewise, addition of the oligomers also led to enhanced water barrier properties. Again, due to the high humidity condition, the decrease in water permeability was greater for the film containing the purified oligomer (PLA-OLLA-P). Nevertheless, for the water permeability measurements, the difference between the permeability reduction in the PLA-OLLA-D and PLA-OLLA-P films was not as pronounced as in the case of the oxygen permeability values measured at 80% RH. This could be explained by the fact that some of the water molecules may be sorbed in the materials structure, being this sorption affected by the number of hydroxyl groups available (greater for the film containing unpurified oligomer) which, thus, reduced the amount of water passing through the film.

4. CONCLUSIONS

Purified and unpurified LA oligomers obtained by a melt polymerization method were blended with a polymeric matrix of PLA by melt mixing, showing a very good compatibility and miscibility with the biopolyester. The optical properties indicated that addition of oligomers to the PLA matrix, did not significantly affect the optical properties of the material. The presence of oligomers slightly hindered crystallization (as lower melting enthalpies were observed) and two different crystalline species were coexisting in the final materials generating double melting peak behaviour. It is worth noting that when the unpurified oligomer was used, the presence of impurities had a negative effect in the melting temperatures, glass transition temperature and in the crystallization process. The purification step used was efficient for the removal of unreacted monomers and very short-chain oligomers as shown by the FTIR results and deduced from the rest of the characterization work. No significant changes were observed in the mechanical properties when the PLA matrix was blended with the purified oligomer. On the other hand, reduction in elastic modulus and tensile strength were obtained when PLA was blended with unpurified oligomer. This was primarily ascribed to the reduction in the T_g of the blend, which is close to room temperature and also to the test temperature for the mechanical properties. Regarding barrier properties, the oligomers were able to reduce the water permeability up to 25% (for PLA-OLLA-P), the oxygen permeability measured at 0%RH by up to 54% (for PLA-OLLA-D) and the oxygen permeability measured at 80%RH by up to 22% (for PLA-OLLA-P). The decrease in the permeability coefficients were associated to an antiplasticization phenomenon explained by reduction in the PLA free volume by oligomer molecules, which was counteracted by the plasticizing effect of water sorption at high humidity conditions.

REFERENCES

[1] Tang XZ, Kumar P, Alavi S, Sandeep KP. (2012) Recent Advances in Biopolymers and Biopolymer-Based Nanocomposites for Food Packaging Materials. Critical Reviews in Food Science and Nutrition 52(5):426-442.

[2] Rhim JW. (2007) Potential use of biopolymer-based nanocomposite films in food packaging applications. Food Science and Biotechnology 16(5):691-709.

[3] Madhavan Nampoothiri K, Nair NR, John RP. (2010) An overview of the recent developments in polylactide (PLA) research. Bioresource Technology 101(22):8493-8501.

[4] Jacobsen S, Fritz HG. (1999) Plasticizing polylactide - the effect of different plasticizers on the mechanical properties. Polymer Engineering and Science 39(7):1303-1310.

[5] Simoes CL, Viana JC, Cunha AM. (2009) Mechanical properties of poly(ε-caprolactone) and poly(lactic acid) blends. Journal of Applied Polymer Science 112(1):345-352.

[6] Sanchez-Garcia MD, Lagaron JM. (2010) On the use of plant cellulose nanowhiskers to enhance the barrier properties of polylactic acid. Cellulose 7(5):987-1004.

[7] Haafiz MKM, Hassan A, Zakaria Z, Inuwa IM, Islam MS, and Jawaid M (2013) Properties of polylactic acid composites reinforced with oil palm biomass microcrystalline cellulose. Carbohydrate Polymers 98, 139-45.

[8] Gorrasi G, Vittoria V, Murariu M, Da Silva Ferreira A, Alexandre M, Dubois P. (2008)

Effect of filler content and size on transport properties of water vapour in PLA/calcium sulfate composites. Biomacromolecules 9(3):984-990.

[9] Singh S, Gupta RK, Ghosh AK, Maiti SN, Bhattacharya SN. (2010) Poly (L-lactic acid)/layered silicate nanocomposite blown film for packaging application: Thermal, mechanical and barrier properties. Journal of Polymer Engineering 30(5-7):361-375.

[10] Katiyar V, Gerds N, Koch CB, Risbo J, Hansen HCB, Plackett D. (2011) Melt processing of poly(L-lactic acid) in the presence of organomodified anionic or cationic clays. Journal of Applied Polymer Science 122(1):112-125.

[11] Picard E, Espuche E, Fulchiron R. (2011) Effect of an organo-modified montmorillonite on PLA crystallization and gas barrier properties. Applied Clay Science 53(1):58-65.

[12] Fortunati E, Peltzer M, Armentano I, Torre L, Jiménez A, Kenny JM. (2012) Effects of modified cellulose nanocrystals on the barrier and migration properties of PLA nano-biocomposites. Carbohydrate Polymers 90 (2):948-956.

[13] Martínez-Sanz M, Lopez-Rubio A, Lagaron JM. (2012) Optimization of the dispersion of unmodified bacterial cellulose nanowhiskers into polylactide via melt compounding to significantly enhance barrier and mechanical properties. Biomacromolecules (11):3887-3899.

[14] Kim HK, Kim SJ, Lee HS, Choi JH, Jeong CM, Sung MH, et al. Mechanical and barrier properties of poly(lactic acid) films coated by nanoclay-ink composition. Journal of Applied Polymer Science 127 (5):3823-3829.

[15] Park SH, Lee HS, Choi JH, Jeong CM, Sung MH, Park HJ. (2012) Improvements in barrier properties of poly(lactic acid) films coated with chitosan or chitosan/clay nanocomposite. Journal of Applied Polymer Science 125(SUPPL. 1):E675-E680.

[16] Svagan AJ, Åkesson A, Cárdenas M, Bulut S, Knudsen JC, Risbo J, et al. (2012) Transparent films based on PLA and montmorillonite with tunable oxygen barrier properties. Biomacromolecules13(2):397-405.

[17] Martucci JF, Ruseckaite RA. (2010) Three-layer sheets based on gelatin and poly(lactic acid), part 1: Preparation and properties. Journal of Applied Polymer Science 118(5):3102-3110.

[18] Busolo MA, Torres-Giner S, Lagaron JM. (2009) Enhancing the gas barrier properties of polylactic acid by means of electrospun ultrathin zein fibers. Annual Technical Conference - ANTEC, Conference Proceedings, 5:2763-2767 2.

[19] Razavi SM, Dadbin S, Frounchi M. (2012) Oxygen-barrier properties of poly(lactic acid)/poly(vinyl acetate-co-vinyl alcohol) blends as biodegradable films. Journal of Applied Polymer Science 125(SUPPL. 2):E20-E26.

[20] Almenar E, Auras R. (2010) Permeation, Sorption, and Diffusion in Poly(Lactic Acid). In: Auras R, Lim L-T, Selke S, Tsuji H Poly(Lactic Acid) Synthesis, Structure, Properties, Processing and Applications: John Wiley & Sons, Inc.; pp. 155-179.

[21] Lee JS, Leisen J, Choudhury RP, Kriegel RM, Beckham HW, Koros WJ. (2012) Antiplasticization-based enhancement of poly(ethylene terephthalate) barrier properties. Polymer 53(1):213-222.

[22] Garcia A, Iriarte M, Uriarte C, Etxeberria A. (2006) Study of the relationship between transport properties and free volume based in polyamide blends. Journal of Membrane Science 284(1-2):173-179.

[23] Garcia A, Iriarte M, Uriarte C, Iruin JJ, Etxeberria A, Del Rio J. (2004) Antiplasticization of a polyamide: A positron

annihilation lifetime spectroscopy study. Polymer 45(9):2949-2957.

[24] Eceolaza S, Iriarte M, Uriarte C, Del Rio J, Etxeberria A. (2012) Influence of the organic compounds addition in the polymer free volume, gas sorption and diffusion. European Polymer Journal 48(7):1218-1229.

[25] Choudalakis G, Gotsis AD. (2012) Free volume and mass transport in polymer nanocomposites. Current Opinion in Colloid and Interface Science 17(3):132-140.

[26] Ni C, Luo R, Xu K, Chen GQ. (2009) Thermal and crystallinity property studies of poly (L-lactic acid) Blended with oligomers of 3-hydroxybutyrate or dendrimers of hydroxyalkanoic acids. Journal of Applied Polymer Science 111(4):1720-1727.

[27] Kanehashi S, Kusakabe A, Sato S, Nagai K. (2010) Analysis of permeability; solubility and diffusivity of carbon dioxide; oxygen; and nitrogen in crystalline and liquid crystalline polymers. Journal of Membrane Science 365(1-2):40-51.

[28] Tsuji H, Okino R, Daimon H, Fujie K. (2006) Water vapor permeability of poly(lactide)s: Effects of molecular characteristics and crystallinity. Journal of Applied Polymer Science 99(5):2245-2252.

[29] Komatsuka T, Kusakabe A, Nagai K. (2008) Characterization and gas transport properties of poly(lactic acid) blend membranes. Desalination 234(1-3):212-220.

[30] Drieskens M, Peeters R, Mullens J, Franco D, Iemstra PJ, Hristova-Bogaerds DG. (2009) Structure versus properties relationship of poly(lactic acid). I. effect of crystallinity on barrier properties. Journal of Polymer Science, Part B: Polymer Physics 47(22):2247-2258.

[31] Burgos N, Martino VP, Jiménez A. (2013) Characterization and ageing study of poly(lactic acid) films plasticized with oligomeric lactic acid. Polymer Degradation and Stability 98(2):651-658.

[32] Fiori S, Ara P. (2009) Method for plasticizing lactic acid polymers. Patent WO 2009/092825.

[33] Kiremitci-Gumusderelioglu M, Deniz G. (1999) Synthesis, characterization and in vitro degradation of poly(dl-lactide)/poly(dl-lactide-co-glycolide) films. Turkish Journal of Chemistry 23(2):153-161.

[34] Auras R, Harte B, Selke S. (2004) An overview of polylactides as packaging materials. Macromolecular Bioscience 4(9):835-864.

[35] Moon SI, Lee CW, Miyamoto M, Kimura Y. (2000) Melt polycondensation of L-lactic acid with Sn(II) catalysts activated by various proton acids: A direct manufacturing route to high molecular weight poly(L-lactic acid). Journal of Polymer Science, Part A: Polymer Chemistry 38(9):1673-1679.

[36] Noël M, Fredon E, Mougel E, Masson D, Masson E, Delmotte L. (2009) Lactic acid/wood-based composite material. Part 1: Synthesis and characterization. Bioresource Technology 100(20):4711-4716.

[37] Aydin E, Planell JA, Hasirci V. (2011) Hydroxyapatite nanorod-reinforced biodegradable poly(l-lactic acid) composites for bone plate applications. Journal of Materials Science: Materials in Medicine 22(11):2413-2427.

[38] Gonçalves CMB, Coutinho JoAP, Marrucho IM. (2010) Optical Properties. In: Auras R, Lim L-T, Selke S, Tsuji H Poly(Lactic Acid) Synthesis, Structure, Properties, Processing and Applications: John Wiley & Sons, Inc.; 97-112.

[39] Ristić IS, Tanasić L, Nikolić LB, Cakić SM, Ilić OZ, Radičević RZ, et al. (2011) The Properties of Poly(l-Lactide) Prepared by Different Synthesis Procedure. Journal of

Polymers and the Environment 19(2):419-430.

[40] Inkinen S, Hakkarainen M, Albertsson AC, Södergård A. (2011) From lactic acid to poly(lactic acid) (PLA): Characterization and analysis of PLA and Its precursors. Biomacromolecules 12(3):523-532.

[41] Zhang J, Duan Y, Sato H, Tsuji H, Noda I, Yan S, et al. (2005) Crystal modifications and thermal behavior of poly(L-lactic acid) revealed by infrared spectroscopy. Macromolecules 38(19):8012-8021.

[42] Kazuyo DS, Aki Sasashige T, Kanamoto T, Hyon SH. (2003) Preparation of oriented β-form poly(L-lactic acid) by solid-state coextrusion: Effect of extrusion variables. Macromolecules 36(10):3601-3605.

[43] Liu D, Yuan X, Bhattacharyya D. (2012) The effects of cellulose nanowhiskers on electrospun poly (lactic acid) nanofibres. Journal of Materials Science 47(7):3159-3165.

[44] Vasanthan N, Ly H, Ghosh S. (2011) Impact of nanoclay on isothermal cold crystallization kinetics and polymorphism of poly(L -lactic acid) nanocomposites. Journal of Physical Chemistry B 115(31):9556-9563.

[45] Braun B, Dorgan JR, Dec SF. (2006) Infrared spectroscopic determination of lactide concentration in polylactide: An improved methodology. Macromolecules 39(26):9302-9310.

[46] Yasuniwa M, Tsubakihara S, Sugimoto Y, Nakafuku C. (2004) Thermal analysis of the double-melting behavior of poly(L-lactic acid). Journal of Polymer Science, Part B: Polymer Physics 42(1):25-32.

[47] Xie J-X, Yang R-J. (2012) Preparation and characterization of high-molecular-weight poly(l-lactic acid) by chain-extending reaction with phosphites. Journal of Applied Polymer Science 124(5):3963-3970.

[48] Zhang J, Tashiro K, Tsuji H, Domb AJ. (2008) Disorder-to-order phase transition and multiple melting behavior of poly(L-lactide) investigated by simultaneous measurements of WAXD and DSC. Macromolecules 41(4):1352-1357.

[49] Olabisi O. (1981) Interpretations of polymer-polymer miscibility. Journal of Chemical Education 58(11):944-950.

[50] Sedlarik V, Kucharczyk P, Kasparkova V, Drbohlav J, Salakova A, Saha P. (2010) Optimization of the reaction conditions and characterization of L-lactic acid direct polycondensation products catalyzed by a non-metal-based compound. Journal of Applied Polymer Science 116(3):1597-1602.

[51] Xing Q, Zhang X, Dong X, Liu G, Wang D. (2012) Low-molecular weight aliphatic amides as nucleating agents for poly (L-lactic acid): Conformation variation induced crystallization enhancement. Polymer 53(11):2306-2314.

[52] Zhang KY, Ran XH, Zhuang YG, Yao B, Dong LS. (2009) Blends of poly(lactic acid) with thermoplastic acetylated starch. Chemical Research in Chinese Universities 25(5):748-753.

[53] Bhattacharyya AR, Sreekumar TV, Liu T, Kumar S, Ericson LM, Hauge RH, et al. (2003) Crystallization and orientation studies in polypropylene/single wall carbon nanotube composite. Polymer 44(8):2373-2377.

[54] Ishihara T, Ogata N, Shinokawa T, Tokunaga Y, Ogihara T, Nakane K. (2006) Structure and physical properties of poly(L-lactic acid)/Oligomeric(D-lactic acid) blends. Sen'i Gakkaishi 62(9):199-204.

[55] Courgneau C, Domenek S, Guinault A, Avérous L, Ducruet V. (2011) Analysis of the Structure-Properties Relationships of Different Multiphase Systems Based on Plasticized Poly(Lactic Acid). Journal of

Polymers and the Environment 19(2):362-371.

[56] Byun Y, Kim YT, Whiteside S. (2010) Characterization of an antioxidant polylactic acid (PLA) film prepared with α-tocopherol, BHT and polyethylene glycol using film cast extruder. Journal of Food Engineering 100(2):239-244.

[57] Larocca NM, Pessan LA. (2003) Effect of antiplasticisation on the volumetric, gas sorption and transport properties of polyetherimide. Journal of Membrane Science 218(1-2):69-92.

[58] Maeda Y, Paul DR. (1987) Effect of antiplasticization on gas sorption and transport. III. Free volume interpretation. Journal of Polymer Science, Part B: Polymer Physics 25(5):1005-1016.

[59] Yeh JT and Chen HY (2007) Blending and oxygen permeation properties of the blown films of blends of modified polyamide and ethylene vinyl alcohol copolymer with varying vinyl alcohol contents. Journal of Materials Science 42, 5742-5751.

[60] Mittal V (2008) Effect of the presence of excess ammonium ions on the clay surface on permeation properties of epoxy nanocomposites. Journal of Materials Science 43, 4972-4978.

[61] Apicella A, Egiziano L, Nicolais L, and Tucci V (1988) Environmental degradation of the electrical and thermal properties of organic insulating materials. Journal of Materials Science 23, 729-735.

[62] Singh VM, Koo D, Palmese GR, Cairncross RA. (2011) Synthesis of polylactide with varying molecular weight and aliphatic content: Effect on moisture sorption. Journal of Applied Polymer Science 120(5):2543-2549.

[63] Koo D, Du A, Palmese GR, Cairncross RA. (2012) Moisture management of polylactides: The effect of heat treatment. Polymer 53(5):1115-1123.

Chapter 2

MELT POLYCONDENSATION TO IMPROVE THE DISPERSION OF BACTERIAL CELLULOSE INTO POLYLACTIDE VIA MELT COMPOUNDING: ENHANCED BARRIER AND MECHANICAL PROPERTIES

J. Ambrosio-Martín, M. J. Fabra, A. Lopez-Rubio and J. M. Lagaron

Cellulose 2015, 22, 1201–1226

Novel Materials and Nanotechnology Group, IATA, CSIC, Av. Agustín Escardino 7, 46980 Paterna (Valencia), Spain.

ABSTRACT

Nanocomposites of polylactide (PLA) and bacterial cellulose nanowhiskers (BCNW) with improved properties were obtained through melt compounding. Prior to melt processing, and with the aim of improving BCNW dispersion, lactic acid oligomers (OLLA) were *in situ* polymerized in the presence of the nanofiller (both freeze-dried and partially hydrated). This *in situ* polymerization reaction enhanced the compatibilization between hydrophilic cellulose and hydrophobic PLA, even leading to chemical grafting of the OLLA onto the surface of BCNW, when this was used in a partially hydrated form. The optimized dispersion attained through this pre-incorporation strategy was confirmed by comparison with materials obtained through direct melt compounding of PLA with BCNW. Differential scanning calorimetry experiments showed that although cellulose content had not effect on melting temperatures, the degree of crystallinity was significantly affected. Addition of grafted BCNW also resulted in improved mechanical properties increasing the elastic modulus and tensile strength up to 52% and 31%, respectively, mainly ascribed to the promotion of filler-filler and filler-matrix interactions. Moreover, the developed nanocomposites showed improvements in the water and oxygen barrier properties (measured at 80% RH), respectively, which make them attractive for food packaging applications. This could be explained by well-dispersed nanocrystals acting as blocking agents within the polymeric matrix, reducing the diffusion through the nanocomposite films and, hence, the water and oxygen permeability. Therefore, this work offers a new route for incorporating well dispersed nanocellulose within a hydrophobic PLA matrix, overcoming the dispersion problems that this entails, especially when working with melt compounding methods.

Keywords: Bacterial cellulose; Cellulose nanowhiskers; Melt compounding; Lactic acid oligomers; Polylactide; *In situ* polymerization.

1. INTRODUCTION

Environmental concerns derived from the massive use of petroleum-based plastics, as well as possible future shortages of fossil resources, have boosted research on alternative bioplastic materials obtained from renewable sources.

Poly (lactic acid) (PLA) is one of the most widely studied thermoplastic sustainable biopolymers [1-4], due to its good optical and processing characteristics [5], in which is the most representative biodegradable and biobased polymer, and cost-competitive with respect to conventional polymers like poly(ethylene terephthalate) (PET) [6, 7]. It is an aliphatic polyester derived from 100% renewable resources that possesses numerous advantages and significantly lower non-renewable energy content compared with various other common polymers [8, 9].

However, PLA presents some drawbacks such as low thermal resistance, low flexibility and low barrier to oxygen and water compared to other benchmark packaging polymers. Therefore, strategies for enhancing its barrier and mechanical properties are needed for the commercial implementation of these materials so that they can broaden their scope of application while maintaining the biodegradable, renewable, and eco-friendly properties [10, 11].

Nanoreinforcement of biopolymers through the addition of, for instance, nanoclays or cellulose nanowhiskers, has already proven to be an effective strategy to enhance these properties [11, 16-19]. The so developed renewable and biodegradable polymer-based nanocomposites, commonly called “new green nanocomposite materials”, are the wave of the future, being considered as the next generation materials.

With the aim of developing fully renewable materials, the interest for cellulose nanowhiskers (CNW), also termed cellulose nanocrystals or nanocellulose, as nanofillers in biopolymer matrices has increased over the last years [20]. This is explained by the wide availability of cellulose from different sources [21], its low cost, easiness to recycle and the low power consumption required in its production [22]. Moreover, the high aspect ratio and good mechanical properties of the extracted cellulose nanowhiskers have made this class of nanomaterial very attractive for the preparation of low cost, lightweight and high mechanical properties nanocomposites [23].

Bacterial cellulose (BC), synthesized by some bacterial species, such as *Gluconacetobacter xylinus, Acetobacter hansenii* or *Acetobacter pasterianus* is an interesting alternative for the production of nanobiocomposites with improved properties. Although the chemical structure of plant cellulose (PC) and BC is the same, they have different structural organization which results in different mechanical properties, improved structure of the fibres and fibres network, higher water retention and higher crystallinity. Moreover, while PC is naturally associated with other biopolymers such as hemicellulose and lignin, BC is practically pure cellulose [24, 25]. Because of that, bacterial cellulose has been widely used as reinforcing filler for different polymeric matrices such as ethylene vinyl alcohol copolymers (EVOH), polyvinyl alcohol (PVA), polypyrrole (PPy), poly (lactic acid) (PLA), polystyrene (PS) and poly (3-hydroxybutyrate) (PHB) [13, 26-30].

Bacterial cellulose nanowhiskers (BCNW) can be obtained by subjecting BC to acid hydrolysis. It is well known that after acid hydrolysis the thermal stability of the BCNW is significantly reduced, making it unsuitable for the most melt-compoundable

polymer-based nanocomposites applications. Nevertheless, recent work has developed a new methodology to overcome this drawback [31]. The dimension of the nanocrystals depend on hydrolysis conditions, reaching cross sections with dimensions ca. 10-50nm [31, 32].

There are several challenges for developing nanobiocomposites containing cellulose nanowhiskers, which are mainly related to the hydrophilic nature of the fillers and their strong self-association, leading to agglomeration [33], when freeze-drying or when mixing through industrial-based melt processing technologies. In order to increase the compatibility of nanocellulose with hydrophobic matrices, either the use of surfactants [17, 34] or chemical surface modification of CNW [35-38] have been common strategies, but these modifications could compromise the biodegradability of CNW, also affecting the production prices. Complications about migration processes can also arise with these modifications in the case of food packaging materials.

Recently, several strategies to improve the dispersion of CNW in melt processed biopolymers have been developed based on the pre-incorporation of the nanocellulose either into EVOH electrospun fibres [39], PLA electrospun fibres or into EVOH matrix through precipitation [13]. Both pre-incorporation methods have demonstrated an improved dispersion of the nanofillers in the biopolymeric matrices, thus, resulting in improvements in mechanical and barrier properties.

A different strategy to enhance the compatibilization between CNW and hydrophobic biopolyesters like PLA, allowing better dispersion in a subsequent melt mixing step, has been to graft PLA onto the surface of the micro or nanocellulose [6, 40, 41]. Ring opening polymerization technique has been used to graft PLA onto CNW surface. Reduction in thermal degradation, increase in crystallization degree, limited reinforcing effect below T_g and an increase in the stiffness of the material above T_g have been reported in materials obtained through this technique [6]. On the other hand, improvements in heat distortion temperature (HDT) and mechanical properties were achieved when the accessible surface hydroxyl groups on the CNW surface were partially substituted by acetate groups prior to the ring opening polymerization. It allowed controlling the molecular weight of the grafted polymer chain, reaching sufficient molecular weight to avoid the necessity to blend the grafted material with neat homopolymer [41]. However, for ring opening polymerization (ROP), the use of organic solvents and catalyst in the reaction is necessary. Apart from the ROP technique to graft PLA onto nanocellulose surface, melt polycondensation polymerization has also been used to graft lactic acid oligomers onto microcrystalline cellulose (MC) surface. Improved dispersion was achieved in a subsequent melt mixing with PLA along with enhancement in thermal properties and mechanical properties. Despite of that, high contents of MC, up to ~30%, were necessary to obtain those enhancements and no barrier properties study was done [40].

In the present work, a methodology to improve the dispersion of the BCNW in a PLA matrix based on pre-incorporation of BCNW in lactic acid oligomers obtained by *in situ* melt polycondensation method has been developed, obtaining grafted lactic acid oligomers chains onto BCNW surface and enhancing the compatibility between BCNW and PLA in a subsequent melt mixing process. BCNW were used partially hydrated instead of freeze-dried, with the corresponding improvements in the final dispersion, as reported [6, 39, 42]. Moreover, in contrast with previous works [6, 13] it was not necessary to use organic

solvents to pre-disperse BCNW, since cellulose nanowhiskers aqueous suspensions are fully compatible with the polymerization process as the initial monomer is also in aqueous medium. The use of aqueous suspensions has some advantages, such as the high stability of cellulose in this solvent, the fact that no extra treatments are necessary, such as solvent exchange steps to use this nanoadditive, and also the reduction of the use of organic solvents during the synthesis of the materials (of paramount importance when used for direct contact with food). Furthermore, no catalyst was used in the oligomerization process.

The morphology, thermal properties and thermal stability, mechanical and barrier properties of the nanocomposites have been studied. For comparison purposes, direct melt mixing of PLA and freeze-dried or partially hydrated BCNW has also been carried out.

2. MATERIALS AND METHODS

2.1. Materials

The semicrystalline poly(lactic acid) (PLA) used was a film extrusion grade with a number average molecular weight (M_n) of 130,000 g mol^{-1} and a weight average molecular weight (M_w) of 150,000 g mol^{-1} manufactured by NatureWorks (USA). Lactic acid (LA) was supplied as a 90 wt.% aqueous solution by Across Organics (Belgium).

Sulphuric acid 96 wt.% and sodium hydroxide pellets were purchased from Panreac (Barcelona, Spain). The bacteria strain *Gluconacetobacter xylinus* was obtained from the Spanish type culture collection (CECT).

2.2. Preparation of bacterial cellulose mats

The bacteria *G. xylinus* was incubated in a modified Hestrin/Schramm medium at 30 °C [42]. All of the cells were pre-cultured in a test tube containing 5mL of media. When a thin layer of cellulose was detected on the surface, they were transferred to 200mL bottles and, subsequently, to containing bigger reactor of 20L. The synthesized bacterial cellulose pellicles, of about 2cm thickness obtained thereof were cut up (ca. 2cm × 2cm), sterilized and cleaned in boiling water and in a 10 wt.% (v/v) NaOH aqueous solution to remove bacterial cells and absorbed culture media. Finally, the pH was adjusted to neutral by boiling in distilled water several times.

2.3. Preparation of bacterial cellulose nanowhiskers (BCNW)

BCNW were obtained by the optimized method reported by Martinez-Sanz et al. [31]. Briefly, small pieces of bacterial cellulose at neutral pH were ground in a blender. A gel-like material was then obtained and compressed in order to remove most of the absorbed water. The partially dried cellulosic material was then treated with 301mL sulfuric acid L^{-1} water, in a cellulose/acid ratio of approximately 7 g L^{-1}, at 50 °C for 3 days, until homogenous solution was obtained. The cellulose nanowhiskers were obtained as a white precipitate after several centrifugations and washing cycles at 12.500 rpm and 15 °C for 20min. The pH of the samples was measured after the washing-centrifugation cycles, being around 2 for all the samples. Then, the material was re-suspended in deionized water and neutralized with sodium hydroxide until neutral pH and, subsequently, centrifuged to obtain the final product as a partially hydrated precipitate. This last step was thought to turn the filler

heat stable. One fraction of this material was freeze-dried and the other fraction was kept refrigerated. The humidity of the partially hydrated fraction was determined.

2.4. *In situ* melt polycondensation.

An initial mixture of lactic acid monomers and fillers (i.e. partially hydrated BCNW) in a weight ratio of 7% of BCNW to 93% of lactic acid oligomers, was performed using a homogenizer (Ultraturrax) for 5 min followed by sonication for another 5min. The mixture was placed in a three-necked flask equipped with mechanical stirrer, temperature controller and a vacuum system through a cold trap. Lactic acid oligomers were obtained after dehydration of the mixture at 150 °C and atmospheric pressure for 2 h. Then, a pressure of 100 mmHg was applied for another 2 h, followed by a final pressure of 30 mmHg for 4 h obtaining BCNW within a viscous liquid of oligo (L-lactic acid). The product was cooled and then ground into powder, washed with diethyl ether, vacuum filtered and dried at 70 °C for 24h in a vacuum oven. A purified material to be used as masterbatch with lactic acid oligomers grafted onto BCNW surface and free lactic acid oligomers was obtained (OLLA-BCNW). With comparative purposes the same procedure was carried out but using freeze-dried BCNW (OLLA-$BCNW_{FD}$). Moreover, using the aforementioned procedure but in absence of BCNW, purified lactic acid oligomers (OLLA) were obtained. The amount of partially hydrated or freeze-dried bacterial cellulose within the masterbatches was calculated by a calibration curve as explained below.

2.5. Preparation of films

Neat PLA as well as blends of OLLA-BCNW, OLLA and PLA were melt-mixed in a Brabender Plastograph internal mixer for 4 min at 162 °C and 100 rpm. Different amounts of OLLA-BCNW masterbatch were blended with neat PLA so as to have BCNW contents of 0.5, 1, 3 and 5 wt.% (sample codes: PLA-BCNW 0.5 %, PLA-BCNW 1 %, PLA-BCNW 3 %, PLA-BCNW 5 %). In the same way, blends of OLLA-$BCNW_{FD}$, OLLA, and PLA were obtained using the same conditions and with the same contents of BCNW specified above (sample codes: PLA-$BCNW_{FD}$ 0.5 %, PLA-$BCNW_{FD}$ 1 %, PLA-$BCNW_{FD}$ 3 %, PLA-$BCNW_{FD}$ 5 %). It should be mentioned that the maximum amount of OLLA added from the masterbatches was 2.75 wt.%, which correspond to the samples with 5 wt.% of BCNW and, thus, in order to keep constant OLLA content, pure OLLA was added to the other compositions developed. An additional blend with PLA and 2.75 % of pure OLLA was prepared and used as control sample (sample code: PLA–OLLA).

Furthermore, with comparative purposes, direct blends of PLA, OLLA and freeze-dried BCNW, (sample code: PLA-$BCNW_{FD}$-D), and PLA, OLLA and BCNW partially hydrated, (sample code: PLA-BCNW-D), were melt-mixed at weight ratios of 0,5 and 3 wt.% for BCNW and 2.75 wt.% OLLA using the same conditions specified above. Additionally, blends with OLLA-BCNW, OLLA and PLA were prepared in the same way with 25 wt.% of OLLA (considering the OLLA from the masterbatch and the free OLLA added) and 5 wt.% of BCNW (sample code: PLA-$OLLA_{25}$-$BCNW_5$). The obtained products were allowed to cool at room temperature and they were subsequently compression-moulded into films using a hot-plate hydraulic press (165 °C and 2MPa for 2 min). The so-obtained films had a thickness of about 100 ± 5 μm as measured with a Mitutoyo micrometer by averaging four measurements on each sample.

Table 1A detailing the compositions and procedures used to develop the different samples is provided in Annex A.

2.6. Transmission and attenuated total reflectance FTIR analysis.

Transmission FTIR experiments were recorded in a controlled chamber at 21 °C and 40 wt.% RH using a Bruker (Rheinstetten, Germany) FTIR Tensor 37 equipment. The spectra were taken at 1 cm^{-1} resolution averaging a minimum of 10 scans. Samples of 6 mg of OLLA-BCNW were ground and dispersed in 200 mg of spectroscopic grade KBr. A pellet was then formed by compressing the sample at 150 MPa. A calibration curve was obtained by recording the IR spectra of pellets containing 6 mg of the mixture of OLLA and BCNW with known concentrations of nanowhiskers in the range of 40 to 70 wt.%. The characteristics bands of cellulose overlapped with infrared bands of PLA due to their similar chemical structure. However, at lower wavenumbers, in the region of the characteristics bands of glucopyranose ring, the band at 560 cm^{-1} was chosen as the characteristic band of cellulose [43]. In this range there was no contribution from the OLLA. On the other hand, the intensity of the band at 872 cm^{-1}, which corresponds to the ν(C-COO) stretching [44], was chosen as the characteristic band for OLLA. The intensity of this band was divided by the intensity of the band at 560 cm^{-1} of cellulose and this ratio was plotted versus BCNW content. Subsequently, the IR spectra of the OLLA-BCNW pellet were recorded and the percentages of BCNW incorporated into the material were estimated.

ATR-FTIR spectra of BCNW, OLLA and OLLA-BCNW were collected in the same environmental conditions as the transmission experiments, coupling the ATR accessory GoldenGate of Specac Ltd. (Orpington, UK) to the above-mentioned FTIR equipment. All spectra were recorded within the wavenumber range of 4000–600 cm^{-1} by averaging 20 scans at 4 cm^{-1} resolution.

2.7. Optical properties

The transparency of the films was determined qualitatively and quantitatively. The qualitative study was performed by the assessment of the contact transparency of the films, while the quantitative analysis was performed through the surface reflectance spectra in a spectrocolorimeter CM-3600d (Minolta Co., Tokyo, Japan) with a 10 mm illuminated sample area in the visible region. Duplicate measurements were taken for each sample both using a white and a black background. Film transparency was evaluated through the internal transmittance (T_i) by applying the Kubelka-Munk theory for multiple scattering to the reflection data [45]. T_i of the films was quantified using Eq. (1). In this equation, R_0 is the reflectance of the film on an ideal black background. Parameters a and b were calculated by Eqs. (2) and eq (3), where R is the reflectance of the sample layer backed by a known reflectance R_g.

$$T_i = \sqrt{\left((a - R_0)^2 - b^2\right)} \quad (1)$$

$$a = \frac{1}{2}\left(R + \frac{R_0 - R + R_g}{R_0 R_g}\right) \quad (2)$$

$$b = \left(a^2 - 1\right)^{1/2} \quad (3)$$

2.8. Differential Scanning Calorimetry (DSC)

Thermal properties of OLLA, OLLA-BCNW, PLA and its nanocomposites (PLA-BCNW and PLA-$BCNW_{FD}$) were studied by DSC using a Perkin-Elmer DSC 7 calorimeter (Perkin–Elmer Cetus Instruments, Norwalk,

CT). DSC experiments were carried out on typically 3mg of dry material at heating rate of 10 °C min^{-1} from 0 °C to 160 °C in a nitrogen atmosphere using a refrigerating cooling accessory (Intracooler 2 from Perkin Elmer). The first and second melting endotherms, after controlled crystallization at 10 °C min^{-1} from the melt, were analysed. Calibration was performed using an indium sample and the slope of the thermal scans was corrected by subtracting similar scans of an empty pan. All tests were carried out, at least, in duplicate.

The degree of crystallinity (%) of PLA was estimated from the corrected enthalpy for biopolymer content in the final materials, using the ratio between the enthalpy of the studied material and the enthalpy of a perfect PLA crystal using the following equation:

$$\%Xc = \frac{\left(\Delta H_f - \Delta H_c\right)}{\Delta H_f^o\left(1-w\right)} \times 100 \qquad (4)$$

where ΔH_f is the enthalpy of fusion and ΔH_c the enthalpy of cold crystallization of the studied specimen. $\Delta H°_f$ is the enthalpy of fusion of a totally crystalline material and w is the weight fraction of the filler. The $\Delta H°_f$ used for this equation was 93 J g^{-1} for PLA [11].

2.9. Thermogravimetric Analysis (TGA)

Thermogravimetric (TG) curves of PLA and its nanocomposites (PLA-BCNW and PLA-$BCNW_{FD}$) were recorded using a thermobalance Setaram Setsys 16/18 (Setaram Instrumentation). Samples were heated from 25 °C to 600 °C at a heating rate of 10 °C min^{-1} under nitrogen atmosphere. Derivative thermogravimetric curves (DTG) express the weight loss rate as a function of temperature.

2.10. Water permeability

Direct permeability to water (P_w) was determined from the slope of weight loss versus time curves at 24 °C. The films were sandwiched between the aluminium top (open O-ring) and bottom (deposit for the permeant) parts of a specifically designed permeability cell with screws containing deionized water as the permeant. A Viton rubber O-ring was placed between the film and the top part of the cell to enhance sealability. The cells were placed inside a desiccator at 0%RH and the water weight loss through a film area of 0.001 m^2 was monitored and plotted as a function of time. In order to estimate the permeability values of the films, only the linear part of the weight loss data was used to ensure sample steady-state conditions. Cells with aluminium films were used as control samples to estimate solvent loss through the sealing. Water weight loss was calculated as the total cell weight loss minus the loss through the sealing. Tests were done in duplicate.

2.11. Oxygen transmission rate

The oxygen permeability coefficient (P) was derived from oxygen transmission rate (OTR) measurements recorded using an Oxtran 100 equipment (Modern Control Inc., Minneapolis, MN, US). Experiments were carried out at 24 °C and at 80% relative humidity conditions. Relative humidity was generated by a built-in gas bubbler and was checked with a hygrometer placed at the exit of the detector. The samples were purged with nitrogen for a minimum of 20 h in the humidity equilibrated samples, prior to exposure to an oxygen flow of 10 ml min^{-1}. A 5 cm^2 sample area was measured by using an in-house developed mask. The measurements were done in duplicate.

The diffusion coefficient, D, was estimated by the half-time method [46]. The

time $t_{1/2}$ is the point at which the transfer rate has reached 50% of the steady state flow. The relationship between the diffusion coefficient (D) and the time $t_{1/2}$ is derived by normalizing the equation of Fick's second law [47] (Eq. 5). Taking into account that for $t_{1/2}$ the OTR is half of the OTR reached in the steady state, D can be calculated from Eq. (6).

$$OTR(t) = \frac{Pp}{l}\left[1 + 2\sum_{n=1}^{\infty}(-1)^n \exp\left(-\frac{D\pi^2 n^2 t}{l^2}\right)\right] \quad (5)$$

$$D = \frac{l^2}{7.199 \cdot t_{1/2}} \quad (6)$$

where p is the oxygen partial pressure, l is the film thickness and t is time. The solubility coefficient (S) was subsequently calculated from the following equation:

$$P = D \times S \quad (7)$$

2.12. Mechanical properties

Tensile tests were carried out at 24 °C and 50% RH on an Instron 4400 Universal Tester. Pre-conditioned dumb-bell shaped specimens with initial gauge length of 25 mm and 5 mm in width were die-stamped from the films in the machine direction. The thickness of all specimens was approximately 100 μm. The storage conditions before test were 24 °C and 0% relative humidity. A fixed crosshead rate of 10 mm min^{-1} was used in all cases, and results were taken as the average of, at least, three tests.

2.13. X-Ray Difraction (XRD)

X-ray diffractograms were obtained using a D5005 Bruker diffractometer using monochromatic Cu-Kα radiation. The configuration of the equipment was θ–2θ and the samples were examined over the angular range of 5° to 45° with a step size of 0.02 and a count time of 4s per point.

2.14. Scanning electron microscopy (SEM)

For scanning electron microscopy (SEM) observation, the samples were cryofractured after immersion in liquid nitrogen, mounted on bevel sample holders and sputtered with Au/Pd under vacuum. The cross section images of the films were examined on a Hitachi microscope (Hitachi S-4100) at an accelerating voltage of 10 KV and a working distance of 12–16 mm.

2.15. Transmission Electron Microscopy (TEM).

Transmission electron microscopy (TEM) was performed using a JEOL 1010 (Jeol, Tokyo, Japan) equipped with a digital Bioscan (Gatan) image acquisition system. TEM observations were performed on one dried drop of a 0.001% aqueous suspension of BNCW on a carbon coated grid (200 mesh). Also ultrathin sections of microtomed nanocomposite films were observed by TEM. All samples were stained with a 2 wt.% solution of uranyl acetate prior to observation.

2.16. Statistical analysis

Results were analysed by multifactor analysis of variance (ANOVA) using Statgraphics Centurion 15.1 software (Statpoint Technologies, INC, Warrenton, VA, USA). Tukey's test was used at the 95% confidence level.

3. RESULTS AND DISCUSSION

3.1. Grafting of OLLA onto BCNW surface

The main objective of the present work was to enhance the barrier and mechanical properties of PLA through the addition of

bacterial cellulose nanowhiskers (BCNW). The strategy followed to improve the dispersion of the hydrophilic nanofillers within the hydrophobic biopolymeric matrix through melt processing was to pre-disperse the nanocellulose in lactic acid oligomers produced using a melt polycondensation reaction.

Initially, the BCNW were obtained following a recently optimized methodology [31]. The average cross-section of these nanofillers was ~22 nm, having a length of ~600 nm, as measured from the TEM images (cf. Figure 1), which was very similar to the morphology obtained by Martínez-Sanz et al. [31]. The crystallinity index (95.6%) and the thermal stability of the BCNW (onset degradation temperature of 228 °C and peak degradation temperature of 323 °C) were also close to those obtained in the mentioned work [31]. These high degradation temperatures ensured the thermal stability of nanocellulose during melt blending with PLA, which required lower processing temperatures.

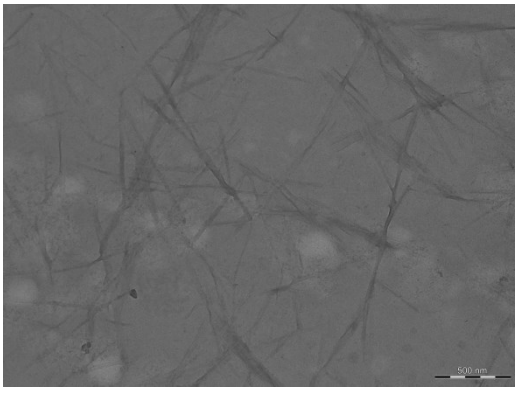

Figure 1. TEM micrographs of BCNW. Scale marker correspond to 500nm

Partially hydrated and freeze-dried BCNW were pre-dispersed in lactic acid oligomers by *in situ* melt polycondensation, using the Moon et al. reported method [48], obtaining grafted and ungrafted lactic acid oligomers onto BCNW surface. In order to remove unreacted monomers and very short chain oligomers, a purification step was carried out after oligomerization. Several methods to purify the material were compared (see General Discussion of the Results section). Purification with chloroform is widely used to purify PLA nanocomposites as previously reported in the literature [41, 49-51]. However, in this case, this purification was not suitable since, firstly, the obtained OLLA-BCNW material could not be properly separated by centrifugation and, secondly, both separation by filtration and direct precipitation generated a material with low OLLA content (~ 90-95 wt.% of cellulose as measured by the calibration curve, explained below) and, hence, strong interactions between cellulose nanocrystals were promoted, which was detrimental for the subsequent melt mixing step in terms of dispersion. On the other hand, washing the material with diethyl ether demonstrated to be a good method to eliminate unreacted monomers and very short chains oligomers, as previously reported, [52]. This method generated a perfectly dispersible material in a subsequent melt mixing process with polymeric matrices, as shown below. A scheme of the general procedure is given in Figure 1A in Annex A.

The material obtained through melt polycondensation was analysed through FTIR. Figure 2 shows the complete infrared spectra of OLLA, BCNW, and OLLA-BCNW (Figure 2a) and the magnification of some characteristics spectral bands (Figure 2b-d). The spectrum of the OLLA-BCNW material clearly shows contributions from both cellulose at 3345, 1164, 1055 and 1035 cm^{-1} and OLLA at 1750, 1130, 1085, 875 cm^{-1} (cf. Figure 2a), thus confirming the presence of both components in the material. Changes in the chemical composition of the material or interactions between the PLA matrix and the reinforcement as a consequence of grafting can be typically observed as shifts of the characteristic bands to higher wave

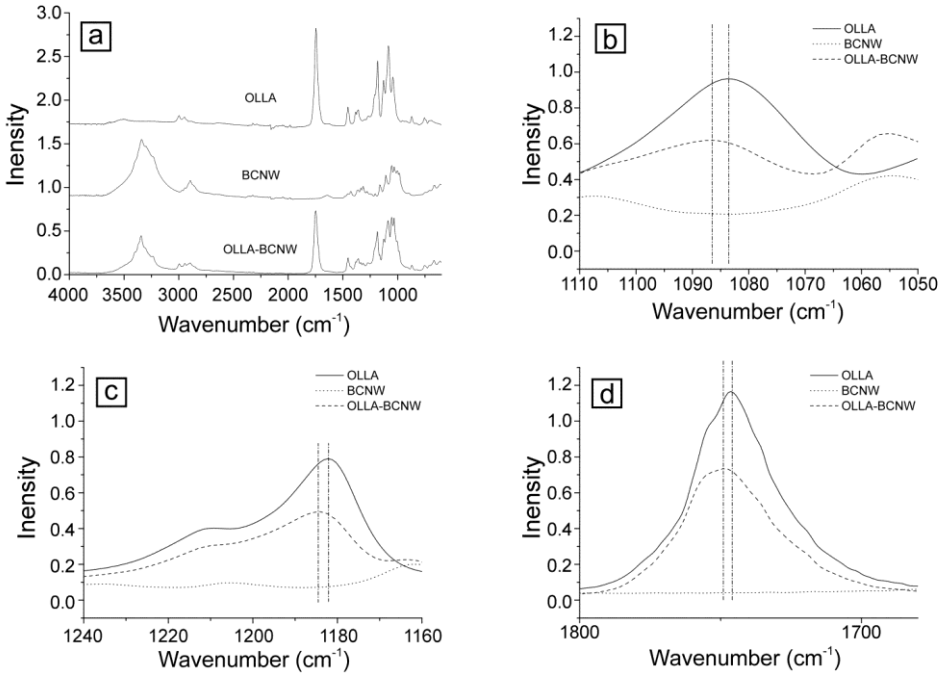

Figure 2. ATR-FTIR spectra of lactic acid oligomers (OLLA), BCNW and OLLA-BCNW (a). Magnifications at 1085 cm^{-1} (b), 1185 cm^{-1} (c), and 1750 cm^{-1} (d) areas.

numbers in the infrared spectra [1]. In this case, shifts to higher wavenumbers of the main bands ascribed to the ester bonds in OLLA-BCNW spectrum were observed if compared with pure oligomers spectrum, as can be seen in the bands around 1085, 1185 and 1750 cm^{-1}, depicted in Figure 2b, c and d, respectively. In comparison with these results, FTIR spectrum of OLLA-$BCNW_{FD}$ was also obtained (see General Discussion of the Results section and Annex A) and, although contributions of BCNW and OLLA were also showed, no shifts were observed for the same bands. This result suggests that the partially hydrated nanocellulose, or at least part of it, was chemically grafted to the oligomers while no chemical grafting seemed to occur when freeze-dried BCNW was used. Long term dispersion stability tests were also performed to further analyse the covalent grafting between the nanocellulose and the lactic acid oligomers. Three suspensions were prepared; two of

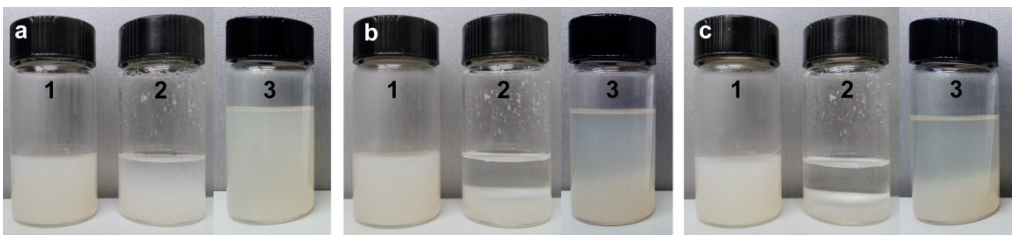

Figure 3. Suspensions of OLLA-BCNW nanocomposites (1), physical mixture of OLLA and BNCW (2) and OLLA-$BCNW_{FD}$ nanocomposites (3) in chloroform. Pictures recorded immediately after the stirring was stopped (a), 1 h later (b) and 72 h later (c)

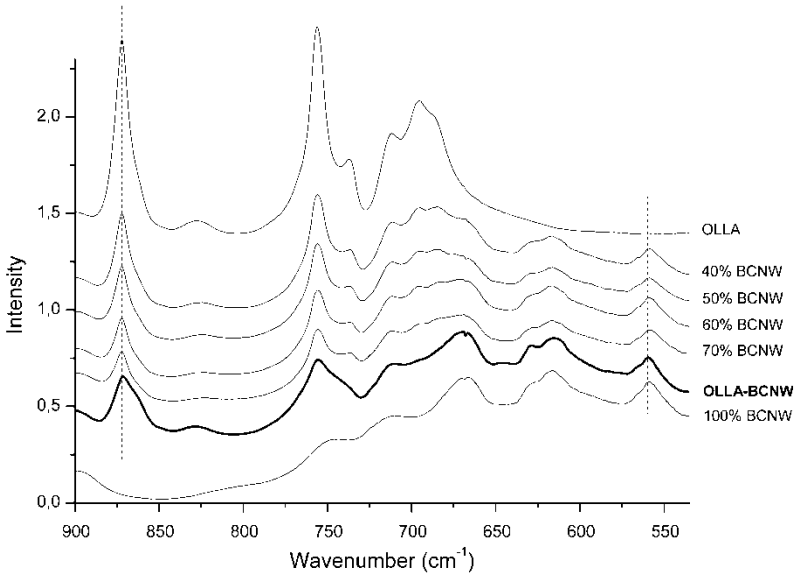

Figure 4. FTIR spectra of OLLA, BCNW, mixtures of OLLA and BCNW with known amounts of BCNW and OLLA-BCNW

them containing polymerized OLLA-BCNW and OLLA-$BCNW_{FD}$ respectively, suspended in chloroform and the last one consisting of a suspension of a physical mixture of OLLA and BCNW in chloroform. The ratio of OLLA/BCNW was kept constant for all suspensions. As previously reported in the literature, more homogenous and stable suspensions could be achieved when PLA chains are grafted on CNW surfaces [6]. Figure 3 clearly shows that the suspension of polymerized OLLA-BCNW was much more stable than the others resulting from OLLA-$BCNW_{FD}$ or physical mixtures of OLLA and BCNW, indicating that, in the polymerized material using partially hydrated BCNW, high solvation of grafted OLLA chains onto BCNW surface was produced, which allowed high stability of the nanocellulose suspended in chloroform. On the contrary, the suspension with the physical mixture of OLLA and BCNW was unstable and precipitation of the material was observed in less than 0.5 h. In the case of the OLLA-$BCNW_{FD}$ suspension, although a small fraction remained stable, precipitation was also observed. As previously reported, when BCNW is freeze-dried strong interactions are promoted between cellulose chains, being difficult to re-disperse individual nanowhiskers [42]. Therefore, this result could indicate that when freeze-dried BCNW were used during the polycondensation process, aggregation of the nanocellulose prevented an intimate mixing with the OLLA, thus leading to only a small fraction of the lactic acid material effectively grafted onto the BCNW. These results are in accordance with those previously observed in the FTIR analysis, where no shifts were observed in the main bands related to the ester bonds for OLLA-$BCNW_{FD}$.

In order to estimate the amount of BCNW incorporated into the polymerized material, a calibration curve was performed with known amounts of the two components. Transmission infrared spectra of KBr pellets containing different concentrations of OLLA and BCNW were analysed to locate characteristic bands

which could be used to estimate the concentration of nanowhiskers. Figure 4 displays the spectral range where not overlapping bands from both materials were present. As previously commented, bands at 560 and 872 cm^{-1} were chosen as the characteristic band of cellulose and OLLA respectively. The calibration curve was performed by relating the ratio of these two characteristic vibrational bands with the known nanocellulose contents. Subsequently, the IR spectra of the polymerized materials were analysed and the estimated percentage of BCNW present within the final materials was 65 wt.% for both OLLA-BCNW and OLLA-$BCNW_{FD}$.

These so-obtained materials were used as a masterbatches to obtain nanocomposites of PLA and BCNW through melt blending. For comparison purposes, nanocomposites of PLA with either freeze-dried or partially hydrated BCNW were also obtained through direct melt mixing.

3.2. Morphological characterization of the nanocomposites

In order to corroborate that the *in situ* polymerization strategy effectively improved the dispersion of nanocellulose in PLA nanocomposites obtained through melt compounding, films of PLA-BCNW, PLA-$BCNW_{FD}$, PLA-BCNW-D and PLA-$BCNW_{FD}$-D were compared. Figure 5 shows the obtained films of these materials with concentrations of 0.5 and 3 wt.% of BCNW. From this figure, agglomerates were clearly observed in the samples produced by direct melt-mixing with both freeze-dried and partially hydrated BCNW, indicating that poor dispersion of BCNW into PLA was obtained through these blending routes. As previously mentioned, in the case of freeze-dried BCNW, agglomeration was mainly related to the difficulty in re-dispersing the nanofiller within the polymer matrix due to the very strong self-association through hydrogen bonding induced upon freeze-drying [42]. When partially hydrated BCNW was directly added to the melt compounding process, flash evaporation of water is also thought to generate strong interactions between cellulose molecules, hence complicating their re-dispersion within the polymeric matrix. Despite the above, when freeze-dried BCNW was pre-incorporated by melt polycondensation no agglomerates were observed to the naked eye, leading to a relative good dispersion observed through macroscopic analysis. Furthermore, no agglomerates were observed in the samples obtained through blending PLA with OLLA-BCNW, suggesting that the used methodology led to a better dispersion of the nanofiller. Due to the poor dispersion of nanocellulose observed in PLA-BCNW-D and PLA-$BCNW_{FD}$-D, no further characterization of these materials was carried out, since it is well-known that agglomeration of the nanofiller in polymer nanocomposites results in poorer mechanical properties, particularly at high concentrations [33], and also in inferior barrier properties, especially in terms of water barrier properties [13]. This is again explained by the strong self-aggregating nature of cellulose nanowhiskers when the water is eliminated, generating poor interfacial filler-matrix adhesion and, thus, creating preferential pathways through the interphases.

The improved dispersion obtained for the nanocomposite containing the OLLA-BCNW was apparent even when increasing the nanofiller concentration. Figure 6 shows the contact transparency of pure PLA and the nanocomposite films. From this figure, a qualitative analysis was performed and similar transparency to that of PLA can be noticed, even for the compositions with higher nanocellulose contents, suggesting that a good dispersion of the filler in the PLA matrix was achieved. Films of OLLA-$BCNW_{FD}$ nanocomposites with concentrations of 0.5

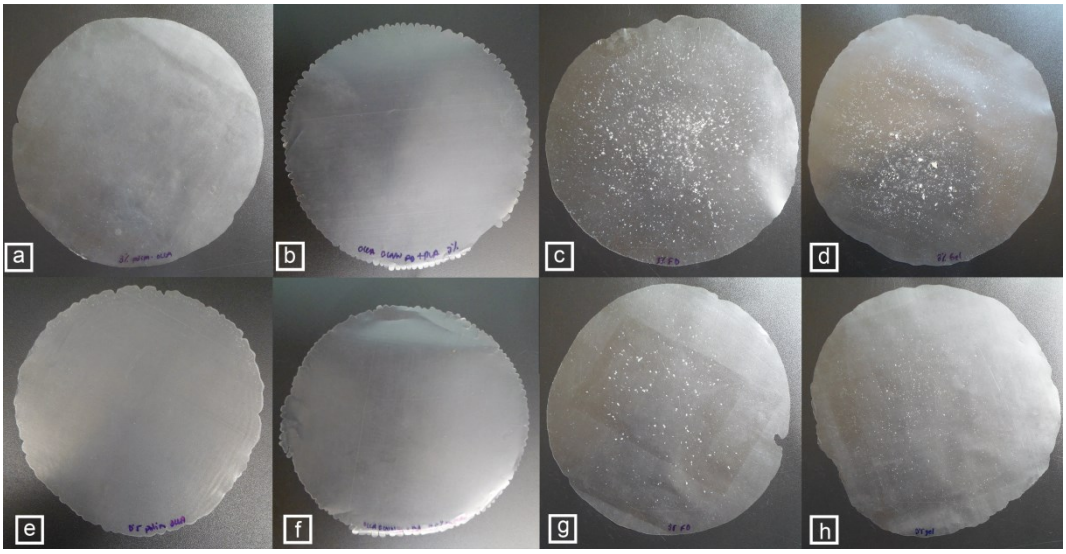

Figure 5. Photographs of ~100μm thickness films showing their contact transparency for films of PLA-BCNW (a, e), PLA-BCNW$_{FD}$ (b, f), PLA-BCNW$_{FD}$-D (c, g) and PLA-BCNW-D (d, h) at 3wt.% (upper) and 0.5 wt.% (bottom)

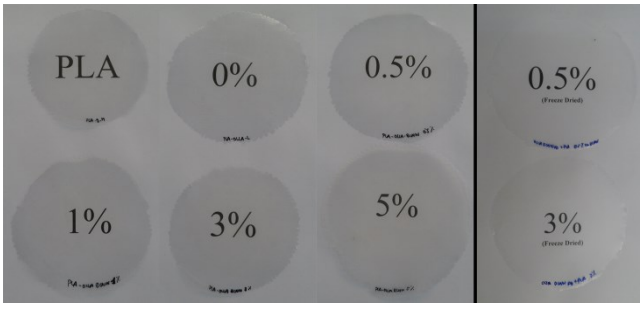

Figure 6. Photographs of ~100μm thickness films showing their contact transparency for films of PLA-BCNW and PLA-BCNW$_{FD}$ at different concentrations

and 3 wt.% are also shown in Figure 6. Good transparency was also observed for these films which were related with the relatively good dispersion of the freeze-dried BCNW when a pre-incorporation method based on *in situ* polymerization was used. The transparency of the films was further evaluated through a quantitative method by means of the visible light internal transmittance (T_i). Figure 7 shows the spectral curves of internal transmittance for PLA and its nanocomposites with partially hydrated and freeze-dried bacterial cellulose. High values of T_i correspond to more transparent films with a more homogeneous refractive index through their structure, whereas lower T_i values are related to more opaque films. As observed, similar behaviour to that of pure PLA was obtained for low BCNW content over the wavelength range studied (visible region) with small differences in T_i. However, as BCNW increased (both partially hydrated and freeze-dried cellulose), a gradual reduction in the internal transmittance was

noticed. As it has been previously reported, chemically pure glucans, such as bacterial cellulose, are poor absorbers of UV and visible light [53]. Hence it could be assumed that the loss of transparency in the visible region for the higher loaded samples was caused by the scattering of nanoparticles. In any case, internal transmittance was above 75% for all samples indicating good transparency of the films.

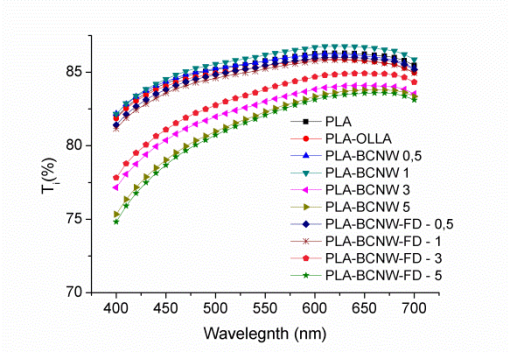

Figure 7. Spectral distribution of internal transmittance (T_i) of PLA and its nanocomposites with bacterial cellulose

The morphology and dispersion of the nanofillers within the PLA matrix were also studied by SEM and TEM experiments. Figure 8a-f shows the cryofractured sections of the nanocomposite films using OLLA-BCNW with increasing nanocellulose content. Good dispersion of BCNW, which appeared as small needles, was observed in all the samples. In the nanocomposites with greater nanocellulose content, i.e. 3 and 5 wt.%, there were areas with more nanofiller concentration, although no agglomerates were observed. Moreover, the fracture surface became less homogeneous for these samples, where some small voids and other surface irregularities, as a rougher surface, were clearly observed. The average cross sections of the BCNW for the different nanocomposites were 66 ± 9, 66 ± 21, 60 ± 23 and 74 ± 17 nm for the composites containing 0.5, 1, 3 and 5 wt.% respectively.

In addition, Figure 8g-h shows the cryofractured sections of the nanocomposite films using OLLA-$BCNW_{FD}$ with 0.5 and 3 wt.% BCNW content. In this case, although relative good dispersion was observed in certain areas (cf. Figure 2A in Annex A), big agglomerates and high concentration areas of BCNW were observed which led to a more open structure of the matrix (specially for the sample with greater BCNW content).Therefore, although good nanocellulose dispersion was suggested through macroscopic analysis when OLLA-$BCNW_{FD}$ was used, the melt polycondensation reaction was not able to proper re-disperse the self-associated cellulose chains generated during freeze-drying, as inferred from the microscopic examination.

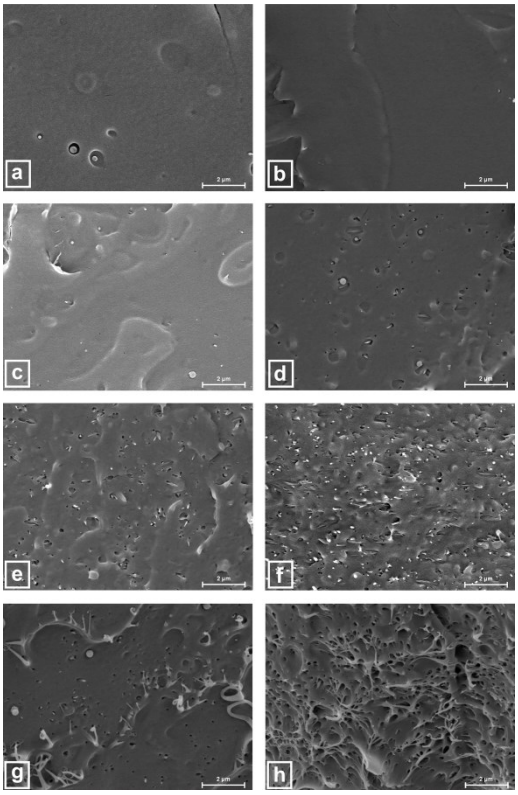

Figure 8. SEM micrographs of cryofractured sections of the PLA (a), PLA-OLLA (b), PLA-BCNW nanocomposites films at 0.5 wt.% (c) , 1 wt.% (d) , 3 wt.% (e) and 5

wt.% (f) and PLA-BCNW$_{FD}$ nanocomposites films at 0.5 wt.% (g) and 3 wt.% (h). Scale markers correspond to 2μm

TEM analysis confirmed the good nanofiller dispersion of BCNW in PLA-BCNW even at high nanocellulose contents. As an example, Figure 9 shows a TEM image for the PLA nanocomposites films containing 3 wt.% of BCNW. As expected, fibrillar morphology of the BCNW was observed having an average length of 465 ± 153 nm and an average cross section of 42 ± 5 nm.

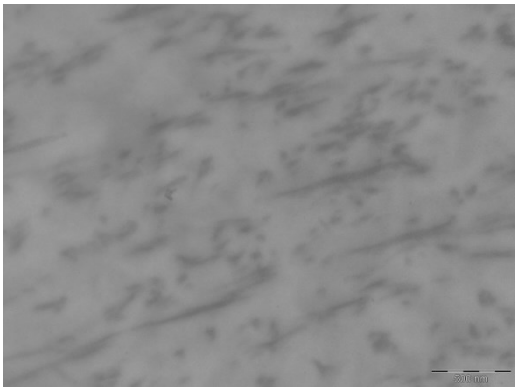

Figure 9. TEM micrographs of PLA-BCNW film containing 3 wt. % BCNW. Scale markers correspond to 500 nm

Therefore, and in agreement with previous works [13, 39, 26], it was possible to obtain highly dispersed nanowhiskers when using a pre-incorporation method prior to the melt blending process, in this case *in situ* melt polycondensation, and using partially hydrated nanowhiskers.

3.3. Thermal properties and thermal stability of PLA nanocomposites

Initially, DSC experiments were carried out to evaluate how the grafting of OLLA onto the BCNW surface affected their thermal properties. From Figure 10 it can be observed that incorporation of BCNW had two main effects regarding thermal properties of the polymerized materials. On one hand, a reduction in glass transition temperature (T_g) was noticeable. Jamshidi et al. (1988) reported the relationship between molecular weight and T_g of PLA [54], showing an increase in T_g with increasing number average molecular weight (M_n) of the samples, especially at low molecular weights.

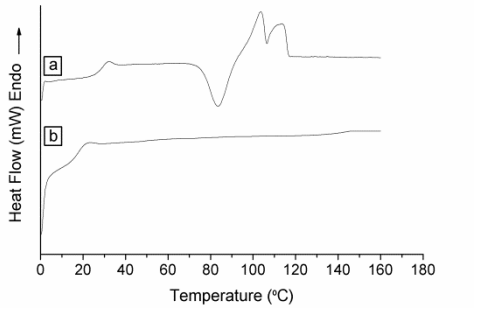

Figure 10. DSC curves of OLLA (a) and OLLA-BCNW (b)

Due to the impossibility of separating OLLA and OLLA-BCNW, it was not possible to measure the molecular weight of polymerized OLLA. However, an increase of the cellulose content results in increased number of initiating hydroxyl groups, which is known to result in a decrease in the average molecular weight of the grafted polymer chains [41]. Therefore, lower molecular weights of OLLA chains are expected upon polymerization in the presence of nanocellulose when compared with the molecular weight of the oligomers obtained in the same conditions without cellulose. This lower average molecular weight expected could thus explain the decrease in the T_g of the grafted material.

On the other hand, no crystallization peaks were observed when BCNW was incorporated. This result suggests that the addition of BCNW prevented proper chain packing of the OLLA chains, impeding crystallization.

Later on, DSC analyses of the melt blended nanocomposites were carried out in order to evaluate if the incorporation of OLLA-BCNW or OLLA-BCNW$_{FD}$ within the PLA matrix affected the thermal properties of the material. Melting temperature (T_m), cold crystallization temperature (T_{cc}), melting enthalpy (ΔH_m) normalized to the PLA content of the nanocomposites and degree of crystalinity (X_c) were determined from the DSC first heating run of the samples. Moreover, glass transition temperature (T_g) and the ratio between melting peak areas, directly related with melting enthalpy, were also evaluated for both the first and the second heating runs.

The effect of BCNW in thermal properties was characterized by comparing with samples developed with the same amount of oligomers. Table 1 gathers all the DSC data for PLA and its nanocomposites. As it can be seen, glass transition temperature slightly decreased for all compositions, both for the materials containing partially hydrated or freeze-dried cellulose. However, in the case of partially hydrated cellulose, only for the nanocomposite with greater loading, i.e. PLA-BCNW 5 wt.%, significant differences were observed when compared with the control sample (PLA-OLLA without BCNW). Despite the inherent rigidity of cellulose, previous works have demonstrated this effect when grafted PLA onto CNW surface or grafted LA oligomers onto microcrystalline cellulose surface were incorporated into PLA through melt blending [6, 40]. This result seems to be related to the molecular weight of the generated oligomer chains. It is well-known that entanglements between grafted and ungrafted polymer chains only occur when the molecular weight of the grafted polymer chains are high enough [6]. In fact, a previous study in which poly(ε-caprolactone) (PCL) chains of different molecular weights were grafted onto microfibrillated cellulose revealed that there

Table 1. DSC glass transition temperature (T_{g1}), maximum of melting peaks (T_m), melting enthalpy (ΔH_m), cold crystallization temperature (T_c), degree of crystallinity (X_c) and ratio between melting peak's areas $(A_1/A_2)_1$ during the first heating run and glass transition temperature (T_{g2}) and ratio between melting peaks areas $(A_1/A_2)_2$ during second heating run.

	T_{g1}(ºC)	T_{m1} (ºC)	T_{m2} (ºC)	T_c (ºC)	ΔH_m(J/g)	X_c(%)	$(A_1/A_2)_1$	T_{g2}(ºC)	$(A_1/A_2)_2$
PLA	55.4 ± 0.4^{a}	150.3 ± 0.4^{a}	112.4 ± 0.3^{a}	2.4 ± 0.4^{ab}	2.6 ± 0.4^{ab}			58.5 ± 0.2^{a}	
PLA-OLLA	55.3 ± 0.7^{a}	147.6 ± 0.4^{a}	151.3 ± 0.2^{b}	111.8 ± 0.3^{ab}	1.9 ± 1.0^{a}	2.0 ± 1.1^{a}	3.6 ± 0.4^{a}	57.2 ± 0.3^{abc}	7.6 ± 0.4^{a}
PLA–BCNW 0.5	53.7 ± 0.9^{ab}	147.8 ± 0.4^{a}	152.5 ± 0.7^{bc}	108.7 ± 2.4^{cde}	2.3 ± 1.3^{ab}	2.5 ± 1.4^{ab}	1.3 ± 0.3^{c}	57.4 ± 0.4^{ab}	6.3 ± 1.2^{b}
PLA–BCNW 1	53.9 ± 0.6^{ab}	145.9 ± 0.7^{a}	151.4 ± 0.7^{ab}	106.8 ± 1.3^{de}	5.0 ± 1.3^{cd}	5.4 ± 1.4^{cd}	1.1 ± 0.1^{cd}	56.7 ± 0.6^{abc}	4.8 ± 0.0^{c}
PLA–BCNW 3	55.3 ± 0.0^{a}	145.6 ± 0.5^{a}	151.2 ± 0.1^{ab}	106.0 ± 0.7^{e}	4.7 ± 0.4^{bcd}	5.0 ± 0.4^{bcd}	0.7 ± 0.1^{e}	55.6 ± 0.4^{cde}	3.8 ± 0.8^{c}
PLA–BCNW 5	52.9 ± 1.0^{b}	142.9 ± 0.9^{b}	150.4 ± 0.1^{a}	95.5 ± 1.2^{f}	5.6 ± 0.5^{d}	6.1 ± 0.6^{d}	0.2 ± 0.1^{f}	54.7 ± 0.0^{e}	1.9 ± 0.1^{de}
PLA–BCNW$_{FD}$ 0.5	53.0 ± 0.8^{b}	145.8 ± 0.3^{a}	152.0 ± 0.4^{abc}	110.6 ± 0.3^{abc}	2.4 ± 0.1^{ab}	2.6 ± 0.1^{ab}	2.1 ± 0.1^{b}	57.2 ± 0.1^{abc}	2.7 ± 0.1^{d}
PLA–BCNW$_{FD}$ 1	52.9 ± 0.6^{b}	145.3 ± 0.8^{a}	151.0 ± 1.2^{ab}	109.2 ± 1.0^{bcd}	3.6 ± 2.7^{bc}	3.9 ± 2.9^{bc}	1.1 ± 0.1^{cde}	56.9 ± 0.3^{bc}	1.3 ± 0.1^{e}
PLA–BCNW$_{FD}$ 3	53.1 ± 0.3^{b}	145.2 ± 1.3^{a}	151.0 ± 1.4^{ab}	108.5 ± 0.9^{cde}	3.0 ± 1.4^{bc}	3.2 ± 1.5^{bc}	1.1 ± 0.0^{cd}	56.0 ± 1.2^{bcd}	1.3 ± 0.0^{e}
PLA–BCNW$_{FD}$ 5	53.0 ± 1.1^{b}	145.0 ± 2.1^{a}	151.4 ± 2.1^{ab}	107.6 ± 1.9^{de}	1.6 ± 0.1^{a}	1.7 ± 0.1^{a}	0.7 ± 0.0^{de}	55.1 ± 1.2^{de}	0.9 ± 0.0^{e}

a-d: different superscripts within the same column indicates significant differences among samples ($p<0.05$)

was a correlation between the formation of physical entanglements and the length of the grafted chains [55].

In this case, even though there is a good compatibility and good miscibility between the OLLA-BCNW and the PLA matrix, it seems that the molecular weight of oligomers was not enough to generate proper entanglements between matrix and filler, thus resulting in a slight plasticization of the material, in terms of glass transition temperature. In addition, another factor that could affect the T_g is the added amount of OLLA-BCNW, as its molecular weight is lower than the molecular weight of OLLA synthesized without cellulose, as previously discussed, which could reduce the glass transition temperature of the final material. In fact, the greatest decrease in glass transition temperature was for PLA-BCNW 5 wt.% sample, where only OLLA-BCNW was added. On the other hand, in the case of the samples containing freeze-dried cellulose, significant differences were observed when compared with the control sample, while no differences were seen the different compositions. This could be ascribed to the lack of grafting of the OLLA molecules to the BCNW surface when freeze-dried cellulose was used, as previously suggested by the FTIR results.

Moreover, addition of oligomers to the PLA matrix gives rise to a double melting peak [52, 56]. This effect can be explained through different theories. Some authors have ascribed the double melting behaviour to the melt-recrystallization model [57], suggesting that small and imperfect crystals are able to evolve during the DSC heating scan into more stable crystals through a melt-recrystallization mechanism. Another hypothesis arises from the work of Zhang et al. [58], who observed that, when the cold crystallization temperature of PLLA was below 120 °C, a modification of the α crystal form occurred, which was named α' (disordered α), corresponding to smaller spherulites. In this case, the presence of two melting peaks could be ascribed to the two species that coexist in the material, i.e. the oligomer and the high molecular weight PLA. In fact, the temperature of the second melting peak remained almost constant in all samples when compared to the melting temperature of pure PLA. This indicates that similar crystals were formed in all materials. On the contrary, the temperature of the first melting peak was reduced when increasing the cellulose content with both partially hydrated of freeze-dried nanocellulose. It could be ascribed to the melting of the OLLA-BCNW, as nanocellulose has been reported to promote crystallization without affecting melting temperature [6, 13, 59] while addition of lactic acid oligomers has been reported to reduce melting temperature [56, 60]. As mentioned before, only OLLA from the masterbatches were incorporated in the nanocomposite with the greatest nanocellulose content (i.e. 5 wt.%), while for the other composites free OLLA (with a comparatively greater molecular weight than OLLA polymerized in the presence of BCNW) was also incorporated so as to have a constant oligomer content in all the samples. Therefore, the greater was the nanocellulose content the greater was the amount of lower molecular weight oligomers from the masterbatches added. This reduction in molecular weight was probably the cause for the reduced first melting peak temperature in the nanocomposites. In fact, lower melting temperature of the first melting peak was obtained as nanocellulose content increased.

To better understand how the incorporation of BCNW affected the crystallization process, the peak areas of the first and second melting peaks were studied. According to the data, the areas of the two meeting peaks appearing when OLLA was added to the PLA matrix were highly influenced by the presence of BCNW. In the

case of PLA-OLLA, a greater peak area was observed for the first melting peak indicating the development of a crystalline fraction mainly composed by smaller and/or less ordered crystals. On the contrary, as the BCNW content increased, the crystalline fraction was composed of more perfect or bigger crystals since the ratio between the areas of the first and second melting peaks (A_1/A_2) was greatly reduced. However, differences between partially hydrate and freeze-dried cellulose were observed since, although a reduction in the values of A_1/A_2 were observed in both cases, higher values of the areas ratio were obtained in the case of freeze-dried cellulose if compare with the same composition of partially hydrated cellulose. This indicated that smaller and/or less ordered crystals were formed when freeze-dried cellulose was used. The same behaviour was observed by Goffin et al. who realized that crystal growth seemed to be affected by the amount of the grafted CNW added to the PLA matrix. An increase in grafted CNW content induced an increase in the relative content of more perfect crystals [6].

It is well-known that cellulose nanowhiskers added into polymeric matrices act as nucleating agents favouring the crystallization process [13, 59, 61, 62]. Moreover, a recent study about the effects of fillers on crystal formation and on the crystalline structure of PLA has demonstrated that microfibrillated cellulose acted as a nucleating agent, accelerating the crystallization rate and reducing the cold crystallization temperature of PLA [63].

This nucleating effect of nanocellulose was also evident in the present study. While a decrease in the melting enthalpy (not statistically significant) was observed for PLA-OLLA when compared with pure PLA, being in accordance with previous work [52], addition of BCNW resulted in greater melting enthalpies and, thus, increased crystallinity of the materials. A threefold increase in the crystalline fraction was observed for the materials containing 5 wt.% of partially hydrated BCNW, indicating that increasing the amount of nanofiller resulted in improved biopolymer chain packing. Lower increments in the melting enthalpies were obtained when freeze-dried cellulose was used with a maximum for the concentration of 1wt.% and with values even lower than that for pure PLA for the sample with 5wt.%. Hence, lower nucleating effect was observed for freeze-dried cellulose which is directly related with the lower dispersion of the filler as observed in the morphological analysis. Moreover, addition of BCNW also favoured the cold crystallization process. Again, the lower nucleating effect of the freeze-dried cellulose was notice since a significantly lower reduction of the cold crystallization temperature was observed for this sample when compared with the nanocomposites containing partially hydrated cellulose (5 vs. 17 °C reduction for the highest loaded samples, respectively).

The thermal stability of PLA and its nanocomposites was evaluated through TGA. As observed in Table 2 addition of BCNW and also OLLA, did not significantly affect the thermal degradation temperature of most of the materials (both for PLA-BCNW and PLA-$BCNW_{FD}$ samples). In fact, a previous work reported that the addition of OLLA up to 25 wt.% in a PLA matrix did not affect the thermal degradation temperature of the biopolyester [52]. Interestingly, in the case of PLA-BCNW 5% a slight increase in the thermal degradation temperature was observed. It has been previously reported that high loadings of cellulose nanocrystals into a PHBV matrix led to a stronger nanowhiskers network and hence, thermal degradation was limited due to the restricted mobility of the polymer chains [64].

Table 2. TGA decomposition temperature. degradation onset and endset temperatures and % residue at 500 °C of PLA and its nanocomposites incorporating BCNW.

	T_d(°C)	T_{Onset} (°C)	T_{Endset} (°C)
PLA	360.8 ± 1.3^{ab}	333.8 ± 5.5^{a}	379.7 ± 6.5^{a}
PLA-OLLA	359.1 ± 2.2^{b}	326.2 ± 0.2^{ab}	377.3 ± 3.1^{a}
PLA –BCNW 0.5	361.5 ± 2.3^{ab}	323.0 ± 10.8^{ab}	380.6 ± 2.1^{a}
PLA –BCNW 1	361.8 ± 5.2^{ab}	324.9 ± 5.7^{ab}	379.2 ± 5.5^{a}
PLA –BCNW 3	362.6 ± 4.1^{ab}	321.4 ± 2.1^{b}	381.6 ± 4.5^{a}
PLA –BCNW 5	365.1 ± 2.5^{a}	323.2 ± 3.8^{ab}	382.0 ± 0.9^{a}
PLA –BCNW$_{FD}$ 0.5	359.1 ± 0.8^{b}	316.2 ± 5.1^{bc}	380.0 ± 0.6^{a}
PLA –BCNW$_{FD}$ 1	358.3 ± 1.1^{b}	310.0 ± 2.1^{c}	376.8 ± 0.7^{a}
PLA –BCNW$_{FD}$ 3	362.1 ± 1.7^{ab}	319.8 ± 4.8^{bc}	382.1 ± 2.2^{a}
PLA –BCNW$_{FD}$ 5	359.6 ± 0.6^{ab}	315.1 ± 2.2^{bc}	381.7 ± 0.9^{a}

a-d: different superscripts within the same column indicates significant differences among samples ($p<0.05$)

Regarding the onset degradation temperature, a reduction was observed for all the nanocomposites. This can be explained by the negative influence that short chain oligomers have on this onset degradation temperature when added to the PLA matrix, as previously reported [52]. No significant differences were observed in the endset degradation temperature suggesting that addition of BCNW had no effect on this property.

3.4. Crystallinity of the PLA nanocomposites

X-ray diffraction experiments were also carried out to evaluate the crystalline structure of PLA and its nanocomposites with partially hydrate cellulose. Figure 11 shows the X-ray diffractograms of the different samples. As it can be seen, PLA was practically an amorphous material. On the other hand, BCNW are highly crystalline materials with characteristic peaks located at 14,5°, 16,4° and 22,5° 2θ which correspond to the 101, 10$\bar{1}$ and 002 crystal planes from cellulose I, respectively [31]. It was difficult to observe these peaks at low nanofiller content due to the overlapping with the amorphous halo from the biopolymer. Nevertheless at higher nanofiller content characteristic bacterial nanocellulose crystalline reflections, especially the most intense cellulose I peak at 22,5° [31] were observed. These reflections were more noticeable as the BCNW content increase, suggesting the presence of crystalline domains which were related to the BCNW content. This was directly related with the results observed in the crystallinity studied by DSC where an increase of the crystallinity and also a promotion of the more perfect or bigger crystals were observed as the BCNW increase.

3.5. Barrier Properties of the PLA nanocomposites

Oxygen transport properties, i.e. permeability (P), diffusion (D) and solubility (S) coefficients measured at 80% relative humidity, as well as water vapour permeability (P_w) coefficients for PLA and its nanocomposites are compiled in Table 3.

The oxygen permeability for pure PLA measured in this study was very similar to that reported in the literature for PLA films processed by melt compounding [13, 16, 52, 65]. Moreover, the oxygen permeability for the PLA-OLLA sample was in accordance with our previous work, where a small addition of lactic acid oligomers resulted in an increase in the oxygen barrier properties [52].

Transport properties are known to be strongly related to different factors that either define the tortuosity of the path that

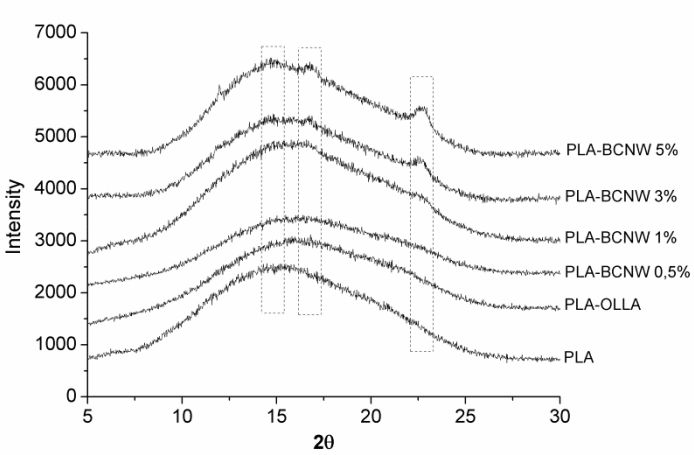

Figure 11. X-ray diffraction patterns of neat PLA and PLA-BCNW nanocomposites films at different concentrations

the permeant molecules need to follow or influence the kinetics of the process, including shape and aspect ratio of the filler, degree of dispersion, filler loading and orientation, adhesion to the matrix, moisture activity, filler-induced crystallinity, polymer chain immobilization, filler-induced solvent retention, degree of purity, porosity and size of the permeant [11]. Therefore, insufficient adhesion to the matrix or relatively low aspect ratios resulted, for instance, in detrimental effects on oxygen permeability [66], while greater aspect ratios (obtained through nanofabrication) and good dispersion yielded a more efficient barrier effect [11].

The first thing to mention is the reduction of the oxygen permeability for all the developed nanocomposites. In fact, the results presented here for PLA-BCNW are even better than those obtained using a casting methodology, while melt processing is known to favour nanofiller agglomeration [11]. These results further demonstrate that pre-dispersing BCNW within lactic acid oligomers obtained through polycondensation was a good strategy to attain a proper dispersion of the nanofiller and a very good interaction with the high molecular weight PLA matrix. Moreover, in contrast with the previously mentioned work [11], which exhibited the highest oxygen barrier improvements up to 2 - 3 wt.% CNW content, in this case, the greatest oxygen permeability decrease was observed for the sample with the highest nanocellulose loading, i.e. 5 wt.%.

The permeation of low-molecular weight chemical species through a polymeric matrix is generally envisaged as a combination of two processes, i.e. solution and diffusion. For PLA, it is has been reported that higher diffusion coefficients are obtained at high relative humidity conditions, due to the plasticization of the amorphous phase by water molecules. On the contrary, PLA solubility coefficients decrease in the same conditions due to the filling of the existing free volume by water molecules [67]. Recently it has been shown that addition of lactic acid oligomers to a PLA matrix resulted in a reduction of the oxygen and water permeability due to the occupancy of free volume by the oligomer molecules [52]. Moreover, it has been reported that addition of nanocellulose into PLA matrices, even when the filler is properly dispersed, generally increases the

Table 3. Oxygen transport properties, permeability (*P*), diffusion (*D*) and solubility (*S*) coefficients and water permeability coefficients (P_w) for PLA and its nanocomposites films incorporating BCNW.

	P (80% RH) ($m^3 m\ m^{-2} s^{-1} Pa^{-1}$)	*D* (80%RH) ($m^2\ s^{-1}$)	*S* (80%RH) ($g\ g^{-1} Pa^{-1}$)	P_w ($Kg\ m\ m^{-2} s^{-1} Pa^{-1}$)
PLA	$1.73 \pm 0.01\ e^{-18\ ab}$	$1.93\ e^{-12}$	$0.89\ e^{-6}$	$1.59 \pm 0.05\ e^{-14\ a}$
PLA-OLLA	$1.76 \pm 0.06\ e^{-18\ a}$	$2.05\ e^{-12}$	$0.86\ e^{-6}$	$1.58 \pm 0.05\ e^{-14\ a}$
PLA –BCNW 0.5	$1.69 \pm 0.13\ e^{-18\ ab}$	$2.12\ e^{-12}$	$0.80\ e^{-6}$	$1.44 \pm 0.01\ e^{-14\ b}$
PLA –BCNW 1	$1.58 \pm 0.02\ e^{-18\ bc}$	$1.91\ e^{-12}$	$0.83\ e^{-6}$	$1.45 \pm 0.06\ e^{-14\ b}$
PLA –BCNW 3	$1.52 \pm 0.07\ e^{-18\ cd}$	$1.98\ e^{-12}$	$0.77\ e^{-6}$	$1.45 \pm 0.02\ e^{-14\ b}$
PLA –BCNW 5	$1.36 \pm 0.04\ e^{-18\ d}$	$1.94\ e^{-12}$	$0.70\ e^{-6}$	$1.34 \pm 0.07\ e^{-14\ b}$
PLA –$BCNW_{FD}$ 0.5	$1.72 \pm 0.06\ e^{-18\ ab}$	$2.28\ e^{-12}$	$0.75\ e^{-6}$	$1.56 \pm 0.04\ e^{-14\ a}$
PLA –$BCNW_{FD}$ 1	$1.72 \pm 0.04\ e^{-18\ ab}$	$2.15\ e^{-12}$	$0.80\ e^{-06}$	$1.54 \pm 0.00\ e^{-14\ a}$
PLA –$BCNW_{FD}$ 3	$1.63 \pm 0.01\ e^{-18\ b}$	$2.15\ e^{-12}$	$0.76\ e^{-06}$	$1.51 \pm 0.01\ e^{-14\ ab}$
PLA –$BCNW_{FD}$ 5	$1.63 \pm 0.02\ e^{-18\ b}$	$2.30\ e^{-12}$	$0.71\ e^{-06}$	$1.46 \pm 0.05\ e^{-14\ b}$
PLA-$OLLA_{25}$-$BCNW_5$	$1.31 \pm 0.02\ e^{-18\ d}$	$2.07\ e^{-12}$	$0.63\ e^{-06}$	$1.28 \pm 0.01\ e^{-14\ c}$

a-c: different superscripts within the same column indicates significant differences among samples ($p<0.05$)

oxygen diffusion coefficient at high relative humidity since water molecules interact with the hydroxyl groups from the nanocellulose surface weakening the matrix-filler adhesion. Despite of that, a reduction in the oxygen permeability measured a 80%RH has been reported when comparing to that measured at 0%RH, mainly due to a reduction in the solubility coefficient [13]. Indeed, some reported studies have demonstrated that these hydroxyl groups significantly affect water sorption [68, 69]. In comparison with recent works [13], slightly lower diffusion coefficients were obtained for the PLA nanocomposites incorporating the OLLA-BCNW, especially at high BCNW content (cf. Table 3). In this case, probably due to the covalent grafting between BCNW and the oligomers, the water molecules found more difficulty to interact as a result of higher bond strength. Therefore, plasticization was slightly reduced due to the good filler-matrix adhesion, limiting to some extent the mobility of the polymeric chains. Apart from that, the solubility coefficient values were also slightly lower than those in the reported work by Martinez-Sanz et al. [13]. As mentioned above, at high relative humidity, water molecules filled the existing free volume in the polymer matrix. In addition, in the materials developed in the present work, the free volume was also occupied by OLLA molecules, as previously observed [52]. As a consequence, OLLA and water competed for the free sites within the polymer matrix resulting in a greater occupied free volume and, hence, in reduced solubility. It is interesting to note that the lowest oxygen solubility coefficient was for the sample containing 5 wt.% BCNW, which could be explained by the lower molecular weight of the added oligomers (no free OLLA added) which would probably had better ability to fill the available free volume. These combined lower diffusion and solubility coefficients in the PLA nanocomposites resulted in reduced oxygen permeability when compared with pure polymer, even for the highest BCNW content, i.e, 5 wt.%. This is contrary to previous work [13], where only there was improvement in barrier properties, measured at 80% RH, for the sample of 1 wt.% of BCNW in PLA, with neat permeability value similar to that reported here for the same content, but when increasing the BCNW content up to 2 or 3 wt.% a decrease in the barrier properties took place.

However, smaller decreases were noticed when freeze-dried cellulose was used in the polymerization process (PLA-$BCNW_{FD}$ samples), due to both the presence

of agglomerates and the more open structure generated. As a result, preferential pathways could be generated for the permeants to pass through the film, thus increasing the diffusion coefficients, as can be seen in Table 3. It is worth mentioning that for the same BCNW content (freeze-dried or partially hydrated) similar solubility coefficients were obtained.

It was previously reported that when only OLLA was added to a PLA matrix, a maximum increase in the barrier properties was observed with the addition 25 wt.% of OLLA [52]. In addition, this study has revealed that 5 wt.% BCNW content seems to have the optimum effect in terms of barrier properties (it should be remembered that this sample contained 2.75% of OLLA). Therefore, in order to study the potential synergistic effect of both components, a sample with 25 wt.% content of OLLA and 5 wt.% of BCNW was developed. Indeed, as observed in Table 3, the greatest reduction in the oxygen permeability was achieved for this sample, mainly ascribed to a combination of increased diffusion, related with an increment of OLLA and hence of hydroxyl groups, and decreased solubility, confirming in this way, the capacity of the lactic acid oligomers to fill the existing free volume within the polymer matrix.

The water permeability coefficient (P_w) of neat PLA was in the range of existing literature data of melt processed PLA [13, 65]. A reduction in water permeation was obtained for the different nanocomposites prepared, suggesting that BCNW acted as a blocking agent, reducing the solubility and/or diffusion of the low molecular weight compound through the films, as previously reported [13].

In contrast, it has been previously reported a detrimental effects on water vapour permeability when unmodified CNW was added to PLA matrix by solvent cast method, increasing the water vapour permeability as a function of the CNW content, due to filler agglomeration. Surface modification of cellulose greatly counteracted this negative effect, but no water vapour permeability improvement was observed [70]. To the best of our knowledge, there is scarce literature about the incorporation of CNW in PLA by melt mixing, and even less about the water barrier properties of the nanocomposites prepared through this technique. Martinez-Sanz et al. reported a significant reduction of the water vapour permeability when incorporating BCNW into PLA by melt compounding through the use of different pre-incorporation methods. Reductions of diffusion and solubility coefficients were achieved when BNCW was added to the PLA matrix. However, as expected, the direct melt mixing of freeze-dried BCNW with PLA resulted in increased water vapour permeability [13]. The reductions were higher than those reported here. As previously commented water sorption is affected by both the free volume fraction and the presence of hydroxyl groups. Therefore, these results could be explained on the basis of the increased number of hydroxyl groups present in the materials developed here as a consequence of oligomer incorporation, leading to greater water solubility through the interaction of water with these groups. In fact, for the compositions containing 0.5, 1 and 3 wt.% BCNW, where additional free OLLA was incorporated, the same reduction in water permeability was observed when compared with neat PLA. On the contrary, for the sample containing 5 wt.% BCNW, where no additional free OLLA was added, and hence, a greater fraction of the hydroxyl groups from the oligomer were covalently bonded, water permeability was further reduced. Therefore, in addition to the blocking effect of cellulose due to its excellent dispersion in the PLA matrix, lower water solubility due to the decreased number of hydroxyl groups

could be expected, thereby decreasing the water permeability to some extent.

As observed for the oxygen permeability, smaller decreases were noticed for PLA-BCNW$_{FD}$ samples due to the different morphology obtained for these films which thus had increased diffusion. Nevertheless, the same trend in the water permeability reduction was observed, i.e. the best performance was displayed for the sample with highest loading.

Water permeability was also evaluated to study the synergistic effect of OLLA and BCNW, added at 25 wt.% and 5 wt.%, respectively. As observed in the oxygen permeability study, the best performance in terms of water permeability was obtained for this sample. Addition of OLLA provided more hydroxyl groups but could also fill a greater free volume fraction within the material. Both issues affected water sorption in a different way. While an increase in hydroxyl groups increased water sorption, this was probably counteracted by the reduction in the free volume. Therefore, as deduced from the results, the added short chain oligomers had the capacity to fill the available free volume, being this effect dominant and giving rise to a reduction in the water vapour permeability.

3.6. Mechanical properties of the nanocomposites

Elastic modulus, tensile strength and elongation at break were measured for the different specimens and the results are gathered in Table 4. Previous works dealing with composite materials containing cellulose, showed a detrimental effect of this filler on the mechanical properties of the polymer, which was mainly ascribed to the lack of interfacial adhesion between the hydrophilic filler and the hydrophobic matrix [11, 71, 72]. Moreover, it is also widely recognized that a good dispersion of nanofillers is crucial for improving the mechanical properties. Both improving the filler-matrix interfacial adhesion through different methods, such as chemical surface modification of the filler [70, 73, 74] and promoting filler-filler interactions [22, 75, 76] have been proven to be successful strategies for enhancing the mechanical properties of cellulose-containing nanocomposites.

In this work, addition of BCNW pre-dispersed in *in situ* polymerized oligomers, resulted in a stiffening of the materials, reflected in an increase in the elastic modulus, up to 52% for the greatest BCNW content (5 wt.%) when it was used from the partially hydrated precipitate (cf. Table 4). This improvement was significantly greater than that reported for similar nanocomposites obtained in a previous study (52% vs. 17%), in which BCNW were incorporated to PLA through electrospun fibres [13]. This result confirms on one hand better filler-matrix adhesion of the materials developed in this work which could be ascribed to the grafting of the oligomers with the nanocellulose and, on the other hand, the greater fraction of the covalently bonded hydroxyl groups for the 5 wt.% BCNW sample which did not contain free oligomers, which inferred better performance in terms of mechanical properties.

On the contrary, when BCNW was used as freeze-dried material, although higher elastic modulus were also obtained when compared to pure PLA, lower improvements than those obtained with the partially hydrated cellulose were achieved, especially at high nanocellulose contents. This could be mainly ascribed to a lack of interfacial adhesion between the filler and the polymeric matrix, reduced dispersion of the freeze-dried filler and also to the presence of agglomerates, in agreement with the morphological and grafting evaluations.

Table 4. Elastic modulus (E), tensile strength and elongation at break (ε_b) for PLA and its nanocomposites incorporating BCNW.

	E (MPa)	Tensile Strength (MPa)	ε_b (%)
PLA	1363.33 ± 152.59^{a}	45.37 ± 3.24^{ab}	5.92 ± 1.26^{a}
PLA-OLLA	1439.08 ± 58.91^{a}	40.03 ± 9.25^{a}	4.08 ± 0.21^{b}
PLA –BCNW 0.5	1566.05 ± 208.03^{abc}	47.40 ± 3.63^{ab}	3.61 ± 0.38^{b}
PLA –BCNW 1	1732.05 ± 30.73^{c}	48.88 ± 4.68^{b}	3.44 ± 0.53^{b}
PLA –BCNW 3	1848.57 ± 54.24^{cd}	50.26 ± 6.72^{b}	3.19 ± 0.68^{b}
PLA –BCNW 5	2074.83 ± 13.24^{d}	59.68 ± 1.32^{c}	3.44 ± 0.13^{b}
PLA –BCNW$_{FD}$ 0.5	1534.44 ± 23.84^{b}	46.52 ± 1.16^{ab}	3.59 ± 0.39^{b}
PLA –BCNW$_{FD}$ 1	1549.28 ± 12.41^{b}	46.41 ± 1.06^{ab}	3.07 ± 0.31^{b}
PLA –BCNW$_{FD}$ 3	1647.99 ± 90.06^{bc}	49.23 ± 3.85^{b}	2.70 ± 0.39^{b}
PLA –BCNW$_{FD}$ 5	1669.25 ± 102.66^{bc}	46.81 ± 0.12^{ab}	2.73 ± 0.16^{b}
PLA-OLLA$_{25}$-BCNW$_5$	1661.23 ± 151.31^{bc}	30.20 ± 5.83^{d}	1.89± 0.63^{c}

a-d: different superscripts within the same column indicates significant differences among samples ($p<0.05$)

Furthermore, the increase in BCNW content in the nanocomposites also led to an increase in the tensile strength of the films. The same effect was reported in several works incorporating nanocellulose in different polymer matrices such as PLA, EVOH or PVA [13, 75, 76]. Lower improvements were also obtained when freeze-dried BCNW were used, especially at high contents due to the morphological characteristics of these samples, as previously commented. These results further prove that good dispersion and proper interfacial interactions favour an effective load transfer from the biopolymer chains to the nanocrystals. This is in accordance with previous studies in which a decrease in tensile strength was observed upon addition of nanocellulose as a consequence of poor dispersion and filler-matrix adhesion [11, 33].

Finally, in general, no significant differences were observed between the elongation at break of the different BCNW-containing nanocomposites with respect to the control sample containing lactic acid oligomers, although the same trend as with the other mechanical parameters studied was observed for the samples with freeze-dried BCNW. It is well-known that addition of reinforcing agents, such as BCNW, reduces the elongation at break of polymeric materials, since they act as stress concentrating components. However, when matrix-filler interactions take place, through hydrogen bonding and van der Waals interactions, this stress concentration effect is prevented to a certain extent [13, 76, 77]. In fact, when matrix-filler interfacial adhesion is promoted, no effect or even improvements in elongation at break have been reported [13, 70, 76].

In a previous work where only OLLA was added to PLA at 25 wt.% loading, no effect was observed in terms of elastic modulus [52]. Nevertheless, when BCNW was incorporated at 5 wt.% loading (PLA-OLLA$_{25}$-BCNW$_5$) an increase in the elastic modulus was observed bearing out the reinforcing effect of nanocellulose. However, due to the addition of free oligomer chains which could hinder filler-matrix adhesion to some extent, the improvement was lower that that for the PLA-BCNW 5 wt.% sample. Moreover, an important embrittlement of this sample was obtained as shown in Table 4, with a reduction of both tensile strength and elongation at break. It seems that addition of high concentration of oligomers in combination with BCNW had a negative synergistic effect in terms of mechanical properties.

Therefore, this pre-incorporation method by *in situ* melt polycondensation has demonstrated not only to improve the dispersion of the nanocellulose in the PLA matrix, but also to enhance the interfacial filler-matrix adhesion and, thus, the mechanical properties of the materials. An important condition to obtain strong mechanical reinforcement is to achieve the so-called percolation threshold, where the nanowhiskers are strongly interconnected by a 3D network. The percolation threshold can be easily estimated using the following equation [22]:

$$\upsilon_{RC} = \frac{0.7}{L/d} \quad (8)$$

where υ_{RC} is the percolation threshold and L/d is the aspect ratio of the filler. For nanocomposites incorporating BCNW with an average cross-section of ~22 nm and length of ~600 nm, as mentioned before, the experimental aspect ratio is about 27 and, hence, the percolation threshold should lay around 2.5 v.%. Interestingly, addition of only 0.8 v.% of BCNW (1 wt.%) resulted in a statistically significant increase in the elastic modulus. This could be explained because in the percolation threshold model only filler-filler interactions are taken into account, while in this case filler-matrix interactions are also of paramount importance as a consequence of the grafted oligomer chains, thus leading to improvements in the elastic modulus with lower contents of filler than those predicted by the percolation threshold model. The best result in terms of elastic modulus was for the material containing 5 wt.% BCNW, highlighting that even for the material with the greatest nanofiller content, a good dispersion and good matrix-filler and filler-filler interactions were achieved.

Modelling of the mechanical properties using the following Halpin–Tsai equations was carried out to correlate our data with the theoretical expectations [66]:

$$E = \frac{E_m(1+\xi\eta\phi)}{1-\eta\phi} \quad (9)$$

$$\eta = \frac{E_r/E_m - 1}{E_r/E_m + \xi} \quad (10)$$

$$\xi = \frac{2\times length}{thickness} \quad (11)$$

where E_m and E_r indicate elastic modulus of matrix and reinforcement respectively, ξ is calculated from the length and thickness of the nanofiller, and ϕ indicates volume fraction.

The following data were used in the calculations: E_{PLA}= 1.36 GPa, $E_{cellulose}$ = 167.5 GPa. [78].

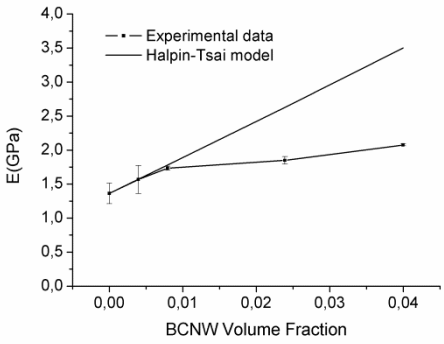

Figure 12. Experimentally measured Young's modulus for PLA-BCNW nanocomposites compared to theoretical predictions by Halpin–Tsai model

The values obtained from the theoretical model in comparison with the experimental values are shown in Figure 12. From this figure it can be observed that the experimental values fitted very well those predicted by the theoretical model only at low concentrations. On the contrary, at higher concentrations the experimental values diverted from those predicted. It is worth noting that the theoretical calculations are based on fully dispersed systems where the filler is aligned in the longitudinal direction and has perfect

interfacial adhesion to the matrix. According to the morphological study, although a good dispersion was achieved for all the samples, in the case of the nanocomposites containing 3 and 5 wt.% BCNW, areas with greater filler concentration, small voids and other irregularities in the polymer matrix were observed. As a result, even though there was an improvement of the mechanical properties for the latter compositions, these were lower if compared with those predicted by the Halpin-Tsai model.

4. CONCLUSIONS

In the present work, PLA-BCNW nanocomposites were successfully developed through a melt compounding method. A pre-incorporation step based on an *in situ* melt polycondensation reaction was carried out to obtain pre-dispersed BCNW within OLLA chains, with grafting between OLLA and BCNW. Morphological studies corroborated that this pre-incorporation step improved the subsequent melt mixing of PLA and BNCW overcoming the lack of dispersion that is obtained when unmodified freeze-dried or partially hydrated BCNW were used.

Analysis of thermal properties revealed that addition of BCNW to the melt polycondensation process directly affected the oligomer properties, especially the molecular weight. Moreover, both addition of neat and nanocellulose-containing oligomer resulted in decreased glass transition temperature of the nanocomposites, indicating a slight plasticization of the materials, in terms of glass transition temperature, upon incorporation of these low molecular weight compounds. On the other hand, a nucleating effect of BCNW was observed and, thus, increased melting enthalpies and decreased cold crystallization temperatures were obtained as a function of the nanocellulose content. In general, no effects were observed in the thermal stability of the obtained nanocomposites, except for the sample with highest cellulose content which displayed increased thermal stability ascribed to the stronger nanocellulose network generated.

Moreover, addition of OLLA-BCNW into PLA also had a beneficial effect in terms of barrier properties. The increase in the oxygen barrier at high relative humidity was due to a combined decrease in the diffusion and solubility coefficients, derived from the covalent grafting of BCNW with the oligomers and from the occupancy of the available free volume by both water and OLLA, respectively. Likewise, a reduction in water permeability was obtained due to the blocking capacity of the highly dispersed cellulose nanoparticles. Enhanced mechanical properties were obtained upon BCNW addition, mainly due to the improvement of the nanofiller dispersion obtained through the *in situ* polymerization technique which facilitated matrix-filler interactions, resulting in improvements of 52% in the elastic modulus and 31% in the tensile strength.

The obtained materials when freeze-dried BCNW was used in the polymerization process had reduced properties in terms of barrier and mechanical properties ascribed to the difficulty of re-dispersing the self-aggregated nanocellulose chains generated during the freeze-drying process. Finally, although the synergistic effect of oligomers loaded at 25 wt.% and BCNW loaded at 5 wt.% improved to some extent the barrier properties mainly due to the capacity of the oligomers to fill the available free volume, this composition with greater free oligomer content was detrimental for the mechanical properties. In summary, a new route to obtain PLA-cellulose nanowhiskers nanocomposites compatible with current industrial processes such as melt

compounding has been developed. The high nanofiller dispersion obtained through this route improved filler-matrix interactions, resulting in improved barrier and mechanical properties.

REFERENCES

[1] Inkinen S, Hakkarainen M, Albertsson AC, Södergård A. (2011) From lactic acid to poly(lactic acid) (PLA): Characterization and analysis of PLA and Its precursors. Biomacromolecules 12(3):523-532.

[2] Auras R, Harte B, Selke S. (2004) An overview of polylactides as packaging materials. Macromolecular Bioscience 4(9):835-864.

[3] Carrasco F, Pagès P, Gámez-Pérez J, Santana OO, Maspoch ML. (2010) Processing of poly(lactic acid): Characterization of chemical structure, thermal stability and mechanical properties. Polymer Degradation and Stability 95(2):116-125.

[4] Carrasco F, Pags P, Gámez-Pérez J, Santana OO, Maspoch ML. (2010) Kinetics of the thermal decomposition of processed poly(lactic acid). Polymer Degradation and Stability 95(12):2508-2514.

[5] Jayaramudu J, Reddy GSM, Varaprasad K, Sadiku ER, Ray SS, Rajulu AV. (2013) Structure and properties of poly (lactic acid)/Sterculia urens uniaxial fabric biocomposites. Carbohydrate Polymers 94(2):822-828.

[6] Goffin AL, Raquez JM, Duquesne E, Siqueira G, Habibi Y, Dufresne A, et al. (2011) From interfacial ring-opening polymerization to melt processing of cellulose nanowhisker-filled polylactide-based nanocomposites. Biomacromolecules 12(7):2456-2465.

[7] Tang XZ, Kumar P, Alavi S, Sandeep KP. (2012) Recent Advances in Biopolymers and Biopolymer-Based Nanocomposites for Food Packaging Materials. Critical Reviews in Food Science and Nutrition 52(5):426-442.

[8] Vink ETH, Rábago KR, Glassner DA, Gruber PR. (2003) Applications of life cycle assessment to NatureWorks™ polylactide (PLA) production. Polymer Degradation and Stability 80(3):403-419.

[9] Braun B, Dorgan JR, Knauss DM. (2006) Reactively compatibilized cellulosic polylactide microcomposites. Journal of Polymers and the Environment 14(1):49-58.

[10] Shen T, Lu M, Zhou D, Liang L. (2012) Effect of reactive blocked polyisocyanate on the properties of solvent cast blends from poly(lactic acid) and poly(ethylene glycol). Journal of Applied Polymer Science 125(3):2071-2077.

[11] Sanchez-Garcia MD, Lagaron JM. (2010) On the use of plant cellulose nanowhiskers to enhance the barrier properties of polylactic acid. Cellulose 17(5):987-1004.

[12] Sanchez-Garcia MD, Laearon JM. Morphology and barrier properties of solvent cast nanocomposites of polylactic acid with cellulose nanowhiskers derived from alpha purified microfibers. 2010. p. 26-29.

[13] Martínez-Sanz M, Lopez-Rubio A, Lagaron JM. (2012) Optimization of the dispersion of unmodified bacterial cellulose nanowhiskers into polylactide via melt compounding to significantly enhance barrier and mechanical properties. Biomacromolecules 13(11):3887-3899.

[14] Singh S, Gupta RK, Ghosh AK, Maiti SN, Bhattacharya SN. (2010) Poly (L-lactic acid)/layered silicate nanocomposite blown film for packaging application: Thermal, mechanical and barrier properties. Journal of Polymer Engineering 30(5-7):361-375.

[15] Gorrasi G, Vittoria V, Murariu M, Da Silva Ferreira A, Alexandre M, Dubois P. (2008) Effect of filler content and size on transport properties of water vapor in PLA/calcium sulfate composites. Biomacromolecules 9(3):984-990.

[16] Katiyar V, Gerds N, Koch CB, Risbo J, Hansen HCB, Plackett D. (2011) Melt processing of poly(L-lactic acid) in the presence of organomodified anionic or cationic clays. Journal of Applied Polymer Science 122(1):112-125.

[17] Fortunati E, Peltzer M, Armentano I, Torre L, Jiménez A, Kenny JM. (2012) Effects of modified cellulose nanocrystals on the barrier and migration properties of PLA nano-biocomposites. Carbohydrate Polymers 90(2):948-956.

[18] Picard E, Espuche E, Fulchiron R. (2011) Effect of an organo-modified montmorillonite on PLA crystallization and gas barrier properties. Applied Clay Science 53(1):58-65.

[19] Kim Y, Jung R, Kim HS, Jin HJ. (2009) Transparent nanocomposites prepared by incorporating microbial nanofibrils into poly(l-lactic acid). Current Applied Physics 9(1 SUPPL.):S69-S71.

[20] Habibi Y, Lucia LA, Rojas OJ. (2010) Cellulose nanocrystals: Chemistry, self-assembly, and applications. Chemical Reviews (Washington, DC, United States) 110(6):3479-3500.

[21] Abdul Khalil HPS, Bhat AH, Ireana Yusra AF. (2012) Green composites from sustainable cellulose nanofibrils: A review. Carbohydrate Polymers 87(2):963-979.

[22] Azizi Samir MAS, Alloin F, Dufresne A. (2005) Review of recent research into cellulosic whiskers, their properties and their application in nanocomposite field. Biomacromolecules 6(2):612-626.

[23] Sánchez-García MD, Hilliou L, Lagarón JM. (2010) Morphology and water barrier properties of nanobiocomposites of κ/l-hybrid carrageenan and cellulose nanowhiskers. Journal of Agricultural and Food Chemistry 58(24):12847-12857.

[24] Iguchi M, Yamanaka S, Budhiono A. (2000) Bacterial cellulose - a masterpiece of nature's arts. Journal of Materials Science 35(2):261-270.

[25] Wan YZ, Huang Y, Yuan CD, Raman S, Zhu Y, Jiang HJ, et al. (2007) Biomimetic synthesis of hydroxyapatite/bacterial cellulose nanocomposites for biomedical applications. Materials Science and Engineering C 27(4):855-864.

[26] Martínez-Sanz M, Lopez-Rubio A, Lagaron JM. (2013) Nanocomposites of ethylene vinyl alcohol copolymer with thermally resistant cellulose nanowhiskers by melt compounding (I): Morphology and thermal properties. Journal of Applied Polymer Science 128(5):2666-2678.

[27] George J, Sajeevkumar VA, Ramana KV, Sabapathy SN, Siddaramaiah. (2012) Augmented properties of PVA hybrid nanocomposites containing cellulose nanocrystals and silver nanoparticles. Journal of Materials Chemistry 22(42):22433-22439.

[28] Tang L, Yin N, Chen S, Ouyang Y, Wang H. Preparation and characterization flexible conductive PPy/BC nanocomposite membrane. 2012. p. 755-758.

[29] Peng K, Wang B, Chen S, Zhong C, Wang H. (2011) Preparation and properties of polystyrene/bacterial cellulose nanocomposites by in situ polymerization. Journal of Macromolecular Science, Part B: Physics 50(10):1921-1927.

[30] Zhijiang C, Guang Y. (2011) Optical nanocomposites prepared by incorporating bacterial cellulose nanofibrils into poly(3-

hydroxybutyrate). Materials Letters 65(2):182-184.

[31] Martínez-Sanz M, Lopez-Rubio A, Lagaron JM. (2011) Optimization of the nanofabrication by acid hydrolysis of bacterial cellulose nanowhiskers. Carbohydrate Polymers 85(1):228-236.

[32] Hirai A, Inui O, Horii F, Tsuji M. (2009) Phase separation behavior in aqueous suspensions of bacterial cellulose nanocrystals prepared by sulfuric acid treatment. Langmuir 25(1):497-502.

[33] Hossain KMZ, Ahmed I, Parsons AJ, Scotchford CA, Walker GS, Thielemans W, et al. (2011) Physico-chemical and mechanical properties of nanocomposites prepared using cellulose nanowhiskers and poly(lactic acid). Journal of Materials Science:1-12.

[34] Petersson L, Kvien I, Oksman K. (2007) Structure and thermal properties of poly(lactic acid)/cellulose whiskers nanocomposite materials. Composites Science and Technology 67(11-12):2535-2544.

[35] Follain N, Belbekhouche S, Bras J, Siqueira G, Marais S, Dufresne A. (2013) Water transport properties of bio-nanocomposites reinforced by Luffa cylindrica cellulose nanocrystals. Journal of Membrane Science 427:218-229.

[36] Hassan ML, Bras J, Hassan EA, Fadel SM, Dufresne A. (2012) Polycaprolactone/modified bagasse whisker nanocomposites with improved moisture-barrier and biodegradability properties. Journal of Applied Polymer Science 125(SUPPL. 2):E10-E19.

[37] Raquez JM, Murena Y, Goffin AL, Habibi Y, Ruelle B, DeBuyl F, et al. (2012) Surface-modification of cellulose nanowhiskers and their use as nanoreinforcers into polylactide: A sustainably-integrated approach. Composites Science and Technology 72(5):544-549.

[38] Frone AN, Berlioz S, Chailan JF, Panaitescu DM, Donescu D. (2011) Cellulose fiber-reinforced polylactic acid. Polymer Composites 32(6):976-985.

[39] Martínez-Sanz M, Olsson RT, Lopez-Rubio A, Lagaron JM. (2012) Development of bacterial cellulose nanowhiskers reinforced EVOH composites by electrospinning. Journal of Applied Polymer Science 124(2):1398-1408.

[40] Xiao L, Mai Y, He F, Yu L, Zhang L, Tang H, et al. (2012) Bio-based green composites with high performance from poly(lactic acid) and surface-modified microcrystalline cellulose. Journal of Materials Chemistry 22(31):15732-15739.

[41] Braun B, Dorgan JR, Hollingsworth LO. (2012) Supra-molecular ecobionanocomposites based on polylactide and cellulosic nanowhiskers: synthesis and properties. Biomacromolecules 13(7):2013-2019.

[42] Martínez-Sanz M, Olsson RT, Lopez-Rubio A, Lagaron JM. (2011) Development of electrospun EVOH fibres reinforced with bacterial cellulose nanowhiskers. Part I: Characterization and method optimization. Cellulose 18(2):335-347.

[43] Kovalenko VI, Mukhamadeeva RM, Maklakova LN, Gustova NG. (1994) Interpretation of the IR spectrum and structure of cellulose nitrate. Journal of Structural Chemistry (Translation of Zhurnal Strukturnoi Khimii) 34(4):540-547.

[44] Radjabian M, Kish MH, Mohammadi N. (2010) Characterization of poly(lactic acid) multifilament yarns. I. The structure and thermal behavior. Journal of Applied Polymer Science 117(3):1516-1525.

[45] Hutchings JB (1999) Food color and appearance. Aspen, Maryland

[46] Hertlein J, Singh RP, Weisser H. (1995) Prediction of oxygen transport parameters

of plastic packaging materials from transient state measurements. Journal of Food Engineering 24(4):543-560.

[47] Hiltner A, Liu RYF, Hu YS, Baer E. (2005) Oxygen transport as a solid-state structure probe for polymeric materials: A review. Journal of Polymer Science, Part B: Polymer Physics 43(9):1047-1063.

[48] Moon SI, Lee CW, Miyamoto M, Kimura Y. (2000) Melt polycondensation of L-lactic acid with Sn(II) catalysts activated by various proton acids: A direct manufacturing route to high molecular weight poly(L-lactic acid). Journal of Polymer Science, Part A: Polymer Chemistry 38(9):1673-1679.

[49] Li Y, Sun XS. (2010) Preparation and characterization of polymer-Inorganic nanocomposites by in situ melt polycondensation of l -Lactic acid and surface-hydroxylated MgO. Biomacromolecules 11(7):1847-1855.

[50] Luo YB, Wang XL, Xu DY, Wang YZ. (2009) Preparation and characterization of poly(lactic acid)-grafted TiO2 nanoparticles with improved dispersions. Applied Surface Science 255(15):6795-6801.

[51] Wu L, Cao D, Huang Y, Li BG. (2008) Poly(l-lactic acid)/SiO2 nanocomposites via in situ melt polycondensation of l-lactic acid in the presence of acidic silica sol: Preparation and characterization. Polymer 49(3):742-748.

[52] Ambrosio-Martín J, Fabra MJ, Lopez-Rubio A, Lagaron JM. (2014) An effect of lactic acid oligomers on the barrier properties of polylactide. Journal of Materials Science 49(8):2975-2986.

[53] Wondraczek H, Kotiaho A, Fardim P, Heinze T. (2011) Photoactive polysaccharides. Carbohydrate Polymers 83(3):1048-1061.

[54] Jamshidi K, Hyon SH, Ikada Y. (1988) Thermal characterization of polylactides. Polymer 29(12):2229-2234.

[55] Lönnberg H, Fogelström L, Zhou Q, Hult A, Berglund L, Malmström E. (2011) Investigation of the graft length impact on the interfacial toughness in a cellulose/poly(ε-caprolactone) bilayer laminate. Composites Science and Technology 71(1):9-12.

[56] Burgos N, Martino VP, Jiménez A. (2013) Characterization and ageing study of poly(lactic acid) films plasticized with oligomeric lactic acid. Polymer Degradation and Stability 98(2):651-658.

[57] Yasuniwa M, Tsubakihara S, Sugimoto Y, Nakafuku C. (2004) Thermal analysis of the double-melting behavior of poly(L-lactic acid). Journal of Polymer Science, Part B: Polymer Physics 42(1):25-32.

[58] Zhang J, Tashiro K, Tsuji H, Domb AJ. (2008) Disorder-to-order phase transition and multiple melting behavior of poly(L-lactide) investigated by simultaneous measurements of WAXD and DSC. Macromolecules 41(4):1352-1357.

[59] Lee JH, Park SH, Kim SH. (2013) Preparation of cellulose nanowhiskers and their reinforcing effect in Polylactide. Macromolecular Research:1-8.

[60] Martin O, Avérous L. (2001) Poly(lactic acid): Plasticization and properties of biodegradable multiphase systems. Polymer 42(14):6209-6219.

[61] Ten E, Jiang L, Wolcott MP. (2012) Crystallization kinetics of poly(3-hydroxybutyrate-co-3-hydroxyvalerate)/ cellulose nanowhiskers composites. Carbohydrate Polymers 90(1):541-550.

[62] Yu HY, Qin ZY, Zhou Z. (2011) Cellulose nanocrystals as green fillers to improve crystallization and hydrophilic property of poly(3-hydroxybutyrate-co-3-

hydroxyvalerate). Progress in Natural Science: Materials International 21(6):478-484.

[63] Song Y, Tashiro K, Xu D, Liu J, Bin Y. (2013) Crystallization behavior of poly(lactic acid)/microfibrillated cellulose composite. Polymer (United Kingdom).

[64] Yu HY, Qin ZY, Liu YN, Chen L, Liu N, Zhou Z. (2012) Simultaneous improvement of mechanical properties and thermal stability of bacterial polyester by cellulose nanocrystals. Carbohydrate Polymers 89(3):971-978.

[65] Sanchez-Garcia MD, Nordqvist D, Hedenqvist M, Lagaron JM. (2011) Incorporating amylopectin in poly(lactic acid) by melt blending using poly(ethylene-co-vinyl alcohol) as a thermoplastic carrier. II. Physical properties. Journal of Applied Polymer Science 119(6):3708-3716.

[66] Petersson L, Oksman K. (2006) Biopolymer based nanocomposites: Comparing layered silicates and microcrystalline cellulose as nanoreinforcement. Composites Science and Technology 66(13):2187-2196.

[67] Auras R, Harte B, Selke S. (2004) Effect of water on the oxygen barrier properties of poly(ethylene terephthalate) and polylactide films. Journal of Applied Polymer Science 92(3):1790-1803.

[68] Singh VM, Koo D, Palmese GR, Cairncross RA. (2011) Synthesis of polylactide with varying molecular weight and aliphatic content: Effect on moisture sorption. Journal of Applied Polymer Science 120(5):2543-2549.

[69] Koo D, Du A, Palmese GR, Cairncross RA. (2012) Moisture management of polylactides: The effect of heat treatment. Polymer 53(5):1115-1123.

[70] Espino-Pérez E, Bras J, Ducruet V, Guinault A, Dufresne A, Domenek S. (2013) Influence of chemical surface modification of cellulose nanowhiskers on thermal, mechanical, and barrier properties of poly(lactide) based bionanocomposites. European Polymer Journal 49(10):3144-3154.

[71] Siqueira G, Bras J, Dufresne A. (2009) Cellulose whiskers versus microfibrils: Influence of the nature of the nanoparticle and its surface functionalization on the thermal and mechanical properties of nanocomposites. Biomacromolecules 10(2):425-432.

[72] Martínez-Sanz M, Abdelwahab MA, Lopez-Rubio A, Lagaron JM, Chiellini E, Williams TG, et al. (2013) Incorporation of poly(glycidylmethacrylate) grafted bacterial cellulose nanowhiskers in poly(lactic acid) nanocomposites: Improved barrier and mechanical properties. European Polymer Journal 49(8):2062-2072.

[73] Chun KS, Husseinsyah S, Osman H. (2013) Properties of coconut shell powder-filled polylactic acid ecocomposites: Effect of maleic acid. Polymer Engineering and Science 53(5):1109-1116.

[74] Chun KS, Husseinsyah S, Osman H. (2012) Mechanical and thermal properties of coconut shell powder filled polylactic acid biocomposites: Effects of the filler content and silane coupling agent. Journal of Polymer Research 19(5).

[75] Martínez-Sanz M, Lopez-Rubio A, Lagaron JM. (2013) Nanocomposites of ethylene vinyl alcohol copolymer with thermally resistant cellulose nanowhiskers by melt compounding (II): Water barrier and mechanical properties. Journal of Applied Polymer Science 128(3):2197-2207.

[76] George J, Ramana KV, Bawa AS, Siddaramaiah. (2011) Bacterial cellulose nanocrystals exhibiting high thermal stability and their polymer nanocomposites.

International Journal of Biological Macromolecules 48(1):50-57.

[77] Fortunati E, Armentano I, Iannoni A, Kenny JM. (2010) Development and thermal behaviour of ternary PLA matrix composites. Polymer Degradation and Stability 95(11):2200-2206.

[78] Tashiro K, Kobayashi M. (1991) Theoretical evaluation of three-dimensional elastic constants of native and regenerated celluloses: role of hydrogen bonds. Polymer 32(8):1516-152.

Chapter 3

SYNERGISTIC EFFECT OF LACTIC ACID OLIGOMERS AND LAMINAR GRAPHENE SHEETS ON THE BARRIER PROPERTIES OF POLYLACTIDE NANOCOMPOSITES OBTAINED BY THE *IN SITU* POLYMERIZATION PRE-INCORPORATION METHOD

J. Ambrosio-Martín[a], A. Lopez-Rubio[a], M. J. Fabra[a], M.A. López Manchado[b], A. Sorrentino[c], G. Gorrasi[d] and J. M. Lagaron[a]

Journal of Applied Polymer Science – Under Review

[a] Novel Materials and Nanotechnology Group, IATA-CSIC, Avda. Agustin Escardino 7, 46980 Paterna (Valencia), Spain.

[b] Institute of Polymer Science and Technology, (CSIC), Juan de la Cierva, 3, 28006 Madrid, Spain.

[c] Institute for Polymers, Composites and Biomaterials (IPCB), National Research Council (CNR), P.le Enrico Fermi 1, 80055 Portici, Italy

[d] Department of Industrial Engineering, University of Salerno, via Giovanni Paolo II, 132 Fisciano (Salerno), Italy.

ABSTRACT

Nanocomposites of polylactide (PLA) and functionalized graphene sheets (FGS) were obtained through melt compounding. Pre-incorporation of the FGS fillers into lactic acid oligomers (OLLA) by *in situ* melt polycondensation was performed with the aim of improving the FGS dispersion and distribution into the polymeric matrix. To evaluate the effect of the pre-incorporation step, a comparison with direct addition of the filler to the melt mixing process was carried out. Addition of OLLA and FGS led to considerably better barrier properties. Specifically, reductions of up to 45% and 41% in oxygen and water vapour permeability were achieved, respectively. Mechanical and electrical properties of the PLA and its nanocomposites were also studied and correlated with both the addition of oligomers and the incorporation method.

Keywords: Polylactide, Graphene sheets, Oligomer, *In situ* polymerization, Barrier properties.

1. INTRODUCTION

One of the main functions of food packaging is the protection and preservation of food products from the adverse effects of external agents such as gases and vapours. Specifically, high barrier materials are required in packages for oxygen sensitive food products. However, plastic packages are permeable to small molecules like gases, vapours and to other low molecular weight compounds like aromas and, thus, a great deal of research has been devoted to improve the barrier properties of polymeric materials through different strategies.

High barrier polymers are already being used in the food packaging field contributing to an increase in the shelf-life of foods [1]. However, most of them are derived from non-renewable petroleum-based sources which, moreover, are rarely reused or recycled, thus generating large volumes of residues.

Given the environmental issues related to the use of petroleum-based plastics and their high consumption of in the food packaging field, which was around 42% of the global consumption of plastics in 2011 [2], it is of great interest to develop materials for these applications based on biodegradable polymers and synthesized from renewable resources.

Poly (lactic acid) is a widely studied biopolymer, attracting great interest both at the academic and industrial levels, due to its renewability and biodegradability character [3]. In fact, PLA is one of the most promising biopolymers to replace non-renewable petroleum-based polymers in many applications, such as packaging, biological and biomedical applications [4, 5].

Despite of this, for high barrier applications, PLA performance needs to be improved because it has insufficient barrier to gases and vapours compared to benchmark polymers for food packaging like PET, which could hardly satisfy current demands. Increasing the barrier properties of PLA would make it more competitive in the polymer market compared to conventional petroleum-based polymers.

Several strategies have been used to improve the barrier properties of PLA. Blending PLA with low molecular weight lactic acid oligomers has been proven effective in reducing its permeability to gases and vapours (50% and 25% respectively) due to occupancy of existing free volume in the PLA matrix by oligomers [6]. Furthermore, the possibility to improve the polymer barrier properties by incorporating nanofillers is one of the most widely explored strategies, being also attractive due to its low cost [1]. For instance, the incorporation of cellulose nanocrystals resulted in significantly improved barrier properties to gases and vapours [7-9]. It is worth mentioning that optimized dispersion of the nanofillers within the polymer matrices is crucial to obtain improved performance of the nanocomposites [10]. There are different methods for the incorporation of nanofillers into polymer matrices. Melt compounding is a common technique used at industrial level, but it has a number of drawbacks for nanocomposite development related to the high temperatures used for processing and the formation of nanofiller agglomerates during the process, regardless of the nanofiller nature [8, 9, 11, 12]. Therefore, different strategies have been developed to improve the dispersion of the fillers through melt mixing with the aim of improving the final properties of the nanocomposites [8, 9,13-15]. Among these strategies, a recently explored approach is the use of masterbatches, which could be prepared by different techniques such as *in situ* polymerization or electrospinning [8, 9]. Specifically, pre-incorporation of cellulose

nanocrystals in lactic acid oligomers through *in situ* polymerization resulted in improved barrier properties (around 20% for both oxygen and water vapour permeability) compared with the same materials synthesized by direct addition of the filler to the melt mixing process, which was mainly ascribed to a significant improvement in nanofiller dispersion. In addition, the synergistic effect of adding cellulose nanocrystals and oligomers, which were able to fill the free volume, as previously mentioned, was assessed achieving greater improvements in barrier performance (25% in oxygen permeability) [9].

Besides the addition of cellulose nanocrystals, compounds with laminar structure are promising materials for improving the barrier properties of polymer matrices, as the impermeable sheets increase the tortuosity of the pathway for permeant molecules, exerting a direct effect on the diffusion phenomenon. Thus, clay nanosheets nanocomposites have been developed demonstrating a significant impact on barrier properties [16-19]. For instance, improvements in oxygen barrier properties of 60%, 32% and 48% and in water barrier properties of 55%, 76% and 63% were obtained for PLA, polyhydroxybutyrate-co-valerate (PHBV), and polycaprolactone (PCL) clay nanocomposites, respectively [20].

Graphene and its derivatives, a relatively new family of compounds also with laminar geometry, have emerged in recent decades due to their excellent properties, not only related to their very good mechanical and electrical properties, but also to the fact that defect-free graphene sheets are impermeable to gases [21]. It is well established that these materials are highly effective for improving the barrier properties due to its planar structure [21-23]. For instance, outstanding improvements, up to 90%, were obtained in polyphenylene sulphide/graphene nanoplatelets nanocomposites, although very high amount of fillers were necessary [24]. In addition, this family of fillers has also been already used to improve the barrier performance of PLA, reporting oxygen permeability reductions up to 45% [23] or 68% [25] for nanocomposites obtained by solution coagulation and solution casting, respectively. Moreover, Kwon et al. has also reported improvements in PLA oxygen barrier properties using octadecylamine-graphene oxide (ODA-GO) as filler, reaching improvements of up to 77% for 10 wt.% of ODA-GO. In this case, solution intercalation was the strategy used to develop the nanocomposites. It is worth to mention that this improvement was greater than that obtained using the same amount of organically modified bentonite clay performed in the same study [26]. To the best of our knowledge, there is no previous study reporting on barrier improvements of PLA-graphene nanocomposites obtained through melt blending.

In the present study, graphene nanosheets have been incorporated into PLA using melt compounding. Derivative graphene material, such as functionalized graphene sheets (FGS), was used since functional sites could favour interactions with the matrix, as previously reported [27]. A comparison between direct addition of the nanofiller and the pre-incorporation of graphene in lactic acid oligomers, synthesized by *in situ* polymerization, was assessed. This incorporation strategy has been recently demonstrated to be effective improving the dispersion of cellulosic fillers into PLA matrix [9, 28]. The effect of the addition of these nanosheets on the thermal, mechanical, electrical and barrier properties of the materials has been evaluated.

2. MATERIALS AND METHODS

2.1. Materials

The semicrystalline poly(lactic acid) (PLA) used was a film extrusion grade with a number average molecular weight (M_n) of 130,000 g mol^{-1} and a weight average molecular weight (M_w) of 150,000 g mol^{-1} manufactured by NatureWorks (USA). Lactic acid (LA) was supplied as a 90 wt.% aqueous solution by Across Organics (Belgium).

2.2. Preparation of functionalized graphene sheets (FGS)

Functionalized graphene sheets (FGS) were synthesized by thermal reduction of graphite oxide at 1000°C for 30 s under air atmosphere. Briefly, graphite powder (purum powder < 0.1 mm, Sigma Aldrich) was dispersed in 20 mL of fuming nitric acid for 20 min; next, potassium chlorate (8 g) was slowly added over 1 h and the reaction mixture was stirred for 21 h at 0°C. Graphene produced through this method leads to the formation of single graphene layers or stacks of up to 7 sheets with hydroxyl, carbonyl and epoxy groups on their surface [27]. A full description of the synthesis and characterization of the FGS can be found elsewhere [29].

2.3. *In situ* melt polycondensation.

An initial mixture of lactic acid monomers with the filler (i.e. FGS), was performed with vigorous stirring overnight. The mixture was placed in a three-necked flask equipped with mechanical stirrer, temperature controller and a vacuum system through a cold trap. Lactic acid oligomers were obtained after dehydration of the mixture at 150 °C and atmospheric pressure for 2 h. Then, a pressure of 100 mmHg was applied for another 2 h, followed by a final pressure of 30 mmHg for 4 h obtaining FGS within a viscous liquid of oligo(L-lactic acid). The product was cooled and then ground into powder, washed with diethyl ether, vacuum filtered and dried at 70 °C for 24h in a vacuum oven. A purified material with lactic acid oligomers and FGS was obtained (OLLA-FGS) and it was used as masterbatch. The FGS content in the obtained hybrid material was determined by means of thermogravimetric analysis (TGA) under nitrogen flow (10 °C min^{-1}) and it was found to be around 9 wt.% of FGS. Moreover, using the aforementioned procedure but in absence of FGS, purified lactic acid oligomers (OLLA) were also obtained.

2.4. Preparation of films

Neat PLA as well as blends of OLLA-FGS, OLLA and PLA were melt mixed in a Brabender Plastograph internal mixer for 5 min at 162 °C and 120 rpm. Different contents of FGS were incorporated at weight ratios of 0.1, 0.5, 1 and 2 wt.% of FGS with respect to the total amount of material, from now on called PLA-FGS. A mixture of PLA and OLLA was also developed as reference material, henceforth called PLA-OLLA. The amount of OLLA added was 25 wt.% and to keep constant this amount in all samples, purified OLLA was used. Furthermore, for comparative purposes, direct blends of PLA, OLLA and FGS, from now on PLA-FGS-D were melt mixed at weight ratios of 0.1, 0.5, 1 and 2 wt.% for FGS and 25 wt.% OLLA using the same conditions specified above. These materials were then compression-moulded into films using a hot-plate hydraulic press (165 °C and 2MPa for 2 min) and allowed to cool at room temperature. The so-obtained films had an average thickness of about 200 μm as measured with a Mitutoyo micrometer by averaging four measurements on each sample.

2.5. Scanning Electron Microscopy (SEM)

For scanning electron microscopy (SEM) observation, the samples were cryo-fractured after immersion in liquid nitrogen, mounted on bevel sample holders and sputtered with Au/Pd in a vacuum. The experiments were conducted on a Hitachi microscope (Hitachi S-4800) at an accelerating voltage of 10 KV and a working distance of 12–16 mm taking pictures for the sample thickness.

2.6. Transmission Electron Microscopy (TEM)

Transmission electron microscopy (TEM) was performed using a JEOL 1010 (Jeol, Tokyo, Japan) equipped with a digital Bioscan (Gatan) image acquisition system. TEM observations were performed on ultrathin sections of microtomed thin composite sheets.

2.7. Differential Scanning Calorimetry (DSC)

Thermal properties of PLA and its nanocomposites with FGS were evaluated by DSC using a Perkin-Elmer DSC 8000 calorimeter under nitrogen atmosphere. The analysis was carried out on samples with a mass ranging between 8 and 10 mg. The samples were heated from 0 °C to 180 °C at 10 °C min^{-1} using a refrigerating cooling accessory (Intracooler 2 from Perkin Elmer). The first and second melting endotherms, after controlled crystallization at 10 °C min^{-1} from the melt, were analysed. To ensure reliability of the obtained data, heat flow and temperature were calibrated with the standard material, indium. The degree of crystallinity (%) of PLA was estimated from the corrected enthalpy for biopolymer content in the final materials, using the ratio between the enthalpy of the studied material and the enthalpy of a perfect PLA crystal using the following equation:

$$\%Xc = \frac{\left(\Delta H_f - \Delta H_c\right)}{\Delta H_f^o\left(1-w\right)} \times 100 \quad (1)$$

where ΔH_f is the enthalpy of fusion and ΔH_c the enthalpy of cold crystallization of the studied specimen. ΔH^o_f is the enthalpy of fusion of a totally crystalline material and w is the weight fraction of the filler. The ΔH^o_f used for this equation was 93 J g^{-1} for PLA [7].

2.8. Thermogravimetric analysis (TGA)

Thermal degradation of materials was investigated by thermogravimetric (TGA) analysis. The tests was carried out by means of a TGA2950 (TA Instruments, U.S.A.) under nitrogen flow. The samples were heated from 40 °C up to 800 °C by applying a heating rate equal to 10 °C min^{-1}. Derivative thermogravimetric curves (DTG) express the weight loss rate as a function of temperature.

2.9. Oxygen transmission rate

The oxygen permeability coefficient was derived from oxygen transmission rate (OTR) measurements recorded using an Oxtran 100 equipment (Modern Control Inc., Minneapolis, MN, US). Experiments were carried out at 24 °C and at 80% relative humidity (RH) conditions. RH was generated by a built-in gas bubbler and was checked with a hygrometer placed at the exit of the detector. The samples were purged with nitrogen for a minimum of 20 h in the humidity equilibrated samples, prior to exposure to an oxygen flow of 10 ml min^{-1}. A 5 cm^2 sample area was measured by using

an in-house developed mask. The measurements were done in duplicate.

2.10. Water permeability

Direct permeability to water was determined from the slope of weight loss vs. time curves at 24 °C. The films were sandwiched between the aluminium top (open O-ring) and bottom (deposit for the permeant) parts of a specifically designed permeability cell with screws containing deionized water as the permeant. A Viton rubber O-ring was placed between the film and the top part of the cell to enhance sealability. The cells were placed inside a desiccator at 0%RH and the water weight loss through a film area of 0.001 m^2 was monitored and plotted as a function of time. In order to estimate the permeability values of the films, only the linear part of the weight loss data was used to ensure sample steady-state conditions. Cells with aluminium films were used as control samples to estimate solvent loss through the sealing. Water weight loss was calculated as the total cell weight loss minus the loss through the sealing. Tests were done in duplicate.

2.11. Mechanical properties

Tensile tests were carried out at 24 °C and 50% RH on an Instron 4400 Universal Tester. Pre-conditioned dumb-bell shaped specimens with initial gauge length of 25 mm and 5 mm in width were die-stamped from the films in the machine direction. The thickness of all specimens was approximately 200 μm which was measured using a digital micrometre (Mitutoyo, Spain, ±0.001 mm). The storage conditions before test were 24 °C and 0% relative humidity. A fixed crosshead rate of 10 mm min^{-1} was used in all cases, and results were taken as the average of, at least, three tests.

2.12. Electrical properties

Electrical characterization has been done, using a Keithley 2400 source measurement unit in a two-probe resistance measurement configuration. However, it should be mentioned that for some selected samples was found that four-point and two-point measurements configuration gave very similar results. The sample thicknesses were carefully measured by a micrometer, whereas the length and the width were 5 and 30 mm, respectively. The electrical conductivity was measured in the voltage range -10 + 10 V. All the samples showed a linear behaviour of the current (I) versus the applied voltage (V).

3. RESULTS AND DISCUSSION

Functionalized graphene sheets (FGS) were pre-incorporated into lactic acid oligomers (OLLA) through *in situ* polymerization to obtain a masterbatch (OLLA-FGS). Different amounts of OLLA-FGS masterbatch prepared by *in situ* polymerization were blended with PLA using melt compounding in order to prepare samples with different FGS content. Moreover, based on previous results which demonstrated that addition of OLLA up to 25wt.% within PLA significantly improved its barrier properties [6], in this study, the amount of total oligomers incorporated into PLA was fixed at 25 wt.%. To this aim, additional OLLA to that included in the masterbatch was added in order to reach this content. Thus, the potential synergistic effect when adding different amounts of FGS on the final properties of the materials were evaluated.

3.1. Morphological characterization

The dispersion of the FGS within the PLA matrix was studied using SEM and TEM.

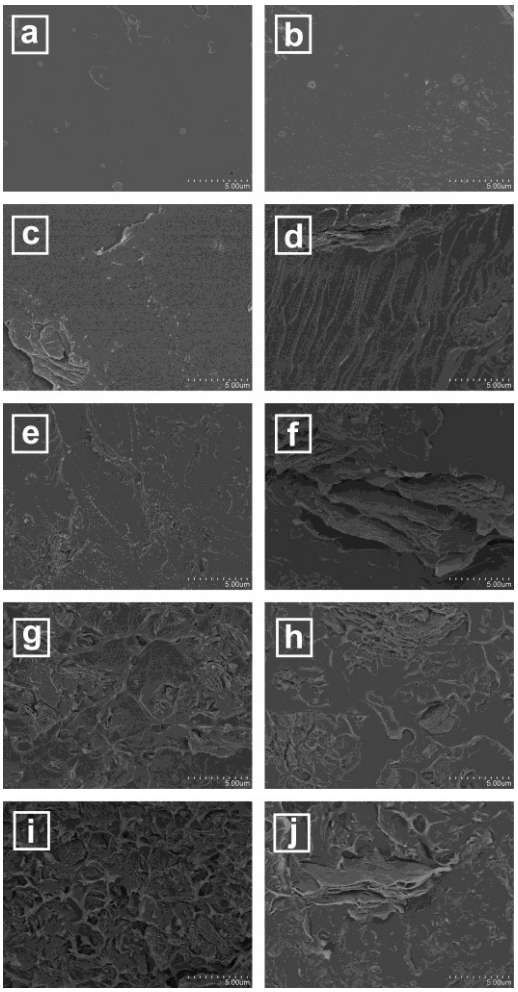

Figure 1. SEM micrographs of the cryo-fractured sections of pure PLA (a), PLA-OLLA (b) and PLA-FGS nanocomposites films at 0.1 wt.% (c, d); 0.5 wt.% (e, f); 1.0 wt.% (g, h) and 2.0 wt.% (i, j) obtained using an *in-situ* polymerization step and by direct addition to the melt mixer respectively. Scale markers correspond to 5μm.

Figure 1 shows the cryo-fractured sections of the neat PLA and its nanocomposite films using both addition routes, i.e. direct addition and with an *in situ* polymerization pre-incorporation step. An initial observation was that while for PLA and PLA-OLLA a smooth fracture surface was clearly seen, when FGS was added the surface became rougher, especially for high FGS contents. This effect has also been reported when high concentration of graphene was incorporated into poly-(vinylidene fluoride) [30] or polylactide (PLA) [31]. Random dispersion and distribution of the filler was generally observed for the samples obtained through a pre-incorporation method although some small aggregates were also present. On the other hand, bigger aggregates were observed when FGS was directly added to the melt mixing process, indicating that better dispersion of the FGS was obtained using the pre-incorporation step with a more intimate mixing between filler and matrix. In a previous work using the same procedure with another additive, direct addition of the filler resulted in very big agglomerates which could be seen by naked eye. This problem was overcome using the *in situ* polymerization pre-incorporation step improving to a great extent the dispersion of the filler [9]. Figure 2 shows the TEM micrographs of PLA-FGS nanocomposites containing 1 wt.% of FGS synthesized through both addition routes. These images further confirm the random filler dispersion and distribution, the presence of filler agglomerates in certain areas and also bigger aggregates when FGS was directly added.

3.2. Thermal properties of PLA and its nanocomposites

With the aim of investigating the effects of the FGS addition on the thermal properties of the PLA nanocomposites, DSC analysis of all the samples was carried out. Glass transition temperature (T_g) and melting enthalpy (ΔH_m) normalized to the PLA content of the nanocomposite films were evaluated from the DSC first and second heating runs. Moreover, the melting temperature (T_m), degree of crystallinity (X_c) and the cold crystallization temperature (T_{cc}) were also measured from the first heating run curve, which provided

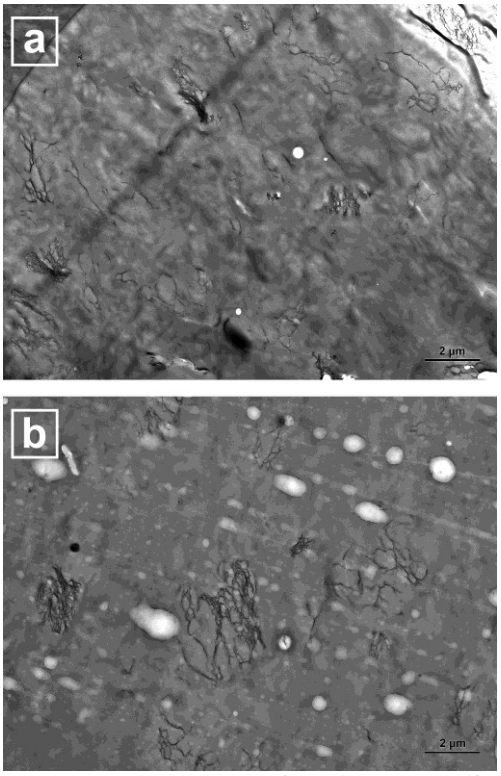

Figure 2. TEM micrographs of PLA-FGS films containing 1 wt.% FGS obtained using an *in situ* polymerization step (a) and by direct addition to the melt mixer (b). Scale markers correspond to 2µm.

information related to the thermal characteristics of the just obtained material. Table 1 gathers the DSC data for PLA and its nanocomposites. The first interesting observation is that after OLLA or OLLA-FGS addition, a double melting peak appeared. It has been reported that this effect could be attributed either to a melt recrystallization mechanism or to the coexistence of two crystals size populations for PLA-based materials containing oligomers [6]. Regarding the glass transition temperature, previous studies have observed that it increased with the addition of graphene nanoplatelets or graphene oxide due to the restriction of the molecular mobility exerted by the laminar structures [25]. On the contrary, addition of OLLA to the PLA matrix resulted in a decrease in the glass transition temperature [6] due to a plasticization effect, in terms of glass transition temperature, exerted by the shorter polymer chains, which require less energy to activate molecular mobility [32]. As observed in Table 1**,** addition of OLLA resulted in a T_g reduction of about ~6 °C. Since neat PLA has different properties to these of PLA blended with oligomers, this last sample was taken as a reference. Thus, while direct addition of FGS led to a further T_g reduction of 6 °C for the 2 wt.% sample, when FGS was added using *in situ* melt polycondensation step, no significant differences in the glass transition temperature were observed. This could indicate that direct addition generated lower dispersion as observed in the morphological analysis and, hence, poorer filler-matrix interfacial interactions were established. Even though it was surprising that no increase in T_g was observed upon addition of FGS, even with the pre-incorporation method, similar results have been observed previously. Specifically, it was observed that addition of epoxidized palm oils (EPO) enhanced the molecular motions of PLA chains, manifested by a decrease in T_g [33] and addition of graphene nanoplatelets into this plasticized system resulted in a further T_g decrease [34]. On the other hand, while differences in the glass transition temperatures were observed depending on the FGS incorporation method, no significant changes in the melting temperatures were seen. Regarding the crystallization process, it is widely recognized that PLA crystallization is influenced by addition of graphene nanosheets or graphene oxide[35-37]. Table 1 shows a decrease of the cold crystallization temperature upon addition of FGS through both direct addition and from the masterbatch. Therefore, it could be stated that an increase in the crystallization rate was promoted by the FGS which acted as nucleating agent. This effect has also been

Table 1. DSC glass transition temperature (T_g), maximum of melting (T_m) and melting enthalpy (ΔH_m) during the first and second heating run and cold crystallization temperature (T_{cc}) and crystallinity index (X_c) during the first heating run.

	First Heating						Second Heating	
	T_{g1} (ºC)	T_{m1} (ºC)	T_{m2} (ºC)	T_{cc} (ºC)	ΔH_m (J/g)	X_c (%)	T_{g2} (ºC)	ΔH_m (J/g)
PLA	57.1 ± 0.2^{a}		147.7 ± 0.7^{a}	116.1 ± 0.0^{a}	3.2 ± 0.8^{a}	3.4 ± 0.9^{a}	58.8 ± 0.8^{a}	2.4 ± 1.0^{abc}
PLA-OLLA	51.7 ± 0.3^{b}	134.7 ± 0.7^{a}	146.4 ± 0.2^{b}	100.4 ± 0.3^{b}	2.5 ± 0.6^{a}	2.7 ± 0.7^{a}	51.6 ± 0.1^{b}	2.1 ± 1.0^{c}
PLA-FGS 0.1 %	50.7 ± 0.4^{b}	134.1 ± 0.1^{b}	145.8 ± 0.0^{bc}	99.7 ± 0.2^{c}	2.4 ± 1.2^{a}	2.6 ± 1.3^{a}	49.5 ± 0.3^{d}	2.0 ± 0.4^{abc}
PLA-FGS 0.5 %	49.3 ± 0.1^{bc}	133.9 ± 0.1^{b}	145.9 ± 0.2^{bc}	99.0 ± 0.2^{d}	1.8 ± 0.7^{a}	1.9 ± 0.7^{a}	49.6 ± 0.3^{cd}	2.8 ± 0.8^{abc}
PLA-FGS 1 %	51.6 ± 0.9^{b}	133.8 ± 0.1^{b}	145.9 ± 0.0^{bc}	97.4 ± 0.1^{f}	2.5 ± 0.5^{a}	2.7 ± 0.6^{a}	49.4 ± 0.2^{d}	3.3 ± 1.1^{ab}
PLA -FGS 2 %	51.0 ± 0.0^{b}	134.5 ± 0.0^{b}	146.3 ± 0.0^{bc}	96.9 ± 0.0^{g}	1.6 ± 0.8^{a}	1.7 ± 0.9^{a}	50.3 ± 0.1^{c}	1.6 ± 0.6^{bc}
PLA-FGS 0.1 % -D	48.2 ± 0.3^{c}	133.7 ± 0.3^{b}	145.7 ± 0.2^{bc}	98.3 ± 0.1^{e}	2.6 ± 0.9^{a}	2.8 ± 1.0^{a}	49.1 ± 0.1^{de}	2.5 ± 0.5^{abc}
PLA-FGS 0.5 % -D	48.0 ± 0.0^{c}	134.2 ± 0.2^{b}	146.0 ± 0.1^{bc}	98.8 ± 0.2^{de}	2.2 ± 0.7^{a}	2.3 ± 0.7^{a}	48.9 ± 0.5^{de}	2.6 ± 0.5^{a}
PLA-FGS 1 % -D	51.0 ± 0.6^{b}	133.8 ± 0.3^{b}	145.4 ± 0.3^{c}	98.3 ± 0.3^{e}	2.4 ± 0.7^{a}	2.6 ± 0.7^{a}	48.4 ± 0.2^{e}	2.1 ± 1.3^{abc}
PLA -FGS 2 % -D	45.1 ± 1.5^{d}	133.7 ± 0.2^{b}	145.8 ± 0.5^{b}	97.8 ± 0.0^{ef}	2.2 ± 0.1^{a}	2.4 ± 0.2^{a}	48.5 ± 0.1^{e}	3.0 ± 0.8^{ab}

a-g: different superscripts within the same column indicates significant differences among samples ($p<0.05$)

reported when graphene was added as nanofiller in different polymer matrices [35, 38, 39]. Nevertheless, different results were obtained depending on the FGS incorporation method used. While for direct FGS addition there were almost no differences with the amount of FGS in the nanocomposite, when FGS was added from an *in situ* polymerized masterbatch with OLLA, T_{cc} decreased as the FGS content increased. This could be related with the morphological study where bigger aggregates were observed when FGS was directly added, impairing to some extent the nucleating effect of the FGS.

The crystallinity degree was also studied to investigate whether the addition of the FGS affected the crystalline fraction of the obtained materials. Surprisingly, even though an increase in the crystallization rate was obtained upon FGS addition, no significant effects on crystallinity were observed, obtaining the same crystalline fraction for all the materials regardless the addition route if compared with the reference material. However, a reduction of the crystalline fraction was obtained for all materials in comparison with pure PLA. This is in agreement with a previously reported work [6] where the addition of high amounts of OLLA into PLA resulted in a reduction of the PLA crystallinity. It seems that the nucleating character of FGS was capable to produce an effect in the initiation of the crystallization, accelerating the process, but on the contrary the high amount of OLLA hindered the growth of the crystalline fraction.

3.3. Thermal stability of PLA and its nanocomposites

The thermal stability of PLA and its nanocomposites with FGS was evaluated through thermogravimetric analysis (TGA). As observed from Table 2**,** addition of OLLA affected only slightly the peak maximum of thermal degradation (T_d). However, a remarkable effect on the onset degradation temperature was observed after incorporation of OLLA, with reductions of up to ~70 °C. These results are consistent with

a previous study which reported that incorporation of the same amount of OLLA into PLA also induced a reduction in the onset degradation temperature, having no significant effect on the T_d [6]. This was mainly ascribed to the earlier degradation of the short oligomer chains in comparison with the onset degradation temperature of the higher molecular weight PLA. Figure 3 shows the derivative weight loss curve of pure PLA and PLA-OLLA where this decrease in the onset of degradation temperature for the material containing the oligomer is clearly observed. Whereas for pure PLA a typical one-step derivative weight loss curve was observed, a shoulder before the main degradation peak appeared when OLLA was added, indicating that the short chain oligomers degraded at lower temperatures. Generally, the addition of increasing amounts of FGS, did not strongly affect the T_d of the matrix, independently of the incorporation route used. However, in the case of direct addition at 2 wt.% loading a relevant reduction in the T_d was observed. It has been previously reported that addition of well dispersed nanofillers into polymeric matrices can generate a strong nanofiller network which delays thermal degradation due to the restricted polymer chains mobility [40]. Therefore, as deduced

Table 2. Maximum of the weight loss first derivate thermogravimetric curve (T_d), the corresponding peak onset values and the residue at 500 °C for the PLA and its nanocomposites films.

	T_d (°C)	Onset T (°C)	Residue 500°C (%)
PLA	357.3	323.8	2.0
PLA-OLLA	352.0	255.6	1.8
PLA-FGS 0.1	353.4	254.2	1.3
PLA-FGS 0.5	355.0	254.5	2.0
PLA-FGS 1	353.1	250.6	2.8
PLA-FGS 2	353.6	250.9	2.8
PLA-FGS 0.1-D	354.7	257.4	1.2
PLA-FGS 0.5-D	352.9	255.0	1.5
PLA-FGS 1-D	352.9	245.4	1.9
PLA-FGS 2-D	347.7	247.7	3.4

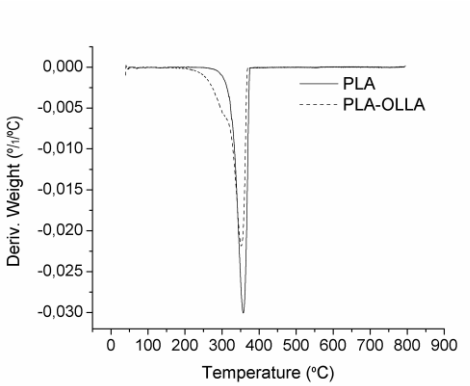

Figure 3. Derivative thermogravimetric (DTG) curves of PLA and PLA-OLLA.

from the thermal properties analysis, in which a lower glass transition temperature was observed for the 2 wt.% sample obtained by direct addition, the reduction in thermal stability could be explained by enhanced polymer chain mobility.

Regarding the onset temperature, since the same amount of OLLA was present in all samples containing FGS than in the PLA-OLLA sample, the same effect was observed, i.e. a remarkable reduction when compared to PLA. In addition, the incorporation of FGS had a further effect on the onset degradation temperature since lower onset temperatures were in general observed for the samples with greater FGS content, as observed in Table 2. The decrease in the onset degradation temperature could be ascribed to the high heat conductivity and low heat barrier effect of graphene in polymer composites. In fact, a recent study reported that PLA-graphene nanocomposites could be ignited with less heat irradiation than the pristine polymer due to the high heat conductivity of graphene which allowed easier and faster heat diffusion through the matrix [38]. Not surprisingly, an increase in the residue at 500 °C was observed as the FGS content increased. Therefore, a negative synergistic effect on the onset degradation temperature was observed upon addition of

both OLLA and FGS, thus decreasing the thermal stability of neat PLA.

3.4. Mechanical properties

The mechanical properties of PLA and its corresponding FGS-containing nanocomposite films obtained using both the masterbatch prepared through *in situ* polymerization and direct addition of the filler with the OLLA in the melt mixing process are summarized in Table 3. Elastic Modulus (E), tensile strength and elongation at break (ε_b) were determined from the stress-strain curves of the different films.

It is widely recognized that addition of graphene and its derivatives within polymer matrices has an important reinforcing effect due to its own nature. Moreover, proper distribution of the filler, the interfacial interaction between polymer and filler and also the reinforcement orientation play an important role in the final mechanical properties. For instance, addition of graphene oxide and graphene nanoplatelets within PLA led to an increase in Young's modulus and in tensile strength for plasticized and unplasticized films obtained through solution casting [25]. Therefore, upon addition of FGS, a reinforcing effect due to the functionalized sites from FGS surface interacting with hydrophilic groups of PLA would be expected. From Table 3, an increase in the elastic modulus was generally observed for each sample obtained from the masterbatch except for the sample with higher FGS content, which remained almost unchanged. A maximum for the elastic modulus was noticed for the sample with 0.1 wt.%, decreasing with further addition of FGS. This effect has been previously observed, showing an optimum loading above which the Young's modulus decreases [25, 34]. This result could be explained on the basis of the agglomeration of FGS at high contents, leading to a poorer dispersion of the filler which counteracts the reinforcement improvement. On the contrary, when FGS was incorporated by direct addition, lower values of the elastic modulus were observed for low loadings probably due to the greater agglomeration of the filler, as observed by the microscopy analysis. Despite that, further addition of FGS (up to 1 and 2 wt.%) through direct incorporation resulted in an increase in the elastic modulus but without significant differences with the same compositions obtained by the pre-incorporation route. It has been recently reported that increasing the filler content leads to an enhanced contact between the nanofillers, resulting in a slight stiffening of the materials [34]. Therefore, addition of FGS at low contents by the melt polycondensation step showed better behaviour in terms of mechanical properties than those obtained by direct addition due to their better dispersion, ascribed to better filler-filler and filler-matrix interactions. However, at high FGS

Table 3. Elastic modulus (E), tensile strength and elongation at break (ε_b) for PLA and its nanocomposites incorporating FGS.

	E (MPa)	TensileStrength (MPa)	ε_b (%)
PLA	1670.4 ± 33.0^{cd}	61.1 ± 1.1^{a}	6.6 ± 1.2^{a}
PLA-OLLA	1701.1 ± 57.3^{c}	54.3 ± 0.8^{b}	3.9 ± 0.8^{b}
PLA-FGS 0.1	1866.0 ± 119.1^{a}	50.3 ± 2.7^{bc}	2.4 ± 0.7^{cd}
PLA-FGS 0.5	1718.0 ± 5.8^{bc}	41.9 ± 0.4^{cde}	2.1 ± 0.6^{cde}
PLA-FGS 1	1797.2 ± 100.8^{ab}	40.8 ± 5.9^{de}	2.1 ± 0.5^{cde}
PLA-FGS 2	1696.9 ± 35.2^{bc}	28.4 ± 1.3^{f}	1.5 ± 0.1^{de}
PLA-FGS 0.1-D	1461.5 ± 7.1^{e}	19.2 ± 5.4^{g}	1.3 ± 0.4^{e}
PLA-FGS 0.5-D	1514.3 ± 30.7^{d}	18.8 ± 1.0^{g}	1.4 ± 0.4^{de}
PLA-FGS 1-D	1796.4 ± 20.8^{ab}	46.2 ± 9.5^{bcd}	3.0 ± 0.2^{bc}
PLA-FGS 2-D	1717.5 ± 22.3^{bc}	32.7 ± 3.0^{ef}	1.9 ± 0.2^{cde}

a-g: different superscripts within the same column indicates significant differences among samples ($p<0.05$)

contents, even though the pre-incorporation step led to better nanofiller dispersion, almost no differences in mechanical properties were observed most likely due to the fact that filler aggregation occurred during both processing methods leading to less property differentiations. Surprisingly, an embrittlement of the materials was observed for all samples with a decrease in the tensile strength upon addition of FGS. Despite that, similar trend to that observed for the elastic modulus was noticed, i.e. better tensile strength for the samples with low FGS content obtained by the pre-incorporation step, and almost no difference between both incorporation methods at high FGS contents. Chieng et al. [34] observed that lower tensile strength values were obtained when increasing the graphene nanoplatelets content in the PLA matrix, which was explained by their stacking above the optimum nanofiller content due to Van der Waals forces. However, in the case of direct addition of the FGS, somewhat higher values of tensile strength were obtained at high filler contents. This could be explained since at low contents higher stacking of FGS was present in samples from direct addition which resulted in lower tensile strength. On the contrary, at high contents, stacking of FGS was also present in samples obtained from the masterbatch which may lead to similar values in tensile strength for both incorporation routes, as observed in the mechanical modulus.

Addition of up to 25 wt.% of oligomers had an important effect regarding the level of interaction between polymer and filler, hindering proper filler-matrix interaction. In fact, in a previous work incorporating nanocellulose using a masterbatch obtained from in situ polycondensation with lactic acid, increasing the amount of oligomers resulted in a reduction in the mechanical properties explained by the reduced filler-matrix adhesion [9]. Regarding the ductility of the materials, a reduction was noticed with a decrease in the elongation at break after addition of OLLA. Further decrease was observed for all samples after addition of FGS, regardless of FGS content. Thus, the main remarkable conclusion from the mechanical tensile tests is that addition of high amounts of lactic acid oligomers into PLA hindered to a great extent the reinforcing effect that could be expected by FGS addition, mainly due to the short-chain feature of the oligomers and also to the highly disturbed filler-matrix interactions.

3.5. Barrier properties

Graphene and its derivatives are considered promising nanomaterials in terms of gas and vapour barrier applications because their laminar structure can potentially block the diffusion of small molecules. The use of these materials in barrier polymers has been studied to some extent. Although a thorough revision about the topic was carried out by Yoo et al. [21], there is scarce literature about the improvements in PLA barrier properties using this type of carbonaceous materials [23, 25] and even less for PLA-graphene or graphene derivatives-based nanocomposites prepared by melt compounding. Oxygen transport properties including permeability (P), diffusion (D) and solubility (S) and water vapour permeability (P_w) of PLA and its nanocomposites were measured and the results are summarized in Table 4.

Figure 4a shows the oxygen barrier properties of PLA and their nanocomposites with FGS. The permeability value for pure PLA was in accordance with that reported in the literature for melt compounded films [8]. Moreover, addition of OLLA resulted in a reduction of the oxygen permeability of about 22%, which was in agreement with a previous work [6]. It is worthy to highlight that further reductions in oxygen permeability were obtained for all the

Table 4. Oxygen transport properties, permeability (*P*), diffusion (*D*) and solubility (*S*) coefficients and water permeability coefficients (P_w) for PLA and its nanocomposites films incorporating FGS.

	P (80% RH) (m^3m/m^2sPa)	*D* (80%RH) (m^2/s)	*S* (80%RH) (g/gPa)	P_w (Kg m/m^2sPa)
PLA	1.81 ± 0.05 $e^{-18\,a}$	2.22 e^{-12}	8.17 e^{-07}	1.54 ± 0.02 $e^{-14\,a}$
PLA-OLLA	1.41 ± 0.07 $e^{-18\,b}$	2.42 e^{-12}	5.82 e^{-07}	1.36 ± 0.03 $e^{-14\,b}$
PLA-FGS 0.1	1.34 ± 0.00 $e^{-18\,bc}$	2.34 e^{-12}	5.75 e^{-07}	1.30 ± 0.02 $e^{-14\,c}$
PLA-FGS 0.5	1.25 ± 0.02 $e^{-18\,cd}$	2.20 e^{-12}	5.66 e^{-07}	1.18 ± 0.01 $e^{-14\,e}$
PLA-FGS 1	1.06 ± 0.03 $e^{-18\,f}$	1.95 e^{-12}	5.42 e^{-07}	1.10 ± 0.02 $e^{-14\,f}$
PLA-FGS 2	1.01 ± 0.04 $e^{-18\,f}$	1.66 e^{-12}	6.09 e^{-07}	0.91 ± 0.00 $e^{-14\,h}$
PLA-FGS 0.1-D	1.35 ± 0.03 $e^{-18\,bc}$	2.18 e^{-12}	6.19 e^{-07}	1.24 ± 0.03 $e^{-14\,cd}$
PLA-FGS 0.5-D	1.26 ± 0.01 $e^{-18\,cd}$	2.23 e^{-12}	5.65 e^{-07}	1.20 ± 0.01 $e^{-14\,d}$
PLA-FGS 1-D	1.20 ± 0.06 $e^{-18\,de}$	2.09 e^{-12}	5.72 e^{-07}	1.13 ± 0.03 $e^{-14\,f}$
PLA-FGS 2-D	1.10 ± 0.08 $e^{-18\,ef}$	1.93 e^{-12}	5.71 e^{-07}	1.03 ± 0.00 $e^{-14\,g}$

a-h: different superscripts within the same column indicates significant differences among samples ($p<0.05$)

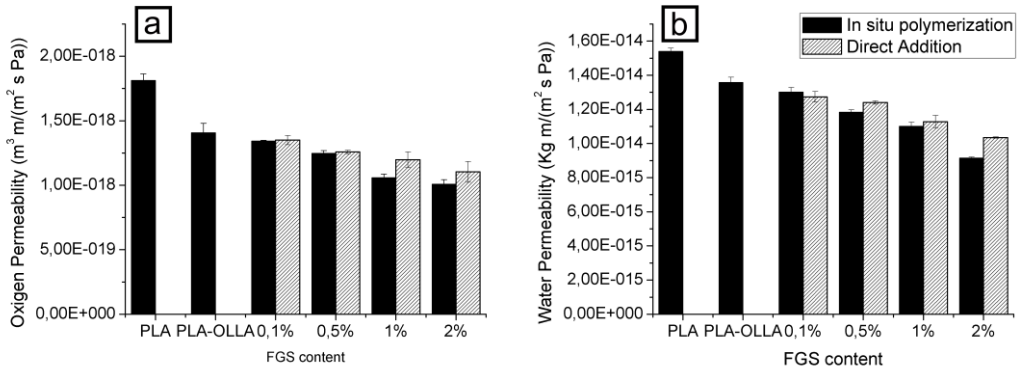

Figure 4. Oxygen (a) and water permeability (b) of pure PLA and its nanocomposites with FGS obtained using an *in situ* polymerization step and by direct addition to the melt mixer.

nanocomposite materials obtained through both incorporation routes when compared to the reference sample. Even though no differences between both routes were observed at low FGS contents, at high contents, slightly higher oxygen barrier performance was obtained for *in situ* polymerized FGS, with the greatest improvement of about 45% for the 2 wt.% loading.

There are several factors that influence the oxygen barrier properties, such as relative humidity, tortuosity of the pathway for the permeant molecules to diffuse through the polymer and the free volume of the polymer matrix, among others. It has been reported that the presence of reactive hydrophilic groups, such as hydroxyl groups from the polymer or polymer nanocomposites, can cause plasticization of the material when exposed to high relative humidity conditions due to the interaction of water with these groups, thus resulting in a higher mobility of the polymer chains and hence easing gas diffusion [8, 41]. Moreover, it is widely known that an increase in tortuosity due to nanofillers and/or crystals translates into a reduction in the vapour and gases permeability values by a drop in diffusion and also that changes in free volume, e.g. amorphous density, are closely related with changes in the transport of low molecular weight compounds. Several works have demonstrated reductions in gas permeability associated with fractional free

volume occupancy phenomena in polymers [42, 43].

In this study, addition of OLLA led to an increase of the hydrophilic groups which resulted in a slight increment in the diffusion coefficient when compared with PLA. Nevertheless a strong effect on the free volume occupancy by oligomers molecules was observed with a considerable reduction in the solubility coefficient, in agreement with previous works [6]. Regardless of the incorporation route, addition of FGS resulted in a further reduction of the diffusion coefficient compared to the reference sample (i.e. PLA-OLLA), even reaching lower values than those for pure PLA. This could mainly be ascribed to the effective blocking effect of the FGS laminar sheets, resulting in an increase in tortuosity. It is widely known that an increase in polymer crystallinity is also closely related to improved barrier properties, as the crystalline domains are considered impermeable to the pass of low molecular weight compounds, thus increasing the tortuous path for the permeant molecules to go through [44-47]. A recent study has demonstrated the high "filler barrier efficiency" of this kind of fillers [48]. This "filler barrier efficiency" factor is intended to separate the effects of filler loading from crystallinity variations in the barrier performance of the materials. As observed in thermal analysis, no effect on the crystallization degree was observed upon addition of FGS, thus corroborating the very good filler barrier efficiency of these nanofillers. In fact, the higher the FGS addition, the higher the tortuosity effect observed, with greater drops in the diffusion coefficient. The higher oxygen permeability obtained for the highly loaded samples prepared from direct addition of FGS in comparison with the same compositions obtained by *in situ* polymerization could be explained by the general poorer dispersion of the nanofiller in the former samples, thus resulting in high diffusion coefficients due to creation of preferential pathways for the oxygen molecules to pass.

Water permeability was also measured and the results are depicted in Figure 4b. Addition of oligomers also resulted in a reduction of the water permeability achieving an improvement of about 12%, which was in line with previous results [6].

Moreover, addition of FGS caused a greater reduction in the water permeability coefficient for all samples regardless of the FGS incorporation route. The effect of dispersion of FGS into PLA matrix was also noticed. While at low contents there were no significant differences between both incorporation routes, high FGS contents led to higher water vapour permeability for the materials synthesized by direct addition, mainly ascribed to preferential paths created by the agglomerated nanofiller. Hence, the maximum reduction in water permeability was achieved for the sample with 2wt.% FGS obtained from an *in situ* polymerized material with an improvement of about 41%, thus confirming the improved nanofiller dispersion obtained through this incorporation route.

3.6. Electrical properties

Conductive carbonaceous materials such as carbon nanotubes, graphite, graphene and/or its derivatives have been widely used as nanofillers to improve the electrical properties of polymeric matrices [12, 24, 49-52]. The dispersion of the filler into de polymeric matrix plays a key role in order to obtain good results. Figure 5 shows the electrical conductivities of PLA and its nanocomposites. Neat PLA is electrically insulating with a low conductivity, which is considered to be in the range of 10^{-16} - 10^{-19} S cm^{-1} by Sullivan et al. [53]. As observed from Figure 5, addition of conducting graphene nanofillers significantly increased

the conductivity of the materials. It is reported that S-shaped curves indicate that the nanocomposites exhibit a typical percolation transition from an insulator to semiconductor [54, 55]. Although it is not the case, it can be noticed the beginning of this typical S-shaped curve, with an exponential increase of the electrical conductivity, suggesting that there is a transition from insulator material to semiconductor. However, higher amounts of FGS would be necessary to obtain the whole curve. In spite of this, differences between both incorporation routes were noticed. Higher conductivity was obtained for the nanocomposites obtained through a pre-incorporation step than that obtained through direct addition of the filler. As previously commented, the dispersion of the filler is an important factor for the electrical properties. Thus, the better FGS dispersion obtained using the pre-incorporation step could be responsible of creating more continuous conductive pathways, thus resulting in higher conductivity. However, although an increase in the conductivity was noticed when FGS nanofiller was added, the increments were not as high as expected. The low conductivity of the materials could be explained by an insufficient dispersion of the nanofiller, combined with the very low crystallinity of the polymer matrix. In fact, it has been reported that there is a strong correlation between the crystallization degree of the polymeric matrix and the electrical conductivity of the polymeric nanocomposites [53]. Samples with higher crystallinity lead to a higher electrical conductivity due to the decreased scattering of electrons through the crystalline lamella. An analytical model has been previously proposed, based on the Fermi-Dirac distribution, to describe the critical insulator to conductor transition [56].

$$\log(\sigma_c) = \log(\sigma_f) + \frac{\log\left(\frac{\sigma_p}{\sigma_f}\right)}{(1+\exp(t(\phi-\phi_c)))} \qquad (2)$$

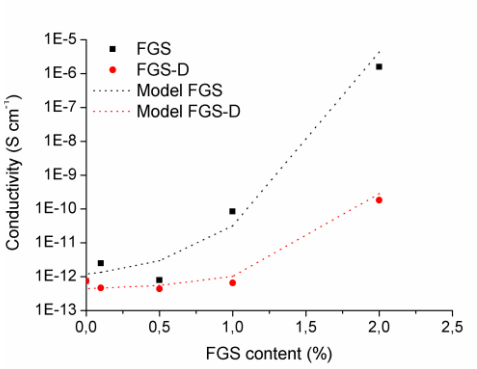

Figure 5. Experimental and calculated electrical conductivity versus filler loading for PLA-FGS nanocomposites.

where σ_c, σ_f and σ_p are the composite, filler, and polymer conductivities, respectively, ϕ is the FGS mass fraction, and t is an empirical parameter that leads to the change in conductivity at the percolation threshold ϕ_c. By assuming a constant value for σ_f and σ_p, from Equation (1) the best fitted values of ϕ_c and t were obtained. Thus, the percolation threshold value of nanocomposites was calculated at about ~1 wt.% for the samples produced from the masterbatch and ~2.8 wt.% for the samples obtained by direct addition of the filler to the melt mixer. Again, due to the relatively bad dispersion of the filler when added directly, an increase in the percolation threshold value was obtained.

4. CONCLUSIONS

Nanocomposites of polylactide (PLA) and functionalized graphene sheets (FGS) were successfully developed through a melt compounding method. In order to improve the dispersion of the filler within the PLA matrix, a pre-incorporation method based on *in situ* polymerization of FGS with lactic acid oligomers (OLLA) was used, obtaining a masterbatch material. Microscopic analysis revealed the efficiency of this pre-

incorporation step to improve the dispersion of FGS into PLA if compared by that observed for the samples obtained by direct addition of the FGS to the melt mixing process. Although thermal properties were not extensively affected upon addition of FGS into PLA, a decrease in the glass transition temperature, mainly ascribed to the oligomers addition, and also, an acceleration of the crystallization process due to the nucleating effect of FGS were observed. Moreover, the thermal stability was affected after the incorporation of OLLA and FGS, with a remarkable reduction in the onset degradation temperature, due one hand to the earlier degradation of the oligomers and on the other hand to the high heat conductivity of the FGS. As expected, improved barrier properties to both oxygen and water were obtained due to the blocking effect exerted by the laminar FGS and also to the occupancy of the free volume by the oligomers molecules, which led to improvements of up to 45% and 41% in oxygen and water vapour permeability, respectively. Addition of FGS simultaneously with OLLA impaired, to some extent, the filler-matrix interactions, counteracting the expected improvement in mechanical properties. Nevertheless, an optimum in the elastic modulus was obtained for the 0.1 wt.% sample obtained from the masterbatch. Lower improvements than expected were obtained in the electrical properties of the PLA nanocomposites after FGS addition, mainly due to most likely still incomplete dispersion and distribution of the filler together with the very low crystallinity of the polymeric material.

REFERENCES

[1] Siracusa V. (2012) Food packaging permeability behaviour: A report. International Journal of Polymer Science 2012.

[2] Silvestre C, Duraccio D, Cimmino S. (2011) Food packaging based on polymer nanomaterials. Progress in Polymer Science (Oxford) 36(12):1766-1782.

[3] Auras R, Harte B, Selke S. (2004) An overview of polylactides as packaging materials. Macromolecular Bioscience 4(9):835-864.

[4] Slomkowski S, Penczek S, Duda A. (2014) Polylactides-an overview. Polymers for Advanced Technologies 25(5):436-447.

[5] Oh JK. (2011) Polylactide (PLA)-based amphiphilic block copolymers: synthesis, self-assembly, and biomedical applications. Soft Matter 7(11):5096-5108.

[6] Ambrosio-Martín J, Fabra MJ, Lopez-Rubio A, Lagaron JM. (2014) An effect of lactic acid oligomers on the barrier properties of polylactide. Journal of Materials Science 49(8):2975-2986.

[7] Sanchez-Garcia MD, Lagaron JM. (2010) On the use of plant cellulose nanowhiskers to enhance the barrier properties of polylactic acid. Cellulose 17(5):987-1004.

[8] Martínez-Sanz M, Lopez-Rubio A, Lagaron JM. (2012) Optimization of the dispersion of unmodified bacterial cellulose nanowhiskers into polylactide via melt compounding to significantly enhance barrier and mechanical properties. Biomacromolecules 13(11):3887-3899.

[9] Ambrosio-Martín J, Fabra MJ, Lopez-Rubio A, Lagaron JM. (2015) Melt polycondensation to improve the dispersion of bacterial cellulose into polylactide via melt compounding: enhanced barrier and mechanical properties. Cellulose 22(2):1201-1226.

[10] Ramanathan T, Abdala AA, Stankovich S, Dikin DA, Herrera-Alonso M, Piner RD, et al. (2008) Functionalized graphene sheets

for polymer nanocomposites. Nature Nanotechnology 3(6):327-331.

[11] Moniruzzaman M, Winey KI. (2006) Polymer nanocomposites containing carbon nanotubes. Macromolecules 39(16):5194-5205.

[12] Potts JR, Dreyer DR, Bielawski CW, Ruoff RS. (2011) Graphene-based polymer nanocomposites. Polymer 52(1):5-25.

[13] Pötschke P, Bhattacharyya AR, Janke A, Pegel S, Leonhardt A, Täschner C, et al. (2005) Melt mixing as method to disperse carbon nanotubes into thermoplastic polymers. Fullerenes Nanotubes and Carbon Nanostructures 13(SUPPL. 1):211-224.

[14] Annala M, Lahelin M, Seppälä J. (2012) Utilization of poly(methyl methacrylate) - Carbon nanotube and polystyrene - Carbon nanotube in situ polymerized composites as masterbatches for melt mixing. Express Polymer Letters 6(10):814-825.

[15] Ayana B, Suin S, Khatua BB. (2014) Highly exfoliated eco-friendly thermoplastic starch (TPS)/poly (lactic acid)(PLA)/clay nanocomposites using unmodified nanoclay. Carbohydrate Polymers 110:430-439.

[16] Al-Qadhi M, Merah N. (2014) Mechanical and physical properties of polymer-based nanocomposites containing different types of clay. Polymer Composites.

[17] Hosseinkhanli H, Aalaie J, Abdollahi M, Khalkhali T, Shojaei M. (2014) Thermal, mechanical, and barrier properties of polyethylene/surlyn/organoclay nanocomposites blown films prepared by different mixing methods. Journal of Vinyl and Additive Technology.

[18] Tentschert J, Jungnickel H, Reichardt P, Leube P, Kretzschmar B, Taubert A, et al. (2014) Identification of nano clay in composite polymers. Surface and Interface Analysis 46(S1):334-336.

[19] Ojijo V, Ray SS. (2014) Nano-biocomposites based on synthetic aliphatic polyesters and nanoclay. Progress in Materials Science 62:1-57.

[20] Sanchez-Garcia MD, Lagaron JM. (2010) Novel clay-based nanobiocomposites of biopolyesters with synergistic barrier to UV light, gas, and vapour. Journal of Applied Polymer Science 118(1):188-199.

[21] Yoo BM, Shin HJ, Yoon HW, Park HB. (2014) Graphene and graphene oxide and their uses in barrier polymers. Journal of Applied Polymer Science 131(1).

[22] Kim H, Abdala AA, MacOsko CW. (2010) Graphene/polymer nanocomposites. Macromolecules 43(16):6515-6530.

[23] Huang HD, Ren PG, Xu JZ, Xu L, Zhong GJ, Hsiao BS, et al. (2014) Improved barrier properties of poly(lactic acid) with randomly dispersed graphene oxide nanosheets. Journal of Membrane Science 464:110-118.

[24] Jiang X, Drzal LT. (2012) Exploring the potential of exfoliated graphene nanoplatelets as the conductive filler in polymeric nanocomposites for bipolar plates. Journal of Power Sources 218:297-306.

[25] Pinto AM, Cabral J, Tanaka DAP, Mendes AM, Magalhães FD. (2013) Effect of incorporation of graphene oxide and graphene nanoplatelets on mechanical and gas permeability properties of poly(lactic acid) films. Polymer International 62(1):33-40.

[26] Kwon K, Chang JH. (2014) Comparison of the properties of poly(lactic acid) nanocomposites with various fillers: Organoclay, functionalized graphene, or organoclay/ functionalized graphene complex. Polymer (Korea) 38(2):232-239.

[27] Schniepp HC, Li JL, McAllister MJ, Sai H, Herrera-Alonson M, Adamson DH, et al. (2006) Functionalized single graphene sheets derived from splitting graphite oxide.

Journal of Physical Chemistry B 110(17):8535-8539.

[28] Xiao L, Mai Y, He F, Yu L, Zhang L, Tang H, et al. (2012) Bio-based green composites with high performance from poly(lactic acid) and surface-modified microcrystalline cellulose. Journal of Materials Chemistry 22(31):15732-15739.

[29] Verdejo R, Barroso-Bujans F, Rodriguez-Perez MA, De Saja JA, Lopez-Manchado MA. (2008) Functionalized graphene sheet filled silicone foam nanocomposites. Journal of Materials Chemistry 18(19):2221-2226.

[30] El Achaby M, Arrakhiz FZ, Vaudreuil S, Essassi EM, Qaiss A, Bousmina M. (2013) Preparation and characterization of melt-blended graphene nanosheets-poly(vinylidene fluoride) nanocomposites with enhanced properties. Journal of Applied Polymer Science 127(6):4697-4707.

[31] Kim IH, Jeong YG. (2010) Polylactide/exfoliated graphite nanocomposites with enhanced thermal stability, mechanical modulus, and electrical conductivity. Journal of Polymer Science, Part B: Polymer Physics 48(8):850-858.

[32] Sedlarik V, Kucharczyk P, Kasparkova V, Drbohlav J, Salakova A, Saha P. (2010) Optimization of the reaction conditions and characterization of L-lactic acid direct polycondensation products catalyzed by a non-metal-based compound. Journal of Applied Polymer Science 116(3):1597-1602.

[33] Giita Silverajah VS, Ibrahim NA, Md Zin Wan Yunus W, Hassan HA, Woei CB. (2012) A comparative study on the mechanical, thermal and morphological characterization of poly(lactic acid)/epoxidized palm oil blend. International Journal of Molecular Sciences 13(5):5878-5898.

[34] Chieng BW, Ibrahim NA, Wan Yunus WMZ, Hussein MZ, Loo YY. (2014) Effect of graphene nanoplatelets as nanofiller in plasticized poly(lactic acid) nanocomposites: Thermal properties and mechanical properties. Journal of Thermal Analysis and Calorimetry 118(3):1551-1559.

[35] Wu D, Cheng Y, Feng S, Yao Z, Zhang M. (2013) Crystallization behavior of polylactide/graphene composites. Industrial and Engineering Chemistry Research 52(20):6731-6739.

[36] Chen Y, Yao X, Gu Q, Pan Z. (2013) Non-isothermal crystallization kinetics of poly (lactic acid)/graphene nanocomposites. Journal of Polymer Engineering 33(2):163-171.

[37] Wang H, Qiu Z. (2012) Crystallization kinetics and morphology of biodegradable poly(l-lactic acid)/graphene oxide nanocomposites: Influences of graphene oxide loading and crystallization temperature. Thermochimica Acta 527:40-46.

[38] Bao C, Song L, Xing W, Yuan B, Wilkie CA, Huang J, et al. (2012) Preparation of graphene by pressurized oxidation and multiplex reduction and its polymer nanocomposites by masterbatch-based melt blending. Journal of Materials Chemistry 22(13):6088-6096.

[39] Sridhar V, Lee I, Chun HH, Park H. (2013) Graphene reinforced biodegradable poly(3-hydroxybutyrate-co-4-hydroxybutyrate) nano-composites. Express Polymer Letters 7(4):320-328.

[40] Yu HY, Qin ZY, Liu YN, Chen L, Liu N, Zhou Z. (2012) Simultaneous improvement of mechanical properties and thermal stability of bacterial polyester by cellulose nanocrystals. Carbohydrate Polymers 89(3):971-978.

[41] Mokwena KK, Tang J. (2012) Ethylene Vinyl Alcohol: A Review of Barrier Properties for Packaging Shelf Stable Foods. Critical Reviews in Food Science and Nutrition 52(7):640-650.

[42] Larocca NM, Pessan LA. (2003) Effect of antiplasticisation on the volumetric, gas sorption and transport properties of polyetherimide. Journal of Membrane Science 218(1-2):69-92.

[43] Maeda Y, Paul DR. (1987) Effect of antiplasticization on gas sorption and transport III. Free volume interpretation. Journal of Polymer Science, Part B: Polymer Physics 25(5):1005-1016.

[44] Colomines G, Ducruet V, Courgneau Ć, Guinault A, Domenek S. (2010) Barrier properties of poly(lactic acid) and its morphological changes induced by aroma compound sorption. Polymer International 59(6):818-826.

[45] Kanehashi S, Kusakabe A, Sato S, Nagai K. (2010) Analysis of permeability; solubility and diffusivity of carbon dioxide; oxygen; and nitrogen in crystalline and liquid crystalline polymers. Journal of Membrane Science 365(1-2):40-51.

[46] Tsuji H, Okino R, Daimon H, Fujie K. (2006) Water vapor permeability of poly(lactide)s: Effects of molecular characteristics and crystallinity. Journal of Applied Polymer Science 99(5):2245-2252.

[47] Komatsuka T, Kusakabe A, Nagai K. (2008) Characterization and gas transport properties of poly(lactic acid) blend membranes. Desalination 234(1-3):212-220.

[48] Ambrosio-Martín J, Gorrasi G, Lopez-Rubio A, Fabra MJ, Mas LC, López-Manchado MA, et al. (2015) On the use of ball milling to develop poly(3-hydroxybutyrate-co-3-hydroxyvalerate)-graphene nanocomposites (II)—Mechanical, barrier, and electrical properties. Journal of Applied Polymer Science 132:42217.

[49] De Vivo B, Lamberti P, Tucci V, Guadagno L, Vertuccio L, Vittoria V, et al. (2012) Comparison of the physical properties of epoxy-based composites filled with different types of carbon nanotubes for aeronautic applications. Advances in Polymer Technology 31(3):205-218.

[50] Gorrasi G, Sorrentino A. (2013) Photo-oxidative stabilization of carbon nanotubes on polylactic acid. Polymer Degradation and Stability 98(5):963-971.

[51] Gorrasi G, Milone C, Piperopoulos E, Lanza M, Sorrentino A. (2013) Hybrid clay mineral-carbon nanotube-PLA nanocomposite films. Preparation and photodegradation effect on their mechanical, thermal and electrical properties. Applied Clay Science 71:49-54.

[52] Mittal G, Dhand V, Rhee KY, Park SJ, Lee WR. (2015) A review on carbon nanotubes and graphene as fillers in reinforced polymer nanocomposites. Journal of Industrial and Engineering Chemistry 21:11-25.

[53] Sullivan EM, Oh YJ, Gerhardt RA, Wang B, Kalaitzidou K. (2014) Understanding the effect of polymer crystallinity on the electrical conductivity of exfoliated graphite nanoplatelet/polylactic acid composite films. Journal of Polymer Research 21(10).

[54] Wu H, Zhao W, Chen G. (2012) One-pot in situ ball milling preparation of polymer/graphene nanocomposites. Journal of Applied Polymer Science 125(5):3899-3903.

[55] Wu H, Zhao W, Hu H, Chen G. (2011) One-step in situ ball milling synthesis of polymer-functionalized graphene nanocomposites. Journal of Materials Chemistry 21(24):8626-8632.

[56] Gorrasi G, Di Lieto R, Patimo G, De Pasquale S, Sorrentino A. (2011) Structure-property relationships on uniaxially oriented carbon nanotube/polyethylene composites. Polymer 52(4):1124-1132.

Chapter 4

ASSESSMENT OF BALL MILLING METHODOLOGY TO DEVELOP POLYLACTIDE-BACTERIAL CELLULOSE NANOWHISKERS NANOCOMPOSITES

J. Ambrosio-Martín[a], A. Lopez-Rubio[a], M. J. Fabra[a], G. Gorrasi[b], R. Pantani[b] and J. M. Lagaron[a]

Journal of Applied Polymer Science 2015, 132(10):41605

[a] Novel Materials and Nanotechnology Group, IATA-CSIC, Avda. Agustin Escardino 7, 46980 Paterna (Valencia), Spain.

[b] Department of Industrial Engineering, University of Salerno, via Giovanni Paolo II, 132 Fisciano (Salerno), Italy.

ABSTRACT

In this work, ball milling is evaluated as a methodology to develop polylactide (PLA)-bacterial cellulose nanowhiskers (BCNW) nanocomposites. This technique, widely used for clay-based nanocomposites, is effective in breaking up to a very large extent the freeze-dried nanocellulose aggregates, giving raise to transparent films similar to the neat PLA films. Incorporation of the nanofiller through this methodology enhances the polymer crystallinity index. An increase in the onset degradation temperature and a significant reinforcing effect in terms of an increase in the storage modulus and in the tan delta peak are also observed. Improved barrier to oxygen at high relative humidity (80 %) is also noticed, reaching the best performance at the lowest BCNW loading (0.5 wt.%). These improvements are related to the relatively good nanocellulose dispersion and distribution attained for low loadings of the nanofiller. Thus, the ball milling methodology appears as a feasible processing methodology for developing PLA-BCNW nanocomposites.

Keywords: Biopolymers & renewable polymers, composites, films, nanoparticles, nanowires and nanocrystals, packaging.

1. INTRODUCTION

The development of fully renewable biopolymer nanocomposites to replace synthetic polymers for different applications has been the subject of numerous studies during the last years. Nanocellulose, also referred to as cellulose nanocrystals (CNW) or cellulose nanowhiskers (CNW) represents one of the most interesting fillers for these applications due to its broad availability, low cost and to the possibility of obtaining different morphological features depending on the cellulose source. In this sense, while cellulose nanowhiskers (CNW) extracted from vegetal resources such as cotton or wood typically have a length of 100–300 nm and width of 5–20 nm [1-3], those obtained from tunicin and bacterial cellulose (BCNW) may have several micrometres in length and a width of 5–50 nm [4-6]. CNW are usually obtained through hydrolysis with strong acids such as sulphuric acid or hydrochloric acid, which produce a preferential digestion of the amorphous domains of the material and cleavage of the nanofibril bundles [7]. One of the main difficulties associated with the use of unmodified CNW as reinforcing agents is their high hydrophilicity, which makes it difficult to disperse them in non-polar media. This is especially relevant when trying to implement the physical properties of biopolyesters using nanocellulose. Among the biopolyesters, polylactide (PLA) obtained from the fermentation of corn starch [8] is one of the most attractive materials due to its high transparency and ease of processability and, thus, has found commercial applications in food packaging and medicine. However, PLA also presents a number of drawbacks such as low thermal resistance, excessive brittleness, and relatively low barrier to oxygen and water vapour as compared to other packaging materials such as polyethylene terephthalate (PET). The other great challenge when trying to develop PLA-based nanocomposites reinforced with CNW is to attain proper nanofiller dispersion through the use of industrial processing techniques, such as melt compounding methods, due to the above mentioned different nature between hydrophobic PLA and hydrophilic CNW. It has been observed that direct melt mixing of the freeze-dried nanocellulose with the polymer or biopolymer matrix provides materials with big nanocelllulose agglomerates and, thus, insufficient physical properties [9]. Several strategies have been recently developed to improve nanocellulose dispersion PLA matrices obtained through melt compounding, based on pre-incorporation of the nanofiller either in electrospun fibres [9] or in lactic acid oligomers [10]. Chemical modification of the nanofiller has also been investigated and although improved adhesion with the PLA matrix was observed, good nanofiller dispersion was only obtained for low nanocellulose loadings [11]. Moreover, chemical modification also resulted in decreased crystallinity and thermal stability of the nanofiller [11]. As an alternative, the potential of ball milling has been previously investigated to develop polymer nanocomposites where hydrophilic filler was introduced in hydrophobic matrix, attempting to overcome the lack of natural affinity between both components [12]. Ball milling is a high-energy grinding technique, able to induce several mechanochemical changes in the materials that occur at different rates. In addition to its use to develop clay-based nanocomposites, this technique has been previously used in the development of graphene-based nanocom-posites as the high-energy milling induces platelet and graphite delamination, respectively, thus improving the final properties of the obtained materials [13]. Very recently, nanofibres of 50 nm diameter were obtained from waste jute fibres using high energy planetary ball milling [14], thus suggesting that this high mechanical energy process could be effectively used for improving

nanocrystals dispersion. To the best of our knowledge, this technique has not been used before to generate cellulose-based nanocomposites and, thus, the objective of the present work was to evaluate the potential of ball milling for the production of PLA-BCNW nanocomposites and to compare it with the existing strategies previously developed. PLA and freeze-dried BCNW were ground together using ball milling and the mixed material obtained was subsequently hot-pressed into films. The morphology, thermal properties, isothermal crystallization, mechanical properties and oxygen barrier performance of the so-obtained nanocomposites were characterized.

2. MATERIALS AND METHODS

2.1. Materials

The semicrystalline poly(lactic acid) (PLA) used was a film extrusion grade with a number average molecular weight (M_n) of 130,000 g mol^{-1} and a weight average molecular weight (M_w) of 150,000 g mol^{-1} manufactured by NatureWorks (USA). Prior to the ball milling process, the material was purified by dissolution in $CHCl_3$ and subsequent precipitation by drop-wise addition to an excess of methanol. The material, in this way, was transformed from pellet to powder form which is necessary for the ball milling process. Sulphuric acid 96 wt.% and sodium hydroxide pellets were purchased from Panreac (Barcelona, Spain). The bacterial strain *Gluconacetobacter xylinus* was obtained from the Spanish type culture collection (CECT).

2.2. Preparation of bacterial cellulose nanowhiskers (BCNW)

Initially, bacterial cellulose mats were obtained using the bacterial strain *Gluconacetobacter xylinus* 7351 as described in previous works [10, 15]. After that BCNW were obtained by acid hydrolysis using the optimized method reported by Martinez-Sanz and coworkers [7]. Full description of the synthesis of the BCNW can be found elsewhere [10].

2.3. Preparation of nanocomposites through ball milling

Grinded BCNW and PLA powder were milled in the solid state in a Retsch (Germany) centrifugal ball mill (model PM100). The milling process was carried out in a cylindrical steel jar of 50 cm^3 with 5 steel balls of 10 mm of diameter. The rotation speed used was 650 rpm, and the milling time was fixed to 60 min. In these experimental conditions, four series of composites PLA-BCNW with 0.5, 1, 3, and 5 wt/wt % of BCNW were prepared. An additional PLA sample to be taken as a reference was also milled in absence of filler. The PLA-BCNW mixtures and the pure milled PLA were molded in a hot press (Carver Inc.) at 165 °C forming 250 ± 50 μm thick films.

2.4. Optical properties of the films

The opacity of the films was measured by using a Konica Minolta CM-2500d X-Rite SP60 Series spectrophotometer following the ASTM E284 ("Terminology of Appearance"). The opacity was defined as ability of a thin film to hide a surface behind and in contact with it, expressed as the ratio of the reflectance factor (R_b) when the material is backed by a black surface to the reflectance factor (R_w) when it is backed by a white surface (usually having a reflectance factor of 0.89). The opacity (O) was calculated using the relationship: O (%) = (R_b/R_w) x 100

2.5. Differential Scanning Calorimetry (DSC)

The thermal properties and isothermal cold crystallization behaviour of PLA and PLA-BCNW nanocomposite films obtained through ball milling were studied by DSC using a DTA Mettler Toledo (DSC 30) under nitrogen atmosphere. DSC experiments were carried out on typically 10-12 mg of dry material at a heating and cooling rate of 10 °C min^{-1}. To ensure reliability of the data obtained, heat flow and temperature were calibrated with standard materials, indium, and zinc.

The degree of crystallinity (%) of PLA was estimated from the corrected enthalpy for biopolymer content in the final materials, using the ratio between the enthalpy of the studied material and the enthalpy of a perfect PLA crystal using the following equation:

$$\%Xc = \frac{\left(\Delta H_f - \Delta H_c\right)}{\Delta H_f^o\left(1-w\right)} \times 100 \quad (1)$$

where ΔH_f is the enthalpy of fusion and ΔH_c the enthalpy of cold crystallization of the of the studied specimen. ΔH^o_f is the enthalpy of fusion of a totally crystalline material and w is the weight fraction of the filler. The ΔH^o_f used for this equation was 93 J g^{-1} for PLA [16].

In addition, isothermal crystallization kinetics study was performed as follow. The samples were heated from room temperature to 180 °C at 75 °C min^{-1} and held for 10 min to erase the thermal history. Then, they were cooled rapidly at 100 °C min^{-1}, to the desired crystallization temperatures (in this case 105, 110 and 115 °C), ensuring that the crystallization process do no start in the cooling step. After that, the temperature was held for about 2 h, until the crystallization process was completed, and finally heated at 10 °C min^{-1} to 180 °C again to get the melting temperature.

2.6. Thermogravimetric Analysis (TGA)

Thermogravimetric (TG) curves were recorded using a thermobalance Mettler TC-10. The samples were heated from 25 °C to 800 °C at a heating rate of 10 °C min^{-1} both under air flow and under nitrogen atmosphere. The weight loss was recorded as function of temperature.

2.7. Dynamic mechanical analysis (DMA)

Mechanical properties were evaluated using a DMA TAQ800. Measurements were conducted at the constant frequency (1Hz) and amplitude (5μm). The temperature was varied between -30 °C and 140 °C at 3 °C min^{-1}.

2.8. Oxygen transmission rate

The oxygen permeability coefficient was derived from oxygen transmission rate (OTR) measurements recorded using an Oxtran 100 equipment (Modern Control Inc., Minneapolis, MN, US). Experiments were carried out at 24 °C and at 80 % relative humidity (RH) conditions. Relative humidity was generated by a built-in gas bubbler and was checked with a hygrometer placed at the exit of the detector. The samples were purged with nitrogen for a minimum of 20 h in the humidity equilibrated samples, prior to exposure to an oxygen flow of 10 ml min^{-1}. A 5 cm^2 sample area was measured by using an in-house developed mask. The measurements were done in duplicate.

2.9. Mechanical properties

Tensile tests were carried out at 24 °C and 50 % RH on an Instron 4400 Universal Tester. Pre-conditioned dumb-bell shaped specimens with initial gauge length of 25 mm and 5 mm in width were die-stamped from the films in the machine direction. The thickness of all specimens was

approximately 100 μm. A fixed crosshead rate of 10 mm min^{-1} was used in all cases, and results were taken as the average of, at least, three tests.

2.10. Scanning electron microscopy (SEM)

For scanning electron microscopy (SEM) observation, the samples were cryofractured after immersion in liquid nitrogen, mounted on bevel sample holders and sputtered with Au/Pd under vacuum. The cross section images of the films were examined on a Hitachi microscope (Hitachi S-4100) at an accelerating voltage of 10 KV and a working distance of 12–16 mm.

2.11. Transmission Electron Microscopy (TEM)

Transmission electron microscopy (TEM) was performed using a JEOL 1010 (Jeol, Tokyo, Japan) equipped with a digital Bioscan (Gatan) image acquisition system. TEM observations were performed on ultrathin sections of microtomed thin composite sheets.

2.12. Statistical analysis

Results were analysed by multifactor analysis of variance (ANOVA) using Statgraphics Centurion 15.1 software (Statpoint Technologies, INC, Warrenton, VA, USA). Tukey's test was used at the 95 % confidence level.

3. RESULTS AND DISCUSSION

3.1. Morphology and optical properties of the PLA-BCNW nanocomposites obtained by ball-milling

The nanocomposite films obtained after compression moulding of the different formulations obtained through ball milling were optically identical to a neat PLA film (it could be observed in Figure A3 in Annex A), which indicated that this processing method effectively broke up the aggregates formed during the freeze-drying of the cellulose nanocrystals. The development of PLA-BCNW films through the direct melt compounding of the biopolyester with the freeze-dried material is known to give rise to materials with aggregates that can be visually observed [9, 10].

The opacity values of the films with different BCNW content are shown in Table 1. From this table it can be observed that only for the film with the greatest nanocellulose content there were significant differences in opacity, which increased with respect to the neat PLA film.

Table 1. Opacity values of films with different BCNW contents.

	Apparent opacity
PLA	16,4 ± 0,2
PLA-BCNW 0.5	16,3 ± 0,1
PLA-BCNW 1	16,0 ± 0,9
PLA-BCNW 3	17,3 ± 0,1
PLA-BCNW 5	19,5 ± 0,2

The microstructure of the films was also evaluated through SEM and TEM analysis. The cryo-fractured surfaces of the various nanocomposites in comparison with that of the neat PLA film are shown in Figure 1. From these images it can be observed, that even though there were little optical differences at the macroscopic level, some nanocellulose aggregates still remain in the materials. Nevertheless, although these aggregates were also observed by TEM analysis, a significant fraction of the filler was properly dispersed and distributed as observed in Figure 2.

From the morphological study, it can be stated that although this technique broke up big aggregates so as to give rise to transparent films (in contrast with direct

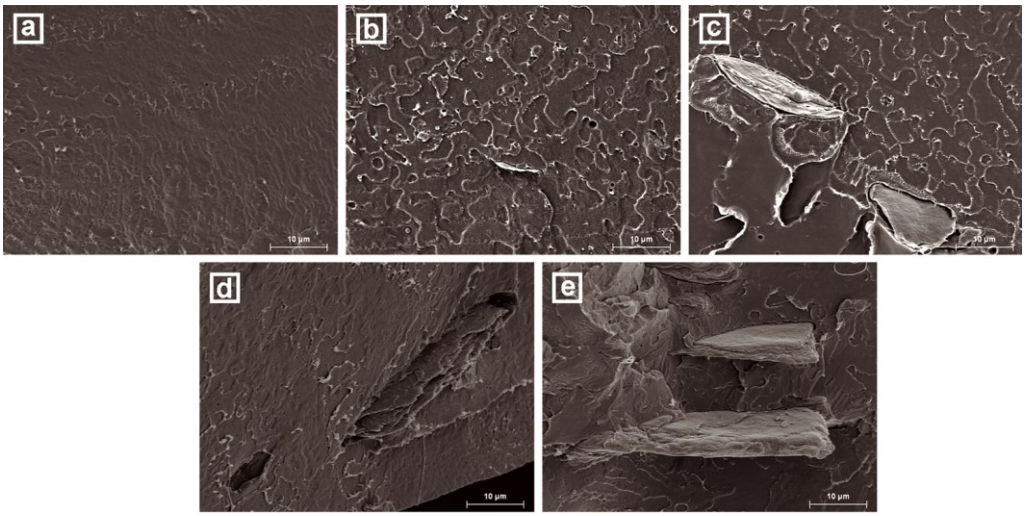

Figure 1. SEM images of the cross-sections of the different films obtained through ball-milling: a) Neat PLA film; b) PLA-BCNW 0.5; c) PLA-BCNW 1; d) PLA-BCNW 3; e) PLA-BCNW 5. Scale markers correspond to 10 µm

melt blending of PLA with freeze-dried BCNW), it was insufficient to attain a proper BCNW dispersion such as the one obtained using other pre-dispersion methods previously described [9, 10]. Moreover, increasing the nanocellulose content in the materials resulted in bigger and more frequent aggregates as observed by SEM (cf. Figure 1).

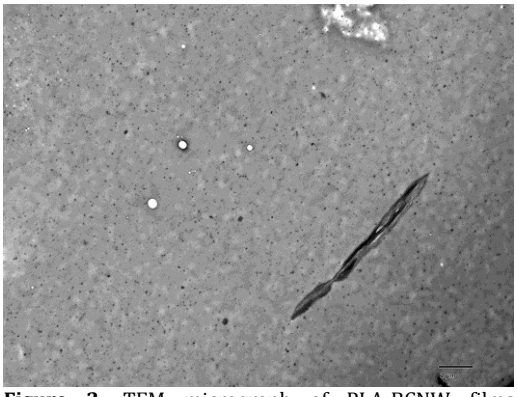

Figure 2. TEM micrograph of PLA-BCNW films containing 1 wt.% BCNW. Scale marker correspond to 2 µm.

3.2. Thermal properties and isothermal crystallization

With the aim of investigating the effects of BCNW addition through the ball milling methodology on the thermal properties of the PLA nanocomposites, DSC analyses of all the samples were carried out. Table 2 compiles the melting temperature (T_m), melting enthalpy (ΔH_m) normalized to the PLA content of the nanocomposite films, the cold crystallization temperature (T_{cc}) and the degree of crystallinity (X_c) which were obtained from the DSC first heating run, and the glass transition temperature which was determined from both the first (T_{g1}) and the second heating run (T_{g2}). Furthermore, Figure 3 shows the thermograms from the first heating scan of each sample.

The first interesting observation was that the neat PLA film obtained after ball milling, showed a double melting event, suggesting the existence of two different crystalline populations, probably generated as a consequence of the mechanical treatment of the polymer. Several authors have reported that high energy ball milling

Table 2. DSC maximums of melting (T_{m1} and T_{m2}), melting enthalpy (ΔH_m), cold crystallization temperature (T_{cc}), cold crystallization enthalpy (ΔH_c), PLA crystallinity (X_c) and glass transition temperature of PLA films processed by ball milling obtained during the first (T_{g1}) and second (T_{g2}) heating runs

	T_{m1} (°C)	T_{m2} (°C)	ΔH_m (J g^{-1})	T_{cc} (°C)	ΔH_c (J g^{-1})	X_c (%)	T_{g1}(°C)	T_{g2} (°C)
PLA	147,3	153,5	34,5	109,7	33,2	1,4	57,9	58,8
PLA-BCNW 0.5	147,0	154,0	31,4	107,7	30,0	1,6	58,8	59,2
PLA-BCNW 1	147,3	153,8	36,3	108,5	33,0	3,6	56,7	56,9
PLA-BCNW 3	147,0	153,5	36,0	108,5	32,2	4,1	56,0	58,9
PLA-BCNW 5	146,9	154,0	35,8	107,0	31,4	4,7	56,3	59,0

applied to different polymers, such as poly(methyl methacrylate) (PMMA) and poly (lactic-co-glycolic acid) (PLGA), results in changes in the molecular weight of the polymers [17, 18]. Specifically, chain scission has been observed in PMMA as a consequence of the intense mechanical treatment [17], which could explain the development of lower melting temperature crystallites.

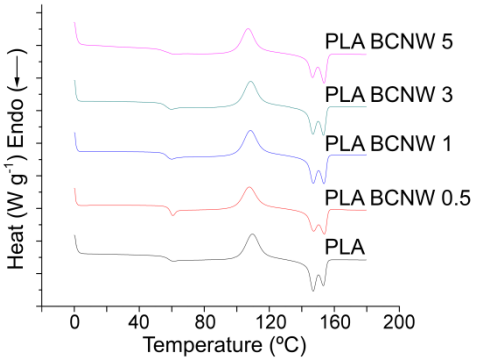

Figure 3. DSC fist heating scan thermograms of PLA and its nanocomposites

As deduced from the results in Table 2, the thermal properties of the nanocomposites were not significantly different from those of the neat PLA film obtained through ball milling. Only a slight decrease in the cold crystallization temperature (T_{cc}) was observed for the nanocomposites. The lower T_{cc} observed in the heating run can be an indication of a faster crystallization induced by the presence of a significant fraction of well dispersed cellulose nanowhiskers, as observed in TEM analysis, which acted as nucleating agents for PLA, as previously reported [9, 19]. In fact, the crystallinity of the nanocomposites increased as a function of nanocellulose loading, supporting the beneficial effect of the fillers on crystallization. This is an interesting result, as it is well-known that, in general, ball milling of semicrystalline polymers results in decreased crystallinity [20, 21].

To further analyse the influence of BCNW on the crystallization process, an isothermal crystallization study was carried out. Three different crystallization temperatures were used (105, 110 and 115 °C) for the study and Table 3 compiles the parameters obtained through fitting the DSC crystallization curves with the Avrami model (Equation (2)).

$$X(t) = 1 - \exp\left(-kt^n\right) \qquad (2)$$

where $X(t)$ is the relative crystallinity at time t, k is the crystallization rate constant and n is the Avrami index. Derivative method reported by De Santis and Pantani [22] was used to directly fit the calorimetric curve of the isothermal crystallization process to the derivative form of Avrami equation.

It is well-known that the value of the Avrami exponent n depends on both the mechanism of nucleation and to the

Table 3. Parameters obtained from the Avrami analysis during isothermal crystallization of PLA and its nanocomposites prepared by ball milling

	105 °C			110 °C			115 °C		
	k (s^{-1})	n	$t_{1/2}$ (s)	k (s^{-1})	n	$t_{1/2}$ (s)	k (s^{-1})	n	$t_{1/2}$ (s)
PLA	1.2 e-3	3.2	734.3	8.0 e-4	3.0	1108.1	3.9 e-4	3.5	2281.4
PLA-BCNW 0.5	1.1 e-3	3.2	845.7	8.4 e-4	3.1	1052.4	5.5 e-4	2.9	1606.2
PLA-BCNW 1	1.1 e-3	3.4	836.4	8.5 e-4	2.9	1034.4	5.8 e-4	2.9	1531.0
PLA-BCNW 3	1.0 e-3	3.3	851.8	9.3 e-4	3.0	956.8	8.6 e-4	2.8	1021.8
PLA-BCNW 5	1.7 e-3	2.8	510.3	1.5 e-3	2.9	573.9	1.2 e-3	2.8	726.5

geometry of the growing crystals, and usually is an integer between 1 and 4. At the different crystallization temperatures investigated, this exponent was in the vicinity of 3, both for the neat polymer and for the nanocomposites, thus suggesting that addition of the nanocellulose did not significantly affected the crystallization mechanism.

On the other hand, the parameter k has contributions from both nucleation and growth and the increase in this parameter could be related with an increase in the crystallization rate and, thus, an improvement in the crystallization process. As shown in Table 3, parameter k increased when increasing the BCNW content when the isothermal crystallization process was carried out at 110 and 115 °C, thus pointing out to an acceleration of the crystallization process. In contrast, at 105 °C, an increase in this parameter was only observed for PLA-BCNW 5% sample. At this temperature, i.e. 105 °C, the crystallization process went faster (as observed if comparing the k parameters at the three different temperatures) and, apparently, small additions of BCNW did not affect it. In contrast, the nanocomposite with 5 wt.% BCNW content showed an acceleration of the crystallization process reflected in an increase of the parameter k. In line with these results, the crystallization half times ($t_{1/2}$, time required for half of the final crystallinity to develop) decreased for the nanocomposites when compared to the neat polymer at 110 and 115 °C. At 105 °C, since $t_{1/2}$ is directly related with the crystallization rate constant, the same trend was observed as for this parameter, no effect on the crystallization process for low contents of BCNW was observed, while the crystallization process was promoted when BCNW content was increased up to 5 wt.%. The decrease of $t_{1/2}$ was also related to the nanofiller content, again indicating an increase in the crystallization rate promoted by the presence of nanocellulose. Increasing the crystallization temperature, the rate of nucleation decreased and thus the overall crystallization rate also decreased. Similar results were obtained during the isothermal cold crystallization of PLA using several nucleating agents [23], thus confirming that BCNW effectively promoted crystallization acting as nucleating sites.

The thermal stability of the different materials obtained through ball milling and subsequently pressed into films were also analysed using TGA in the presence of air and under a nitrogen atmosphere. In general, as observed in Table 4, incorporation of BCNW through the ball milling methodology did not alter the thermal stability of the nanocomposites. Despite the fact that native BCNW are less thermally stable than PLA [7, 9], no significant decrease in the thermal stability of the materials was observed and even a slight increase in the onset degradation temperature was noticed when the samples were analysed in the presence of oxygen.

Table 4. TGA maximum of the weight loss first derivate (*Td*) and the corresponding peak onset values and the residue at 600°C for the PLA Films, analysed in the presence of air (O_2) and under a nitrogen atmosphere (N_2).

	Oxygen			Nitrogen		
	Onset T (°C)	*Td* (°C)	Residue at 600 °C	*Onset T* (°C)	*Td* (°C)	Residue at 600 °C
PLA	325.8	362.7	2.6	329.5	366.4	2.1
PLA-BCNW 0.5	329.0	363.6	1.8	331.2	366.9	2.1
PLA-BCNW 1	332.3	361.5	2.2	331.2	366.5	1.9
PLA-BCNW 3	330.2	361.4	1.8	330.1	366.2	2.3
PLA-BCNW 5	330.4	362.2	1.9	330.4	365.4	2.8

3.3. Mechanical and thermo mechanical characterization

The mechanical properties of PLA and its corresponding BCNW-containing nanocomposite films obtained through ball milling are summarized in Table 5. In general, the PLA films containing nanocellulose exhibited a higher Young's modulus and tensile strength and lower elongation at break than the neat PLA film, regardless of the nanofiller content. It is interesting to note that the greatest reinforcing effect observed corresponded to the film with lowest BCNW content (0.5 wt.%), probably as a consequence of the better dispersion of the nanofiller within the polymeric matrix, as inferred from the SEM micrographs. When comparing the ball milling methodology presented in this work with other strategies previously reported to develop PLA-BCNW nanocomposites [9, 10], the improvements in Young's modulus and tensile strength were lower than the previously reported ones, about a 10 % improvement of both parameters using the ball milling approach vs. 52 % or 17 % Young's modulus increase and 31 % or 14 % tensile strength increase for BCNW incorporation through grafting with lactic acid oligomers [10] or pre-incorporation through electrospinning [9], respectively. Chemical grafting of BCNW with poly-(glycidyl methacrylate) (PGMA) before incorporation into PLA also resulted in slightly better mechanical properties, reaching improvements of ca. 16% and 22% in Young's modulus and tensile strength, respectively [11].

The load bearing capacity of neat PLA and BCNW-containing nanocomposites obtained through ball milling was studied from the storage modulus. The results are shown in Figure 4a. The storage modulus of the PLA nanocomposite films improved over the entire temperature span as compared to neat PLA. The increase in the storage modulus was directly related to the nanofiller content and could be attributed, not only to the presence of the nanofiller, but also to the observed increase in crystallinity of the nanocomposites (cf. Table 2).

The ratio of loss modulus to storage modulus is defined as mechanical loss factor or tan δ. Figure 4b shows that incorporation of the BCNW led to an increase of about 3 °C in the tan delta peak of PLA. These increments were attributed to the restricted segmental mobility of the matrix chains

Table 5. Young's modulus (*E*), tensile strength and elongation at break (ε_b) for PLA and its nanocomposites with BCNW obtained through ball milling.

	E (MPa)	Tensile Strength (MPa)	ε_b (%)
PLA	2091.9 ± 190.6	41.36 ± 4.5	4.8 ± 2.0
PLA-BCNW 0.5	2305.4 ± 96.0	45.40 ± 2.4	3.4 ± 0.4
PLA-BCNW 1	2120.7 ± 136.6	42.67 ± 2.5	3.4 ± 0.5
PLA-BCNW 3	1953.6 ± 125.9	38.83 ± 3.9	2.6 ± 0.4
PLA-BCNW 5	2176.2 ± 56.6	40.24 ± 4.3	2.4 ± 0.4

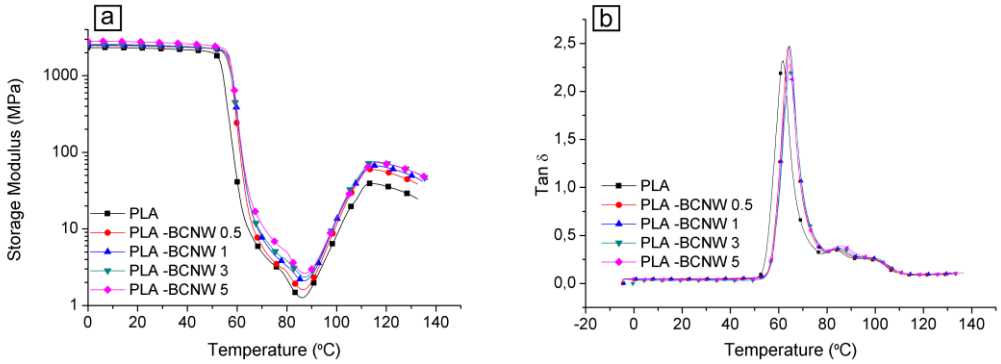

Figure 4. Storage modulus (a) and tan δ plots versus temperature for neat PLA and its nanocomposites with BCNW

around the nanofillers [24]. However, the increase was not proportional to the nanofiller content, probably due to agglomeration and, thus, increasing the BCNW amount did not correlate with increased surface area for interaction with the biopolyester.

3.4. Barrier properties

Finally, the oxygen permeability of the nanocomposites obtained through ball milling in comparison with the neat PLA film was also characterized at 80 % RH. The results are plotted in Figure 5.

The oxygen permeability of neat PLA obtained through ball milling was very similar to that previously reported in the literature [25, 26], even though that, as previously stated, ball milling processing leads to an increase in density of the material [27].

From Figure 5 it can be observed that a significant reduction in the oxygen permeability was obtained for the materials containing BCNW, suggesting that the well dispersed fraction of crystalline nanofillers effectively blocked the oxygen flow, although the greatest reduction was seen for the lowest nanocellulose content, highlighting again the importance of dispersion to optimize the performance improvements in this kind of films. When comparing the results of this study with previous PLA-BCNW nanocomposites prepared using different routes and methodologies, it can be stated that ball milling improved the dispersion of the nanofillers when compared to PGMA-grafted BCNW nanocomposites [11] or direct freeze-dried nanocellulose addition, which led to a lower improvements or deleterious effect on barrier properties, respectively. However, greater improvements were obtained using pre-incorporation methods such as dispersion in electrospun fibres [9] or grafting with lactic acid oligomers [10], which improved the further dispersion in PLA matrix through melt compounding. Moreover, in a comparision with PLA-based nanocompounds reinforced with nanoclays

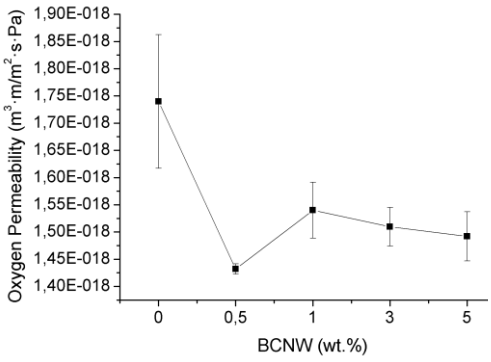

Figure 5. Oxygen permeability measured at 80% RH for neat PLA and its nanocomposites with BCNW prepared by ball milling

[28, 29], lower improvements were obtained in this study. It is important to mention that, in one hand, the used methodology to incorporate the nanofiller were different to that used in this study. In fact, to the best of our knowledge, there is no any literature about the incorporation of nanoclays into PLA through ball milling. On the other hand, the better improvements obtained in those studies were due to the filler nature. It is widely known that its lamellar structure induced higher blocking effect to the vapour and gases pathways.

4. CONCLUSIONS

In this work it has been demonstrated that ball milling can lead to a significant dispersion of the BCNW filler within a PLA matrix when compared to direct addition of freeze-dried nanocellulose in a melt mixing process. The morphological studies showed that this technique was able to disperse and distribute the freeze dried BCNW fillers, although some agglomerates remained. Upon increasing the BCNW content an increase in the number of aggregates were observed. The well dispersed fraction of BCNW acted as nucleating sites, increasing the crystallization rate and the final crystallinity index of the materials. Moreover, thermal stability was not significantly affected and even a slight increase in the onset degradation temperature was observed in the nanocomposites obtained through ball milling. Improved thermo-mechanical and barrier properties were observed for nanocomposites as compared to the neat PLA. In spite of this, the nanocomposite film with lowest BCNW content displayed the best performance in terms of mechanical and thermo-mechanical properties, as well as permeability to oxygen measured at high relative humidity, which was related to a better dispersion of the nanofiller at this loading level.

REFERENCES

[1] Araki J, Wada M, Kuga S, Okano T. (1998) Flow properties of microcrystalline cellulose suspension prepared by acid treatment of native cellulose. Colloids and Surfaces A: Physicochemical and Engineering Aspects 142(1):75-82.

[2] Favier V, Chanzy H, Cavaille JY. (1995) Polymer nanocomposites reinforced by cellulose whiskers. Macromolecules 28(18):6365-6367.

[3] Siqueira G, Bras J, Dufresne A. (2009) Cellulose whiskers versus microfibrils: Influence of the nature of the nanoparticle and its surface functionalization on the thermal and mechanical properties of nanocomposites. Biomacromolecules 10(2):425-432.

[4] Araki J, Kuga S. (2001) Effect of trace electrolyte on liquid crystal type of cellulose microcrystals. Langmuir 17(15):4493-4496.

[5] De Souza Lima MM, Wong JT, Paillet M, Borsali R, Pecora R. (2003) Translational and rotational dynamics of rodlike cellulose whiskers. Langmuir 19(1):24-29.

[6] Hirai A, Inui O, Horii F, Tsuji M. (2009) Phase separation behavior in aqueous suspensions of bacterial cellulose nanocrystals prepared by sulfuric acid treatment. Langmuir 25(1):497-502.

[7] Martínez-Sanz M, Lopez-Rubio A, Lagaron JM. (2011) Optimization of the nanofabrication by acid hydrolysis of bacterial cellulose nanowhiskers. Carbohydrate Polymers 85(1):228-236.

[8] Lunt J. (1998) Large-scale production, properties and commercial applications of

poly lactic acid polymers. Polymer Degradation and Stability 59(1-3):145-152.

[9] Martínez-Sanz M, Lopez-Rubio A, Lagaron JM. (2012) Optimization of the dispersion of unmodified bacterial cellulose nanowhiskers into polylactide via melt compounding to significantly enhance barrier and mechanical properties. Biomacromolecules 13(11):3887-3899.

[10] Ambrosio-Martín J, Fabra MJ, Lopez-Rubio A, Lagaron JM. (2015) Melt polycondensation to improve the dispersion of bacterial cellulose into polylactide via melt compounding: enhanced barrier and mechanical properties. Cellulose 22(2):1201-1226.

[11] Martínez-Sanz M, Abdelwahab MA, Lopez-Rubio A, Lagaron JM, Chiellini E, Williams TG, et al. (2013) Incorporation of poly(glycidylmethacrylate) grafted bacterial cellulose nanowhiskers in poly(lactic acid) nanocomposites: Improved barrier and mechanical properties. European Polymer Journal 49(8):2062-2072.

[12] Perrin-Sarazin F, Sepehr M, Bouaricha S, Denault J. (2009) Potential of ball milling to improve clay dispersion in nanocomposites. Polymer Engineering and Science 49(4):651-665.

[13] Wu H, Zhao W, Chen G. (2012) One-pot in situ ball milling preparation of polymer/graphene nanocomposites. Journal of Applied Polymer Science 125(5):3899-3903.

[14] Baheti V, Militky J, Marsalkova M. (2013) Mechanical properties of poly lactic acid composite films reinforced with wet milled jute nanofibers. Polymer Composites 34(12):2133-2141.

[15] Martínez-Sanz M, Olsson RT, Lopez-Rubio A, Lagaron JM. (2011) Development of electrospun EVOH fibres reinforced with bacterial cellulose nanowhiskers. Part I: Characterization and method optimization. Cellulose 18(2):335-347.

[16] Sanchez-Garcia MD, Lagaron JM. (2010) On the use of plant cellulose nanowhiskers to enhance the barrier properties of polylactic acid. Cellulose 17(5):987-1004.

[17] Pantaleón R, González-Benito J. (2010) Structure and thermostability of PMMA in PMMA/silica nanocomposites: Effect of high-energy ball milling and the amount of the nanofiller. Polymer Composites 31(9):1585-1592.

[18] Shabir A, Alhusban F, Perrie Y, Mohammed AR. (2011) Effects of ball-milling on PLGA polymer and its implication on lansoprazole-loaded nanoparticles. J Basic Clin Pharm 2(2):71-82.

[19] Suryanegara L, Nakagaito AN, Yano H. (2010) Thermo-mechanical properties of microfibrillated cellulose-reinforced partially crystallized PLA composites. Cellulose 17(4):771-778.

[20] Ishida T. (1994) Mechanical alloying of polytetrafluoroethylene with polyethylene. Journal of Materials Science Letters 13(9):623-628.

[21] Olmos D, Domínguez C, Castrillo PD, Gonzalez-Benito J. (2009) Crystallization and final morphology of HDPE: Effect of the high energy ball milling and the presence of TiO2 nanoparticles. Polymer 50(7):1732-1742.

[22] De Santis F, Pantani R. (2013) Nucleation density and growth rate of polypropylene measured by calorimetric experiments. Journal of Thermal Analysis and Calorimetry 112(3):1481-1488.

[23] Liao R, Yang B, Yu W, Zhou C. (2007) Isothermal cold crystallization kinetics of polylactide/nucleating agents. Journal of Applied Polymer Science 104(1):310-317.

[24] Avérous L, Fringant C, Moro L. (2001) Plasticized starch-cellulose interactions in

polysaccharide composites. Polymer 42(15):6565-6572.

[25] Petersen K, Nielsen PV, Olsen MB. (2001) Physical and mechanical properties of biobased materials - Starch, polylactate and polyhydroxybutyrate. Starch/Staerke 53(8):356-361.

[26] Sanchez-Garcia MD, Nordqvist D, Hedenqvist M, Lagaron JM. (2011) Incorporating amylopectin in poly(lactic acid) by melt blending using poly(ethylene-co-vinyl alcohol) as a thermoplastic carrier. II. Physical properties. Journal of Applied Polymer Science 119(6):3708-3716.

[27] Takamatsu H, Miyazaki T, Ishida E, Ashizuka M, Abe H. (2006) Mechanical properties of β-tricalcium phosphate/polylactic acid composites prepared through ball-milling. Journal of the Ceramic Society of Japan 114(1328):332-335.

[28] Tenn N, Follain N, Soulestin J, Crétois R, Bourbigot S, Marais S. (2013) Effect of nanoclay hydration on barrier properties of PLA/montmorillonite based nanocomposites. Journal of Physical Chemistry C 117(23):12117-12135.

[29] Sanchez-Garcia MD, Lopez-Rubio A, Lagaron JM. (2010) Natural micro and nanobiocomposites with enhanced barrier properties and novel functionalities for food biopackaging applications. Trends in Food Science and Technology 21(11):528-536.

Chapter 5

ASSESSMENT OF BALL MILLING AS A COMPOUNDING TECHNIQUE TO DEVELOP NANOCOMPOSITES OF POLY (3-HYDROXYBUTYRATE-CO-3-HYDROXYVALERATE) AND BACTERIAL CELLULOSE NANOWHISKERS

J. Ambrosio-Martín[a], M. J. Fabra[a], A. Lopez-Rubio[a], G. Gorrasi[b], A. Sorrentino[c] and J. M. Lagaron[a]

Journal of Polymers and the Environment – Under Review

[a] Novel Materials and Nanotechnology Group, IATA-CSIC, Avda. Agustin Escardino 7, 46980 Paterna (Valencia), Spain.

[b] Department of Industrial Engineering, University of Salerno, via Giovanni Paolo II, 132 Fisciano (Salerno), Italy.

[c] Institute for Polymers, Composites and Biomaterials (IPCB), National Research Council (CNR), P.le Enrico Fermi 1, 80055 Portici, Italy

ABSTRACT

The aim of this study was the assessment of high energy ball milling technique to develop poly(3-hydroxybutyrate-co-3-hydroxyvalerate) (PHBV) nanocomposites containing bacterial cellulose nanowhiskers (BCNW). Crystallization behaviour of PHBV/BCNW nanocomposites was studied under non-isothermal and isothermal conditions using differential scanning calorimetry (DSC). The changes in PHBV crystalline structure were also studied using X-ray diffraction. The results confirmed that BCNW acted as nucleating agents and, hence, favored the crystallization of the PHBV. The oxygen permeability of the nanocomposites was reduced by ~22% when compared to that of the neat PHBV. This work provides a new insight into the development of polyhydroxyalkanoate (PHA) composites by means of the high energy ball milling technique.

Keywords: Polyhydroxyalkanoates, Bacterial cellulose nanowhiskers, Bacterial cellulose nanocrystals, Oxygen barrier, Ball milling.

1. INTRODUCTION

Currently, there is a great interest in developing effective biodegradable materials to counteract the existing plastic waste management issues. Nowadays, in the food packaging area, the bio-based materials with greatest commercial potential are some biodegradable polyesters, which can be transformed using conventional plastic processing equipment. Among the most widely researched thermoplastic biodegradable materials, poly(lactic acid) (PLA) and polyhydroxyalkanoates (PHAs) present an interesting balance of properties, they are synthesized from renewable resources and have become commercially available. Specifically, PHAs are biopolyesters synthesized by a wide variety of microorganisms and degraded by numerous microorganism (bacteria, fungi and algae) in various ecosystems [1]. Due to their biodegradability, biocompatibility and adaptable mechanical properties, PHAs have been quickly identified as good candidates to replace fossil-based commodity polymers. However, widespread applications of PHAs are still hindered by several material drawbacks such as high material costs, relatively low barrier performance, poor thermal stability, brittleness and low crystallization rates.

The use of nanoparticles is attractive because they can act as nucleating agents, not only improving the polymer crystallization rates, but also increasing the mechanical, thermal and/or barrier performance of the composites. For instance, inorganic nano-fillers such as carbon nanotubes [2] and nanoclays [3, 4] have demonstrated to increase the crystallization rate of poly(3-hydroxybutyrate-co-3-hydroxyvalerate) (PHBV), and enhance the stiffness and thermal stability of the nanocomposites. Moreover, improvements on the barrier properties of PHBV upon addition of nanoclays have also been reported with reductions of 76% and 32% in water and oxygen permeability respectively using 5 wt.% of filler [5]. However, the non biodegradable character of these inorganic fillers make them non suitable in order to develop fully renewable materials.

Cellulose nanowhiskers (CNW) also called cellulose nanocrystals (CNC), which can be extracted from different sources, even from food by-products as recently reported [6], have attracted considerable attention as reinforcing agents in nanocomposites due to their attractive properties, such as low density, renewable character and biodegradability [7-9]. Several works have reported on the production of PHBV nanocomposites incorporating CNW attempting to improve the properties of the polymer matrix [6, 9-12]. Nevertheless, CNW obtained from bacerial cultures, the so-called bacterial cellulose nanowhiskers (BCNW) have gained even more attention due to their high purity and outstanding properties [13, 14]. Traditionally, solution casting has been the most extended method to prepare CNW-based nanocomposites. As it has been previously reported, this method is time-consuming, requiring repeated successive centrifugation steps [15], and it does not guarantee a good dispersion of the CNW because of the inherent difficulty to properly disperse these hydrophilic nanofillers in organic solvents [6], which have to be used in large amounts. In fact, one of the main drawbacks associated with the use of unmodified cellulose nanowhiskers as reinforcing agents is their very strong water sensitivity, which makes them difficult to disperse in non-polar media. As a consequence, the development of CNW-containing nanocomposites with improved properties remains as a great challenge and many scientific efforts are being put into it. Thus, several works have been published reporting different strategies to solve this problem, such as choosing the optimum

solvent or chemically modifying the CNW surface in order to produce PHBV/CNW nanocomposites with improved properties [10, 15, 16]. The previous strategies have shown to result in better mechanical properties (up to 282% and 166% increase in the Young's Modulus and tensile strength respectively) [11] and improved thermal stability up to 30 °C [15, 16] for PHBV nanocomposites reinforced with CNW. Moreover, a reduced water uptake and water vapour permeability was also obtained reaching improvements of 74% and 56%, respectively [16]. Despite such improvements, the casting technique used to develop these nanocomposites requires important amounts of organic solvents which are toxic and expensive and, moreover, it is not an appropiate and practical technique from the industrial applications point of view. Melt compounding techniques, such as extrusion or injection moulding, are the most widely used processing techniques at industrial scale. However, regardless the polymer matrix, there is scarce literature about the production of CNW-containing nanocomposites throuth melt compounding methods. Again the challenge is to attain a good dispersion of CNW within the biopolymer matrix due to the hydrophobic nature of the most polymeric matrices resulting in poor interfacial interactions between filler and polymer. As previously reported, several alternatives have been successfully proposed to resolve the above disturbing problems, mainly based in the development of a initial compounded material which is used as masterbatch and subsequently diluted in melt state with different polymer matrices. For instance, the dispersion of CNW into PLA matrix has been improved using this strategy by several authors [13, 17-20], with improvements in Young's modulus, tensile strength and oxygen and water vapour permeability up to 52%, 31%, 22% and 18%, respectively [19]. Furthermore, it has been recently published that PLA-cellulose nanofibrils nanocomposites were succesfully prepared by melt extrusion. A plasticizer was used as processing aid to facilitate the nanofiller dispersion and also the cellulose was feeded from a liquid medium [21], thus avoiding nanofiller agglomeration, which is in accordance with previous findings from Martinez Sanz et al. [22] who demonstrated that unmodified cellulose nanowhiskers should be handled in a partially hydrated state instead of freeze-dried, as it is very difficult to re-disperse them due to the strong hydrogen bonding and subsequent self-association. However, only slight improvements in mechanical properties were obtained and no barrier properties were reported for this melt extruded CNW-containing nanocomposites. Poor compatibility between highly hydrophilic cellulose nanowhiskers and the hydrophobic PHBV in the melt state was observed by Jiang et al [10] which complicated the filler dispersion and gave rise to weak polymer-nanofiller interactions. They observed that, despite using polyethylene glycol as a compatibilizer, cellulose nanowhiskers agglomerated during freeze-drying and could not be broken and well-dispersed by the extrusion process. Using the previously mentioned technique of creating an initial masterbatch prior to the melt mixing step, Srithep et al. [23] incorporated nanofibrilated cellulose (NFC) into PHBV. Improvements in Young´s Modulus (90%) and in storage modulus (137%) were obtained for the materials with 10 wt.% of NFC. However, even though individual fibers were observed, some NFC agglomerates were still distinguished. Moreover, NFC triggered the PHBV degradation at high processing temperatures, thus precluding its use in processes such as melt compounding.

Ball milling technique is an efficient and green strategy, constituting another alternative to develop composites. It is considered a novel compounding method

being previouslly used in the development of clay, layered double hydroxide or carbon-based nanocomposites [24-32]. Moreover, it has also been used for polymer nanocomposites where there was low compatibility between filler and matrix aiming to overcome the lack of affinity between both components [25]. However, there is scarce literature reporting on the use of ball milling to generate cellulose-based nanocomposites. Moreira et al. [33] dispersed cellulose nanowhiskers in starch-based thermoplastics using solid state ball milling. Nanowhiskers agglomeration was minimized using a polysaccharide as a coating in a previous step and a reinforcing effect was noticed with improvements in Young's modulus from 29 to 132 MPa and tensile strength from 1.8 to 4.9 MPa. In addition, high energy ball milling has also been used to incorporate BCNW into PLA without the need of any previous nanofiller treatment [34]. Increased mechanical and oxygen barrier properties up to 10% (in Young's Modulus and tensile strength) and 18%, respectively, were obtained.

This work describes the preparation of nanocomposites using BCNW as a filler via the ball-milling technique. The main objetive was to evaluate the potential of this easy, one single step and "green" technique to produce PHBV/BCNW nanocomposites with improved properties. Thermal properties, thermal stability, morphology, mechanical and barrier properties of the developed nanocomposites were studied.

2. MATERIALS AND METHODS

2.1. Materials

Poly (hydroxybutyrate-co-valerate) (PHBV) was supplied by Goodfellow Cambrigde Limited (Hurtingdon, England). This grade consisted of a PHBV copolymer containing 12% mol of hydroxyvalerate plasticized with citric ester. Prior to the ball milling process, the material was purified by dissolution in $CHCl_3$ and subsequently precipitated by drop-wise addition to an excess of methanol. The material, in this way, was transformed from pellet to powder form which was necessary for the ball milling process. Sulphuric acid 96 wt.% and sodium hydroxide pellets were purchased from Panreac (Barcelona, Spain). The bacteria strain *Gluconacetobacter xylinus* was obtained from the Spanish type culture collection (CECT).

2.2. Preparation of bacterial cellulose mats

The bacteria *Gluconacetobacter xylinus* was incubated in a modified Hestrin-Schramm medium at 30 °C [22]. All of the cells were pre-cultured in a test tube containing 5 mL of media. When a thin layer of cellulose was detected on the surface, they were transferred to 200 mL bottles and, subsequently, to a bigger reactor of 20 L. The synthesized bacterial cellulose pellicles, of about 2 cm thickness obtained thereof were cut up (ca. 2cm×2cm), sterilized and cleaned in boiling water and in a 10 wt.% (v/v) NaOH aqueous solution to remove bacterial cells and absorbed culture media. Finally, the pH was adjusted to neutral by boiling in distilled water several times.

2.3. Preparation of bacterial cellulose nanowhiskers (BCNW)

BCNW were obtained by the optimized method reported by Martínez-Sanz et al. [35]. Briefly, small pieces of bacterial cellulose at neutral pH were ground in a blender. A gel-like material was obtained and compressed in order to remove most of the absorbed water. The partially dried cellulosic material was then treated with 301 mL sulfuric acid/L water, in a

cellulose/acid ratio of approximately 7 g L^{-1}, at 50 °C for three days, until a homogenous solution was obtained. The cellulose nanowhiskers were obtained as a white precipitate after several centrifugations and washing cycles at 12.500 rpm and 15 °C for 20 min. The pH of the samples was measured after the washing-centrifugation cycles, being around 2 for all the samples. Then, the material was re-suspended in deionized water and neutralized with sodium hydroxide until neutral pH and, subsequently, centrifuged to obtain BCNW as a partially hydrated precipitate. Finally, the material was freeze dried and ground prior to its use in the ball milling process.

2.4. Preparation of PHBV/BCNW nanocomposites

Ground BCNW and PHBV powders were milled in the solid state in a Retsch (Germany) centrifugal ball mill (model PM100). The milling process was carried out in a cylindrical steel jar of 50 cm^3 with 5 steel balls of 10 mm of diameter. The rotation speed used was 650 rpm and the milling time was fixed at 60 min. In these experimental conditions, three series of composites PHBV/BCNW with 0.5, 1 and 3 wt.% of BCNW were prepared. An additional PHBV sample without nanofiller to be used as a reference was also milled in the same conditions. The PHBV/BCNW mixtures and the pure milled PHBV were moulded in a hot press (Carver Inc.) at 170 °C and cooled at room temperature forming 250 ± 50 μm thick films.

2.5. Characterization of the nanocomposites

2.5.1. *Scanning Electron Microscopy (SEM).*

The microstructural analysis of the PHBV/BCNW nanocomposites was carried out by SEM using a scanning electron microscope (Hitachi S4100). Samples were frozen in liquid nitrogen and cryo-fractured to observe the cross-section of the nanocomposites. The samples were mounted on bevel sample holders, sputtered with Au/Pd under vacuum and observed using an accelerating voltage of 10 kV.

2.5.2. *Transmission Electron Microscopy (TEM)*

Transmission electron microscopy (TEM) was performed using a JEOL 1010 (Jeol, Tokyo, Japan) equipped with a digital Bioscan (Gatan) image acquisition system. TEM observations were performed on ultrathin sections of microtomed thin composite sheets.

2.5.3. *Differential Scanning Calorimetry (DSC)*

Differential scanning calorimetry (DSC) analysis was carried out, in duplicate, on 10-12 mg of dry samples at a heating rate of 10 °C min^{-1} from 0 °C to 180 °C in a nitrogen atmosphere by means of a DTA Mettler Toledo (DSC 30). The first and second melting endotherms, after controlled crystallization at 10 °C min^{-1} from the melt, were analysed. The crystallinity (%) was estimated from the corrected enthalpy for biopolymer content in the samples, following the Eq. (1).

$$\%Xc = \frac{\Delta H_f}{\Delta H_f^o(1-w)} \times 100 \quad (1)$$

where ΔH_f is the enthalpy of fusion of the studied specimen, ΔH^o_f is the enthalpy of fusion of a totally crystalline material and w is the weight fraction of the filler. The ΔH^o_f used for this equation was 109 J g^{-1} for PHBV [36, 37].

In addition, an isothermal crystallization kinetics study was performed as follows: The samples were heated from room temperature to 180 °C at 75 °C min^{-1} and held for 10 min to erase the thermal history. Then, they were cooled rapidly, at 100 °C min^{-1}, to the desired crystallization temperatures (in this case 133, 135 and 137 °C), ensuring that the crystallization process did not start during the cooling step. After that, the temperature was held until the crystallization process was completed and, finally, the samples were heated at 10 °C min^{-1} to 180 °C again to obtain the melting temperature.

2.5.4. *X-ray Diffraction*

X-ray diffraction (XRD) measurements were performed with a Brucker diffractometer (equipped with a continuous scan attachment and a proportional counter) with Ni-filtered Cu Kα radiation (λ= 1.54050 Å). The samples were examined over the angular range of 2° to 40° with a step size of 0.03° and a count time of 0.2 s per point.

Peak fitting was carried out using Igor software package (Wavemetrics, Lake Oswego, Oregon). Gaussian function was used to fit the experimental diffraction profiles obtained. For the fitting procedure, the reflections considered were eight at 13.4°, 16.8°, 19.8°, 21.4°, 22.3°, 25.5°, 27.0° and 30.0° 2θ (corresponding to the 020, 110, 021, 101, 111, 121, 040 and 002 crystal planes, respectively) assigned to the crystalline part of the semicrystalline PHBV and one assigned to the amorphous halo centred at ~16 2θ. The crystallinity index *CI (X_i)* was determined by the method reported by Martínez Sanz et al. [22].

$$CI(X_i) = \frac{\sum A_{Crystal}}{\sum A_{Total}} x100 \qquad (2)$$

where ΣA_{Total} is the sum of the areas under all the diffraction peaks and $\Sigma A_{Crystal}$ is the sum of the areas corresponding to crystalline peaks.

2.5.5. *Thermogravimetric analysis (TGA)*

Thermogravimetric (TG) curves were recorded using a Mettler TC-10 thermobalance. The samples (~5 mg) were heated from 25 °C to 800 °C at a heating rate of 10 °C min^{-1} under air and nitrogen atmosphere. Derivate thermogravimetric curves (DTG) express the weight loss rate as a function of temperature.

2.5.6. *Dynamic Mechanical Analysis (DMA)*

Mechanical properties were evaluated using a DMA TAQ800. Measurements were conducted at constant frequency (1Hz) and amplitude (5μm). The temperature was varied between -30 °C and 140 °C at 3 °C min^{-1}.

2.5.7. *Mass transport properties.*

The oxygen transmission rate of the various samples was determined at 80% relative humidity (RH) and 25 °C using an Oxtran 100 equipment (Modern Control Inc., Minneapolis, MN, USA). 80% RH was generated by a built-in gas bubbler and was checked with a hygrometer placed at the exit of the detector. Samples were purged with nitrogen for a minimum of 20 h in the previously relative humidity equilibrated samples, prior to exposure to an oxygen flow of 10 mL min^{-1}. The exposure area during the test was 5 cm^2 for each sample. In order to obtain the oxygen permeability, film thickness and gas partial pressure were considered in each case.

Water sorption was measured on different strips of the sample by subjecting the samples to a 100% relative humidity

conditions at 25 °C. The weight uptake was followed as a function of time. Equilibrium sorption was assumed when no further weight changes were observed. The data were averaged on at least two samples. Since all the samples analysed showed Fickian behaviour, i.e. a linear dependence of water sorption with the square root of time, it was possible to derive the mean diffusion coefficient D (cm^2 s^{-1}) from the linear part of the reduced sorption curve:

$$\frac{C_t}{C_{eq}} = \left(\frac{16D}{\pi l^2}\right)^{1/2} t^{1/2} \quad (3)$$

where l is the thickness of the sample, C_t is the penetrant concentration at the time t, and C_{eq} is the penetrant concentration at the equilibrium value.

2.5.8. *Statistical analysis*

Some of the results were analysed by multifactor analysis of variance (ANOVA) using Statgraphics Centurion 15.1 software (Statpoint Technologies, INC, Warrenton, VA, USA). Tukey's test was used at the 95% confidence level.

3. RESULTS AND DISCUSSION

3.1. Morphology and optical properties of the PHBV/BCNW nanocomposites obtained by ball-milling

Bacterial cellulose nanowhiskers (BCNW) were successfully obtained with average cross-sections of ~22 nm and length of ~600 nm, as previously reported [19]. To study the dispersion of the BCNW within the PHBV matrix, the cryo-fractured surface of nanocomposite films were examined by SEM (c.f. Figure 1). For the nanocomposite films, the figures correspond to the areas were some agglomerates were detected. SEM

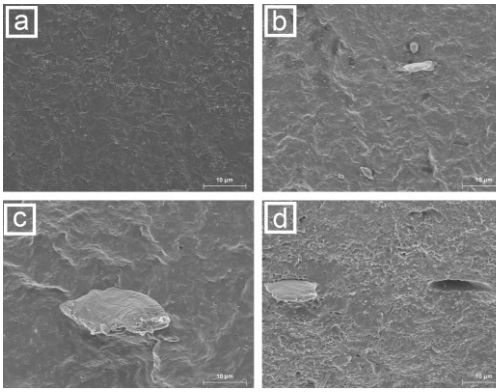

Figure 1. SEM micrographs of the cryo-fractured section obtained from PHBV films: (a) neat PHBV; (b) PHBV/BCNW 0.5 wt.%; (c) PHBV/BCNW 1 wt.% and (d) PHBV/BCNW 3 wt.%. Scale markers correspond to 10 μm.

images of the samples confirmed that BCNW were agglomerated within the nanocomposites, even for the sample with the lowest nanofiller content, and a lack of interfacial interaction between the polymer matrix and the BCNW agglomerates was apparent. This could be attributed, not only to the discrete compatibility between the hydrophilic nanofiller and PHBV, but also to the fact that the BCNW were added as a freeze-dried product with strong hydrogen bonding self-association which could not be disrupted even with the intense mechanical treatment applied during ball milling. Moreover, increasing the nanocellulose content up to 1 or 3 wt.% in the materials resulted in bigger aggregates, as observed from the SEM images. In spite of that, from the TEM micrographs shown in Figure 2, it can be observed that a significant fraction of the filler was properly dispersed and distributed at the nanoscale level, even though the previously mentioned aggregates were also present in the TEM images. Therefore, although a complete dispersion of the nanofiller could not be attained through ball milling, a fraction of the added BCNW was properly dispersed and distributed within the polymeric matrix as a result of the processing step.

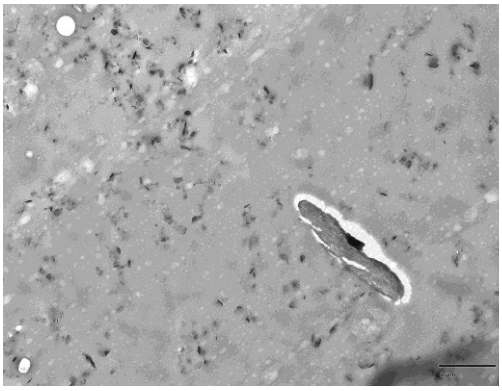

Figure 2. TEM micrographs of PHBV-BCNW films containing 1 wt.% BCNW. Scale markers correspond to 2μm.

Figure 3 shows the contact transparency images of the nanocomposite films with different BCNW loadings. It was observed that the nanocellulose aggregates present in the nanocomposites did not significantly affect the optical properties at the macroscopic level and, thus, the nanocomposite films obtained after compression moulding of the different formulations performed through ball milling were optically identical to the neat PHBV film, indicating that the transparency of the pure PHBV was kept for all the specimens developed.

Figure 3. Contact transparency pictures of PHBV and PHBV/BCNW nanocomposites films.

3.2. FTIR study of PHBV/BCNW nanocomposites

Figure 4 illustrates FTIR spectra of the nanocomposites. Characteristic peaks from both PHBV and BCNW were present in the FTIR spectra of the nanocomposites. For instance, the broad bands at 3400 cm^{-1} and 2900 cm^{-1} were assigned to O-H stretching vibration and C-H stretching vibrations modes of BCNW, respectively [16, 38, 39]. Bands at 3436 and 3342 cm^{-1} have been typically ascribed to free and hydrogen bonded O-H stretching vibrations, respectively [11, 16, 39]. From Figure 4, it can be observed that upon increasing the BCNW content, the intensity of the broad band at 3400 cm^{-1} increased and the band related to the hydrogen bonded O-H stretching vibrations was more noticeable. This result suggests that although a chemical grafting between the hydroxyl groups from BCNW and the reactive groups from the PHBV did not occur, hydrogen bonds could be generated within the nanocomposites between hydroxyl groups from BCNW surface and carbonyl groups present in the PHBV. An increase and sharpening of the previously reported bands associated to hydrogen bonded carbonyl groups at around 1723 cm^{-1} [16, 39, 40] further confirms the interaction between both components. Moreover, it has been demonstrated that this band is sensitive to the PHBV crystallinity [41] and, thus, the observed increase in the intensity of this band upon increasing BCNW content could also be related to an increase in the polymer crystallinity. This result can be corroborated by the increase in the FTIR band located at 1381 cm^{-1}, which is also known to be sensitive to changes in PHBV crystallization [15].

3.3. Thermal properties and thermal stability of PHBV/BCNW nanocomposites

The degree of crystallinity plays an important role in the physical properties and biodegradability of polymers. Thermal properties of neat PHBV and the nanocomposite materials were evaluated by means of DSC analyses. The melting temperature (T_m) and heat of fusion (ΔH_m) were determined from the first and second heating runs. The degree of crystallinity (X_c)

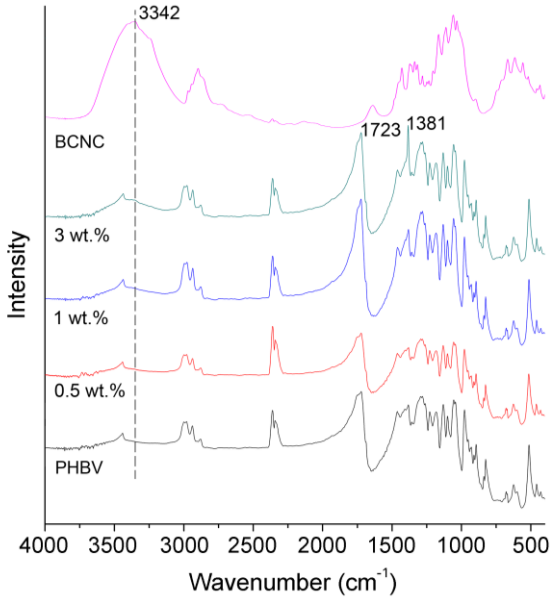

Figure 4. ATR-FTIR spectra of the neat PHBV and nanocomposites films containing BCNW.

of the specimens was determined from the first heating run curve, offering information related to the thermal characteristics of the just obtained material. Crystallization temperature (T_c) and enthalpy (ΔH_c) values were also obtained from the cooling run. Table 1 shows the thermal parameters of the neat PHBV and the BCNW-containing nanocomposites.

As shown in Figure 5a, the DSC traces of the first heating scan showed two melting peaks, which have been previously reported [6, 42] and interpreted as an effect of the melting-recrystallization process occurring during subsequent heating [43]. During the slow heating scans, unstable crystals have sufficient time to melt and reorganize into more stable crystals which lead to this bimodal melting peak behaviour. The reorganized crystals are subsequently re-melted at higher temperatures [44, 45]. Moreover, Wang et al. [46] observed the same bimodal effect in PHBV/clays nanocomposites with an increase in the high-temperature melting peak area upon addition of clays. It was pointed out that the low-temperature melting peak was probably related to homogeneous nucleation of PHBV which started spontaneously by PHBV chain aggregation below the melting point. On the contrary, the high-temperature melting peak was related to heterogeneous nucleation of PHBV, and its increase was associated to the

Table 1. DSC maximum of melting (T_m), melting enthalpy (ΔH_m) and degree of crystallinity (X_c) during the first heating run, crystallization temperature (T_c) and crystallization enthalpy (ΔH_c) during the cooling run, and maximum of melting (T_m) and melting enthalpy (ΔH_m) during second heating run.

	1st Heating				Cooling		2nd Heating	
	T_{m1} (°C)	T_{m2} (°C)	ΔH_m (J g^{-1})	X_c (%)	T_c (°C)	ΔH_c (J g^{-1})	T_{m1} (°C)	ΔH_m (J g^{-1})
PHBV	149.5	158.7	62.5	57.4	113.2	65.5	153.5	69.4
PHBV-BCNW 0.5	150.3	158.9	63.3	58.0	112.5	65.9	153.4	69.7
PHBV-BCNW 1	148.0	158.2	64.7	59.4	113.2	66.4	153.5	70.3
PHBV-BCNW 3	144.8	157.5	69.9	64.1	114.0	67.9	152.7	72.4

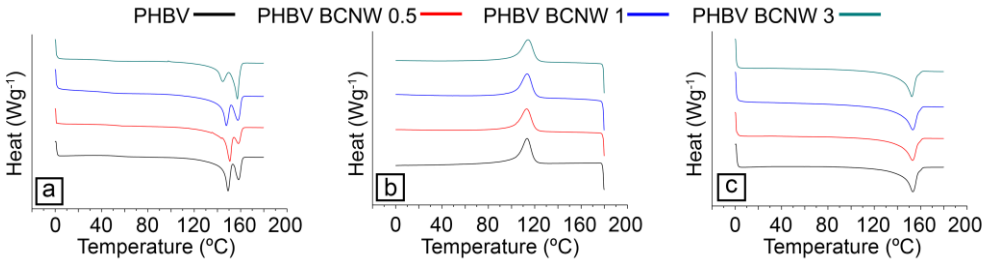

Figure 5. DSC first heating scan (a), cooling scan (b) and second heating scan (c) of the neat PHBV and the PHBV/BCNW nanocomposites prepared by ball-milling.

existence of much more crystalline nuclei after addition of clays than in neat PHBV. DSC results showed that while for lower loadings there was no effect in the low melting peak temperature, addition of greater amounts of BCNW up to 3 wt.% decreased the lower melting peak temperature ca. 5 °C, when compared with the neat PHBV. Nevertheless, although at high loadings the fraction of crystals that melted at low temperature was composed by smaller or more defective crystals, its proportion was substantially reduced as could be discerned from the area ratio of both melting peaks areas, hence reducing its contribution to the total enthalpy of the material (cf. Figure 5a.). In fact, an increase in the area and height of the second melting peak related to the first melting peak was observed with increasing BCNW content. Moreover, a sharpening of the high temperature melting peak was also observed. From all the previous observations it could be stated that at higher loadings the fraction of crystals which melted at higher temperature (heterogeneous crystallization) increased, being in accordance with the observations of Wang et al. [46] and, hence, suggesting that BCNW could act as nucleating agents. These results were similar to those observed by Jiang et al. [10] who reported an enhancement of the crystallization ability upon addition of CNW into PHBV, but different from those reported by Martínez-Sanz et al. [6] who suggested that the CNW somehow hindered the crystallization process of PHBV. Both studies were carried out with cellulose-based nanocomposites obtained by solution casting with the same PHBV grade as the one used in this study. Therefore, the addition of BCNW affected the heterogeneous and homogeneous crystallization of the PHBV with a clear promotion of the heterogeneous crystallization process. As shown in Table 1, the melting enthalpy values increased with BCNW addition, indicating an increase in the crystallinity, mainly for higher BCNW loadings. As already mentioned, this could be ascribed to a nucleating effect exerted by the well dispersed and distributed fraction of the BCNW. These results are well correlated with the previous FTIR observations. In fact, it is well established that nanowhiskers and other nanofillers in nanocomposites may act as nucleating sites and, thus, affect the crystallization kinetics of the polymeric matrix. An exothermic peak was observed for all specimens during the cooling scan which corresponded to the crystallization of PHBV (Figure 5b). Although there were no great differences in the crystallization temperature, increased crystallization enthalpies were observed when BCNW were added, particularly at high concentrations. This again confirmed the nucleation ability of the nanowhiskers. After erasing the thermal history of the materials, only one melting peak was observed in the thermograms (cf. Figure 5c) and the melting temperature values ranged

between those obtained in the first and second melting peaks from the first heating run. It should be mentioned that while melting temperature was almost unaltered with the addition of BCNW, an increase in the melting enthalpy and a sharpening of the melting peaks were observed for the nanocomposite materials (cf. Table 1 and Figure 5c).

The thermal stability of the neat PHBV and PHBV/BCNW nanocomposite samples were examined using TGA. Figure 6 shows TG and DTG curves under air and nitrogen environments. The temperatures corresponding to the onset of decomposition (T_{onset}) are essential for evaluating the thermal stability of the nanocomposites and are reported in Table 2. Several studies reported that cellulose nanowhiskers were able to improve the thermal stability of the PHBV [11, 15, 16, 39], while a slight decrease on thermal degradation was observed in other cases [9].

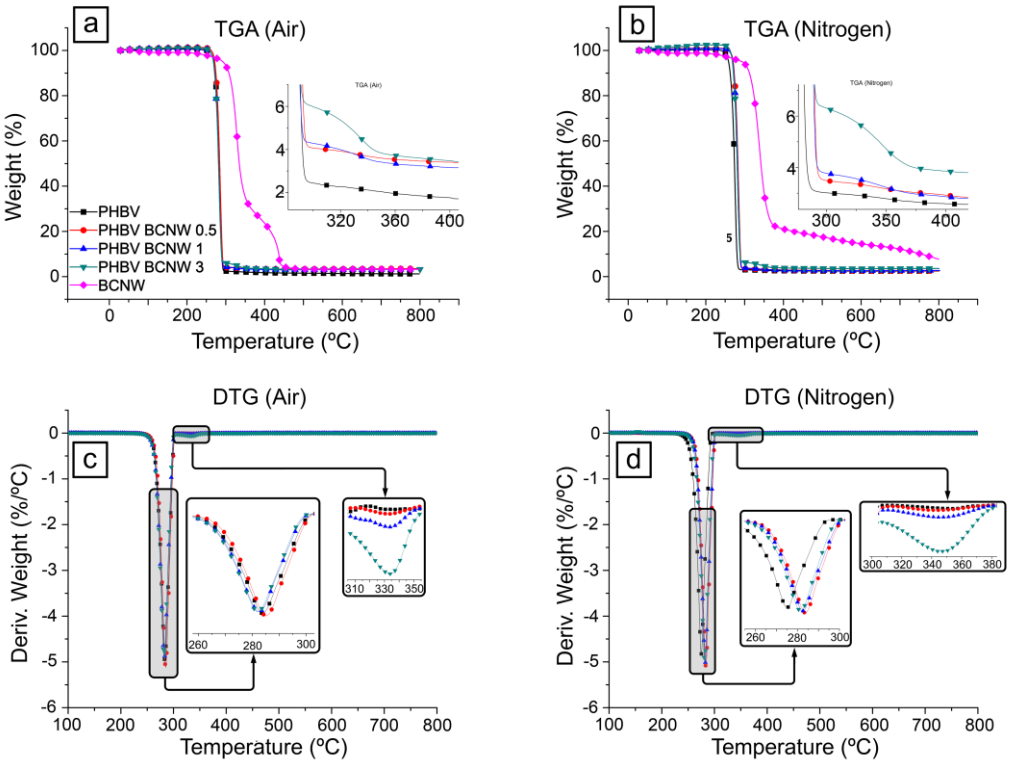

Figure 6. TGA curves of pure BCNW, pure PHBV and its nanocomposites with BCNW (a, b) and DTG curves of pure PHBV and its nanocomposites with BCNW (c, d) in air and nitrogen environments (left and right respectively). The insets are expanded views at different temperature ranges.

Table 2. TGA decomposition temperature (T_d), onset temperature (T_{onset}) and the residue at 600°C for neat PHBV and its nanocomposites incorporating BCNW evaluated in air and nitrogen environment.

	T_d (°C)		T_{onset} (°C)		% Residue at 600 °C	
	Air	N_2	Air	N_2	Air	N_2
PHBV	284.2	276.0	266.7	259.6	1.4	2.4
PHBV-BCNW 0.5	286.1	284.8	266.9	266.3	3.4	2.6
PHBV-BCNW 1	282.7	283.0	264.3	265.0	3.1	2.6
PHBV-BCNW 3	282.9	282.2	264.3	264.1	3.2	3.5

Thermal degradation through a one-step process was observed in both environments, although a small shoulder was observed around 320-350 °C. Under inert atmosphere the thermal stability of the nanocomposites was better than that for the neat PHBV but worse than that for the pure BCNW. It fact, it was found that with the increase in BCNW contents, the degradation temperature (T_d) increased from 276.0 °C for the neat PHBV to 284.8 °C for the nanocomposite film with 0.5 wt.%, showing at this concentration the maximum improvement, and then decreased slightly to 282.2 °C for 3 wt.% BCNW. Similar behaviour has been recently reported with a maximum improvement at low loading levels above which the degradation temperature was decreased [14]. It is widely recognized that the general mechanism of thermal degradation of PHBV is the scission of PHBV molecules by a random cis-elimination reaction at a six-membered ring ester intermediate which take place at the initial steps of PHBV decomposition. It has been observed that addition of CNW suppressed the formation of this intermediate due to the strong hydrogen bonds interactions [39]. However, once the maximum degradation temperature was reached, the degradation process was accelerated due to the increased thermal conductivity of the CNW [39]. As observed in the morphological analysis, more agglomerates were noticed at high BCNW addition. This implies a reduction of the hydroxyl groups from BCNW surface available to form hydrogen bonds with the PHBV matrix, thereby reducing the thermal stability to some extent at those loading levels. However, results obtained in air conditions showed a different trend. While for 0.5 wt.% a slight improvement in thermal stability was detected, higher loadings led to a decrease in degradation temperature, probably due to the fact that oxidative degradation took place in this atmosphere. Therefore, it can be stated that nanocomposites containing BCNW behaved differently depending on the environmental conditions, i.e. oxidative thermal degradation of the PHBV or thermal degradation by pyrolysis. Regarding the small shoulder observed in both air and nitrogen environments and taking in account the degradation curve of the pure BCNW, the mass loss could be attributed to the degradation of BCNW present in the nanocomposite. In fact, the higher the BCNW concentration, the larger the weight loss observed at this point. Results also showed that addition of BCNW increased the residual content at 600 °C of the PHBV/BCNW nanocomposites, indicating that a higher fraction of the material did not volatilize upon thermal degradation.

3.4. Thermo-mechanical properties of PHBV and its nanocomposites.

The thermo-mechanical properties of neat PHBV and its nanocomposites prepared with BCNW were also investigated using dynamo mechanical analysis (DMA). DMA can also be used to determine how the mechanical properties of specimens vary with temperature. The resulting storage modulus and tanδ relaxation temperature of neat PHBV and PHBV/BCNW nanocomposites are shown in Figure 7 and 8, respectively. Glass transition temperature (T_g) values could not be discerned by DSC, but they can be obtained through DMA. Figure 8 shows that tanδ relaxation of PHBV increased with BCNW addition, which can be caused by the restriction of the chain mobility within the polymer matrix after nanofiller incorporation. The neat PHBV exhibited a tanδ transition around 16 °C, which could corresponds to the T_g of the PHB [47] and it increased with the increase in BCNW content. The results also showed that the nanofiller increased the storage modulus of the neat PHBV at temperatures below the tanδ relaxation temperature

(Figure 7). The increase in the storage modulus can be ascribed to the reinforcing effect of the nanofillers. Similar effects were observed in PHBV-based nanocomposites with CNW [10] or carbon nanotubes [48].

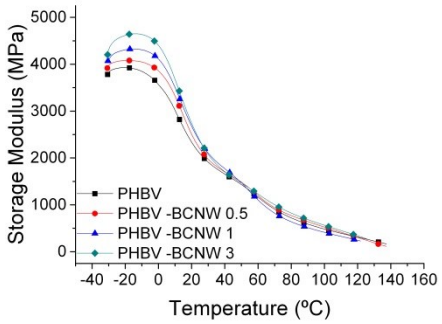

Figure 7. Temperature dependence of the storage modulus of the neat PHBV and the PHBV/BCNW nanocomposites prepared by ball-milling.

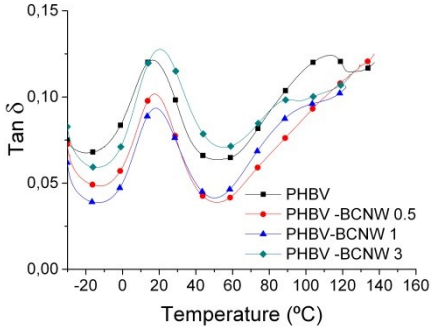

Figure 8. Tanδ of the net PHBV and the PHBV/BCNW nanocomposites prepared by ball-milling.

3.5. Crystal structure and crystallinity of PHBV/BCNW nanocomposites

Crystal structures of the neat PHBV and PHBV/BCNW nanocomposites were studied by X-ray diffraction. The diffraction patterns are shown in Figure 9 and the crystal parameters and polymer crystallinity index (X_i) were calculated and are summarized in Table 3. The diffractogram of the neat PHBV shows that this biopolyester is a semicrystalline material. Nanocomposites containing BCNW showed PHBV reflections at the same values as the neat biopolymer, indicating that, in the nanocomposites, PHBV crystallized in its typical orthorhombic crystalline form [48-50]. In fact, the same interplanar distances were obtained for PHBV and its nanocomposites using Bragg´s law (cf. Table 3) defined by the following equation:

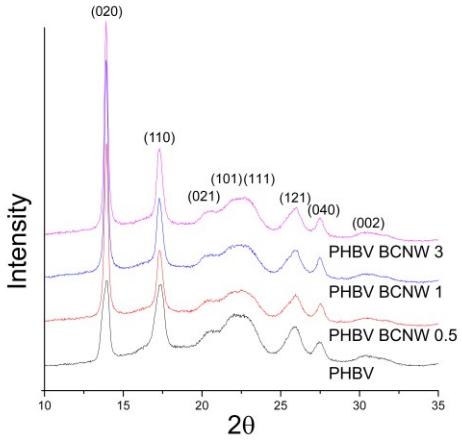

Figure 9. X-Ray diffraction patterns of neat PHBV and nanocomposites containing BCNW.

$$n\lambda = 2d\sin\theta \qquad (4)$$

where n is an integer, λ is the wavelength of incident wave, d is the interplanar spacing, and θ is the angle between the incident ray and the scattering planes. The results

Table 3. Effect of BCNW content on the crystallite size for (020) reflections

	d-spacing (nm)	Crystallite size D_{020} (nm)	Crystallinity Index (X_i)
PHBV	0.64	16.28	53.5
PHBV-BCNW 0.5	0.65	27.63	60.2
PHBV-BCNW 1	0.66	30.28	61.0
PHBV-BCNW 3	0.66	28.06	62.0

suggest that the parameters of PHBV unit cell were not influenced by BCNW addition. However, as shown in Figure 9, sharper and more intense peaks can be discerned for the (020) plane upon BCNW addition, which is related with the crystallite size that was determined using the well-known Scherrer equation (Eq. 4) [48]:

$$L(nm) = \frac{K \cdot \lambda}{\beta \cdot \cos\theta} \quad (5)$$

where L is the crystallite size (nm), K is a dimensionless shape factor with a value close to unity, which is K=0.94 for an orthorhombic cell [48], λ is the wavelength of the X-ray radiation which for CuKα radiation is 1.54Å, θ is the Bragg angle and β is the full width half maximum (FWHM). Table 3 shows an increase in the crystal lamella size in the direction normal to the (020) plane with increasing BCNW content. Crystallinity values were also obtained from PHBV and its nanocomposite diffractograms. It is worth noting that the data calculated from the diffractograms were in very good agreement with those calculated by DSC. As observed before, an increase in the crystallinity took place after BCNW addition. Once again, these results confirm that higher crystalline fraction was obtained in PHBV/BCNW nanocomposites. In line with the above, it is has been reported that CNW could affect the crystallization of PHBV in two opposite ways. CNW can act as nucleating agent increasing the nucleation and, hence, the overall crystallization rate, thus leading to more perfect crystals, but, on the contrary, when strong interactions take place between CNW and PHBV, the mobility of PHBV chains become more limited and hence crystallinity decreases [40]. Thus, attending to the morphological analysis performed here, due to the existence of some agglomerates, the hydroxyl groups from BCNW surface were reduced, hence reducing the BCNW-PHBV interactions. Because of that, polymer chains could easily move generating an increment in the polymer crystallinity, as observed by DSC and X-ray diffraction.

3.6. Isothermal crystallization of PHBV/BCNW nanocomposites

Isothermal crystallization of neat PHBV and PHBV/BCNW nanocomposites was inves-tigated at three crystallization temperatures 133, 135 and 137 °C. The crystallization kinetics of neat PHBV and PHBV/BCNW nanocomposites under isothermal crystallization conditions were analysed by the Avrami equation [51-53]. The derivative method reported by De Santis and Pantani [54] was used to directly fit the calorimetric curve of the isothermal crystallization process to the derivative form of the Avrami equation. Figure 10 shows, as an example, the DSC curves for PHBV/BCNW 1 wt.% nanocomposites obtained at the different isothermal crystallization temperatures, with the corresponding Avrami fittings. The data obtained from the plots corresponding to Avrami kinetic parameters are listed in Table 4. Parameter K represents the overall kinetics rate constant and n is a parameter which depends on the type of nucleation and the geometry of growing crystals. The half-time of crystallization ($t_{½}$) is defined as the

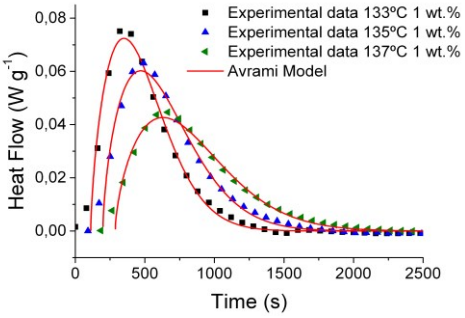

Figure 10 DSC curves of isothermal crystallization at 133 °C, 135 °C and 137 °C of the PHBV/BCNW 1 wt.% nanocomposites obtained by ball-milling.

Table 4. Avrami kinetic parameters for the crystallization of the neat PHBV and the PHBV/BCNW nanocomposites

	133 °C			135 °C			137 °C		
	$K\ (s^{-1})$	n	$t_{1/2}$	$K\ (s^{-1})$	n	$t_{1/2}$	$K\ (s^{-1})$	n	$t_{1/2}$
PHBV	2.5E-03	1.6	318.2	1.8E-03	1.6	442.1	1.6E-03	2.2	521.9
PHBV-BCNW 0.5	2.6E-03	1.6	304.4	2.0E-03	1.7	391.7	1.7E-03	1.8	470.7
PHBV-BCNW 1	2.4E-03	1.7	331.3	2.0E-03	1.6	392.4	1.6E-03	1.6	489.7
PHBV-BCNW 3	2.7E-03	1.6	298.0	2.0E-03	1.6	395.5	1.8E-03	1.7	455.1

time needed to reach 50% crystallization. It is also used to directly characterize the crystallization rate, since the reciprocal half-time of crystallization ($1/t_{½}$) can be considered approximately proportional to the crystal growth rate [55]. Thus, it can be said that the shorter the half-time of crystallization, the higher the crystallization rate. In view of the results, although a slight increment in the K parameter was observed, $t_{½}$ was, in general, clearly reduced for all nanocomposites, indicating that the presence of BCNW facilitated the crystallization process. This effect is in agreement with the above mentioned non-isothermal crystallization study performed by DSC.

3.7. Mass transport properties

Oxygen permeability (P) of PHBV and PHBV/BCNW nanocomposites was measured at 80% RH and the results are gathered in Table 5. The permeability value of neat PHBV obtained through ball milling was lower to that reported in the literature for PHBV films obtained through melt compounding or solution casting [6, 56]. One of the factors that could explain this effect is the higher crystallinity obtained for the neat PHBV processed by ball milling, which was almost double than the crystallinity reported in those studies [6, 56], as crystalline domains are considered impermeable to low molecular weight molecules increasing the tortuosity [5, 16]. In fact, this oxygen permeability value was found to be close to that of similarly processed PHBV which also reached similar values in crystallinity, as reported in a previous work [57]. Moreover, oxygen barrier properties improved upon addition of BCNW, as can be seen in Table 5, suggesting that the dispersed fraction of crystalline nanofillers partially blocked the oxygen diffusion. A maximum oxygen permeability drop of ca. 22% was attained for the samples with 0.5 wt.% of BCNW. To the best of our knowledge, this is the largest oxygen permeability reduction reported for PHBV nanocomposites loaded with BCNW up to date. This reduction in the oxygen permeability values highlights the oxygen barrier properties of the so-obtained PHBV/BCNW nanocomposites demonstrating the blocking capacity of BCNW. Increasing the BCNW content, i.e. for 1 and 3 wt.%, did not result in further improvements on barrier properties, but it did not grow worse. This reduction in oxygen permeability could be also related to the further increase on crystallinity degree of the polymeric matrices upon addition of BCNW as observed by DSC, which could lead to a greater tortuosity as mentioned above. At high contents a balance between tortuosity due to the blocking effect created by addition of well dispersed fillers [14, 16] and filler agglomeration of the BCNW, creating preferential paths, could take place since although greater improvements could be expected upon addition of higher amounts of BCNW, the presence of higher agglomerates at those loading levels generated preferential paths to the permeant pass through. Similar results were obtained after incorporation of BCNW into PLA by ball milling where the best result was also obtained for the lowest loading, 0.5

wt.%, as in this case. Higher loading of BCNW did not result in further improvements of the oxygen permeability [34]. Moreover, although addition of low amounts of BCNW into polymeric matrices such as PLA by melt mixing resulted in a reduction of the oxygen permeability measured at high relative humidity, an increase of the BCNW loading led to a detrimental effect in the oxygen barrier performance [13]. These effects were mainly due to the presence of filler agglomerates at high contents highlighting the importance of dispersion to optimize the performance improvements in this kind of films.

Table 5. Oxygen permeability values of the neat PHBV and its nanocomposites with BCNW.

	P (m^3 m m^{-2} s^{-1} Pa^{-1})
PHBV	2.8 ± 0.1 e^{-19b}
PHBV-BCNW 0.5	2.2 ± 0.3 e^{-19c}
PHBV-BCNW 1	2.3 ± 0.2 e^{-19c}
PHBV-BCNW 3	2.3 ± 0.3 e^{-19c}

a-b: different superscripts within the same column indicate significant differences between samples.

Table 6. Sorption and diffusion coefficients of water vapour of PHBV and its nanocomposites with BCNW.

	Sorption (Ceq (g/100g))	Diffusion (cm^2 s^{-1})
PHBV	0.66 ± 0.03[a]	1.6 ± 0.0 $e^{-8\,ab}$
PHBV-BCNW 0.5	0.63 ± 0.06[a]	1.4 ± 0.1 $e^{-8\,b}$
PHBV-BCNW 1	0.68 ± 0.13[a]	1.0 ± 0.1 $e^{-8\,c}$
PHBV-BCNW 3	0.66 ± 0.06[a]	1.3 ± 0.1 $e^{-8\,b}$

a-c: different superscripts within the same column indicate significant differences between samples.

Water vapour sorption and diffusion were also measured, and the data are reported in Table 6. Although no statistically significant differences were noticed for the water vapour sorption of the various samples, an increasing tendency was observed when incorporating BCNW, mainly due as a consequence of the presence of hydroxyl groups on cellulose surface. This result was in accordance with previous results incorporating different kinds of CNW, which included BCNW, into PHBV, where although a trend of increased water uptake was observed, there were not statistically significant differences upon filler addition [6]. Moreover, a reduction in the diffusion coefficients was generally observed. In agreement with the oxygen permeability measurements, apart from the blocking effect exerted by BNCW, the crystallinity degree was closely related with these results. However, for loadings of 3 wt.%, no further improvements were observed for the diffusion coefficient, probably due to the presence of more frequent and bigger agglomerates, as observed by microscopic analysis, which was also in accordance with the observations in the oxygen permeability study. In any case, this coefficient remained below the values of the unfilled polymer.

4. CONCLUSIONS

In this work, PHBV nanocomposite films loaded with bacterial cellulose nanowhiskers (BCNW) were produced by the potentially environmentally-friendly technique of ball-milling and the effects of cellulose nanowhiskers loading in the morphology, thermal properties and stability, isothermal crystallization, dynamo-mechanical properties and barrier properties were studied. Morphological evaluation clearly revealed a relative good dispersion and distribution of the BCNW within the polymeric matrix although some BCNW aggregates remained present in the nanocomposites after the ball milling process. The results confirmed that the well dispersed fraction of BNCW acted as nucleating agents and their addition favored the crystallization phenomena of the PHBV, which was corroborated by the isothermal crystallization study. Thermal stability of the

PHBV was improved by addition of BCNW when measured under inert atmosphere but, on the contrary, under air conditions, only the nanocomposite with 0.5 wt.% BCNW showed an improvement. Regarding the barrier properties, the oxygen permeability was improved up to 22% after addition of 0.5 wt.% of BCNW. A reduction of the water vapour diffusion coefficient was also obtained. Although some BCNW aggregates were present after the ball milling process, in general, this processing method resulted in materials with improved thermal stability, crystallinity, oxygen barrier properties and reduced water vapour diffusion coefficient, showing its potential for nanocomposite development.

REFERENCES

[1] Gonzalez-Lopez J, Pozo C, Martinez-Toledo MV, Rodelas B, Salmeron V. (1996) Production of Polyhydroxyalkanoates by Azotobacter chroococcum H23 in Wastewater from Olive Oil Mills (Alpechin). International Biodeterioration and Biodegradation 38(3-4):271-276.

[2] Lai M, Li J, Yang J, Liu J, Tong X, Cheng H. (2004) The morphology and thermal properties of multi-walled carbon nanotube and poly(hydroxybutyrate-co-hydroxyvalerate) composite. Polymer International 53(10):1479-1484.

[3] Chen GX, Hao GJ, Guo TY, Song MD, Zhang BH. (2004) Crystallization kinetics of poly(3-hydroxybutyrate-co-3-hydroxyvalerate)/ clay nanocomposites. Journal of Applied Polymer Science 93(2):655-661.

[4] Ublekov F, Baldrian J, Nedkov E. (2009) Crystalline β-structure of PHBV grown epitaxially on silicate layers of MMT. Journal of Polymer Science, Part B: Polymer Physics 47(8):751-755.

[5] Sanchez-Garcia MD, Lagaron JM. (2010) Novel clay-based nanobiocomposites of biopolyesters with synergistic barrier to UV light, gas, and vapour. Journal of Applied Polymer Science 118(1):188-199.

[6] Martínez-Sanz M, Vicente AA, Gontard N, Lopez-Rubio A, Lagaron JM. (2014) On the extraction of cellulose nanowhiskers from food by-products and their comparative reinforcing effect on a polyhydroxybutyrate-co-valerate polymer. Cellulose 22(1):535-551.

[7] Kvien I, Sugiyama J, Votrubec M, Oksman K. (2007) Characterization of starch based nanocomposites. Journal of Materials Science 42(19):8163-8171.

[8] Petersson L, Kvien I, Oksman K. (2007) Structure and thermal properties of poly(lactic acid)/cellulose whiskers nanocomposite materials. Composites Science and Technology 67(11-12):2535-2544.

[9] Ten E, Turtle J, Bahr D, Jiang L, Wolcott M. (2010) Thermal and mechanical properties of poly(3-hydroxybutyrate-co-3-hydroxyvalerate)/cellulose nanowhiskers composites. Polymer 51(12):2652-2660.

[10] Jiang L, Morelius E, Zhang J, Wolcott M, Holbery J. (2008) Study of the poly(3-hydroxybutyrate-co-3-hydroxyvalerate)/cellulose nanowhisker composites prepared by solution casting and melt processing. Journal of Composite Materials 42(24):2629-2645.

[11] Yu HY, Qin ZY, Liu L, Yang XG, Zhou Y, Yao JM. (2013) Comparison of the reinforcing effects for cellulose nanocrystals obtained by sulfuric and hydrochloric acid hydrolysis on the mechanical and thermal properties of bacterial polyester. Composites Science and Technology 87:22-28.

[12] Ten E, Jiang L, Wolcott MP. (2012) Crystallization kinetics of poly(3-

hydroxybutyrate-co-3-hydroxyvalerate)/ cellulose nanowhiskers composites. Carbohydrate Polymers 90(1):541-550.

[13] Martínez-Sanz M, Lopez-Rubio A, Lagaron JM. (2012) Optimization of the dispersion of unmodified bacterial cellulose nanowhiskers into polylactide via melt compounding to significantly enhance barrier and mechanical properties. Biomacromolecules 13(11):3887-3899.

[14] Martínez-Sanz M, Villano M, Oliveira C, Albuquerque MGE, Majone M, Reis M, et al. (2014) Characterization of polyhydroxyalkanoates synthesized from microbial mixed cultures and of their nanobiocomposites with bacterial cellulose nanowhiskers. New Biotechnology 31(4):364-376.

[15] Yu HY, Qin ZY, Yan CF, Yao JM. (2014) Green nanocomposites based on functionalized cellulose nanocrystals: A study on the relationship between interfacial interaction and property enhancement. ACS Sustainable Chemistry and Engineering 2(4):875-886.

[16] Yu H, Yan C, Yao J. (2014) Fully biodegradable food packaging materials based on functionalized cellulose nanocrystals / poly(3-hydroxybutyrate-co-3-hydroxyvalerate) nanocomposites. RSC Advances 4(104):59792-59802.

[17] Arias A, Heuzey MC, Huneault MA, Ausias G, Bendahou A. (2014) Enhanced dispersion of cellulose nanocrystals in melt-processed polylactide-based nanocomposites. Cellulose.

[18] Martínez-Sanz M, Lopez-Rubio A, Lagaron JM. (2013) Nanocomposites of ethylene vinyl alcohol copolymer with thermally resistant cellulose nanowhiskers by melt compounding (I): Morphology and thermal properties. Journal of Applied Polymer Science 128(5):2666-2678.

[19] Ambrosio-Martín J, Fabra MJ, Lopez-Rubio A, Lagaron JM. (2015) Melt polycondensation to improve the dispersion of bacterial cellulose into polylactide via melt compounding: enhanced barrier and mechanical properties. Cellulose 22(2):1201-1226.

[20] Goffin AL, Raquez JM, Duquesne E, Siqueira G, Habibi Y, Dufresne A, et al. (2011) From interfacial ring-opening polymerization to melt processing of cellulose nanowhisker-filled polylactide-based nanocomposites. Biomacromolecules 12(7):2456-2465.

[21] Herrera N, Mathew AP, Oksman K. (2015) Plasticized polylactic acid/cellulose nanocomposites prepared using melt-extrusion and liquid feeding: Mechanical, thermal and optical properties. Composites Science and Technology 106:149-155.

[22] Martínez-Sanz M, Olsson RT, Lopez-Rubio A, Lagaron JM. (2011) Development of electrospun EVOH fibres reinforced with bacterial cellulose nanowhiskers. Part I: Characterization and method optimization. Cellulose 18(2):335-347.

[23] Srithep Y, Ellingham T, Peng J, Sabo R, Clemons C, Turng LS, et al. (2013) Melt compounding of poly (3-hydroxybutyrate-co-3-hydroxyvalerate)/ nanofibrillated cellulose nanocomposites. Polymer Degradation and Stability 98(8):1439-1449.

[24] Vertuccio L, Gorrasi G, Sorrentino A, Vittoria V. (2009) Nano clay reinforced PCL/starch blends obtained by high energy ball milling. Carbohydrate Polymers 75(1):172-179.

[25] Perrin-Sarazin F, Sepehr M, Bouaricha S, Denault J. (2009) Potential of ball milling to improve clay dispersion in nanocomposites. Polymer Engineering and Science 49(4):651-665.

[26] Bugatti V, Gorrasi G, Montanari F, Nocchetti M, Tammaro L, Vittoria V. (2011) Modified layered double hydroxides in polycaprolactone as a tunable delivery system: In vitro release of antimicrobial

benzoate derivatives. Applied Clay Science 52(1-2):34-40.

[27] Tammaro L, Vittoria V, Bugatti V. (2014) Dispersion of modified layered double hydroxides in Poly(ethylene terephthalate) by High Energy Ball Milling for food packaging applications. European Polymer Journal 52(1):172-180.

[28] Gorrasi G, Bugatti V, Vittoria V. (2012) Pectins filled with LDH-antimicrobial molecules: Preparation, characterization and physical properties. Carbohydrate Polymers 89(1):132-137.

[29] Gorrasi G, Sarno M, Di Bartolomeo A, Sannino D, Ciambelli P, Vittoria V. (2007) Incorporation of carbon nanotubes into polyethylene by high energy ball milling: Morphology and physical properties. Journal of Polymer Science, Part B: Polymer Physics 45(5):597-606.

[30] Gorrasi G, Piperopoulos E, Lanza M, Milone C. (2013) Effect of morphology of the filler on the electrical behaviour of poly(L-lactide) nanocomposites. Journal of Physics and Chemistry of Solids 74(1):1-6.

[31] Gorrasi G, Di Lieto R, Patimo G, De Pasquale S, Sorrentino A. (2011) Structure-property relationships on uniaxially oriented carbon nanotube/polyethylene composites. Polymer 52(4):1124-1132.

[32] Wu H, Zhao W, Chen G. (2012) One-pot in situ ball milling preparation of polymer/graphene nanocomposites. Journal of Applied Polymer Science 125(5):3899-3903.

[33] Moreira FKV, Marconcini JM, Mattoso LHC. (2012) Solid state ball milling as a green strategy to improve the dispersion of cellulose nanowhiskers in starch-based thermoplastic matrices. Cellulose 19(6):2049-2056.

[34] Ambrosio-Martín J, Lopez-Rubio A, Fabra MJ, Gorrasi G, Pantani R, Lagaron JM. (2015) Assessment of ball milling methodology to develop polylactide-bacterial cellulose nanocrystals nanocomposites. Journal of Applied Polymer Science 132(10):41605.

[35] Martínez-Sanz M, Lopez-Rubio A, Lagaron JM. (2011) Optimization of the nanofabrication by acid hydrolysis of bacterial cellulose nanowhiskers. Carbohydrate Polymers 85(1):228-236.

[36] Buzarovska A, Bogoeva-Gaceva G, Grozdanov A, Avella M, Gentile G, Errico M. (2007) Crystallization behavior of poly(hydroxybytyrate-co-valerate) in model and bulk PHBV/kenaf fiber composites. Journal of Materials Science 42(16):6501-6509.

[37] Scandola M, Focarete ML, Adamus G, Sikorska W, Baranowska I, Świerczek S, et al. (1997) Polymer blends of natural poly(3-hydroxybutyrate-co-3-hydroxyvalerate) and a synthetic atactic poly(3-hydroxybutyrate). Characterization and biodegradation studies. Macromolecules 30(9):2568-2574.

[38] Chen G, Dufresne A, Huang J, Chang PR. (2009) A novel thermoformable bionanocomposite based on cellulose nanoerystal-graft-Poly(e-caprolactone). Macromolecular Materials and Engineering 294(1):59-67.

[39] Yu HY, Qin ZY, Liu YN, Chen L, Liu N, Zhou Z. (2012) Simultaneous improvement of mechanical properties and thermal stability of bacterial polyester by cellulose nanocrystals. Carbohydrate Polymers 89(3):971-978.

[40] Yu HY, Yao JM, Qin ZY, Liu L, Yang XG. (2013) Comparison of covalent and noncovalent interactions of carbon nanotubes on the crystallization behavior and thermal properties of poly(3-hydroxybutyrate- co-3-hydroxyvalerate). Journal of Applied Polymer Science 130(6):4299-4307.

[41] Fei B, Chen C, Wu H, Peng S, Wang X, Dong L. (2003) Quantitative FTIR study of PHBV/bisphenol A blends. European Polymer Journal 39(10):1939-1946.

[42] Sanchez-Garcia MD, Gimenez E, Lagaron JM. (2008) Morphology and barrier properties of solvent cast composites of thermoplastic biopolymers and purified cellulose fibers. Carbohydrate Polymers 71(2):235-244.

[43] Gunaratne LMWK, Shanks RA. (2005) Multiple melting behaviour of poly(3-hydroxybutyrate-co-hydroxyvalerate) using step-scan DSC. European Polymer Journal 41(12):2980-2988.

[44] Jiang L, Wolcott MP, Zhang J. (2006) Study of biodegradable polylactide/poly-(butylene adipate-co-terephthalate) blends. Biomacromolecules 7(1):199-207.

[45] Owen AJ, Heinzel J, Škrbić Ž, Divjaković V. (1992) Crystallization and melting behaviour of PHB and PHB/HV copolymer. Polymer 33(7):1563-1567.

[46] Wang S, Song C, Chen G, Guo T, Liu J, Zhang B, et al. (2005) Characteristics and biodegradation properties of poly(3-hydroxybutyrate-co-3-hydroxyvalerate) /organophilic montmorillonite (PHBV/OMMT) nanocomposite. Polymer Degradation and Stability 87(1):69-76.

[47] Cimmino S, Iodice P, Silvestre C, Karasz FE. (2000) Atactic poly(methyl methacrylate) blended with poly(3-D(-)hydroxybutyrate): Miscibility and mechanical properties. Journal of Applied Polymer Science 75(6):746-753.

[48] Vidhate S, Innocentini-Mei L, D'Souza NA. (2012) Mechanical and electrical multifunctional poly(3-hydroxybutyrate-co-3-hydroxyvalerate)-multiwall carbon nanotube nanocomposites. Polymer Engineering and Science 52(6):1367-1374.

[49] Sridhar V, Lee I, Chun HH, Park H. (2013) Graphene reinforced biodegradable poly(3-hydroxybutyrate-co-4-hydroxybutyrate) nano-composites. Express Polymer Letters 7(4):320-328.

[50] Kunioka M, Tamaki A, Doi Y. (1989) Crystalline and thermal properties of bacterial copolyesters: Poly(3-hydroxybutyrate-co-3-hydroxyvalerate) and poly(3-hydroxybutyrate-co-4-hydroxybutyrate). Macromolecules 22(2):694-697.

[51] Avrami M. (1939) Kinetics of phase change. I: General theory. The Journal of Chemical Physics 7(12):1103-1112.

[52] Avrami M. (1940) Kinetics of phase change. II Transformation-time relations for random distribution of nuclei. The Journal of Chemical Physics 8(2):212-224.

[53] Avrami M. (1941) Granulation, phase change, and microstructure kinetics of phase change. III. The Journal of Chemical Physics 9(2):177-184.

[54] De Santis F, Pantani R. (2013) Nucleation density and growth rate of polypropylene measured by calorimetric experiments. Journal of Thermal Analysis and Calorimetry 112(3):1481-1488.

[55] Iannace S, Nicolais L. (1997) Isothermal crystallization and chain mobility of poly(L-lactide). Journal of Applied Polymer Science 64(5):911-919.

[56] Fabra MJ, Lopez-Rubio A, Lagaron JM. (2013) High barrier polyhydroxyalcanoate food packaging film by means of nanostructured electrospun interlayers of zein. Food Hydrocolloids 32(1):106-114.

[57] Ambrosio-Martín J, Gorrasi G, López-Rubio A, Fabra MJ, Mas LC, López-Manchado MA, et al. (2015) On the use of ball milling to develop PHBV-graphene nanocomposites (I) - Morphology, thermal properties, and thermal stability. Journal of Applied Polymer Science 132(24):42101.

Chapter 6

ON THE USE OF BALL MILLING TO DEVELOP PHBV-GRAPHENE NANOCOMPOSITES (I): MORPHOLOGY, THERMAL PROPERTIES AND THERMAL STABILITY

J. Ambrosio-Martín[a], G. Gorrasi[b], A. Lopez-Rubio[a], M. J. Fabra[a], L. Cabedo[c], M.A. López Manchado[d] and J. M. Lagaron[a]

Journal of Applied Polymer Science 2015, 132(24):42101

[a] Novel Materials and Nanotechnology Group, IATA-CSIC, Avda. Agustin Escardino 7, 46980 Paterna (Valencia), Spain.

[b] Department of Industrial Engineering, University of Salerno, via Giovanni Paolo II, 132 84084 Fisciano (Salerno), Italy.

[c] ESID, Universitat Jaume I, Av. Vicent Sos Baynat s/n, 12071 Castellón, Spain.

[d] Institute of Polymer Science and Technology, (CSIC), Juan de la Cierva, 3, 28006 Madrid, Spain.

ABSTRACT

In the first part of this work, novel nanocomposites based on poly (3-hydroxybutyrate co-3-hydroxyvalerate) (PHBV) and functionalized graphene nanosheets (FGS) were prepared through ball milling. As revealed by morphological characterization, this blending methodology was able to allow proper nanofiller dispersion and distribution into the matrix. Thermal properties were studied under non-isothermal and isothermal conditions and the addition of FGS into PHBV matrix, although no changes in crystallization mechanism were observed, it modified the crystallization kinetics leading to increased crystallinity. Thermal stability analysis revealed that FGS affected the mechanism of oxidative thermal degradation and had no effect on thermal degradation by pyrolysis. Furthermore, an analysis of isothermal degradation kinetics showed that FGS speeded up the degradation rate. The Sestak-Berggren model was used as a model to explain the isothermal degradation behaviour of the obtained materials in good agreement with the experimental data.

Keywords: Biodegradable; Biomaterials; Biopolymers and Renewable Polymers; Composites; Graphene and Fullerenes

1. INTRODUCTION

The massive use of petroleum-based polymers has resulted in environmental concerns derived not only from waste management issues, but also from their low degradation rates. As a result, there is a growing interest in the development of renewable and biodegradable materials to partially replace the oil-based ones. Alternatives such as polyhydroxyalkanoates (PHAs) have sparked great interest due to their biodegradable, biocompatible and renewable features. PHAs can be produced in different ways, i.e. chemically or biologically through fermentation from feedstock. This family comprises mainly the homopolymer, polyhydroxybutyrate (PHB), which has been extensively studied since it presents mechanical properties similar to those of conventional petroleum-based polymers, relatively good thermal properties and high stiffness due to its high crystallinity degree [1]. However, although high crystallinity is useful for some applications, the high stiffness limits its usage in other commercial applications. Moreover, another drawback of this polymer is its low thermal stability, making it unstable during melt processing and also limiting its applicability [2]. Several strategies have been developed to overcome these drawbacks, including blending with other polymers, such as poly (vinyl alcohol) (PVA) [3], polypropylene glycol (PPG) [4] and poly-ε-caprolactone (PCL) [5] or modification of the homopolymer by incorporation of different monomer types during the fermentation process. Copolymerization with hydroxyvalerate (HV) results in poly(3-hydroxybutyrate-co-3-hydroxyvalerate) (PHBV) which has improved mechanical and thermal properties, since incorporation of HV reduces the crystallinity, thus decreasing stiffness and brittleness, and also reducing the melting point without decreasing the thermal stability of the material, although greater improvements in this parameter are still needed [1, 6]. However, reduction in crystallinity is widely known to affect the barrier properties of materials to low molecular weight substances, which is a key property of materials intended to be used in packaging applications [7, 8]. Because of that, PHBV copolymers still present several drawbacks including high cost, relative brittleness and thermal instability, which had hampered the widespread usage of this family of polymers. As a strategy to improve biopolymer performance, many studies have focussed on the development of composites and, especially, nanocomposites using a variety of fillers. Natural fibres such as kenaf fibres have been incorporated into PHBV matrix achieving significant improvements in mechanical properties [9]. Furthermore, the addition of cellulose nanowhiskers resulted in significant improvements in thermal, mechanical and barrier properties, as well as in thermal stability [1]. Apart from natural organic fillers, lamellar inorganic reinforcing fillers, including nanoclays or double layered hydroxides, among others, have been widely studied, giving rise to materials with improved mechanical, barrier and thermal stability properties [10-13]. It is noteworthy that the improved performance of nanocomposites is achieved, not only by using the inherent properties of the nanofiller, but more importantly by optimizing the dispersion, interface chemistry and nanoscale morphology [14]. Great interest has recently arisen about carbonaceous nanofillers such as carbon nanotubes and carbon nanosheets due to their excellent mechanical, thermal and electrical properties. Several works have been published about the effect of carbon nanotubes in polymer matrices [15-19], and more specifically in PHBV matrix [20-24]. Graphene, another carbon-filler material which is the elementary structure of

graphite, composed of one atomic thick layer of sp^2-bonded carbon atoms arranged in a honey comb structure, has emerged in last years. The interest in this specific nanofiller derives not only from its excellent mechanical strength, electrical and thermal conductivity, but also from its high surface area and, thus, high barrier effect on polymer matrices [25, 26]. Therefore, its inherent physical properties along with its lamellar structure have made it excellent reinforcing nanofiller for polymer and biopolymer nanocomposites [27]. It has been, for instance used as filler in many polymer matrices such as poly (lactic acid) (PLA) [26, 28], PVA [29], polyethylene (PE) [30] and polystyrene (PS) [31] among others, improving their barrier, mechanical and electrical properties. Recent works have also incorporated low contents of graphene sheets in PHBV matrices through solution casting methods improving, in the same way, the final properties of the obtained materials [6, 32].

The ball milling technique is an alternative and efficient method to produce novel composites with high performances since during the milling "intimate mixing" is promoted [17, 33]. It is considered a novel compounding method and it is based in a high-energy grinding technique, able to induce several mechano-chemical changes in the materials. This technique has been previously used in the development of clay-based and carbon nanotubes-based nanocomposites [17, 34-36]. Moreover, graphene-based nanocomposites have also been synthesized by ball milling since the high energy milling induces graphite delamination, thus improving the final properties of the obtained materials [37]. An effective grafting of polystyrene matrix (PS) onto the surface of graphene sheets using ball milling was reported. With this aim, graphite nanoplatelets were used as initial material, corroborating the effectiveness of its mechano-chemical characteristic of this technique [38]. To the best of our knowledge, the high energy ball milling technique has not been used up to date to develop PHBV-graphene nanocomposites. Because of that, the aim of this work was to evaluate the ball milling technique capacity for the production of PHBV-graphene nanocomposites and the study of the final properties of the so-obtained materials. It has been previously reported that when graphene is functionalized, single-sheet graphene is expected to serve as nanofiller in nanocomposites applications, as functional sites will favor interactions with the matrix [39]. Because of that, a derivative graphene material such as functionalized graphene sheets was used attempting to optimize the filler-matrix compatibilization. This paper is the first part of a wide work in which we aimed to prepare novel PHVB-graphene nanocomposites using mechanical energy. Morphological organization, through SEM and TEM analysis was analyzed. It was conducted a detailed study of behaviour in the molten state of PHVB as function of filler content, either in isothermal or in non-isothermal conditions. The degradation behaviour of PHVB, either in inert atmosphere or in air, depending on graphene content was also analyzed.

2. MATERIALS AND METHODS

2.1. Materials

The bacterial polyhydroxyalkanoate grade was purchased from Goodfellow Cambridge Limited, UK, in pellet form (density 1.25 g cm^{-3}). The supplied material was a melt-processable semicrystalline thermoplastic PHBV12 (polyhydroxybuty-rate with 12 mol% of valerate and containing 10 wt.% of the plasticizer citric ester) copolymer made by biological fermentation from renewable carbohydrate feedstocks. Prior to the ball milling process,

the material was purified by dissolution in chloroform and subsequent precipitation by drop-wise addition to an excess of methanol. The material, in this way, was transformed from pellet to powder form which was necessary for the ball milling process.

Functionalized graphene sheets (FGS) were synthesized by thermal reduction of graphite oxide at 1000°C for 30 s under air atmosphere. Briefly, graphite powder (purum powder < 0.1 mm, Sigma Aldrich) was dispersed in 20 mL of fuming nitric acid for 20 min; next, potassium chlorate (8 g) was slowly added over 1 h and the reaction mixture was stirred for 21 h at 0°C. Graphene produced through this method leads to the formation of single graphene layers or stacks of up to 7 sheets with hydroxyl, carbonyl and epoxy groups on their surface [39]. A full description of the synthesis and characterization of the FGS can be found elsewhere [40].

2.2. Sample Preparation (High Energy Ball Milling - HEBM)

FGS and PHBV powder were milled in the solid state in a Retsch (Germany) centrifugal ball mill (model PM100). The milling process was carried out in a cylindrical steel jar of 50 cm^3 with 5 steel balls of 10 mm of diameter. The rotation speed used was 650 rpm and the milling time was fixed to 60 min. In these experimental conditions, six series of composites PHBV-FGS with 0.1, 0.5, 1.0, 1.5, 2.0, and 3.0 wt.% of FGS were prepared. An additional PHBV sample without filler to be taken as a reference was also milled in the same conditions. The PHBV-FGS mixtures and the pure milled PHBV were molded in a hot press (Carver Inc.). To this aim the material was heated up to 175 °C and kept at this temperature for 5 min. Subsequently, the material was hot pressed and cooled at room temperature giving rise to 250 ± 50 μm thick films. Preparation of the PHBV/FGS nanocomposites is shown in Figure 1.

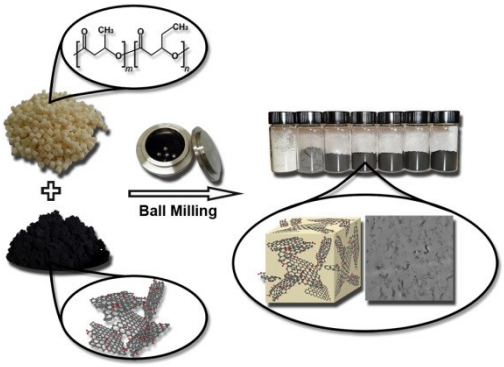

Figure 1. Preparation of PHBV/FGS nanocomposites.

2.3. Characterization

2.3.1. *Scanning Electron Microscopy (SEM)*

For scanning electron microscopy (SEM) observation, the samples were cryofractured after immersion in liquid nitrogen, mounted on bevel sample holders and sputtered with Au/Pd in a vacuum. The experiments were conducted on a Hitachi microscope (Hitachi S-4100) at an accelerating voltage of 10 KV and a working distance of 12–16 mm taking pictures for the sample thickness.

2.3.2. *Transmission Electron Microscopy (TEM)*

Transmission electron microscopy (TEM) was performed using a JEOL 1010 (Jeol, Tokyo, Japan) equipped with a digital Bioscan (Gatan) image acquisition system. TEM observations were performed on ultrathin sections of microtomed thin composite sheets.

2.3.3. *Differential Scanning Calorimetry (DSC)*

Thermal properties of PHBV and its nanocomposites with FGS were evaluated by

DSC using a DTA Mettler Toledo (DSC 30) under nitrogen atmosphere. The analysis was carried out on samples with a mass ranging between 10 and 12 mg. The heating and cooling rate for the runs was 10 °C min^{-1} with a temperature range for the assays between 0 and 180 °C. To ensure reliability of the data obtained, heat flow and temperature were calibrated with standard materials, indium, and zinc. The degree of crystallinity was calculated by taking the specific heat of fusion of perfectly crystalline PHBV. For materials with HV contents equal or higher than 10 mol%, the classical value reported was used, $\Delta H_m° = 109$ J g^{-1} [41].

In addition, the isothermal crystallization kinetics experiments were evaluated at different temperatures. The samples were heated to 180 °C and annealed at that temperature for 10 min to eliminate the thermal history of any specimen. After that, the samples were cooled rapidly at 100 °C min^{-1}, to the desired crystallization temperatures, T_c, ensuring that the crystallization process did not start during the cooling step. Finally, the temperature was held until crystallization was complete. The exothermic crystallization peaks were recorded as a function of time at T_c.

2.3.4. *Thermogravimetric Analysis (TGA)*

Thermogravimetric analysis (TGA) was carried out with a Mettler TC-10 thermobalance. The samples were heated from 25°C to 800°C at 10 °C min^{-1} heating rate under air flow and nitrogen flow. The weight loss was recorded as function of temperature. Moreover, isothermal TGA was performed in nitrogen environment for pure PHBV and its composites with 0.5, 1.5 and 3 wt.%. The temperature was raised from room temperature to 100 °C at 75 °C min^{-1} and kept for 3 minutes to eliminate the water. From 100 °C to the respective isothermal degradation temperature, T_d, the temperature was raised at 100 °C min^{-1} heating rate. After that, the sample was subjected to T_d for a predetermined time.

3. RESULTS AND DISCUSSION

3.1. Morphological Characterization

To study the dispersion of the FGS within the PHBV matrix, SEM and TEM experiments were carried out. Figure 2 shows the cryofractured sections of the neat PHBV and its nanocomposite films.

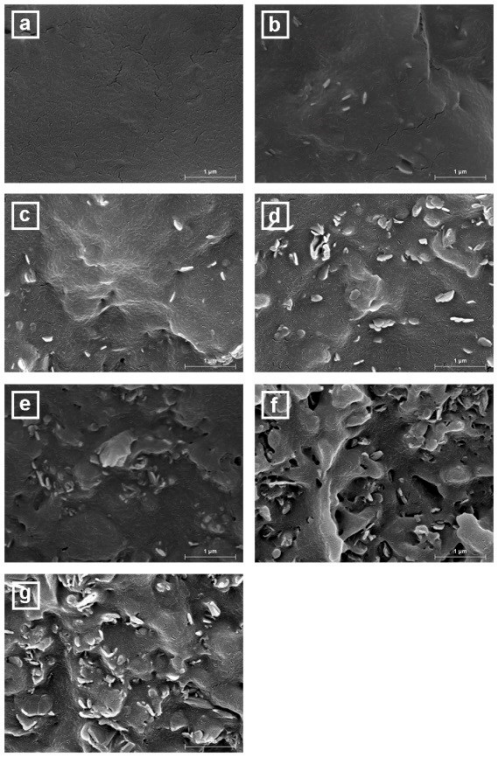

Figure 2. SEM micrographs of the cryo-fractured sections of pure PHBV (a) and PHBV-FGS nanocomposites films at 0.1 wt.% (b); 0.5 wt.% (c); 1.0 wt.% (d); 1.5 wt.% (e); 2.0 wt.% (f) and 3.0 wt.% (g). Scale markers correspond to 1μm.

Homogeneous dispersion and distribution of the filler, which appears as laminar structures, was observed, especially at low contents. When the amount of FGS increased, although the filler was randomly dispersed, filler concentration areas were noticed. Moreover, while the neat polymer showed a rather flat, clean and smooth fracture surface due to the known brittleness of PHBV [42, 43], as the FGS content increased, the materials exhibited less homogeneous and rougher fractured surfaces with more irregularities. This effect has also been reported when high concentration of graphene was incorporated into poly (vinylidene fluoride) [44] or polylactide (PLA) [45]. Figure 3 shows TEM micrographs of PHBV-FGS nanocomposites with high and low FGS content. These images further confirm the good filler dispersion in PHBV matrix as well as the fact that the filler was concentrated in certain areas for highly loaded nanocomposites. Consequently, the ball milling technique seems to be an appropriate tool to obtain a homogeneous distribution of FGS within the PHBV biopolymeric matrix, especially at low content.

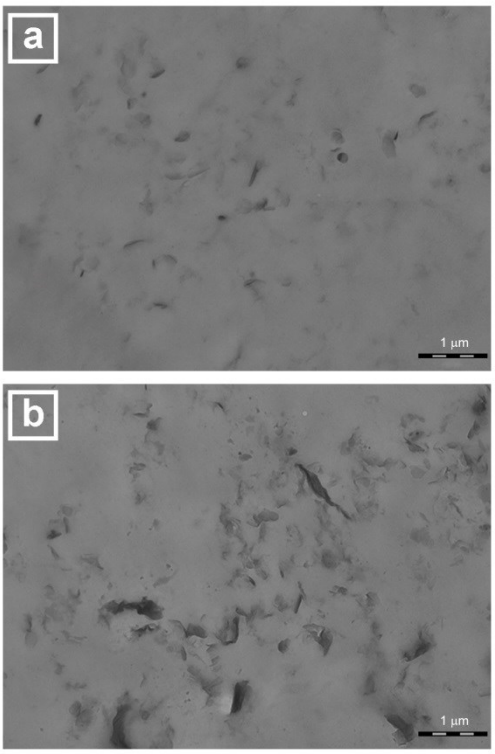

Figure 3. TEM micrographs of PHBV-FGS films containing 0.5 wt.% FGS (a) and 2.0 wt.% FGS (b). Scale markers correspond to 1µm.

3.2. Melting and Crystallization Behaviour of PHBV and its Nanocomposites

With the aim of investigating the effects of the FGS addition on the thermal properties of the PHBV nanocomposites, DSC analyses of all samples were carried out. The melting temperatures (T_m) and melting enthalpy (ΔH_m) normalized to the PHBV content of the nanocomposite films were evaluated from the DSC first and second heating runs. The degree of crystallinity (X_c) was only calculated from the DSC first heating run and crystallization temperature (T_c) and crystallization enthalpy (ΔH_c) were also obtained from DSC cooling run. Table 1 gathers all the DSC data for PHBV and its nanocomposites.

As shown in Figure 4, neat PHBV displays multiple melting peaks in the first heating, which occurred between 150°C and 180 °C. Multiple melting peaks behaviour of PHBV copolymer was interpreted previously as an effect of the melting-recrystallization process occurring during subsequent heating [46]. During the slow heating scans, unstable crystals have sufficient time to melt and reorganize into more stable crystals which lead to this bimodal melting peak behaviour. The reorganized crystals are then subsequently re-melted at higher temperatures [47, 48]. Wang et al. [49] observed the same bimodal effect in PHBV/clays nanocomposites with an increase of the high-temperature melting peak area upon addition of clays. It was pointed out that the low-temperature melting peak was probably related to

Table 1. DSC glass transition temperature (T_{g1}), maximum of melting (T_m), melting enthalpy (ΔH_m), during the first heating run, crystallization temperature (T_c), crystallization enthalpy (ΔH_c), during the cooling run, and maximum of melting (T_m) and melting enthalpy (ΔH_m) during second heating run.

	First Heating				Cooling		Second Heating	
	T_{m1} (°C)	T_{m2} (°C)	ΔH_m (J g^{-1})	X_c (%)	T_c (°C)	ΔH_c (J g^{-1})	T_m (°C)	ΔH_m (J g^{-1})
PHBV	143.3	157.5	58.01	53.22	111.2	59.70	152.0	59.76
PHBV-FGS 0,1 %	142.5	155.5	64.88	59.53	112.0	63.04	151.8	65.86
PHBV-FGS 0,5 %	143.5	156.5	65.34	59.94	112.2	63.05	152.3	66.34
PHBV-FGS 1 %	141.7	155.8	67.53	61.95	113.2	64.54	152.0	67.54
PHBV-FGS 1,5 %	142.8	156.8	67.04	61.50	113.8	62.16	152.3	67.33
PHBV-FGS 2 %	148.3	158.3	62.41	57.26	114.2	56.52	154.0	60.65
PHBV-FGS 3 %	146.3	156.5	61.03	55.99	114.7	55.48	152.0	59.53

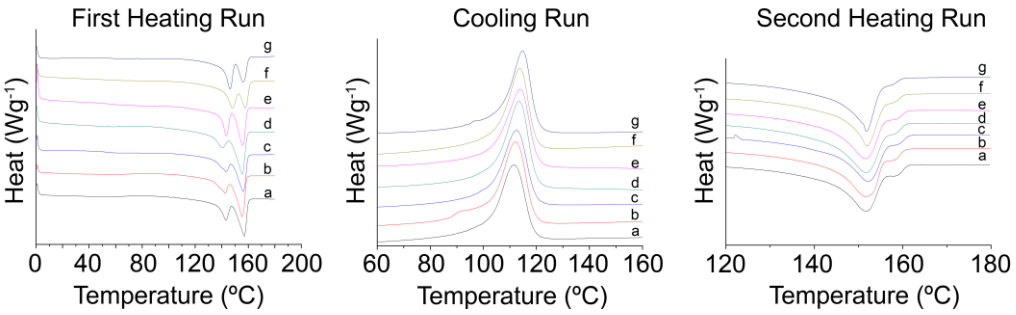

Figure 4. DSC thermograms of first heating, cooling and second heating runs of pure PHBV (a) and PHBV-FGS nanocomposites at 0.1 wt% (b); 0.5 wt% (c); 1.0 wt% (d); 1.5 wt% (e); 2.0 wt% (f) and 3.0 wt% (g).

homogeneous nucleation of PHBV which started spontaneously by PHBV chain aggregation below the melting point. On the contrary, the high-temperature melting peak was related to heterogeneous nucleation of PHBV, and its increase was associated to the existence of much more crystalline nuclei after addition of clays than in neat PHBV. Addition of low amounts of FGS into PHBV matrix did not result in big changes in the low melting temperature peak. However, at high contents, an increase in the melting temperature of the low melting temperature peak was observed. This allows hypothesizing that the fraction of crystals that melted at lower temperatures was composed by bigger or more perfect crystals if compared with the neat polymer. On the other hand, the high melting peak temperature remained almost unaltered for the PHBV nanocomposites in regard to neat polymer. These results differ to some extent with previous studies about the incorporation of graphene [6], nanoclays [49, 50] or carbon nanotubes [24] into PHBV, where a decrease in the melting temperature peak was observed as the nanofiller concentration was increased.

In spite of this, an analysis of the ratio of the melting peak areas demonstrated that at low FGS content there was an increase of the fraction of more stable crystals related to an increase of the high-temperature melting peak area which remained more or less constant up to 1 wt.% (cf. Figure 5). This fraction was then dramatically reduced when high contents of FGS were introduced within the PHBV matrix. This could indicate that at low loadings, the well dispersed FGS acted as nucleating sites increasing the heterogeneous crystallization which is consistent with the observations of Wang et al. [49], discussed above. On the contrary, high contents of FGS hindered the

crystallization process to some extent and the nucleating effect was not as pronounced as at low loadings, generating more defective or unstable crystals. A reduction of the second melting peak area relative to the first melting peak area was also observed when MWCNT were incorporated into PHBV biopolymer [23, 24].

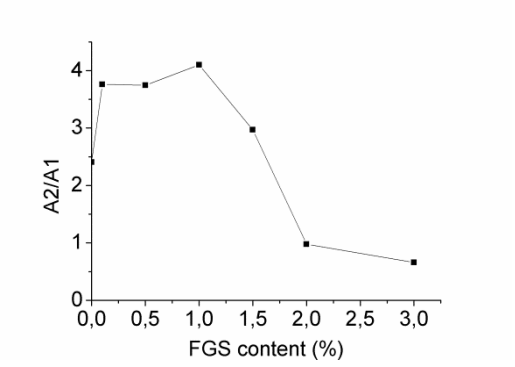

Figure 5. Melting peaks areas ratio as function of FGS content. A_1 and A_2 are the areas of the lower and higher melting temperature peaks, respectively.

From Table 1, it can be seen that the melting enthalpy values increased at each PHBV-FGS composition when compared with neat biopolymer, which was associated to an increase in the crystallinity degree. However, the maximum crystallinity degree was obtained for the nanocomposite containing 1 wt.% FGS. For higher nanofiller loading, although crystallinity was still higher than that for the pure polymer, the crystallization degree underwent a slight decrease. This is in accordance with the data reported in the melting peak areas study where high FGS contents were considered to hinder the crystallization process to some extent. The increase in crystallinity could be ascribed to the nucleating effect of the FGS which increased the nucleation rate of PHBV and thus, improved the overall crystallization rate, as previously reported for PHBV nanocomposites containing graphene [6], multiwalled carbon nanotubes [21] or cellulose nanowhiskers [51]. Moreover, it was reported that well-dispersed multi-walled carbon nanotubes led to an increased number of sites available for nucleation, thereby enhancing the crystallization rate of PHBV [20]. Therefore, DSC results are consistent with SEM observations where, although no agglomerates were observed for high loadings, filler concentration areas could be observed, which could hinder the nucleation effect to some extent and hence, generating lower crystallization degree than that obtained for lower loadings.

The crystallization behaviour of the PHBV-nanocomposites during the DSC cooling run was also analysed. A clear trend of increased crystallization temperature with increasing FGS content was observed, corroborating the nucleating effect of FGS. In addition, the crystallization peaks of nanocomposites became slightly sharper, which can be related to an acceleration of the non-isothermal crystallization rate in the presence of FGS [23]. The crystallization enthalpy of the nanocomposites was generally higher than that of the pure polymer, except for higher loadings, as shown in Table 1. Once again, it could be observed that high FGS contents hindered the crystallization process, as mentioned above.

The double melting peak noted in the first heating scan was eliminated after the DSC cooling process. Only one melting peak was obtained in the second heating scan with a melting temperature between the low and high temperature melting peaks observed in the first heating run, although a small shoulder was observed after the crystallization peak. Similar results were reported for PHBV nanocomposites with double layered hydroxides [10]. For the samples with 2 and 3 wt.% FGS content, sharper melting peaks were obtained and the shoulder became smaller, almost disappearing. This indicates that, during the controlled DSC cooling process, the polymer

chains were able to crystallize in a more homogeneous way.

The isothermal crystallization kinetics of PHBV and its nanocomposites were investigated in order to obtain further information about the effect of FGS addition on the crystallization process of PHBV. The crystallization exothermic peaks of PHBV and its nanocomposites at different temperatures (T_i), 133°C, 135°C and 137 °C were analyzed. As an example, Figure 6 shows the crystallization peaks of neat PHBV, and the nanocomposites containing 1 wt.% and 3 wt.% FGS at those temperatures. From this figure it can be stated that the crystallization process occurred more slowly with increasing T_i and it became shorter with addition of FGS. The crystallization kinetics of neat PHBV and its nanocomposites was analysed by the well established model for isothermal crystallization, i.e. the Avrami model.

$$X_t = 1 - \exp(-Kt^n) \quad (1)$$

where X_t is the relative degree of crystallinity after crystallization time t, n is the Avrami exponent which is related to the type of nucleation mechanism and to the geometry of the growing crystals, and K is the overall (macroscopic) kinetics rate constant (it contains contributions from both nucleation and growth).

A derivative method reported by De Santis and Pantani [52] was used to directly fit the calorimetric curve of the isothermal crystallization process to the derivative form of the Avrami equation. The data obtained from the Avrami fitting is compiled in Table 2. The half-time of crystallization $t_{½}$ is defined as the time required to reach 50% of the total crystallinity and was calculated from the values of n and K [52]. The determination of the crystallization half-time under isothermal conditions is an interesting method to provide clear-cut evidence of the effectiveness of nucleating agents on polymer matrices [53]. In fact, it is also used to directly characterize the crystallization rate, since the reciprocal half-time of crystallization ($1/t_{½}$) can be considered approximately proportional to the crystal growth rate [54]. Thus, it can be observed that the shorter half-time of crystallization the higher the crystallization rate. Data in Table 2 demonstrated that the values of the overall crystallization rate constant increased as the FGS content increased. At the same time, $t_{½}$ parameter decreased with addition of FGS. Therefore, an acceleration of the crystallization process took place when FGS was incorporated. Regarding the Avrami exponent, it was not altered with the FGS incorporation, indicating that the crystallization mechanism was probably the same. In fact, for all the samples a bimodal melting peak was observed suggesting that the same crystallization mechanism occurred. As mentioned above, the low-temperature melting peak was probably related to homogeneous nucleation of PHBV and the high temperature melting peak was related

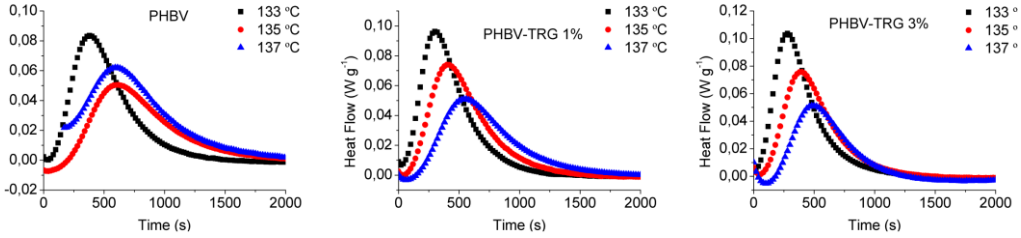

Figure 6. DSC experimental curves during isothermal crystallization study of PHBV and its nanocomposites with 1.0 wt.% and 3.0 wt.% FGS.

Table 2. The values of kinetic rate constant (*K*), Avrami exponent (*n*), and half-time of crystallization ($t_{1/2}$) as function of crystallization temperature of PHBV and its nanocomposites.

Temperature (ºC)	FGS (wt%)	K x 10^3 (s^{-1})	n	$t_{1/2}$ (s)
130	0	2,5	1,6	318,1
	0.1	2,6	1,6	309,6
	0.5	2,7	1,5	293,2
	1.0	2,9	1,6	270,7
	1.5	2,8	1,7	290,3
	2.0	3,2	1,6	244,6
	3.0	3,3	1,5	240,1
135	0	1,8	1,6	443,0
	0.1	2,1	1,7	383,9
	0.5	2,2	1,7	361,2
	1.0	2,4	1,6	330,7
	1.5	2,5	1,6	320,4
	2.0	2,7	1,6	297,2
	3.0	2,6	1,7	303,5
137	0	1,6	1,7	511,9
	0.1	1,6	1,7	495,9
	0.5	1,8	1,8	454,7
	1.0	1,9	1,6	410,9
	1.5	2,0	1,6	394,9
	2.0	2,1	1,7	385,4
	3.0	2,5	1,8	328,9

to heterogeneous nucleation of PHBV. The effect of increasing the crystallization rate with increasing nanofiller concentration is also in agreement with the non-isothermal crystallization study carried out by DSC where an acceleration of the crystallization process was observed due to the FGS nucleating effect.

Therefore, it could be concluded that although there were no changes in the crystallization mechanism, the presence of FGS had an effect on the kinetics and dynamics of PHBV crystallization. The well dispersed FGS altered the crystallization rate and the crystal size and shape, accelerating the crystallization process and giving rise to changes in the heterogeneity of the crystals. Similar effect has been reported for nanocomposites of PHBV and MWCNT [20, 23]. These effects were strongly dependent on the FGS content. Thus, for high FGS content, the crystallization process was somehow hindered, generating more defective and/or smaller crystals when compared with the nanocomposites with lower FGS content. In contrast, increasing the FGS content led to an acceleration of the crystallization process, showing an increase in the crystallization temperature, which was directly related with the non-isothermal crystallization rate, and also an increase in the isothermal crystallization rate.

3.3. Thermal Stability of PHBV and its Nanocomposites

The thermal stability of the neat PHBV and PHBV-FGS nanocomposites were analysed using TGA. Thermal degradation temperatures, onset temperatures and the residues at 400 and 800 °C were evaluated and the results are presented in Table 3. Figure 7 shows the TGA curves of pure FGS and the TGA and DTG curves of PHBV and PHBV-FGS nanocomposites under air and nitrogen conditions. It is clearly observed

Table 3. TGA decomposition temperatures (T_d), onset temperature and the difference between % residue at 400 °C and 800 °C of PHBV and its nanocomposites incorporating FGS evaluated in air and nitrogen environment.

	Air				Nitrogen			
	T_{d1} (ºC)	T_{d2} (ºC)	T_{onset} (ºC)	$R_{400ºC} - R_{800ºC}$ (%)	T_{d1} (ºC)	T_{d2} (ºC)	T_{onset} (ºC)	$R_{400ºC} - R_{800ºC}$ (%)
PHBV	284.2	-	269.3	0.2	276.6	-	259.6	0.1
PHBV-FGS 0,1	282.3	-	266.2	0.3	278.3	-	262.4	0.3
PHBV-FGS 0,5	280.0	472.8	263.7	0.7	276.1	495.9	259.3	0.6
PHBV-FGS 1	279.9	483.5	259.0	1.1	277.6	511.8	258.9	1.2
PHBV-FGS 1,5	278.9	508.5	263.3	1.4	278.4	558.0	262.0	1.6
PHBV-FGS 2	273.8	500.4	257.4	2.0	276.6	580.7	257.9	2.3
PHBV-FGS 3	273.4	522.3	257.0	3.1	275.5	645.2	255.3	3.2

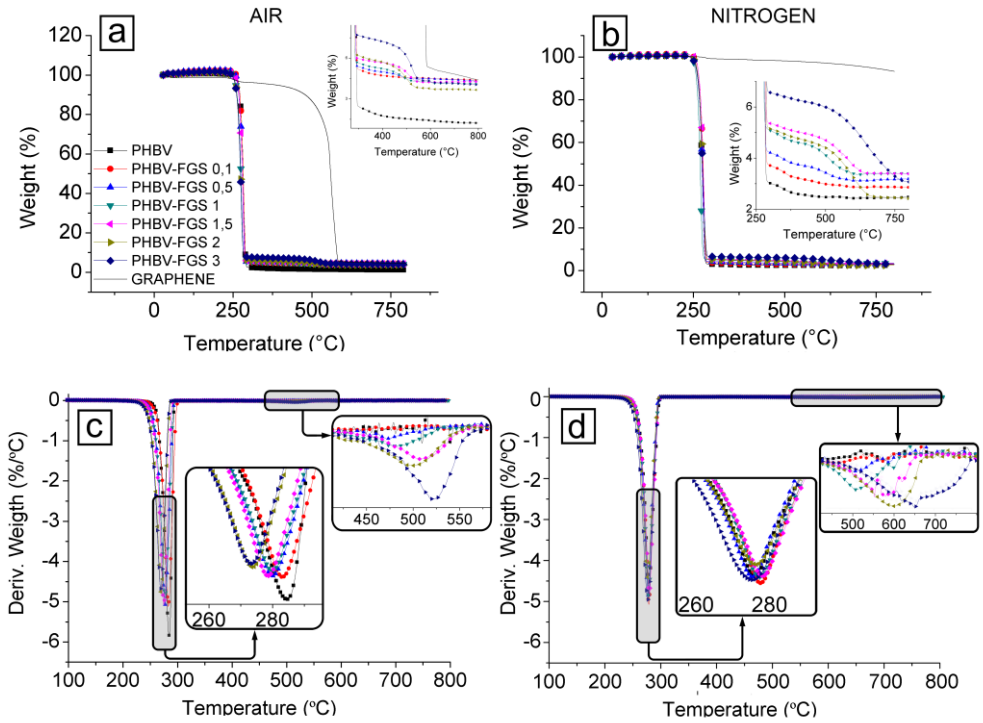

Figure 7. TGA curves of pure FGS, pure PHBV and its nanocomposites with FGS (a, b) and DTG curves of pure PHBV and its nanocomposites with FGS (c, d) in air and nitrogen environments (left and right respectively). The insets are expanded views at different temperature ranges.

better thermal stability of FGS than that for the neat polymer and polymer nanocomposites in both air and nitrogen environments. All nanocomposites showed similar degradation behaviour if compared to neat polymer. However, despite the high thermal stability of the FGS, while for nitrogen environment there was no change on the thermal degradation temperature of PHBV matrix with FGS addition, a decrease was noticed when thermal stability was analysed in the presence of air. In this case, the greater the FGS content the lower the thermal degradation temperature observed for the nanocomposites. Moreover, onset degradation temperatures shifted to lower temperatures with increasing FGS, unlike in nitrogen environment, where they remained more or less constant. Therefore, it seems that addition of FGS affected the mechanism of oxidative thermal degradation of PHBV while had no effect on thermal degradation by pyrolysis. Indeed, it was observed that for pure FGS different degradation mechanism took place in presence of air or nitrogen environment. Polymers loaded with layered nanofillers, such as layered silicates, layered double hydroxide or layered metallic phosphate usually exhibit an increased thermal stability being attributed to the mass and heat barrier effects that this kind of fillers infer to the matrix [28]. In this case, although graphene can be considered a good mass barrier for volatile degradation products, it has high heat conductivity. Therefore, the decrease in degradation temperature can be ascribed to the low heat barrier effect of graphene in polymer composites. In fact, a recent study reported that PLA-graphene nanocomposites could be

ignited with less heat irradiation than the pristine polymer. The reason of that was the high heat conductivity of graphene which allowed easier and faster heat diffusion through the matrix [28]. A small shoulder was observed around 500 °C for all PHBV-FGS nanocomposites in both air and nitrogen environment, except for 0.1 wt.%. Attending to the degradation curve of pure graphene, the mass loss at this point could be attributed to the degradation of graphene present in the nanocomposite. Focusing on This high temperature area of the graph (cf. Figure 7 insets), it was observed that there was a direct and accurate relationship between the mass loss after 400 °C and the FGS content of the nanocomposites both in air and nitrogen environments (cf. Table 3). Moreover, higher thermal degradation temperatures were observed when the experiments were performed under nitrogen atmosphere, which is in accordance with the higher thermal stability of FGS in these conditions.

The isothermal degradation kinetics of PHBV and PHBV-FGS at 0.5 wt.%, 1.5 wt.% and 3 wt.% nanocomposites were investigated at predetermined temperatures, 230 °C, 240 °C and 250 °C in order to further study the effect of FGS addition on the degradation process of PHBV. The weight loss profiles of PHBV and its nanocomposites during isothermal heating at the established temperatures are shown in Figure 8a. A normal one step isothermal degradation process was observed, where higher isothermal degradation temperatures produced faster weight loss. Moreover all composites could speed up the degradation rate of pristine matrix at any determined degradation temperature since the establishments of constant mass plateau were shifted to lower degradation times compared with pure PHBV, i.e., reducing its thermal stability, as observed by TGA.

To evaluate the kinetics of the degradation process, it was assumed that the weight loss during degradation process was associated with the depolymerization reaction. Thus, the degree of depolymerization can be defined as:

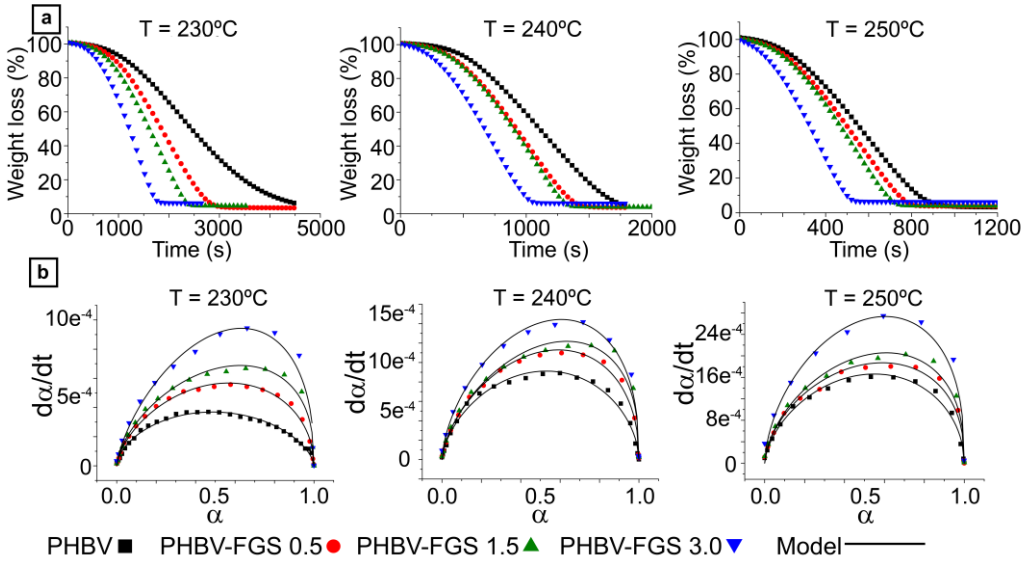

Figure 8. Weight loss profiles versus time (a) and the experimental and calculated data using the Sestak Berggren model of dα /dt versus α (b) of PHBV and its nanocomposites with 0.5 wt%, 1.0 wt% and 3.0 wt% FGS at 230 °C, 240 °C and 250 °C isothermal temperatures.

$$\alpha = \frac{m_0 - m_t}{m_0 - m_f} \quad (2)$$

with m_0 is the initial weight, m_t is the weight at any time and m_f is the weight at the end of the degradation process.

To describe the kinetic of polymer degradation, a single step kinetic equation is normally used.

$$\frac{d\alpha}{dt} = k(T) f(\alpha) \quad (3)$$

where $k(T)$ is a temperature dependent rate constant which is expressed as Arrhenius type equation, i.e, $k(T)=A \cdot exp(-E_a/RT)$, with A and E_a the pre-exponential factor and activation energy respectively, and $f(\alpha)$ expresses the reaction model which describe dependence of the reaction rate on the extent of reaction. Different expressions of $f(\alpha)$ for the most frequently used mechanism are proposed in the literature [12, 55, 56]. The general form of nth-order of $f(\alpha)$ is $f(\alpha)=(1-\alpha)^n$. Figure 8b shows the $d\alpha/dt$ as a function of degree of depolymerisation, α, for PHBV and its nanocomposites at different temperatures. There was non-linear relationship between $d\alpha/dt$ and α, and thus, the simple first-order kinetic model (n=1) could not be used as a model to explain the isothermal degradation behaviour of these materials. On the contrary, the peak profiles of the data plots were in the form of a parabola. This non-linear dependence of the kinetics degradation model with de depolymerization degree of PHB incorporating different kinds of nanofillers has been previously reported [12, 55-57], where a contribution of further reactions mechanism such as autocatalytic reactions or chain scission mechanism were proposed. Moreover, it has been reported that the kinetics degradation model of PHBV does not follow simple first-order kinetics. A more complex degradation process was considered involving degradation of different compounds with different decomposition rates [58].

To understand the degradation reaction of our materials, Sestak-Berggren (Eq. 4) model was used to adjust our isothermal degradation data.

$$\frac{d\alpha}{dt} = k(1-\alpha)^n \alpha^m \quad (4)$$

The relative values of n and m determine relative contributions from decay and acceleratory regions of the thermal degradation process, respectively. This model is known as autocatalytic model and is considered one of the more satisfactory models to describe the observed phenomena [12, 57]. As observed in Figure 8, there was good agreement between the experimental data and the model prediction for pure polymer and for any composition at the various isothermal degradation temperatures. The fitting parameters k, n, m were obtained and are reported in Table 4 along with the correlation factor of the fitting. As observed from this table, an increment in the degradation rate constant was observed for the nanocomposites when compared with the neat PHBV at each temperature. This again indicates reduction in the thermal stability of the obtained nanocomposites. Furthermore the accelera-tory reaction of thermal degradation was larger than decay reaction ($m > n$) for each material at each temperature. These results confirmed the ability of autocatalytic degradation model as a good general model to describe the degradation of PHBV and its nanocomposites with FGS. To evaluate the well known "kinetic triplet", i.e, A, E_a and $f(\alpha)$, the Arrhenius equation was transformed to its logarithmic form and the Arrhenius plots of ln(k) vs 1/T were achieved. The pre-exponential factor and activation energy were calculated from slope and intercept of the linear fitting respectively (cf. Figure 9). A reduction in the activation energy was

Table 4. Fitting parameters of Sestak-Berggren model to the isothermal degradation data.

Temperatura (°C)	Sample	k (s^{-1})	n	m	R^2
230	PHBV	11.6 e^{-4}	0.616	0.582	0.98
	PHBV-FGS 0,5	12.4 e^{-4}	0.492	0.645	0.99
	PHBV-FGS 1,5	13.6 e^{-4}	0.385	0.646	0.98
	PHBV-FGS 3	19.7 e^{-4}	0.412	0.708	0.98
240	PHBV	20.9 e^{-4}	0.563	0.634	0.99
	PHBV-FGS 0,5	23.8 e^{-4}	0.452	0.651	0.99
	PHBV-FGS 1,5	23.9 e^{-4}	0.376	0.651	0.97
	PHBV-FGS 3	28.7 e^{-4}	0.404	0.620	0.98
250	PHBV	36.1 e^{-4}	0.507	0.619	0.98
	PHBV-FGS 0,5	36.9 e^{-4}	0.412	0.591	0.98
	PHBV-FGS 1,5	40.2 e^{-4}	0.390	0.610	0.98
	PHBV-FGS 3	52.8 e^{-4}	0.388	0.591	0.97

observed when the FGS content increased. This indicated that lower energy was necessary to start the degradation process, which was reflected in the increase of the isothermal degradation kinetic rate constant and hence in the thermal degradation rate.

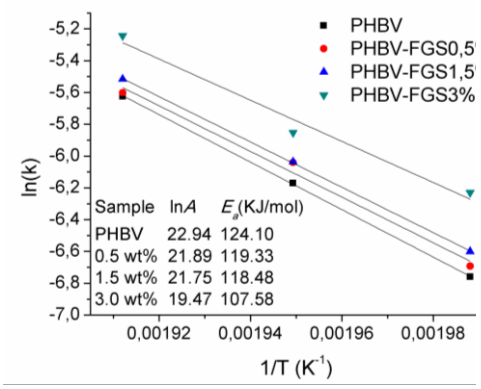

Figure 9. Arrhenius plots of ln(k) versus 1/T for PHBV and PHBV-FGS nanocomposites.

4. CONCLUSIONS

In this work PHBV-FGS nanocomposites were successfully obtained through the ball milling technique and the effect of FGS addition was studied. The morphological characterization revealed good dispersion of the filler which was also well distributed, although for high loadings, filler concentration areas were observed. Isothermal and non-isothermal crystallization analysis confirmed that addition of FGS did not lead to changes in the crystallization mechanism. However, an effect in the crystallization rate and in the crystal shape was observed. FGS was seen to act as a nucleating agent, increasing the overall crystallization rate and the crystallization degree leading to a more heterogeneous crystallization. It was demonstrated that these effects were strongly dependent on the FGS content since at high loadings, the nucleation effect was hindered to some extent, negatively affecting the crystallization process even after a controlled cooling process. Furthermore, a decrease in thermal stability was observed, especially under air conditions, mainly ascribed to the low heat barrier effect of the FGS which made heat diffusion easier and faster through the matrix. This work provides evidence that the ball milling technique can be successfully applied to develop graphene-based nanocomposites with good dispersion and distribution of the filler into the polymer matrix.

REFERENCES

[1] Martínez-Sanz M, Villano M, Oliveira C, Albuquerque MGE, Majone M, Reis M, et al. (2014) Characterization of polyhydroxyalkanoates synthesized from microbial mixed cultures and of their nanobiocomposites with bacterial cellulose nanowhiskers. New Biotechnology 31(4):364-376.

[2] Pardo-Ibáñez P, Lopez-Rubio A, Martínez-Sanz M, Cabedo L, Lagaron JM. (2014) Keratin-polyhydroxyalkanoate melt-compounded composites with improved barrier properties of interest in food packaging applications. Journal of Applied Polymer Science 131(4).

[3] Yoshie N, Azuma Y, Sakurai M, Inoue Y. (1995) Crystallization and compatibility of poly(vinyl alcohol)/poly(3-hydroxybutyrate) blends: influence of blend composition and tacticity of poly(vinyl alcohol). Journal of Applied Polymer Science 56(1):17-24.

[4] Roa JPB, De O. Patrício PS, Oréfice RL, Lago RM. (2013) Improvement of the thermal properties of poly(3-hydroxybutyrate) (PHB) by low molecular weight polypropylene glycol (LMWPPG) addition. Journal of Applied Polymer Science 128(5):3019-3025.

[5] Hinüber C, Häussler L, Vogel R, Brünig H, Heinrich G, Werner C. (2011) Hollow fibers made from a poly(3-hydroxybutyrate)/poly-ε-caprolactone blend. Express Polymer Letters 5(7):643-652.

[6] Sridhar V, Lee I, Chun HH, Park H. (2013) Graphene reinforced biodegradable poly(3-hydroxybutyrate-co-4-hydroxybutyrate) nano-composites. Express Polymer Letters 7(4):320-328.

[7] Guinault A, Sollogoub C, Domenek S, Grandmontagne A, Ducruet V. (2010) Influence of crystallinity on gas barrier and mechanical properties of pla food packaging films. International Journal of Material Forming 3(SUPPL. 1):603-606.

[8] Drieskens M, Peeters R, Mullens J, Franco D, Iemstra PJ, Hristova-Bogaerds DG. (2009) Structure versus properties relationship of poly(lactic acid). I. effect of crystallinity on barrier properties. Journal of Polymer Science, Part B: Polymer Physics 47(22):2247-2258.

[9] Russo P, Carfagna C, Cimino F, Acierno D, Persico P. (2013) Biodegradable composites reinforced with kenaf fibers: Thermal, mechanical, and morphological issues. Advances in Polymer Technology 32(SUPPL.1):E313-E322.

[10] Dagnon KL, Chen HH, Innocentini-Mei LH, D'Souza NA. (2009) Poly[(3-hydroxybutyrate)-co-(3-hydroxyvalerate)]/layered double hydroxide nanocomposites. Polymer International 58(2):133-141.

[11] Sanchez-Garcia MD, Lagaron JM. (2010) Novel clay-based nanobiocomposites of biopolyesters with synergistic barrier to UV light, gas, and vapour. Journal of Applied Polymer Science 118(1):188-199.

[12] Achilias DS, Panayotidou E, Zuburtikudis I. (2011) Thermal degradation kinetics and isoconversional analysis of biodegradable poly(3-hydroxybutyrate)/ organo-modified montmorillonite nanocom-posites. Thermochimica Acta 514(1-2):58-66.

[13] Sorrentino A, Gorrasi G, Vittoria V. Permeability in Clay/Polyesters Nano-Biocomposites. In: Avérous L, Pollet E, editors. Environmental Silicate Nano-Biocomposites: Springer London; 2012. p. 237-264.

[14] Ramanathan T, Abdala AA, Stankovich S, Dikin DA, Herrera-Alonso M, Piner RD, et al. (2008) Functionalized graphene sheets for polymer nanocomposites. Nature Nanotechnology 3(6):327-331.

[15] Gorrasi G, Bredeau S, Candia CD, Patimo G, Pasquale SD, Dubois P. (2012) Carbon nanotube-filled ethylene/vinylacetate copolymers: From in situ catalyzed polymerization to high-performance electro-conductive nanocomposites. Polymers for Advanced Technologies 23(11):1435-1440.

[16] Gorrasi G, Bredeau S, Di Candia C, Patimo G, De Pasquale S, Dubois P. (2011) Electroconductive polyamide 6/MWNT nanocomposites: Effect of nanotube surface-coating by in situ catalyzed polymerization. Macromolecular Materials and Engineering 296(5):408-413.

[17] Gorrasi G, Sarno M, Di Bartolomeo A, Sannino D, Ciambelli P, Vittoria V. (2007) Incorporation of carbon nanotubes into polyethylene by high energy ball milling: Morphology and physical properties. Journal of Polymer Science, Part B: Polymer Physics 45(5):597-606.

[18] Ouyang C, Luo J, Wang Y, Zhang Z. (2012) Preparation of modified multiwalled carbon nanotubes reinforcing poly(lactic acid) composites. Lizi Jiaohuan Yu Xifu/Ion Exchange and Adsorption 28(4):343-351.

[19] Dottori M, Armentano I, Fortunati E, Kenny JM. (2011) Production and properties of solvent-cast poly(ε-caprolactone) composites with carbon nanostructures. Journal of Applied Polymer Science 119(6):3544-3552.

[20] Lai M, Li J, Yang J, Liu J, Tong X, Cheng H. (2004) The morphology and thermal properties of multi-walled carbon nanotube and poly(hydroxybutyrate-co-hydroxy-valerate) composite. Polymer International 53(10):1479-1484.

[21] Shan GF, Gong X, Chen WP, Chen L, Zhu MF. (2011) Effect of multi-walled carbon nanotubes on crystallization behavior of poly(3-hydroxybutyrate-co-3-hydroxyvalerate). Colloid and Polymer Science 289(9):1005-1014.

[22] Yu HY, Yao JM, Qin ZY, Liu L, Yang XG. (2013) Comparison of covalent and noncovalent interactions of carbon nanotubes on the crystallization behavior and thermal properties of poly(3-hydroxybutyrate- co-3-hydroxyvalerate). Journal of Applied Polymer Science 130(6):4299-4307.

[23] Ma Y, Zheng Y, Wei G, Song W, Hu T, Yang H, et al. (2012) Processing, structure, and properties of multiwalled carbon nanotube/poly(hydroxybutyrate-co-valerate) biopolymer nanocomposites. Journal of Applied Polymer Science 125(SUPPL. 1):E620-E629.

[24] Vidhate S, Innocentini-Mei L, D'Souza NA. (2012) Mechanical and electrical multifunctional poly(3-hydroxybutyrate-co-3- hydroxyvalerate)-multiwall carbon nanotube nanocomposites. Polymer Engineering and Science 52(6):1367-1374.

[25] Jiang X, Drzal LT. (2012) Exploring the potential of exfoliated graphene nanopla-telets as the conductive filler in polymeric nanocomposites for bipolar plates. Journal of Power Sources 218:297-306.

[26] Pinto AM, Cabral J, Tanaka DAP, Mendes AM, Magalhães FD. (2013) Effect of incorporation of graphene oxide and gra-phene nanoplatelets on mechanical and gas permeability properties of poly(lactic acid) films. Polymer International 62(1):33-40.

[27] Verdejo R, Bernal MM, Romasanta LJ, Lopez-Manchado MA. (2011) Graphene filled polymer nanocomposites. Journal of Materials Chemistry 21(10):3301-3310.

[28] Bao C, Song L, Xing W, Yuan B, Wilkie CA, Huang J, et al. (2012) Preparation of graphene by pressurized oxidation and multiplex reduction and its polymer nanocomposites by masterbatch-based melt blending. Journal of Materials Chemistry 22(13):6088-6096.

[29] Wang J, Wang X, Xu C, Zhang M, Shang X. (2011) Preparation of graphene/poly(vinyl alcohol) nanocomposites with enhanced mechanical properties and water resistance. Polymer International 60(5):816-822.

[30] El Achaby M, Qaiss A. (2013) Processing and properties of polyethylene reinforced by graphene nanosheets and carbon nanotubes. Materials and Design 44:81-89.

[31] Stankovich S, Dikin DA, Dommett GHB, Kohlhaas KM, Zimney EJ, Stach EA, et al. (2006) Graphene-based composite materials. Nature 442(7100):282-286.

[32] Wang BJ, Zhang YJ, Zhang JQ, Gou QT, Wang ZB, Chen P, et al. (2013) Crystallization behavior, thermal and mechanical properties of PHBV/graphene nanosheet composites. Chinese Journal of Polymer Science (English Edition) 31(4):670-678.

[33] Shaw WJD. Current understanding of mechanically alloyed polymers. Switzerland: Trans Tech Publication 1998. p. 19-30.

[34] Gorrasi G, Piperopoulos E, Lanza M, Milone C. (2013) Effect of morphology of the filler on the electrical behaviour of poly(L-lactide) nanocomposites. Journal of Physics and Chemistry of Solids 74(1):1-6.

[35] Vertuccio L, Gorrasi G, Sorrentino A, Vittoria V. (2009) Nano clay reinforced PCL/starch blends obtained by high energy ball milling. Carbohydrate Polymers 75(1):172-179.

[36] Perrin-Sarazin F, Sepehr M, Bouaricha S, Denault J. (2009) Potential of ball milling to improve clay dispersion in nanocomposites. Polymer Engineering and Science 49(4):651-665.

[37] Wu H, Zhao W, Chen G. (2012) One-pot in situ ball milling preparation of polymer/graphene nanocomposites. Journal of Applied Polymer Science 125(5):3899-3903.

[38] Wu H, Zhao W, Hu H, Chen G. (2011) One-step in situ ball milling synthesis of polymer-functionalized graphene nanocomposites. Journal of Materials Chemistry 21(24):8626-8632.

[39] Schniepp HC, Li JL, McAllister MJ, Sai H, Herrera-Alonson M, Adamson DH, et al. (2006) Functionalized single graphene sheets derived from splitting graphite oxide. Journal of Physical Chemistry B 110(17):8535-8539.

[40] Verdejo R, Barroso-Bujans F, Rodriguez-Perez MA, De Saja JA, Lopez-Manchado MA. (2008) Functionalized graphene sheet filled silicone foam nanocomposites. Journal of Materials Chemistry 18(19):2221-2226.

[41] Branciforti MC, Corrêa MCS, Pollet E, Agnelli JAM, Nascente PADP, Avérous L. (2013) Crystallinity study of nano-biocomposites based on plasticized poly(hydroxybutyrate-co-hydroxyvalerate) with organo-modified montmorillonite. Polymer Testing 32(7):1253-1260.

[42] Horng YT, Chien CC, Huang CT, Wei YH, Chen SY, Lan JCW, et al. (2013) Biosynthesis of poly(3-hydroxybutyrate-co-3-hydroxy-valerate) with co-expressed propionate permease (prpP), beta-ketothiolase B (bktB), and propionate-CoA synthase (prpE) in Escherichia coli. Biochemical Engineering Journal 78:73-79.

[43] Wang X, Chen Z, Chen X, Pan J, Xu K. (2010) Miscibility, crystallization kinetics, and mechanical properties of poly(3-hydroxybutyrate - co - 3-hydroxyvalerate) (PHBV) /poly(3-hydroxybutyrate-co-4-hydroxybutyrate)(P3/4HB) blends. Journal of Applied Polymer Science 117(2):838-848.

[44] El Achaby M, Arrakhiz FZ, Vaudreuil S, Essassi EM, Qaiss A, Bousmina M. (2013) Preparation and characterization of melt-blended graphene nanosheets-poly(vinylidene fluoride) nanocomposites

with enhanced properties. Journal of Applied Polymer Science 127(6):4697-4707.

[45] Kim IH, Jeong YG. (2010) Polylactide/exfoliated graphite nanocomposites with enhanced thermal stability, mechanical modulus, and electrical conductivity. Journal of Polymer Science, Part B: Polymer Physics 48(8):850-858.

[46] Gunaratne LMWK, Shanks RA. (2005) Multiple melting behaviour of poly(3-hydroxybutyrate-co-hydroxyvalerate) using step-scan DSC. European Polymer Journal 41(12):2980-2988.

[47] Jiang L, Morelius E, Zhang J, Wolcott M, Holbery J. (2008) Study of the poly(3-hydroxybutyrate-co-3- hydroxyvalerate) /cellulose nanowhisker composites prepared by solution casting and melt processing. Journal of Composite Materials 42(24):2629-2645.

[48] Owen AJ, Heinzel J, Škrbić Ž, Divjaković V. (1992) Crystallization and melting behaviour of PHB and PHB/HV copolymer. Polymer 33(7):1563-1567.

[49] Wang S, Song C, Chen G, Guo T, Liu J, Zhang B, et al. (2005) Characteristics and biodegradation properties of poly(3-hydroxybutyrate-co- 3-hydroxyvalerate)/organophilic montmorillonite (PHBV/OMMT) nanocomposite. Polymer Degradation and Stability 87(1):69-76.

[50] Bittmann B, Bouza R, Barral L, Diez J, Ramirez C. (2013) Poly(3-hydroxybutyrate-co-3-hydroxyvalerate)/clay nanocomposites for replacement of mineral oil based materials. Polymer Composites 34(7):1033-1040.

[51] Ten E, Jiang L, Wolcott MP. (2012) Crystallization kinetics of poly(3-hydroxybutyrate-co-3-hydroxyvalerate)/ cellulose nanowhiskers composites. Carbohydrate Polymers 90(1):541-550.

[52] De Santis F, Pantani R. (2013) Nucleation density and growth rate of polypropylene measured by calorimetric experiments. Journal of Thermal Analysis and Calorimetry 112(3):1481-1488.

[53] Goffin AL, Raquez JM, Duquesne E, Siqueira G, Habibi Y, Dufresne A, et al. (2011) From interfacial ring-opening polymerization to melt processing of cellulose nanowhisker-filled polylactide-based nanocomposites. Biomacromolecules 12(7):2456-2465.

[54] Mensitieri G, Di Maio E, Buonocore GG, Nedi I, Oliviero M, Sansone L, et al. (2011) Processing and shelf life issues of selected food packaging materials and structures from renewable resources. Trends in Food Science and Technology 22(2-3):72-80.

[55] Erceg M, Kovačić T, Klarić I. (2009) Poly(3-hydroxybutyrate) nanocomposites: Isothermal degradation and kinetic analysis. Thermochimica Acta 485(1-2):26-32.

[56] Erceg M, Kovačić T, Sanja P. (2010) Isothermal degradation of poly(3-hydroxybutyrate)/organically modified montmorillonite nanocomposites. Polymer Composites 31(2):272-278.

[57] Wu TM, Hs SF, Shih YF, Liao CS. (2008) Thermal degradation kinetics of biodegradable poly(3-hydroxybutyrate)/ layered double hydroxide nanocomposites. Journal of Polymer Science, Part B: Polymer Physics 46(12):1207-1213.

[58] Cyras VP, Vázquez A, Rozsa C, Galego Fernández N, Torre L, Kenny JM. (2000) Thermal stability of P(HB-co-HV) and its blends with polyalcohols: crystallinity, mechanical properties, and kinetics of degradation. Journal of Applied Polymer Science 77(13):2889-2900.

Chapter 7

ON THE USE OF BALL MILLING TO DEVELOP PHBV-GRAPHENE NANOCOMPOSITES (I): MECHANICAL, BARRIER AND ELECTRICAL PROPERTIES

J. Ambrosio-Martín[a], G. Gorrasi[b], A. Lopez-Rubio[a], M. J. Fabra[a], L. Cabedo[c], M.A. López Manchado[d] and J. M. Lagaron[a]

Journal of Applied Polymer Science 2015, 132(29):42217

[a] Novel Materials and Nanotechnology Group, IATA-CSIC, Avda. Agustin Escardino 7, 46980 Paterna (Valencia), Spain.

[b] Department of Industrial Engineering, University of Salerno, via Giovanni Paolo II, 132 84084 Fisciano (Salerno), Italy.

[c] ESID, Universitat Jaume I, Av. Vicent Sos Baynat s/n, 12071 Castellón, Spain.

[d] Institute of Polymer Science and Technology, (CSIC), Juan de la Cierva, 3, 28006 Madrid, Spain.

ABSTRACT

In this work, poly (3-hydroxybutyrate-co-3-hydroxyvalerate) (PHBV) nanocomposites containing functionalized graphene sheets (FGS) were prepared by means of high energy ball milling. The crystalline structure, oxygen barrier, mechanical and electrical properties and biodegradability of the developed nanocomposites were analysed and correlated with the amount of FGS incorporated and with their morphology, which was reported in a previous study. Addition of FGS into the PHBV matrix did not affect the crystal morphology of the material but led to somewhat enhanced crystallinity. The good dispersion and distribution of the nanofiller within the polymeric matrix, revealed in the first part of this study, was thought to be crucial for the mechanical reinforcing effect of FGS and also resulted in enhanced gas barrier properties at high relative humidity. Additionally, the conducting behaviour of the nanocomposites, as interpreted by the percolation theory, displayed a very low percolation threshold set at ~0.3 vol% of FGS, while the materials exhibited an overall significantly enhanced conductivity.

Keywords: Biopolymers & Renewable Polymers; blends; graphene and fullerenes

1. INTRODUCTION

Great efforts have been focused on the development of environmentally friendly biodegradable polymers in the last decades due to the non renewable and non biodegradable character of the petroleum-based synthetic polymers, particularly in the packaging area, where a huge amount of plastic waste is generated on a daily basis. Polyhydroxyalkanoates (PHAs) are one of the most studied families of thermoplastic biodegradable polymers not only due to their environmentally-friendly properties such as biodegradability, biocompatibility and renewable character but also because these materials have mechanical properties similar to those of conventional petroleum-based polymers, relatively good thermal properties, melt compounding processability and high stiffness due to its high crystallinity degree [1]. Specifically, poly (3-hydroxybutyrate-co-3- hydroxyvalerate) (PHBV), the copolymers which belong to the PHAs family, have been extensively studied and quickly identified as good candidates to replace fossil-based commodity polymers. However, several properties of these biopolymers, including the mechanical, thermal and barrier properties need to be balanced or improved in order to extend their field of application [1,2]. Among the strategies used to balance these physical properties, the use of organic and inorganic nanofillers as reinforcing agents have been extensively used. For instance, inorganic nanofillers such as carbon nanotubes [3] and nanoclays [4-6] have been used. In the case of organic fillers, cellulose nanocrystals [1, 7-9] have been the most widely used material for this purpose.

In last years, graphene, a two dimensional material consisting of a single layer of carbon atoms packed in a hexagonal lattice, has gained much attention due to its remarkable physical properties such as mechanical, thermal and electrical properties. Because of that, graphene materials are expected to be used in a variety of applications including sensors, batteries, supercapacitors, active and intelligent packaging devices and hydrogen storage systems [10].

Out of all the processes for the production of graphene, e.g. mechanical exfoliation, chemical exfoliation, chemical vapour deposition or epitaxial growth, the reduction of graphene derivatives such as graphene oxide has attracted more attention since it is a route able to produce graphene sheets in both colloidal dispersions and powder forms with high processability. Moreover, the presence of oxygen functionalities in the graphene oxide is very interesting from a chemical point of view. Therefore, graphene derivatives are also expected to serve as reinforcement fillers in nanocomposite materials since they provide reactive sites for chemical interactions with the matrix [10, 11]. The most well-known processes to prepare polymer nanocomposites are solution casting, *in situ* polymerization and melt blending [12, 13]. Graphene and its derivatives have already been extensively used as reinforcing agents in different polymer and biopolymer matrices such as polyvinyl alcohol (PVA) [14] , polyethylene (PE) [15], polyamide-6 (PA6) [16], polystyrene (PS) [17, 18], poly (lactic acid) (PLA) [13] and PHBV [2]. In these studies, improved mechanical, thermal and/or electrical properties were reported. Thus, for example, improvement in Young's Modulus (of up to 10 fold) [19] and in electrical conductivity (up to 13 orders of magnitude) [20] were reported after incorporation of graphene in PVA by solution casting. Similar reinforcing effects, where the storage modulus was seen to increase by up to 118% for PE-nanocomposites obtained by solution casting [21] and 87% and 77% in Young's Modulus and tensile strength, respectively,

for those PE-nanocomposites obtained by melt compounding [15] were also reported. Moreover, PE-graphene nanocomposites obtained by *in situ* polymerization showed improvements in thermal stability with an increase in thermal degradation temperature of up to 30 °C and in electrical properties of up to 9 orders of magnitude [22]. Regarding the use of graphene and its derivatives to reinforce biopolymer matrices, Kim et al. [23] prepared polylactide nanocomposites with exfoliated graphite via melt compounding. The thermal stability, mechanical modulus and electrical conductivity were significantly improved. Pinto et al. [24] showed improvements of up to 85% and 15% in Young's Modulus and tensile strength, respectively, after addition of both graphene oxide and graphene nanoplatelets in PLA via solution casting with no differences between both fillers. Moreover, in the work of Shen et al. [25] an increased electrical conductivity of up to 15 orders of magnitude, was also reported upon addition of chemically reduced graphene oxide into PLA using the same incorporation route. Although, it is widely known that solution casting leads to a relative good dispersion of graphene within polymeric matrices, a recent study demonstrated that surface modification of graphene oxide by grafting PLA chains prior to the solution casting further enhances the dispersion of the filler and resulted in higher mechanical properties [26]. *In situ* ring opening polymerization has also been used to prepare PLA grafted to thermally reduced graphene oxide (TRG) sheets with improvements of up to 18 °C in thermal degradation temperature and up to 12 orders of magnitude in electrical conductivity. An enhanced dispersion was obtained if compared with the materials obtained by melt blending PLA with TRG [27]. In the open literature, there are very few studies reporting on the incorporation of graphene into PHBV. Sridhar et al. [2] reported enhancements in mechanical properties and thermal stability of PHBV with improvements in tensile strength (25%), elastic modulus (higher than 100%) and thermal degradation temperature (10 °C) after incorporation of 6 wt.% of graphene into PHBV by solution casting. Furthermore, Wang et al. [28] observed similar effects, with an increase of 18 °C on thermal degradation temperature and improvements in the storage modulus in the whole temperature range analyzed. In this case, solution casting was also used to incorporate graphene into PHBV but lower amount of filler, 1wt.%, was necessary to achieve those improvements. To the best of our knowledge, there is no previous study dealing with the effect of graphene on the electrical and barrier properties of PHBV-based nanocomposites.

As it is widely recognized, *in situ* polymerization and solution casting are the most widely used routes to prepare polymer-graphene nanocomposites, mainly due to dispersion issues, since good results can be obtained through these methodologies [13]. However, both of them require a significant amount of organic solvents which are toxic and expensive and hence not convenient for industrial applications. On the contrary, although melt mixing is a more appropriate technique from an industrial view point, it leads to poorer dispersion of graphene into the polymer matrices. Despite of that, melt mixing can still be employed as a post-treatment after solution processing to develop graphene-based nanocomposites as previously described in different studies [13, 29, 30]. This strategy, which is a two steps process including the handling of liquids, has limited industrial scalability, although it provides an uniform dispersion of the filler avoiding the stacking or re-aggregation of the nanosheets.

Besides the mechanical reinforcing effect discussed above, graphene has a lamellar

impermeable structure which can, in principle, should perform as a barrier element in polymer nanocomposites potentially decreasing gas and vapour permeability [2]. As previously reported, the incorporation of nanoplatelet structured fillers into polymer matrices has demonstrated to be an effective strategy to generate high barrier polymer films, mainly due to two factors, (i) increased tortuosity of the pathway leading to a reduction in the diffusion coefficient and (ii) reduction of the free volume by modification of the polymer chains mobility due to the adhesion between the filler and the polymer matrix [31]. Previous studies in the literature have corroborated the barrier effect of graphene-based nanofillers in polymer matrices [12]. For instance, reduced oxygen permeability of PLA-graphene nanocomposites has been reported showing reductions of up to 45% [31] or 68% [24]. Higher permeability reductions of up to 90%, were obtained in polyphenylene sulfide nanocomposites, although a high loading of the filler was required [32].

A novel strategy that is being explored for the development of nanocomposites, is the solvent free processing method of the ball milling technique, which has demonstrated to be specially interesting for clay-based and carbon-based nanocomposites [33-38]. This technique is based in a high-energy milling, able to induce several mechanical and chemical changes in the materials. Moreover, graphene-based nanocomposites have also been synthesized by ball milling since this high energy milling induces graphite delamination improving the final properties of the obtained materials [37]. An effective grafting of polystyrene matrix (PS) onto the surface of graphene sheets using ball milling was reported, demonstrating, in this way, the effectiveness of the mechano-chemical character of this technique [38]. Furthermore, graphene nanoplateles were successfully incorporated into polyphenylene sulfide by ball milling with enhancement in mechanical, electrical and barrier properties [32]. To the best of our knowledge, the high energy ball milling technique (HEBM) has not been used up to date to develop PHBV-graphene nanocomposites or to show the effect of this processing technique in barrier properties. Because of this, the aim of the current study was to assess the use of this technique for the production of PHBV-graphene nanocomposites. As mentioned above this technique does not require the use of solvents or pre-treatments of the filler, thus being a one step process. The presence of oxygen functionalities in the graphene surface is very interesting from a chemical point of view, making it a suitable filler to create nanocomposites, as commented. Because of that, functionalized graphene sheets were used in an attempt to optimize the filler-matrix compatibilization.

In the first part of this study, functionalized graphene sheets were introduced into PHBV by means of HEBM. The morphology, thermal properties and thermal stability of the obtained materials were evaluated and it was found that this technique led to a relatively good dispersion and distribution of the nanofiller within the polymer matrix, resulting in enhanced crystallinity due to the nucleating effect of the FGS. In the present work, the crystalline structure, mechanical, barrier and electrical properties as well as the biodegradability of the nanocomposites developed were evaluated, and related to their earlier morphological and thermal characterization.

2. MATERIALS AND METHODS

2.1. Materials

The bacterial polyhydroxyalkanoate grade was purchased from Goodfellow Cambridge Limited, UK, in pellet form

(density 1.25 g cm^{-3}). The supplied material was a melt-processable semicrystalline thermoplastic PHBV12 (polyhydroxybutyrate with 12 mol% of valerate and containing 10 wt.% of the plasticizer citric ester) copolymer made by biological fermentation from renewable carbohydrate feedstocks. Prior to the ball milling process, the material was purified by dissolution in $CHCl_3$ and subsequent precipitation by drop-wise addition to an excess of methanol. The material, in this way, was transformed from pellet to powder form which was necessary for the ball milling process.

Functionalized graphene sheets (FGS) were synthesized by thermal reduction of graphite oxide at 1000°C for 30s under air atmosphere. Briefly, graphite powder (purum powder < 0.1 mm, Sigma Aldrich) was dispersed in 20 mL of fuming nitric acid for 20 min; next, potassium chlorate (8 g) was slowly added over 1 h and the reaction mixture was stirred for 21 h at 0°C. Graphene produced through this method leads to the formation of single graphene layers or stacks of up to 7 sheets with hydroxyl, carbonyl and epoxy groups on their surface [11]. A full description of the synthesis and characterization of the FGS can be found elsewhere [39].

2.2. Sample preparation (High energy ball milling - HEBM)

FGS and PHBV powder were milled in the solid state in a Retsch (Germany) centrifugal ball mill (model PM100). The milling process was carried out in a cylindrical steel jar of 50 cm^3 with 5 steel balls of 10 mm of diameter. The rotation speed used was 650 rpm and the milling time was fixed to 60 min. In these experimental conditions, six series of composites PHBV-FGS with 0.1, 0.5, 1.0, 1.5, 2.0, and 3.0 wt.% of FGS were prepared. An additional PHBV sample without filler to be taken as a reference was also milled in the same conditions. For the characterization, PHBV-FGS mixtures and the pure milled PHBV were molded in a hot press (Carver Inc.). To this aim the material was heated up to 175 °C and kept at this temperature for 5 min. Subsequently, the material was hot pressed and cooled at room temperature giving rise to 250 ± 50 μm thick films. An illustration about the preparation of the PHBV/FGS nanocomposites can be seen in the first part of this work.

2.3. X-ray (XRD)

X-ray diffraction measurements (XRD) were performed with a Brucker diffractometer (equipped with a continuous scan attachment and a proportional counter) with Ni-filtered Cu Kα radiation (λ= 1.54050 Å). The samples were examined over the angular range of 2° to 40°.

2.4. Mass transport properties

Water barrier properties (sorption, diffusion) were evaluated using a microbalance SMS DVS Advantage-2 system. This system has a sensitivity of ±1.0μg, and allows the measurements of mass changes due to sorption or desorption of vapour molecules. In this work the chosen method consisted in submitting the sample to pressure steps at constant temperature. The tests were conducted using water vapour in a nitrogen atmosphere at 30 °C. The starting samples were dry, square films having a thickness of 200 μm and a side of 15 mm. The experimental protocol considered steps of relative humidity (RH) from 0 to 98%.

2.5. Oxygen transmission rate

The oxygen permeability coefficient was derived from oxygen transmission measurements recorded using an Oxtran

100 equipment (Modern Control Inc., Minneapolis, MN, US). Experiments were carried out at 24 °C and at 80% RH conditions. RH was generated by a built-in gas bubbler and was checked with a hygrometer placed at the exit of the detector. The samples were purged with nitrogen for a minimum of 20 h in the humidity equilibrated samples, prior to exposure to an oxygen flow of 10 ml min^{-1}. A 5 cm^2 sample area was measured by using an in-house developed mask. The measurements were done in duplicate.

2.6. Dynamic mechanical analysis (DMA)

Mechanical properties were evaluated using a DMA TAQ800. Measurements were conducted at the constant frequency (1Hz) and amplitude (5μm). The temperature was varied between -30 °C and 140 °C at 3 °C min^{-1}.

2.7. Electrical properties

The electrical conductivity was measured at room temperature with a Keithley 6517A electrometer unit in a two-probe resistance measurement configuretion controlled by a computer. The source delay for each point of measurement was about 3 s. For each measurement, the sample was placed between two copper electrodes. To enhance the electrical contact between the samples and the electrodes, metallization with Au was used. The metallization was conducted using an Agar Auto Sputter Coater (Agar Scientific Limited-UK-). The metallization time was 180 sec, for a metal deposition of about 22 nm. The electrical conductivity was measured in the voltage range -10 to 10 V. The electrical conductivity, σ (S cm^{-1}), of all the samples was obtained by using the basic equation:

$$\sigma = \frac{L}{\tau W}\frac{1}{R} = \frac{L}{\tau W}\frac{I_{measured}}{V_{applied}} \quad (1)$$

where $R(\Omega)=V_{applied}/I_{measured}$, τ (m), W (m), and L (m) are the resistance, the thickness, the width and the length of the specimens, respectively.

2.8. Biodisintegration in composting conditions

The biodesintegration of the samples under controlled composting condition was evaluated according to standard ISO 20200 [40]. The solid waste was prepared by mixing 10% of compost (inoculum), 30% rabbit food, 10% starch, 5% sugar, 1% urea, 10% corn oil and 40% sawdust. The inoculum used in the present study was mature compost supplied by Burés Profesional, SA (Girona, España). Prior to the mixing step, the compost was sieved through a 5 mm sieve. According to the standard, the water content was adjusted to 55 wt.% and kept at this level throughout the whole duration of the experiment by adding water periodically. The samples were cut into squares of 1.5x1.5 cm^2, buried inside the waste at a depth of approximately 6cm and incubated at 58 °C during 90 days inside polypropylene boxes. The specimens were individually sandwiched in between two stainless steel meshes, thus allowing full direct contact with the waste, while simplifying the extraction and labeling of the samples. In order to ensure aerobic conditions to take place, holes were performed on the boxes and, according to the standard, the waste was periodically stirred gently. The samples were extracted at different disintegration times (7, 15, 27, 41, 56, 69, 76, 83 and 90 days) washed with distilled water, dried at 40 °C under vacuum for 24 h, and weighed. The disintegration degree was determined by normalizing the

sample weight for every incubation time to its initial weight.

3. RESULTS AND DISCUSSION

3.1. Crystal morphology of the nanocomposites

In the previous part of this study [41], DSC analysis under isothermal and non-isothermal conditions showed an influence of FGS incorporation on the kinetics and dynamics of PHBV crystallization. Specifically, the crystallization rate and the homogeneity of the crystals were altered and these effects were strongly dependent on the amount of FGS added to the polymer matrix. It was observed that addition of high concentrations of FGS somehow hindered the crystallization process, i.e. the increase in crystallinity was not as pronounced as with lower FGS contents but, at the same time, an acceleration of the crystallization process was observed. As a consequence, more defective or unstable crystals and a faster crystallization process were obtained when high FGS concentrations were used.

The crystal structure of the nanocomposite films was studied in the second part of this work by X-ray analysis. It has been previously reported that PHBV exhibits an isodimorphism phenomenon, and as a consequence the material could crystallize in either PHB unit cell or PHV unit cell, depending on the HV content. The transformation from the PHB lattice to the PHV lattice has been reported to occur at about 30 mol % HV [42]. However, Scandola et al. [43] reported that while for 34 mol% of HV, PHB crystalline phase was developed, and for 55 mol% of HV the X-ray diffraction spectra showed the pattern of the PHV crystalline phase, for 41 mol% of HV, PHB and PHV type crystals coexisted. It has also been previously reported that the reflection

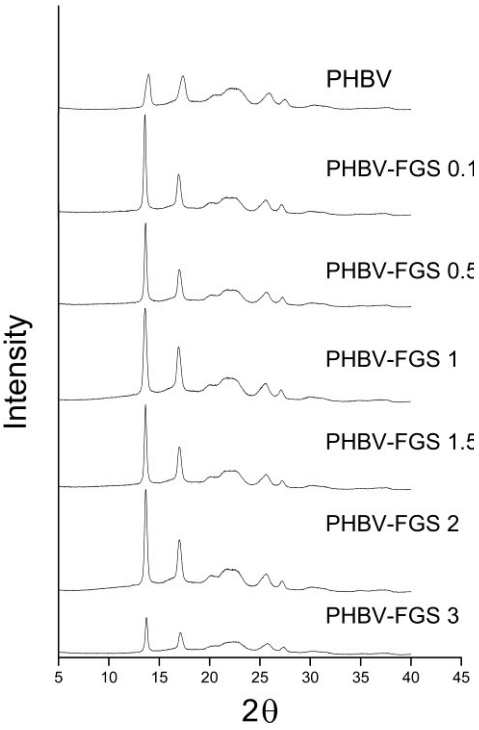

Figure 1. X-ray patterns of PHBV and its

at 2θ = 17° is associated with the (110) diffraction of PHB lattice, while that at 2θ = 18° is associated with the (020) diffraction of PHV lattice [44]. Figure 1 shows the diffractograms of the different samples. The diffractogram of PHBV shows that this biopolyester is a semicrystalline material with the characteristic reflections from an orthorhombic cell [2, 42, 45]. It can be observed that there was no diffraction peak at 2θ = 18° and, thus, only the typical PHB lattice was developed in the different materials. This result suggests that addition of graphene did not modify the crystal unit cell since the reflections for the nanocomposites appeared at the same diffraction angles than those from the neat polymer. In fact, the same spacing between planes were obtained for PHBV and its nanocomposites when applying Bragg´s law (cf. Table 1) suggesting that the parameters of PHBV unit cell were not influenced by FGS

addition. Nevertheless, addition of FGS resulted in sharper peaks for the (020) and (110) PHBV reflections when compared to those of pure PHBV. This could be related with an increase in the crystallites lamella size, thus confirming that addition of these nanofillers promoted crystallization [45]. Scherrer equation (Eq.2) was used to determine the crystallite size for the peak corresponding to the (020) reflection of PHBV and its nanocomposites.

$$L(nm) = \frac{K \cdot \lambda}{\beta \cdot \cos\theta} \quad (2)$$

where K is a dimensionless shape factor with a value close to unity, which is K=0.94 for orthorhombic cell [45], λ is the wavelength of the X-ray radiation which for CuKα radiation is 1.54Å, θ is the Bragg angle and β is the full width half maximum. From Table 1 it can be observed that the lamella size for the (020) reflection increased with the addition of FGS, confirming that addition of FGS effectively promoted the crystallization of PHBV, which is in agreement with previous works [45], although the increase observed here was much more pronounced. A slight decrease in crystal lamella size was observed for high loadings. This is in agreement with the observations reported in the first part of this work [41] related to reduced crystallization at high loadings. Moreover, in order to evaluate how the addition of FGS affected the crystal growth, the ratio between the intensity of the peaks related to (020) and (110) crystal planes was calculated and can also be seen in Table 1. An increase in the ratio was noticed with FGS addition, pointing out that the crystals grew preferentially in the direction of the (020) crystal plane, since an increase in the relative intensity of PHBV crystallite in a particular direction indicates that the PHBV crystals grow in a preferential orientation along that direction, as previously reported [45].

Therefore, taking into account the DSC analysis performed in the previous work in combination with the X-ray analysis, it could be concluded that addition of FGS to the PHBV matrix did not alter the morphology of the crystalline unit cell, but had an effect on the kinetics and dynamics of PHBV crystallization, leading to an increased crystallinity content in the nanocomposites.

Table 1. Calculated lamellar spacing and crystallite sizes of PHBV and its nanocomposites with FGS.

	d-spacing (nm)	Crystallite size L_{020} (nm)	$I_{(020)}/I_{(110)}$
PHBV	0.64	16.29	1.1
PHBV-FGS 0,1	0.65	30.80	2.3
PHBV-FGS 0,5	0.65	30.45	2.1
PHBV-FGS 1	0.65	29.88	1.6
PHBV-FGS 1,5	0.65	30.07	1.9
PHBV-FGS 2	0.65	26.49	1.9
PHBV-FGS 3	0.65	27.44	1.6

3.2. Mass Transport Properties

Graphene is considered a promising nanomaterial to promote gas or vapour barrier applications because perfect graphene sheets are able to block the diffusion of small molecules. A thorough revision about the use of graphene to improve barrier properties in polymer nanocomposites was carried out by Yoo et al. [12]. However, although a broad range of polymers, graphene types, and processing methods to develop graphene-based nanocomposite have been studied, no data was shown for PHBV nanocomposites nor for nanocomposites developed using ball milling. Although several works have reported about the incorporation of graphene into PHBV matrices [2, 28], to the best of our knowledge, the effect of this nanofiller on the transport properties of low molecular weight components through PHBV have not been previously investigated.

Mass transport properties such as water sorption and diffusion were evaluated for PHBV and PHBV-FGS 3.0 wt.%

nanocomposite. By measuring the normalized weight uptake over time, it is possible to infer the equilibrium concentration of sorbed water vapour, i.e. C_{eq} ($g_s/100g_p$), where g_s stands for grams of sorbed water vapour and g_p stands for grams of dry polymeric sample. Figure 2a reports the isotherms of water vapour sorption as a function of water activity (a_w). Similar water sorption isotherms were previously reported for PHB where a moderately hydrophobic character was assumed [46]. The hydrophobic character of the polymer was also reported for PHBV by others authors [47]. From the results, it can be seen that incorporation of FGS of 3 wt.% had no effect on water sorption since no changes in the isotherms were observed when compared with this of the neat PHBV.

Moreover, by fitting the experimental data to the corresponding Fick´s law (see Eq. 3), the diffusion coefficient, D ($cm^2\ s^{-1}$), can be calculated:

$$\frac{C_t}{C_{eq}} = 4\left(\frac{Dt}{\pi l^2}\right)^{1/2} = \left(\frac{16D}{\pi l^2}\right)^{1/2} t^{1/2} \qquad (3)$$

where C_t and C_{eq} are the weight uptake for a given time t and at equilibrium, respectively, and l is the sample thickness.

Figure 2b shows the diffusion coefficients, D ($cm^2\ s^{-1}$), as a function of the equilibrium water uptake, C_{eq} ($g_s/100g_p$). The diffusion behaviour was found to be very similar for both samples at each concentration with no effect on the water vapour diffusion coefficient upon addition of FGS. Recently published works, in which cellulose nanowhiskers or keratin were incorporated into PHBV, reported that only for filler loadings of 1 wt.% there was a positive effect on water barrier properties. For higher filler loadings, no effect or even negative effects on water barrier properties were found [1, 48].

The oxygen permeability measured at 80% RH was also evaluated. Figure 3 displays the oxygen permeability of the PHBV and its nanocomposites. A decrease in oxygen permeability was observed for all the nanocomposites in comparison with the neat PHBV. Generally, it could be said that the oxygen barrier increases with the FGS content, reaching a maximum in barrier performance at 3 wt.% filler loading exhibiting an oxygen permeability reduction of 41%. This barrier improvement is somehow in line with the oxygen barrier improvements reported in the existing literature by other preparation methods (see the Introduction section), indicating that ball milling appears to be an alternative processing route to generate nanocomposites for these materials. Previous works have also reported a decrease in oxygen permeability when

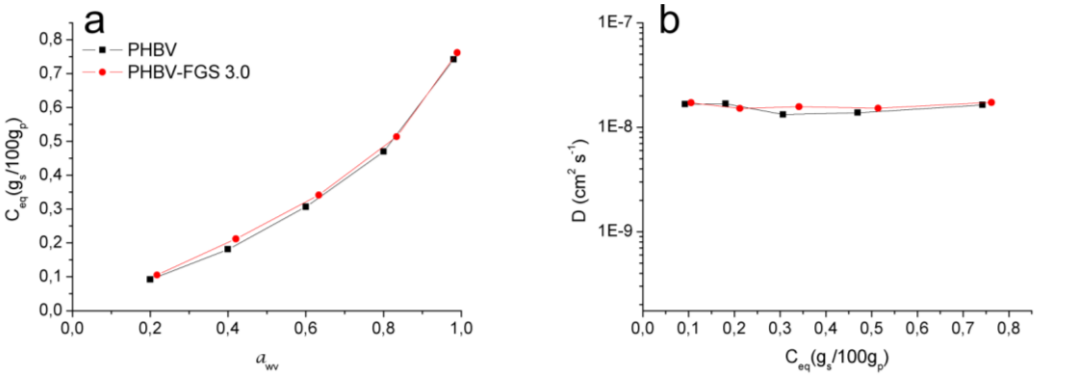

Figure 2. Sorption isotherms as function of water vapour activity (a_{wv}) (a) and diffusion coefficients versus equilibrium sorbed water (C_{eq}) (b) of water vapour for pure PHBV and PHBV-FGS 3.0 wt% nanocomposites.

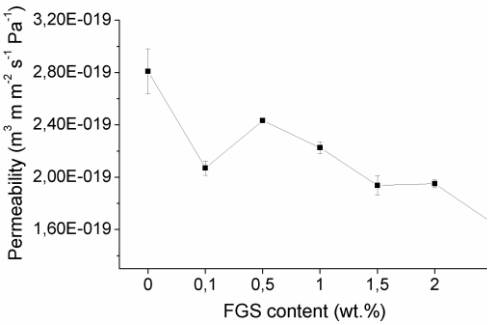

Figure 3. Oxygen permeability of pure PHBV and its nanocomposites with FGS.

graphene nanoplatelets are used as filler [24, 32, 46, 47]. It has been widely demonstrated that a good dispersion of the fillers and a good filler-matrix adhesion are crucial for improving barrier properties in polymer nanocomposites [49]. As observed in the morphological characterization of PHBV and its nanocomposites in the first part of this study [41] a good dispersion and distribution of the graphene lamellar structures were achieved. As a result, the improved barrier properties observed in the composites are here directly correlated with the favourably morphology observed in the results of the previous study. Moreover, as it is also widely known, an increase in crystallinity of semicrystalline biopolyesters has also been related to improved barrier properties mainly due to the tortuousity concept linked to the presence of the crystalline domains [50-53]. Addition of FGS into PHBV led to an increase in polymer crystallinity as measured by DSC in the first part of this study. Therefore, the increased oxygen permeability could also be ascribed to the increase in the crystalline fraction. In order to separate the effect of filler loading on the barrier performance from crystallinity alterations, the permeability drop across composition was divided by the crystallinity of the sample, to study, in relative terms, the impact of the filler in the barrier performance. This factor, which has been termed before as the filler efficiency barrier drop [6], is gathered in Table 2. From the results, an increased permeability drop compared to the neat polymer was observed as the FGS content increased except for the 0.5 and 1 wt.% of FGS compositions. As observed, higher crystallinity was obtained for the latter two compositions if compared, for instance, with that of the 0.1 wt.% FGS sample. Hence, the lower relative permeability drop for these two particular samples was directly ascribed to a lower blocking capacity per filler loading for these two particular samples. The samples with 0.1 wt.% and higher than 1 wt.% FGS led to more efficiency of the filler per filler loading in terms of blocking permeation.

3.3. Dynamic Mechanical Analysis

In many current applications, polymer and polymer-nanocomposites are subjected to many temperature and frequency fluctuations. In order to evaluate the effect of graphene on temperature dependent relaxation behaviour of PHBV matrix, thermo-mechanical properties were evaluated in some of the samples developed. Figure 4 shows the storage modulus and tan δ, also known as loss factor, as a function

Table 2. Filler barrier efficiency data for PHBV and its nanocomposites.

	Permeability Drop (%)	Simple crystallinity* (%X_c)	Filler Barrier Efficiency Permeability Drop(%)/%Crystallinity
PHBV	-	53.2	-
PHBV-FGS 0,1	26.3	59.5	0.44
PHBV-FGS 0,5	13.4	59.9	0.22
PHBV-FGS 1	20.8	61.9	0.33
PHBV-FGS 1,5	31.0	61.5	0.50
PHBV-FGS 2	30.6	57.3	0.53
PHBV-FGS 3	41.2	56.0	0.73

* Calculated in the first part of this work [41]

of temperature as well as the storage modulus at 25 °C and the maximum of tan δ which is related with the glass transition tempera-ture of the nanocomposites (T_g). T_g values of the developed materials could not be discerned by a conventional method of T_g measurement by DSC. Nevertheless, the glass transition temperature measured by DMA generally increased with FGS addition. This trend is consistent with previous works where graphene or multi-walled carbon nanotubes (MWNT) were incorporated in PHBV [2, 45]. The increase in T_g may be due to the restriction of the chain mobility within the polymer matrix upon addition of FGS. The neat PHBV exhibited a tan δ transition around 17 °C, which could be related to the glass transition of the amorphous PHBV molecules [54], whereas for PHBV-FGS nanocomposites the glass transition temperatures were around, 21 °C, 19 °C, 22 °C, and 24 °C for 0.5, 1, 2 and 3 wt.% respectively. In fact, at temperatures lower than T_g the loss factor for the pristine polymer was higher than for the nanocomposites. This means that high energy was dissipated, which could be mainly ascribed to internal frictions of polymer chains which, in turn, were related to increased mobility of those chains. The results also showed that the FGS nanofiller increased the storage modulus of the neat PHBV in the whole temperature span (cf. Figure 4). However at 0.5 wt.% filler content no effects were observed since no changes in the storage modulus curve were noticed. The reinforcing effect of graphene has been previously reported by several authors [2,13-15, 19, 55]. Although the storage modulus of nanocomposites was always

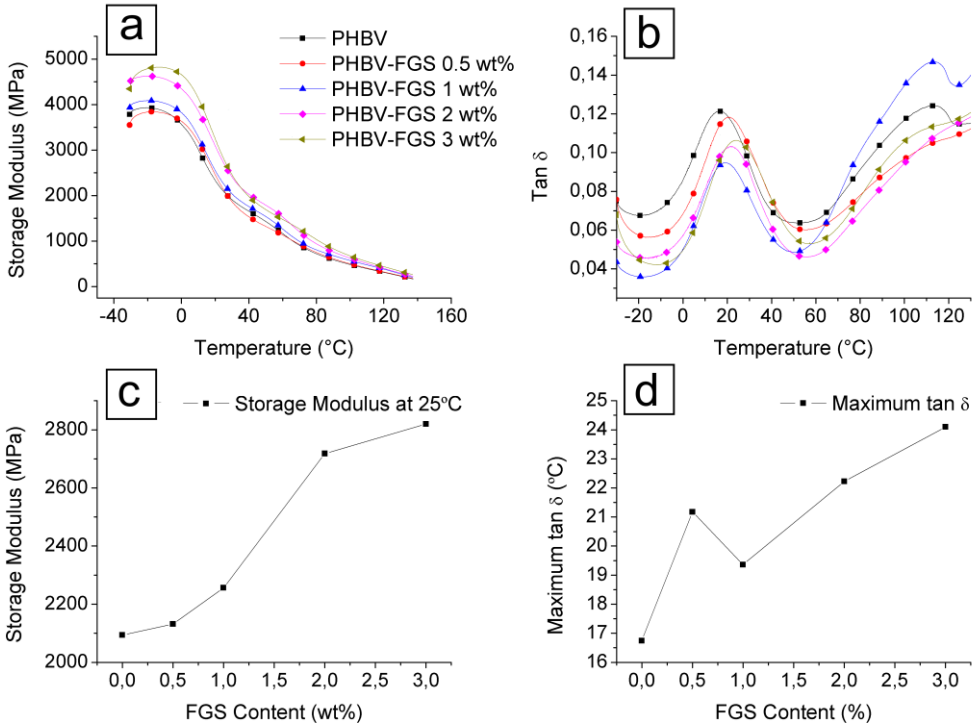

Figure 4. Dynamo-mechanical analysis of PHBV and its nanocomposites. Storage modulus (a) and tan δ (b) versus temperature, storage modulus at 25 °C (c) and maximum of tan δ (d).

higher than that for neat polymer, greater increases were observed at low temperatures ("glassy modulus") than those observed at temperatures above T_g ("rubbery modulus"). Evaluation of the storage modulus at 25 °C was carried out and the same trend was noticed, i.e an increase from 2.1 to 2.8 GPa (enhancement of 35%) for neat PHBV and PHBV-FGS 3 wt.% respectively (cf. Figure 4c). The same effects were observed for PHBV-graphene nanocomposites prepared through solution casting [2], and also in PHBV-MWNT prepared by means of direct melt mixing [45]. In addition, previous works incorporating graphene into PLA have reported that the storage modulus increased when increasing the graphene content even at low filler loadings [13]. The homogeneous dispersion of nanofillers and filler-matrix interfacial interactions are important factors in the development of high-performance polymer materials, which are directly related with improvements in mechanical properties. A comparative study of highly and poorly dispersed graphene/epoxy nanocomposites revealed that the highly dispersed graphene fillers are more efficient than the aggregated ones in transferring the applied load [56]. In view of the results, it could be generally stated that a good dispersion and filler-matrix adhesion were attained, being this premise supported by the oxygen barrier data.

3.4. Electrical Properties

A good dispersion of conductive carbonaceous materials such as carbon nanotubes, graphite, graphene and/or its derivatives into polymeric matrices, is widely known to improve the electrical properties of the final composite materials. Figure 5 shows the electrical conductivities of PHBV and its nanocomposites. Neat PHBV is electrically insulating with a low conductivity (~10^{-13} S cm^{-1}). Nevertheless,

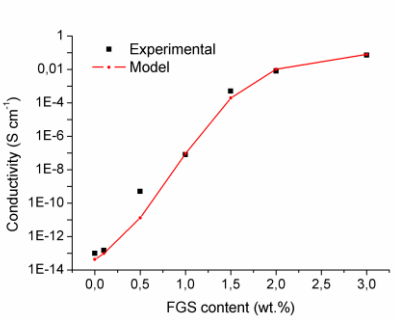

Figure 5. Experimental and calculated electrical conductivity versus filler loading for PHBV-FGS nanocomposites.

the addition of conducting FGS nanofillers significantly increased the conductivity of the materials. The S-shaped curves indicate that the nanocomposites exhibited a typical percolation transition from an insulator to a semiconductor [37, 38]. The percolation theory describes the behaviour of connected fillers in a randomly dispersed system. In this case, the connected fillers were FGS. An analytical model has been previously proposed, based on the Fermi-Dirac distribution, to describe the critical insulator to conductor transition [33].

$$\log(\sigma_c) = \log(\sigma_f) + \frac{\log\left(\frac{\sigma_p}{\sigma_f}\right)}{(1+\exp(t(\phi-\phi_c)))} \qquad (4)$$

where σ_c, σ_f and σ_p are the composite, filler, and polymer conductivities, respectively, ϕ is the FGS mass fraction, and t is an empirical parameter that leads to the change in conductivity at the percolation threshold ϕ_c. By assuming a constant value for σ_f and σ_p, from Eq. (4), the best fitted values of ϕ_c and t were obtained. Thus, the percolation threshold value of nanocomposites was calculated to be about ~0.8 wt.% (~ 0.3 vol%). It is thought that the low FGS content for electrical percolation threshold is related with the high aspect ratio of FGS and also to a homogeneously and well dispersed nanofiller into the polymer matrix, as observed by SEM and TEM (see the previous

study) [41], which allowed the conductive filler to form an extensive network of connected paths through the insulating matrix. Room temperature conductivities (RTC) of up to ~0.1 S cm^{-1} were achieved for samples with 3 wt.% filler loading, sufficient for many electrical applications.

3.5. Biodisintregration in composting conditions

As a biodegradable material, PHA's are susceptible to be degraded under natural environmental conditions upon disposal. In order to evaluate the effect of graphene-based fillers addition into PHBV on its biodegradation, bio-disintegration of the PHBV and its nanocomposites were studied in composting conditions. Figure 6 shows the bio-disintegration (as percentage of weight loss) as a function of time. As observed, despite the fact that some studies about the cyto- and genotoxicity of the graphene have been recently published [57, 58], no detrimental effect upon addition of FGS at different concentrations on the biodegradation process were observed but rather the opposite. Thus, it is worth mentioning that an acceleration of the process was mostly observed for the samples loaded with the carbonaceous material since higher weight losses were appreciated at determined tested times for the nanocomposites. Moreover, as observed from Figure 6, the sample with the highest graphene loading degraded faster. Specifically, while the weight loss of pure PHBV was 33% after 56 days of compost incubation, weight losses of 60% and 94.6% were observed for the samples loaded with 1 wt.% and 3 wt.%, respectively.

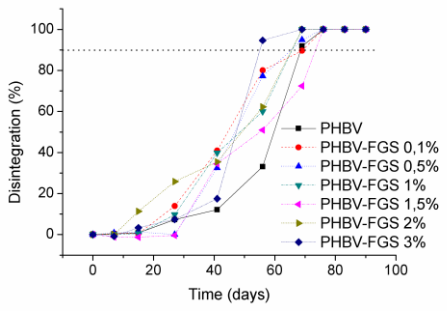

Figure 6. Loss in weight as a result of the biodegradation of PHBV and PHBV-FGS nanocomposites in composting conditions for up to 90 days.

4. CONCLUSIONS

In this article a PHBV polymer containing functionalized graphene sheets (FGS) obtained by ball milling were characterized in terms of physical properties to assess its applicability as barrier, mechanical and electrically conductive materials. The resulted nanocomposites showed improved crystallinity and physical properties. X-ray diffraction, in combination with isothermal and non-isothermal crystallization studies performed in the first part of this work, indicated that addition of FGS did not modify the crystal morphology of the PHBV matrix but led to an increase in crystallinity content. A reduction in oxygen permeability was observed upon addition of FGS which was ascribed most likely to the combined effect of the highly dispersed and distributed laminar filler and increased crystallinity. However, no effects were observed in terms of water vapour mass transport properties across the composition range study. Addition of FGS resulted in an increase in the storage modulus mainly due to the reinforcing effect of FGS homogeneously dispersed and distributed in the PHBV matrix. The electrical percolation threshold of PHBV-FGS nanocomposites was attained at ~ 0.3 vol.%, increasing the PHBV matrix conductivity 12 log units to reach a room temperature conductivity of up to ~0.1 S cm^{-1}. Finally, acceleration of the bio-disintegration process of the PHBV was

observed upon addition of FGS. This study proves that the ball milling technique can be successfully applied to generate gas barrier and mechanically reinforced nanocomposites with enhanced conductivity of interest in various application fields such as barrier and intelligent packaging.

REFERENCES

[1] Martínez-Sanz M, Villano M, Oliveira C, Albuquerque MGE, Majone M, Reis M, et al. (2014) Characterization of polyhydroxyalkanoates synthesized from microbial mixed cultures and of their nanobiocomposites with bacterial cellulose nanowhiskers. New Biotechnology 31(4):364-376.

[2] Sridhar V, Lee I, Chun HH, Park H. (2013) Graphene reinforced biodegradable poly(3-hydroxybutyrate-co-4-hydroxybutyrate) nano-composites. Express Polymer Letters 7(4):320-328.

[3] Lai M, Li J, Yang J, Liu J, Tong X, Cheng H. (2004) The morphology and thermal properties of multi-walled carbon nanotube and poly(hydroxybutyrate-co-hydroxyvalerate) composite. Polymer International 53(10):1479-1484.

[4] Ten E, Jiang L, Wolcott MP. (2012) Crystallization kinetics of poly(3-hydroxybutyrate-co-3-hydroxyvalerate)/ cellulose nanowhiskers composites. Carbohydrate Polymers 90(1):541-550.

[5] Ublekov F, Baldrian J, Nedkov E. (2009) Crystalline β-structure of PHBV grown epitaxially on silicate layers of MMT. Journal of Polymer Science, Part B: Polymer Physics 47(8):751-755.

[6] Sanchez-Garcia MD, Lagaron JM. (2010) Novel clay-based nanobiocomposites of biopolyesters with synergistic barrier to UV light, gas, and vapour. Journal of Applied Polymer Science 118(1):188-199.

[7] Martínez-Sanz M, Vicente AA, Gontard N, Lopez-Rubio A, Lagaron JM. (2014) On the extraction of cellulose nanowhiskers from food by-products and their comparative reinforcing effect on a polyhydroxybutyrate-co-valerate polymer. Cellulose.

[8] Yu HY, Qin ZY, Yan CF, Yao JM. (2014) Green nanocomposites based on functionalized cellulose nanocrystals: A study on the relationship between interfacial interaction and property enhancement. ACS Sustainable Chemistry and Engineering 2(4):875-886.

[9] Yu H, Yan C, Yao J. (2014) Fully biodegradable food packaging materials based on functionalized cellulose nanocrystals/poly(3-hydroxybutyrate-co-3-hydroxyvalerate) nanocomposites. RSC Advances 4(104):59792-59802.

[10] Marques PAAP, Gonçalves G, Cruz S, Almeida N, Singh MK, Grácio J, et al. Functionalized Graphene Nanocomposites. In: Hassim A, editor. Advances in Nanocomposite Technology: InTech Rijeka Croatia; 2011. p. 247-273.

[11] Schniepp HC, Li JL, McAllister MJ, Sai H, Herrera-Alonson M, Adamson DH, et al. (2006) Functionalized single graphene sheets derived from splitting graphite oxide. Journal of Physical Chemistry B 110(17):8535-8539.

[12] Yoo BM, Shin HJ, Yoon HW, Park HB. (2014) Graphene and graphene oxide and their uses in barrier polymers. Journal of Applied Polymer Science 131(1).

[13] Bao C, Song L, Xing W, Yuan B, Wilkie CA, Huang J, et al. (2012) Preparation of graphene by pressurized oxidation and multiplex reduction and its polymer nanocomposites by masterbatch-based melt blending. Journal of Materials Chemistry 22(13):6088-6096.

[14] Wang J, Wang X, Xu C, Zhang M, Shang X. (2011) Preparation of graphene/poly(vinyl

alcohol) nanocomposites with enhanced mechanical properties and water resistance. Polymer International 60(5):816-822.

[15] El Achaby M, Qaiss A. (2013) Processing and properties of polyethylene reinforced by graphene nanosheets and carbon nanotubes. Materials and Design 44:81-89.

[16] Ding P, Su S, Song N, Tang S, Liu Y, Shi L. (2014) Highly thermal conductive composites with polyamide-6 covalently-grafted graphene by an in situ polymerization and thermal reduction process. Carbon 66:576-584.

[17] Stankovich S, Dikin DA, Dommett GHB, Kohlhaas KM, Zimney EJ, Stach EA, et al. (2006) Graphene-based composite materials. Nature 442(7100):282-286.

[18] Fang M, Wang K, Lu H, Yang Y, Nutt S. (2009) Covalent polymer functionalization of graphene nanosheets and mechanical properties of composites. Journal of Materials Chemistry 19(38):7098-7105.

[19] Zhao X, Zhang Q, Chen D, Lu P. (2010) Enhanced mechanical properties of graphene-based polyvinyl alcohol composites. Macromolecules 43(5):2357-2363.

[20] Salavagione HJ, Martínez G, Gómez MA. (2009) Synthesis of poly(vinyl alcohol)/reduced graphite oxide nanocomposites with improved thermal and electrical properties. Journal of Materials Chemistry 19(28):5027-5032.

[21] Kuila T, Bose S, Mishra AK, Khanra P, Kim NH, Lee JH. (2012) Effect of functionalized graphene on the physical properties of linear low density polyethylene nanocomposites. Polymer Testing 31(1):31-38.

[22] De C. Fim F, Basso NRS, Graebin AP, Azambuja DS, Galland GB. (2013) Thermal, electrical, and mechanical properties of polyethylene-graphene nanocomposites obtained by in situ polymerization. Journal of Applied Polymer Science 128(5):2630-2637.

[23] Kim IH, Jeong YG. (2010) Polylactide/exfoliated graphite nanocomposites with enhanced thermal stability, mechanical modulus, and electrical conductivity. Journal of Polymer Science, Part B: Polymer Physics 48(8):850-858.

[24] Pinto AM, Cabral J, Tanaka DAP, Mendes AM, Magalhães FD. (2013) Effect of incorporation of graphene oxide and graphene nanoplatelets on mechanical and gas permeability properties of poly(lactic acid) films. Polymer International 62(1):33-40.

[25] Shen Y, Jing T, Ren W, Zhang J, Jiang ZG, Yu ZZ, et al. (2012) Chemical and thermal reduction of graphene oxide and its electrically conductive polylactic acid nanocomposites. Composites Science and Technology 72(12):1430-1435.

[26] Li W, Xu Z, Chen L, Shan M, Tian X, Yang C, et al. (2014) A facile method to produce graphene oxide-g-poly(L-lactic acid) as an promising reinforcement for PLLA nanocomposites. Chemical Engineering Journal (Lausanne) 237:291-299.

[27] Yang JH, Lin SH, Lee YD. (2012) Preparation and characterization of poly(l-lactide)-graphene composites using the in situ ring-opening polymerization of PLLA with graphene as the initiator. Journal of Materials Chemistry 22(21):10805-10815.

[28] Wang BJ, Zhang YJ, Zhang JQ, Gou QT, Wang ZB, Chen P, et al. (2013) Crystallization behavior, thermal and mechanical properties of PHBV/graphene nanosheet composites. Chinese Journal of Polymer Science (English Edition) 31(4):670-678.

[29] Song P, Cao Z, Cai Y, Zhao L, Fang Z, Fu S. (2011) Fabrication of exfoliated graphene-based polypropylene nanocomposites with

enhanced mechanical and thermal properties. Polymer 52(18):4001-4010.

[30] Song P, Liu L, Fu S, Yu Y, Jin C, Wu Q, et al. (2013) Striking multiple synergies created by combining reduced graphene oxides and carbon nanotubes for polymer nanocomposites. Nanotechnology 24(12).

[31] Huang HD, Ren PG, Xu JZ, Xu L, Zhong GJ, Hsiao BS, et al. (2014) Improved barrier properties of poly(lactic acid) with randomly dispersed graphene oxide nanosheets. Journal of Membrane Science 464:110-118.

[32] Jiang X, Drzal LT. (2012) Exploring the potential of exfoliated graphene nanoplatelets as the conductive filler in polymeric nanocomposites for bipolar plates. Journal of Power Sources 218:297-306.

[33] Gorrasi G, Di Lieto R, Patimo G, De Pasquale S, Sorrentino A. (2011) Structure-property relationships on uniaxially oriented carbon nanotube/polyethylene composites. Polymer 52(4):1124-1132.

[34] Gorrasi G, Sarno M, Di Bartolomeo A, Sannino D, Ciambelli P, Vittoria V. (2007) Incorporation of carbon nanotubes into polyethylene by high energy ball milling: Morphology and physical properties. Journal of Polymer Science, Part B: Polymer Physics 45(5):597-606.

[35] Vertuccio L, Gorrasi G, Sorrentino A, Vittoria V. (2009) Nano clay reinforced PCL/starch blends obtained by high energy ball milling. Carbohydrate Polymers 75(1):172-179.

[36] Perrin-Sarazin F, Sepehr M, Bouaricha S, Denault J. (2009) Potential of ball milling to improve clay dispersion in nanocomposites. Polymer Engineering and Science 49(4):651-665.

[37] Wu H, Zhao W, Chen G. (2012) One-pot in situ ball milling preparation of polymer/graphene nanocomposites. Journal of Applied Polymer Science 125(5):3899-3903.

[38] Wu H, Zhao W, Hu H, Chen G. (2011) One-step in situ ball milling synthesis of polymer-functionalized graphene nanocomposites. Journal of Materials Chemistry 21(24):8626-8632.

[39] Verdejo R, Barroso-Bujans F, Rodriguez-Perez MA, De Saja JA, Lopez-Manchado MA. (2008) Functionalized graphene sheet filled silicone foam nanocomposites. Journal of Materials Chemistry 18(19):2221-2226.

[40] ISO Standard 20200:2004. "Determination of the degree of disintegration of plastic materials under simulatd composting conditions in a laboratory-scale test". International Organization for Standarization

[41] Ambrosio-Martín J, Gorrasi G, Lopez-Rubio A, Fabra MJ, Cabedo L, López-Manchado MA, et al. (2015) On the use of ball milling to develop PHBV-graphene nanocomposites (I) – morphology, thermal properties and thermal stability. Journal of Applied Polymer Science.

[42] Kunioka M, Tamaki A, Doi Y. (1989) Crystalline and thermal properties of bacterial copolyesters: Poly(3-hydroxybutyrate-co-3-hydroxyvalerate) and poly(3-hydroxybutyrate-co-4-hydroxybutyrate). Macromolecules 22(2):694-697.

[43] Scandola M, Ceccorulli G, Pizzoli M, Gazzano M. (1992) Study of the crystal phase and crystallization rate of bacterial poly(3-hydroxybutyrate-co-3-hydroxyvalerate). Macromolecules 25(5):1405-1410.

[44] Shan GF, Gong X, Chen WP, Chen L, Zhu MF. (2011) Effect of multi-walled carbon nanotubes on crystallization behavior of poly(3-hydroxybutyrate-co-3-hydroxyvalerate). Colloid and Polymer Science 289(9):1005-1014.

[45] Vidhate S, Innocentini-Mei L, D'Souza NA. (2012) Mechanical and electrical multifunctional poly(3-hydroxybutyrate-co-3-hydroxyvalerate) - multiwall carbon nanotube nanocomposites. Polymer Engineering and Science 52(6):1367-1374.

[46] Kalaitzidou K, Fukushima H, Drzal LT. (2007) Multifunctional polypropylene composites produced by incorporation of exfoliated graphite nanoplatelets. Carbon 45(7):1446-1452.

[47] Potts JR, Dreyer DR, Bielawski CW, Ruoff RS. (2011) Graphene-based polymer nanocomposites. Polymer 52(1):5-25.

[48] Pardo-Ibáñez P, Lopez-Rubio A, Martínez-Sanz M, Cabedo L, Lagaron JM. (2014) Keratin-polyhydroxyalkanoate melt-compounded composites with improved barrier properties of interest in food packaging applications. Journal of Applied Polymer Science 131(4).

[49] Sorrentino A, Gorrasi G, Vittoria V. Permeability in Clay/Polyesters Nano-Biocomposites. In: Avérous L, Pollet E, editors. Environmental Silicate Nano-Biocomposites: Springer London; 2012. p. 237-264.

[50] Colomines G, Ducruet V, Courgneau Ć, Guinault A, Domenek S. (2010) Barrier properties of poly(lactic acid) and its morphological changes induced by aroma compound sorption. Polymer International 59(6):818-826.

[51] Kanehashi S, Kusakabe A, Sato S, Nagai K. (2010) Analysis of permeability; solubility and diffusivity of carbon dioxide; oxygen; and nitrogen in crystalline and liquid crystalline polymers. Journal of Membrane Science 365(1-2):40-51.

[52] Tsuji H, Okino R, Daimon H, Fujie K. (2006) Water vapor permeability of poly(lactide)s: Effects of molecular characteristics and crystallinity. Journal of Applied Polymer Science 99(5):2245-2252.

[53] Komatsuka T, Kusakabe A, Nagai K. (2008) Characterization and gas transport properties of poly(lactic acid) blend membranes. Desalination 234(1-3):212-220.

[54] Cimmino S, Iodice P, Silvestre C, Karasz FE. (2000) Atactic poly(methyl methacrylate) blended with poly(3-D(-)hydroxybutyrate): Miscibility and mechanical properties. Journal of Applied Polymer Science 75(6):746-753.

[55] Zhao J, Wang X, Zhou W, Zhi E, Zhang W, Ji J. (2013) Graphene-reinforced biodegradable poly(ethylene succinate) nanocomposites prepared by in situ polymerization. Journal of Applied Polymer Science 130(5):3212-3220.

[56] Tang LC, Wan YJ, Yan D, Pei YB, Zhao L, Li YB, et al. (2013) The effect of graphene dispersion on the mechanical properties of graphene/epoxy composites. Carbon 60:16-27.

[57] Akhavan O, Ghaderi E, Akhavan A. (2012) Size-dependent genotoxicity of graphene nanoplatelets in human stem cells. Biomaterials 33(32):8017-8025.

[58] Akhavan O, Ghaderi E, Emamy H, Akhavan F. (2013) Genotoxicity of graphene nanoribbons in human mesenchymal stem cells. Carbon 54:419-431.

IV. General Discussion

1. GENERAL DISCUSSION OF THE RESULTS

1.1. Initial studies. Analyses and optimization.

One of the first objectives of this work was the production of bacterial cellulose nanowhiskers (BCNW) for their subsequent incorporation within polymeric matrices. For that means, bacterial cultures were prepared as described in the previous chapters obtaining bacterial cellulose which was purified and hydrolysed to finally obtain BCNW, with an average cross section of 22 nm and lengths of around 600 nm (as commented in Chapter 2). These highly crystalline materials exhibited a crystallinity of 95.6% and good thermal stability with a degradation temperature of 323°C, allowing their use in processes requiring high temperatures, such as melt blending. The so-obtained materials were stored both freeze-dried and partially hydrated until their use. Figure 4A in Annex A shows a TEM micrograph of the structure of the BCNW in aqueous suspension obtained from partially hydrated BCNW (Figure 4Aa) and SEM micrograph of freeze-dried BCNW (Figure 4Ab). The relevance of the handling state of these BCNW is reflected in this Figure, as aggregation arising from molecular interactions between the crystals occurred upon freeze-drying, which influences their subsequent dispersion in the polymeric matrices and, thus, in the final properties of the nanocomposite materials.

After that, the main pursued objective was the incorporation of BCNW within PLA by *in situ* polymerization using methodologies which could result in a good BCNW dispersion. An *in situ* melt polycondensation reaction using concentrated lactic acid aqueous solutions was initially optimized prior to the incorporation of BCNW, following a previously reported method by Moon et al. (see references in Chapter 1), obtaining PLA with a molecular weight of about 20,000 g/mol. ATR-FTIR spectroscopy was used to follow the chemical structure of the material at different stages of the polymerization process.

The polymerization process was divided into two stages, an initial oligomerization which takes place at 150°C and where the initial linkage of several monomers occurred, followed by the polymerization process at 180°C, where the elongation of the polymer chain took place. After the first stage of polymerization, lactic acid oligomers (OLLA) (low molecular weight PLA) were obtained. The spectrum from OLLA reflected several changes in comparison with the spectrum of initial monomers, i.e. lactic acid, mainly related with a decrease in the presence of hydroxyl groups, which are considered to be the main reaction centers, giving rise to the generation of ester bonds between the monomers which was confirmed by new spectral bands detected, as discussed in Chapter 1.

After the oligomerization stage, the catalyst was added and the polymerization reaction took place, generating higher molecular weight PLA. The completion of the polymerization reaction was confirmed by the total disappearance of the band associated to the hydroxyl groups in the infrared spectrum, indicating that all the lactic acid molecules had reacted and contributed to the formation of the PLA chain as can be observed in Figure 5A in Annex A. Even though the PLA obtained through the polycondensation reaction had a similar spectrum to that of commercial PLA, the polymerized material had a low molecular weight, it was too brittle and did not have film forming ability. Therefore, the strategy followed to

obtain a PLA-based material for food packaging with improved properties was based on developing a masterbatch with the nanofiller through the *in situ* polymerization reaction and the subsequent melt blending with commercial high molecular weight PLA in order to obtain materials with high performance.

This seemed perfectly feasible due to the predictable high compatibility of PLA synthesized by *in situ* polymerization with the high molecular weight PLA ensuring uniform mixing and good BCNW dispersion in the final material. The miscibility of high molecular weight PLA with PLA from *in situ* polymerization was confirmed, as shown in Figure 6A in Annex A, by the single glass transition temperature obtained for the blend of both materials. After the optimization of the polycondensation reaction for PLA, BCNW were also introduced in the reaction media in order to generate PLA chains containing bacterial cellulose nanocrystals so as to improve dispersion of these nanofillers during the subsequent melt mixing step.

Despite the high thermal stability of BCNW with thermal degradation temperature higher than the temperature for the polycondensation reaction, trying to carry out a complete polymerization reaction in the presence of the nanocrystals resulted in thermal degradation of BCNW, probably due to the combination of high temperatures (180°C as mentioned before for the polymerization stage), high reaction times (around 20 hours for the two stages of polymerization) and the initial acid conditions of the reaction medium (as lactic acid monomers were used). Addition of the nanocrystals after the initial oligomerization stage neither avoided thermal degradation, and materials with dark brown color were obtained. Figure 7A in Annex A depicts the so-obtained materials after the polymerization process, both with the addition of BCNW at the beginning and after the oligomerization process. In contrast, no thermal degradation of the BCNW was observed during the oligomerization stage which took place at lower temperature (150°C) and shorter times (8 hours) as can be seen in Figure 7A in Annex A. Thus, this process was used to generate masterbatches of BCNW incorporated into lactic acid oligomers (OLLA-BCNW) for subsequent melt blending. As commented in Chapter 2, hydroxyl groups on the BCNW surface were implied in the polycondensation reaction generating covalent bonds between OLLA and BCNW.

The product obtained after the oligomerization process had impurities such as unreacted monomers, short chain oligomers and lactide, which is a cyclic dimer of lactic acid which appears during oligomerization, as described in Chapter 1. Several purification processes were evaluated in order to generate materials compatible with the subsequent process of melt blending with high molecular weight PLA, which ensure a proper dispersion of BCNW within the PLA.

Initially purification was performed using chloroform, solvent widely used in the purification of PLA systems. Given that some covalent bonds were formed between OLLA and BCNW, as demonstrated in Chapter 2 of this thesis work, using chloroform to purify the obtained masterbatches, led to the dissolution of free oligomer chains not covalently bond to cellulose, leaving in suspension cellulose nanocrystals (attached or not to oligomer chains) since they are not soluble in chloroform. Two different routes were then explored. The first one was to take the suspended fraction and washed it several times, resulting in a material composed by oligomer chains grafted on the cellulose surface and free cellulose nanocrystals, eliminating ungrafted free oligomers (from now on purification process 1). The

second route involved the precipitation of the chloroform system with the dissolved/suspended masterbatches in excess of diethyl ether, followed by filtering. In this case, the lower molecular weight fraction of ungrafted oligomers was eliminated (from now purification process 2). Both purification routes resulted in materials with high cellulose concentration due to the elimination of a substantial fraction of the synthesized oligomers. It led to a strongly aggregation between cellulose chains during the drying process after purification and, thus, resulted in materials that were very difficult to re-disperse by melt mixing. Figure 8A in Annex A shows the agglomerates from the masterbatch purified by the purification process 2 after melt mixed with commercial PLA.

As an alternative, a purification method giving rise to a material with higher oligomer content was developed, which consisted on grinding the obtained masterbatches and subsequently washing with diethyl ether (cf. to Figure 9A in Annex A, showing the greater intensity of the spectral bands related to OLLA). After this purification process, the impurities previously discussed were effectively removed. Figure 10A in Annex A shows the FTIR spectra of pure diethyl ether and the residue after the evaporation of the diethyl ether of purification. It is clearly seen that spectral bands related to OLLA appeared after evaporation of the diethyl ether and also a relative intense band at 3500 cm^{-1} which could be associated to hydroxyl groups from short chain oligomers and to non reacted monomers, as discussed in Chapter 1. It suggested an efficient extraction of these impurities from the polymerized material. The increased amount of oligomers in the material purified with diethyl ether avoided strong aggregation and improved the dispersion of the masterbatch into PLA by melt mixing as demonstrated in Chapter 2 of this work. This methodology also resulted in a patent application (PCT/ES2014/070443).

1.2. An effect of lactic acid oligomers on the properties of polylactide

Once the pre-incorporation process was developed and optimized, the first study focused on studying how incorporation of the lactic acid oligomers (OLLA), without cellulose and synthesized and purified as above commented, affected the properties of commercial PLA. Interestingly, a reduction in the oxygen and water vapour permeability was observed upon oligomer addition as described in Chapter 1, which also includes an optimization of the amount of oligomer which can be melt blended with PLA keeping the film-forming ability and having the optimum barrier properties. The effect of adding purified and unpurified oligomers on the final properties of the PLA blends was also discussed.

The best materials were obtained for oligomer contents of 25 wt%. A comparison between incorporation of purified and unpurified OLLA to the PLA revealed that, although both materials showed good miscibility with commercial PLA by melt mixing, the impurities present in the unpurified oligomer somehow hindered PLA crystallization, generating more defective and heterogeneous crystals, and giving rise to a lower crystalline fraction. Moreover, a greater drop in the glass transition temperature (T_g) of PLA was observed in comparison with the blends with the purified oligomers, which was also associated with a reduction in the elastic modulus of the material. Moreover, no significant changes were observed in the mechanical properties of the materials obtained after mixing purified OLLA and PLA. Regarding the barrier properties, both water and oxygen permeability (measured at two different relative humidities) was reduced upon addition of the oligomers, which

could be explained by oligomer molecules occupying the available free volume in the PLA matrix and, thus, slowing down the passage of permeant molecules through. The permeability values were very dependent of the humidity conditions. The best results in terms of oxygen barrier improvements were observed in dry conditions, as water sorption negatively affected to the materials, generating preferential paths for the oxygen molecules to permeate. In humid conditions, the PLA blends with purified oligomers displayed better barrier properties as the purification process led to less hydrophilic groups, such as hydroxyl groups, available to interact with water and, thus, with less impact on barrier properties.

1.3. Using melt polycondensation of lactic acid as pre-incorporation method

Purified masterbatches of oligomers and BCNW obtained by melt polycondensation were incorporated into PLA through melt mixing. In order to evaluate the effect of the nanofiller, PLA samples were generated with different amounts of BCNW but keeping constant the amount of OLLA. The effect of using partially hydrated BCNW vs. freeze-dried BCNW during the oligomerization process was also evaluated. Furthermore, direct addition of partially hydrated or freeze-dried BCNW to PLA through melt compounding was also carried out for comparison purposes (keeping constant the amounts of BCNW, OLLA and PLA).

In the masterbatch prepared with freeze-dried BCNW, given the strong intermolecular forces established between the cellulose chains during the drying process, only a small fraction of oligomers was effectively grafted to the BCNW surface, as inferred from the long term stability tests (showing a small fraction suspended after 72h as observed in Chapter 2) and the corresponding infrared spectrum showed in Figure 11A in Annex A where no shifts of the spectral bands were obtained. It seemed that the small fraction of grafted oligomers were insufficient to generate a shifting of the corresponding bands, unlike in the case of masterbatch prepared with partially hydrated BCNW (cf. Chapter 2). This resulted in a worse dispersion of the filler in the PLA matrix and also to lower interfacial interactions between BCNW and the polymer, having detrimental effects on thermal, mechanical and barrier properties, thus reaching poorer material properties than in the blends containing the masterbatch obtained from partially hydrated BCNW. A nucleating effect of BCNW was observed in the PLA-based nanocomposites, although it was much more noticeable in the blends where the BCNW were incorporated partially hydrated, due to the improved dispersion obtained in this case. This effect can be observed in the Figure 12A in Annex A where higher increases in the second melting peak area was more noticeable after first heating scan by differential scanning calorimetry and moreover, more homogeneous crystallization took place even after a controlled cooling process when partially hydrated BCNW was used.

Regarding the materials obtained by direct BCNW addition, nanofiller aggregation within the PLA matrix was observed, thus, corroborating the suitability of the incorporation route based on the use of masterbatches obtained through polycondensation for improved material development. Indeed, as shown in Chapter 2, the major improvements in terms of barriers and mechanical properties were achieved for the highest loaded sample (5 wt% BCNW) obtained from the masterbatch with partially hydrated BCNW indicating that, even at

high contents, proper dispersion of the nanocrystals were achieved by the proposed route, thus generating good filler-filler and filler-matrix interactions.

From the previous studies it was observed that addition of 25 wt% of purified OLLA into PLA produced a reduction of up to 22% in oxygen permeability measured under high relative humidity conditions and a reduction of up to 25% in water vapor permeability. Furthermore, it was found that addition of 5 wt% of partially hydrated BCNW into PLA also resulted in a reduction of up to 22% in oxygen permeability measured under the same conditions and 18% in water vapor permeability. Therefore, the potential synergistic effect of combining 5 wt% of partially hydrated BCNW and 25 wt% of purified OLLA on the mechanical and barrier properties of PLA was studied. Although the improvement was not as high as expected, the combination of such amounts of OLLA and BCNW resulted in a greater reduction in oxygen and water vapor permeability of up to 25% and 20 %, respectively. This was mainly due to the occupancy of the free volume by OLLA molecules, corroborating the previous results, which led to the greatest reduction in the oxygen solubility coefficient in the polymer matrix. However, simultaneous addition of 25 wt% of OLLA and 5 wt% of BCNW did not improve the mechanical properties when compared with the sample with 5 wt% of partially hydrated BCNW previously studied. This could be explained by the worse interactions between the filler and the PLA matrix due to the high amount of OLLA. Nevertheless, in comparison with the PLA material incorporating 25 wt% of purified OLLA showed in Chapter 1 where no effect in the elastic modulus was noticed, an increase in this property was observed upon addition of 25% of OLLA and 5 wt% of BCNW, thus highlighting the reinforcing ability of the nanofiller. On the other hand, a significant embrittlement of the material took place with a sharp drop in tensile strength and elongation at break. Therefore it seemed that the addition of large amounts of oligomers in combination with BCNW had a negative synergistic effect in terms of mechanical properties.

Summarizing, the polycondensation-based preincorporation method proposed improved not only the dispersion of the cellulose nanocrystals within the polymer matrix but also the interfacial adhesion between filler and matrix, which was crucial to improve the final properties. In addition, it was a strategy compatible with aqueous based systems avoiding the necessity of organic solvents during the synthesis.

Moreover, although the use of masterbatches with freeze-dried BCNW gave rise to worse results than those with partially hydrated BCNW, it is noteworthy that improvements in barrier and mechanical properties were always obtained. Therefore, hypothetically, these results were expected to be better than those expected upon direct addition of BCNW during the melt mixing process where a very poor dispersion of the filler within the matrix was observed, which is closely related with poor mechanical and barrier properties, as discussed in Chapter 2 of this work.

Using the same strategy described in Chapter 2, i.e. an initial pre-incorporation followed by melt mixing, nanocomposites of PLA with functionalized graphene sheets (FGS) were developed. In this case, due to the greatest improvements in barrier properties obtained when the synergistic effect of the incorporation of OLLA and BCNW was studied, different amounts of FGS were added keeping constant the amount of OLLA at 25 wt%. As discussed in the present work, from the chemical point of view, the presence of functional groups on the surface of graphene made this material especially interesting to be used as nanofiller because functional sites could favor the interaction with the polymer matrix. Thus,

masterbatches composed of FGS and OLLA were developed through *in situ* polymerization and subsequently melt mixed with PLA. Similarly to the previous study performed with BCNW, direct FGS incorporation to the melt mixing step keeping constant the amounts of FGS, OLLA and PLA was also performed for comparison purposes.

In this case, there were no evidences of chemical interactions between nanofiller and oligomer as shown in Figure 13A in Annex A where no shifts of the bands related to the ester groups were observed, unlike when the masterbatches with BCNW were obtained through polycondensation. This was corroborated by the long term dispersion stability tests performed (c.f. Figure 14A in Annex A), where a suspension of the masterbatch in chloroform precipitated in less than 48 hours, behaving similarly as a physical mixture of FGS and OLLA in chloroform. The lower density of hydroxyl and/or carboxyl groups in FGS surface capable of reacting with lactic acid monomers during the polycondensation reaction in comparison with the large amount of hydroxyl groups present on the surface of BCNW could explain this result.

In spite of that, the use of masterbatches during the melt mixing process with PLA resulted in better dispersion and distribution of the FGS in comparison with direct melt mixing of the materials. Nevertheless, at high FGS contents, a relatively good distribution was also achieved for the direct melt mixing, as noticed in Chapter 3 through microscopic analysis.

Again, the final properties of the materials were influenced by the nanofiller dispersion, reflected, for instance, in a lower decrease in the glass transition temperature for the nanocomposites obtained with the masterbatch and a decrease in the cold crystallization temperature with increasing FGS content for these nanocomposites (indicating a better ability to crystallize). The larger aggregates and poorer interfacial filler-matrix interactions in the nanocomposites obtained through direct FGS addition somehow hindered the nucleating effect of FGS and, thus, no differences in the cold crystallization temperature were seen between the different compositions. However, similar crystallinity to that of the reference material was obtained for all compositions, probably ascribed to the large amount of OLLA which, as shown in Chapter 1, resulted in a substantial decrease in the crystallinity of the material, thus counteracting the nucleating effect of FGS. This high OLLA content could also explain the slight improvement in mechanical properties (10% increase in the elastic modulus) observed for the FGS-containing nanocomposites, while from the inherent characteristics of the nanofiller one would expect significantly greater mechanical improvements. Besides, a reduction in tensile strength was observed for all samples regardless of incorporation procedure, i.e. direct addition or pre-incorporation in masterbatch through polycondensation. However, while at low FGS contents, the blends obtained from the masterbatches presented higher values of elastic modulus and tensile strength, at high FGS contents no differences were found between both incorporation routes. It was most likely due to the fact that filler aggregation occurred during both processing methods leading to less property differentiations.

Nevertheless, a quite remarkable synergistic effect on the barrier properties after addition of lactic acid oligomers and different amounts of FGS was observed, reaching improvements of up to 45 and 41% for oxygen and water vapor permeability, respectively, for PLA nanocomposites with 25 wt% OLLA and only 2 wt% of FGS. This considerable drop in permeability was the result of both the filling of the free volume by OLLA combined with

the blocking ability of the lamellar structures, being more effective for that means that the fibrillar nanocellulose ones (improvements of 25% and 20% for oxygen and water vapor permeability, respectively, were obtained for PLA nanocomposites with 25 wt% OLLA and even higher amount of BCNW nanofiller, 5 wt%, as shown in Chapter 2). This blocking ability of the lamellar structures was observed even in the samples developed by direct addition. In fact, no significant differences with the barrier properties of the samples with low FGS content obtained through a pre-incorporation were found. However, increasing the amount of FGS higher differences were observed resulting in higher permeability for the samples developed by direct addition. Addition of FGS also provided the PLA samples with electrical conductivity and, thus, it was found that the nanocomposites containing 2% FGS behaved as a semiconductor material with an increase of about 10^6 orders of magnitude in its electrical conductivity with respect to neat PLA which can be considered an insulator material. Higher conductivity values were observed for the samples synthesized through FGS pre-incorporation by *in situ* polymerization, again explained by the better dispersion of the nanofiller. In fact, percolation thresholds of 1 and 2.8% were found for samples obtained from the masterbatch and synthesized by direct addition, respectively.

Thus, these first chapters demonstrate that a pre-incorporation step based on *in situ* polymerization of nanofillers with highly compatible matrices such as lactic acid oligomers, is a proper strategy to develop PLA-based nanocomposite materials. It increased the compatibility between hydrophilic nanofillers and hydrophobic matrices leading to improved nanofiller dispersion and, thus, improved final properties.

1.4. Using ball milling to synthesize polymer nanocomposites

Focusing on the other major objective of this work based on the development of nanocomposites using one-step procedures, PLA and PHBV nanocomposites containing either BCNW or FGS were developed using a ball milling technology (Chapters 4-7).

For the BCNW-based nanocomposites, generally and regardless of the matrix used, the use of ball milling for incorporating BCNW broke up the biggest aggregates formed during the freeze-drying of the nanofiller. It is important to note that in this case freeze-dried BCNW were used because of technical requirements, having the disadvantage of generating strong intermolecular forces between the cellulose chains which hindered their proper subsequent dispersion. Therefore, although no differences in film appearance were observed macroscopically, under microscopic analysis aggregates were observed even at low BCNW contents, which increased as the concentration of BCNW increased. Nevertheless, it should also be emphasized that the ball milling technology was able to disperse relatively well a certain fraction of the nanofiller.

BCNW addition through ball milling led to improvements in the crystallization process of the polymer matrices, mainly ascribed to the nucleating effect of the well dispersed fraction of BCNW, which in turn led to an increase in the crystalline fraction, also affecting the heterogeneity of the crystalline population generated.

It is important to highlight that differences between pure PLA processed by melt blending and using ball milling were found. In the latter, a decrease in crystallinity and a bimodal melting behavior was observed, which could be related to the mechanical treatment

applied to the samples during the ball milling process which could generate two different crystalline populations. In the Chapter 4 of this work it was already noted that processing by ball milling of semi-crystalline polymers could result in a decrease in crystallinity and it may also result in changes in the molecular weight. Comparing the infrared spectra of PLA processed by melt mixing vs. ball milling (cf. Figure 15 in Annex A), a band around 826 cm^{-1} corresponding to the vibration of the *v*(C-COOH) bonds appear for the ball milled sample, which could be indicative of greater presence of carboxylic groups generated by breaking up the PLA chains during the high energy process.

Similarly, and again regardless of the polymer matrix used, the incorporation of BCNW by ball milling produced a reinforcing effect on the polymeric matrices, mainly due to the intrinsic properties of the BCNW. However, the greatest improvements were obtained for low BCNW contents due to better dispersion achieved at these loading levels. In the case of PLA nanocomposites with BCNW, higher improvements were obtained using the pre-incorporation step through *in situ* polymerization, mainly due to better dispersion of the nanofiller which resulted in better interaction between the matrix and filler leading to a better load transfer.

Barrier properties were also improved after addition of BCNW through ball milling. In the case of PLA-based materials improved oxygen permeability was observed, although it was almost independent of the nanocellulose content. As for the mechanical properties, the sample with lower BCNW content presented the best performance, highlighting the importance of proper nanofiller dispersion to optimize improvements in these nanocomposites materials. In spite of the better dispersion obtained for PLA containing BCNW nanocomposites synthesized through the pre-incorporation method, no great differences were observed.

The same trend in the oxygen permeability was observed for the nanocomposites of PHBV and BCNW, being the barrier improvements independent of the loading level and showing the greatest improvements for low loading levels. In this case, it should be mentioned that the permeability value of neat PHBV obtained through ball milling was lower to that reported in the literature for the same PHBV grade, as reported in Chapter 5 of this work, mainly due to the higher crystallinity obtained for the neat PHBV processed by ball milling. However, addition of BCNW further decreased the oxygen permeability corroborating the blocking effect of BCNW. Furthermore, because of the blocking effect of this nanofiller, a decrease in the water vapor diffusion coefficient was also observed.

Therefore, the ball milling process has shown potential to develop BCNW-based nanocomposites with biopolymer matrices like PHBV and PLA with improved properties, even though a proper dispersion of the nanocrystals within the matrices was not attained. Further work for the optimization of these materials, focusing on improving nanofiller dispersion, should be performed.

Regarding the nanocomposites based on PHBV and FGS, better nanofiller dispersion was reached through ball milling than in the case of BCNW. However, it should be emphasized that although no agglomerates were observed by microscopic analysis of the developed films, at high FGS contents, areas of high nanofiller concentration were present, although relatively good dispersion and distribution was generally observed.

Addition of FGS facilitated the crystallization process, with an acceleration of the process and increasing the crystalline fraction of the polymer. Greater increases in crystallinity were achieved for low FGS contents, giving raise to heterogeneous crystals, mainly due to increased nucleation sites induced by nanofiller addition, in a similar way to what happened when incorporating BCNW. On the contrary, at high nanofiller contents there was a certain reduction in the crystalline fraction with the generation of more unstable crystals due to the hindering of the nucleating character of FGS at high concentration levels.

The thermal stability of PHBV nanocomposites was highly dependent on both the type of nanofiller (FGS vs. BCNW) and the measuring conditions. Regarding the last parameter, a lower thermal stability of PHBV was generally observed under an oxidative atmosphere, due to oxidation reactions taking place, thus, accelerating thermal degradation. Interestingly, in such oxidative conditions, lower reductions in thermal stability were observed for the samples incorporating BCNW if compared to those containing FGS. Conversely, under inert nitrogen atmosphere, whereas for nanocomposites of PHBV and cellulose nanocrystals an improved thermal stability was observed, no effects were observed after addition of FGS. This filler-dependent behavior was mainly based on two aspects. As discussed in Chapter 5 of this work, it is widely known that the general mechanism of thermal degradation of PHBV is the scission of PHBV molecules by a random cis-elimination reaction at a six-membered ring ester intermediate which takes place at the initial steps of PHBV decomposition. This process is suppressed by the generation of hydrogen bonds between the polymer matrix and BCNW thus generating an increase in thermal stability. Moreover, as discussed in Chapter 6 of this work, an increase in thermal stability is also related to the addition of nanofillers with high heat and mass barrier effect. Thus, while both nanofillers were characterized by good mass barrier properties, graphene-based materials were much more thermally conductive than the cellulosic materials, hence facilitating the diffusion of heat throughout the sample.

The above mentioned issues were also closely related to the results of thermal stability of the materials obtained after addition of BCNW or FGS within PLA studied in Chapters 2 and 3 of this work, respectively. Similarly, an increase in the thermal stability of PLA was observed upon BCNW addition, while a certain reduction in thermal stability took place when FGS were added.

The better dispersion of FGS within PHBV through ball milling than that of BCNW using the same technology led to greater improvements in both mechanical and barrier properties. Nevertheless, the increase in barrier properties with the use of FGS was also explained by the morphology of the nanofiller, in a similar way to the differences observed after addition of both nanofillers, BCNW and FGS, into PLA using the pre-incorporation method.

Focusing on the mechanical properties, samples with an increase in storage modulus over the whole temperature span were obtained for PHBV-FGS nanocomposites processed through ball milling. In addition, the Table 2A in Annex A shows the value of the storage modulus of PHBV after addition of both BCNW and FGS at different compositions at 25°C. Although at low nanofiller contents similar values were obtained with the use of both fillers, at high contents a greater increase was observed after addition of FGS reaching improvements of up 35% vs. 13% in the case of BCNW.

Regarding barriers properties, the greatest oxygen permeability reductions were obtained for materials with a 3 wt% of FGS content, reaching improvements of up to 41%. These improvements were much higher than the maximum achieved when BCNW was

incorporated within PHBV through ball milling, where a maximum improvement of up to 21% was observed for the composition containing 0.5 wt% of BCNW. Higher BCNW contents resulted in lower improvements due to the presence of agglomerates at those loading levels, as previously commented. Apart from the already mentioned factors influencing barrier properties, i.e. dispersion and shape of nanofiller, the crystallinity of the polymers also play an important role on the mass transport properties. In fact, in Chapter 7 of this work, a methodology to separate the effect of filler loading on the barrier performance from the crystallinity alterations was developed. The calculated factor has been previously termed as the "filler barrier efficiency". On Table 3A in Annex A a similar comparative study is presented comparing both nanofillers. This table includes the oxygen permeability for each composition, the attained reduction in oxygen permeability and the corresponding filler barrier efficiency. From the results it can be seen that while the BCNW barrier efficiency underwent a drop as BCNW content increased, in the case of FGS an increase took place with FGS addition confirming the better barrier efficiency of this filler.

Unexpected result in regard to water vapor permeability was observed for FGS-containing PHBV nanocomposite films obtained through ball milling, as no improvements were observed with respect to the neat polymer matrix. Further studies are needed to corroborate these results, since from comparison with either the same polymer matrix and processing technology (PHBV with BCNW obtained through ball milling) or the same filler and a different processing technology (PLA with FGS through *in situ* polymerization), one would expect a certain decrease in water vapor permeability.

As previously mentioned, addition of FGS inside the polymer matrices resulted in materials with electrical conductivity. In this case, the electrical conductivities measured for materials synthesized from PHBV and FGS through ball milling were much higher than those achieved when the FGS was introduced into PLA using a pre-incorporation step. Two factors can help explaining this better result in terms of electrical conductivity. On one hand, the improved dispersion of FGS was decisive, as it was also a crucial factor for determining the rest of the properties analyzed. By a comparison of both studies better dispersion of the FGS was achieved by ball milling on the basis of microscopic analysis performed in each case. On the other hand, as discussed in Chapter 3 of this work, the crystallization degree of the polymeric materials is strongly correlated with the electrical conductivity since samples with higher crystallinity led to a higher electrical conductivity due to the decreased scattering of electrons through the crystalline lamella. The crystallinity of the PHBV-based materials was much higher than that for the PLA-based ones. Thus, while the maximum value of electrical conductivity for materials based on PLA was 1.6 e^{-6} S/cm, containing 2 wt% of FGS, in the case of PHBV, with 1.5 wt% of FGS the conductivity was 5.0 e^{-4} S/cm reaching a maximum conductivity of about 0.1 S/cm for a FGS content of 3 wt%.

1.5. Final and complementary studies

To complete the characterization work of the developed nanocomposites, a study of their thermal degradation and degradation under composting conditions was carried out.

Chapters 6 and 7 of the present work show how addition of FGS caused an acceleration of both thermal degradation and degradation under composting conditions, respectively. In

the case of thermal degradation, there was an increase of the degradation kinetics constant and a reduction in the activation energy with increasing the concentration of FGS, indicating that less energy was needed to start the degradation process. In the case of degradation in composting conditions, although several studies have been published on the cyto- and genotoxicity of graphene, an acceleration of the process was also observed indicating that addition of graphene within polymer matrices could have positive effects removing such materials under controlled biodegradation conditions.

In addition to these studies, another study of biodegradation under composting conditions was performed for materials composed by PLA and OLLA and also for the nanocomposites based on PLA and BCNW obtained by melt blending performed as described in Chapters 1 and 2 of this work, respectively. Figure 16A in Annex A represents the weight loss as a result of biodegradation in composting conditions of these materials. The first thing to highlight is the very fast degradation of these materials compared to materials based on PHBV. Despite of that, the incorporation of BCNW further increased the degradation rate since at certain times, such as 8 days, the weight loss for the samples with 3 wt% of BCNW was 66.9% while the weight loss of pure PLA was 15.8%. Moreover, the addition of high amounts of OLLA, up to 25 wt%, into PLA generated even higher increases with weight losses around 75% after 8 days.

Finally, having in mind that these materials were in principle conceived for food packaging applications, a thermoforming study was developed for the nanocomposite films based on PLA and BCNW obtained by melt mixing which have been described in Chapter 2 of this thesis work. Thermoformed trays were easily obtained with these materials and the reinforcing effect of BCNW in the trays was palpable by simple manual manipulation. Figure 17A in Annex A shows some images of the obtained trays. Additionally, a water vapor permeability study of some of the developed trays was performed, obtaining a close relationship with the permeability measured for the films having the same composition. These results are shown in Table 4 of Annex A where the permeability values for both systems, i.e. films and trays, at the studied compositions are compiled.

V. Conclusions/Conclusiones

CONCLUSIONS

The present work investigated on the development of commercial promising biopolyesters-based nanocomposites (specifically PLA and PHBV) of interest in food packaging applications. Two different nanofillers, i.e. bacterial cellulose nanowhiskers (BCNW) and functionalized graphene nanosheets (FGS) were added within the biopolymeric matrices through various processing methods in order to improve their barrier properties, among others. Moreover, the effect that those nanofillers had on the biodegradation process of the different biopolymer matrices was also investigated.

From the results of this work several conclusions can be drawn:

- In order to incorporate the nanofillers into PLA using a melt polycondensation reaction of lactic acid, a two-steps process was necessary, involving an initial pre-incorporation step and a subsequent melt mixing step.

- The presence of enough chemically reactive groups in the nanofiller surface which could take part on the polycondensation reaction such as hydroxyl and carboxyl groups made of especial interest this incorporation route due to the generation of covalent bonds between filler and matrix during the pre-incorporation step.

- Purification of the obtained materials from the pre-incorporation step played a key role for the subsequent dispersion of the nanofiller within the biopolymer matrix during the melt mixing step.

- Addition of lactic acid oligomer molecules (OLLA) within PLA up to 25 wt% resulted in a reduction of the oxygen and water vapour permeability due to their free-volume filling capacity. The use of purified and unpurified oligomers led to different effects on the PLA final properties mainly due to the presence of impurities in the non-purified one.

- The addition of different nanofillers within PLA using the pre-incorporation method based on *in situ* polymerization has proven to be an efficient strategy reducing or even avoiding nanofiller agglomeration in melt compounded nanocomposites, increasing the compatibility of the hydrophilic nanofillers, such as BCNW, and hydrophobic matrices, such as PLA. This strategy resulted in considerable improvements in the mechanical and barrier properties of the biopolymers and even in the electrical properties (for the nanocomposites containing FGS).

- Addition of high amounts of OLLA up to 25 wt.% simultaneously with nanofillers led to good results in terms of barrier properties although mechanical properties were only slightly improved or even deteriorated.

- Regarding the second method to develop nanocomposites based on ball milling technology, its efficiency for materials improvement was highly dependent on the nanofiller used. While for FGS a homogeneous dispersion and distribution of the filler was observed, when BCNW was used, this technology was insufficient to achieve a proper dispersion of the filler within the biopolymeric matrices and some agglomerates remained present. This was mainly due to the fact that BCNW were used as a freeze-dried material, where strong interactions between cellulose molecules existed making it very difficult to re-disperse.

- In spite of that, addition of BCNW through ball milling resulted in improvements in the mechanical and barrier properties although much lower than those obtained through the addition of BCNW by means of pre-incorporation based on *in situ* polymerization. Higher dispersion was obtained when FGS was used which led to greater improvements in the mechanical and barrier properties than in the case of BCNW.

- Comparing the addition of FGS in the studied systems through the different strategies, better dispersion of the filler was noticed using the ball milling technology, which gave rise to materials with an enhanced percolation network which led to a comparatively greater reinforcing effect and better electrical properties.

- Addition of FGS or BCNW had positive effects on the biodegradation rate under composting conditions as a somewhat accelerated degradation was observed in the nanocomposites.

- Summarizing, two different strategies have been developed to incorporate nanofillers within biopolyester matrices with good results in terms of final properties of the obtained materials. Moreover, these strategies avoided the use of organic solvents which could lead to potentially lower environmental impact. On the one hand, the use of strategies compatibles with aqueous-based systems has avoided the use of organic solvents during the synthesis of biopolymer nanocomposites. On the other hand, the use of ball milling as a one single step and free solvent methodology has proven to be an efficient technology for the development of biopolymer nanocomposites. Using both strategies, improvements in mechanical, barrier and electrical properties were obtained.

CONCLUSIONES

El presente trabajo se centró en el desarrollo de nanocompuestos basados en biopoliésteres comerciales con buenas perspectivas de futuro (específicamente PLA y PHBV) de interés en aplicaciones de envasado de alimentos. Dos nanocargas diferentes, concretamente nanocristales de celulosa bacteriana (BCNW) y nanoláminas de grafeno funcionalizado (FGS), se incorporaron en las matrices biopoliméricas a través de diversos métodos de procesado con el fin de mejorar sus propiedades de barrera, entre otras. Por otra parte, se evaluó el efecto que dichas nanocargas en el proceso de biodegradación de las diferentes matrices de biopolímeros.

De los resultados de este trabajo se extraen las siguientes conclusiones:

- Para la incorporación de las nanocargas en el interior de PLA a través de la reacción de policondensación en estado fundido de ácido láctico, fue necesario llevar a cabo un proceso de dos pasos, que incluía una etapa de pre-incorporación inicial de las nanocargas en una matriz de oligómeros de ácido láctico y una etapa posterior de mezclado en fundido de dicho "masterbatch" con PLA comercial de alto peso molecular.

- Esta ruta de incorporación basada en la reacción de policondensación era especialmente interesante debido a la presencia de suficientes grupos químicamente reactivos (tales como grupos hidroxilo y carboxilo) en la superficie de las nanocargas, que participaban durante dicha reacción, siendo capaces de generar enlaces covalentes con la matriz durante la etapa de pre-incorporación .

- La purificación de los materiales obtenidos a partir de la etapa de pre-incorporación jugó un papel clave para la posterior dispersión de las nanocargas dentro de la matriz de biopolímero durante la etapa de mezclado en estado fundido.

- La incorporación de oligómeros de ácido láctico (OLLA) en PLA comercial hasta un 25% en peso dio lugar a una reducción de la permeabilidad al oxígeno y vapor de agua debido a su capacidad de ocupar el volumen libre de dicho material. El uso de oligómeros purificados y no purificados condujo a diferentes efectos sobre las propiedades finales de PLA principalmente debido a la presencia de impurezas en el no purificado.

- La adición de diferentes nanocargas en PLA utilizando el método de pre-incorporación basado en la polimerización *in situ* ha demostrado ser una estrategia eficaz para reducir o incluso evitar la aglomeración de las nanocargas en

nanocompuestos obtenidos por mezclado en fundido, aumentando la compatibilidad entre nanocargas hidrofílicas, tales como BCNW, y matrices hidrofóbicas, tales como PLA. Esta estrategia resultó en mejoras considerables en las propiedades mecánicas y de barrera de los biopolímeros e incluso en las propiedades eléctricas (para los nanocompuestos que contenían FGS).

- La adición de altas cantidades de OLLA, hasta un 25% en peso, simultáneamente con nanocargas condujo a buenos resultados en términos de propiedades de barrera aunque las propiedades mecánicas fueron sólo ligeramente mejoradas o incluso se deterioraron.

- En cuanto al segundo método para desarrollar nanocompuestos basado en la tecnología de "ball milling", su eficiencia para la mejora de los biopolímeros fue altamente dependiente de la nanocarga utilizada. Mientras que para FGS se observó una dispersión y distribución homogénea de las nanocargas, cuando se utilizó BCNW, esta tecnología fue insuficiente para conseguir una dispersión adecuada dentro de las matrices biopoliméricas, apareciendo algunos aglomerados. Esto se debió principalmente al hecho de que las nanocargas de celulosa bacteriana (BCNW) se incorporaron en forma de liofilizado, donde fuertes interacciones entre las moléculas de celulosa tenían lugar, por lo que fueron muy difíciles de redispersar.

- A pesar de ello, la adición de BCNW utilizando ball milling dio lugar a mejoras en las propiedades mecánicas y de barrera aunque mucho menores que los obtenidos mediante pre-incorporación de BCNW basada en polimerización *in situ*. Como ya se ha comentado, se obtuvo una mayor dispersión al utilizar FGS lo cual condujo a mayores mejoras en las propiedades mecánicas y de barrera que en el caso de BCNW.

- Comparando la adición de FGS en los sistemas estudiados a través de las diferentes estrategias, se observó una mejor dispersión de las nanocargas utilizando la tecnología de ball milling dando lugar a materiales con una red de percolación mejorada que resultó, consecuentemente, en un mayor efecto de refuerzo y mejores propiedades eléctricas.

- La adición de FGS o BCNW tuvo efectos positivos en la velocidad de biodegradación en condiciones de compostaje ya que se observó una aceleración en el proceso de degradación de los nanocompuestos.

- En resumen, dos estrategias diferentes se han desarrollado para incorporar nanocargas en matrices de biopoliésteres con buenos resultados en términos de propiedades finales del los materiales obtenidos. Por otra parte, estas estrategias

evitaron el uso de disolventes orgánicos y, por tanto, podrían contribuir a un menor impacto ambiental. Por un lado, el uso de estrategias compatibles con sistemas en base acuosa ha evitado el uso de disolventes orgánicos durante la síntesis de nanocompuestos biopoliméricos. Por otro lado, el uso de ball milling como metodología en un solo paso y libre de disolventes ha demostrado ser una tecnología eficaz para el desarrollo de nanocompuestos de biopolímeros. Con el uso de ambas estrategias, se obtuvieron mejoras en la propiedades mecánicas, de barreras y eléctricas.

VI. Annexes

ANNEX A

Supplementary data. Tables and Figures

Table 1A. Description of the samples used with the corresponding composition of the PLA nanocomposites (polylactide (PLA), lactic acid oligomers (OLLA) and bacterial cellulose nanowhiskers (BCNW)).

Samples Codes	PLA (%)	OLLA (%)*		BCNW (%)
		OLLA from Masterbatches	Pure OLLA	
PLA	100.00	-	-	-
PLA-OLLA	97.25	-	2.75	-
Samples from OLLA-BCNW masterbatch (using partially hydrated BCNW)				
PLA-BCNW 0.5%	96.75	0.27	2.48	0.50
PLA-BCNW 1%	96.25	0.55	2.20	1.00
PLA-BCNW 3%	94.25	1.65	1.10	3.00
PLA-BCNW 5%	92.25	2.75	-	5.00
Samples from OLLA-$BCNW_{FD}$ masterbatch (using freeze-dried BCNW)				
PLA-$BCNW_{FD}$ 0.5%	96.75	0.27	2.48	0.50
PLA-$BCNW_{FD}$ 1%	96.25	0.55	2.20	1.00
PLA-$BCNW_{FD}$ 3%	94.25	1.65	1.10	3.00
PLA-$BCNW_{FD}$ 5%	92.25	2.75	-	5.00
Samples synthesized by direct addition of all components into melt mixer (not from masterbatches) using partially hydrated BCNW (direct blends)				
PLA-BCNW –D 0.5%	96.75	-	2.75	0.50
PLA-BCNW –D 3%	94.25	-	2.75	3.00
Samples synthesized by direct addition of all components into melt mixer (not from masterbatches) using freeze-dried BCNW (direct blends)				
PLA-$BCNW_{FD}$ –D 0.5%	96.75	-	2.75	0.50
PLA-$BCNW_{FD}$ –D 3%	94.25	-	2.75	3.00
Sample prepared with 25wt% of OLLA and 5wt% of BCNW (using OLLA-BCNW masterbatch)				
PLA-$OLLA_{25}$-$BCNW_5$	70.00	2.75	22.25	5.00

* When masterbatches were used, the total amount of OLLA was from both masterbatches and pure OLLA, with the aim to keep constant the OLLA loading in all samples

Table 2A. Addition of different fillers into PHBV by ball milling. Effects on the storage modulus.

Filler concentration	FGS addition Storage Modulus at 25ºC	BCNW addition Storage Modulus at 25ºC
0	2093.7	2093.7
0.5	2131.7	2193.5
1	2256.4	2301.4
3	2819.7	2365.8

Table 3A. Addition of different fillers into PHBV by ball milling. Effects on the oxygen permeability and Filler Barrier Efficiency.

Filler (%)	FGS addition				BCNW addition			
	P O_2	Reduction in P O_2 (%)	X_c (%)	Filler barrier efficiency	*P* O_2	Reduction in P O_2 (%)	X_c (%)	Filler barrier efficiency
0	2.8 e^{-19}	0	53.2	-	2.8 e^{-19}	0	57.4	-
0.5	2.4 e^{-19}	13.4	59.9	0.22	2.2 e^{-19}	21.5	58.0	0.37
1	2.2 e^{-19}	20.8	61.9	0.33	2.3 e^{-19}	18.0	59.4	0.30
3	1.6 e^{-19}	41.2	56.0	0.73	2.3 e^{-19}	18.0	64.1	0.28

P O_2 : Oxygen permeability ($m^3 m\ m^{-2} s^{-1} Pa^{-1}$), X_c: Sample crystallinity

Table 4A: Water vapour permeability of films and trays of PLA and its nanocomposites incorporating BCNW.

Samples	Water vapour permeability (Kg m $m^{-2}s^{-1}Pa^{-1}$)	
	Films	Trays
PLA	1.59 e^{-14}	1.58 e^{-14}
PLA-OLLA	1.58 e^{-14}	1.60 e^{-14}
PLA-BCNW 0.5%	1.44 e^{-14}	1.54 e^{-14}
PLA-BCNW 5%	1.34 e^{-14}	1.39 e^{-14}

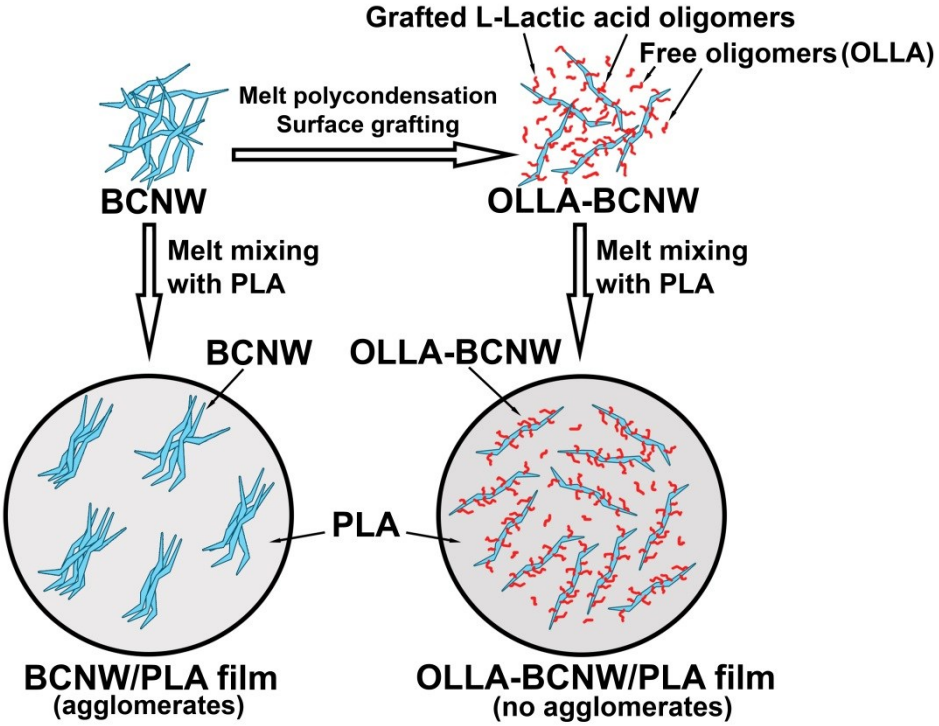

Figure 1A. General procedure to improve the dispersion of the bacterial cellulose nanowhiskers (BCNW) within polylactide (PLA) matrix by *in situ* melt polycondensation.

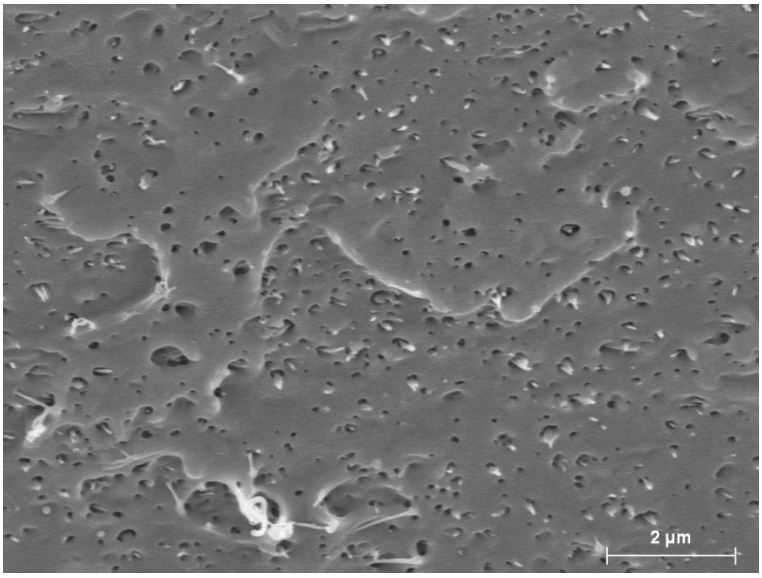

Figure 2A. SEM micrograph of PLA-BCNW with 3 wt% of freeze-dried BCNW.

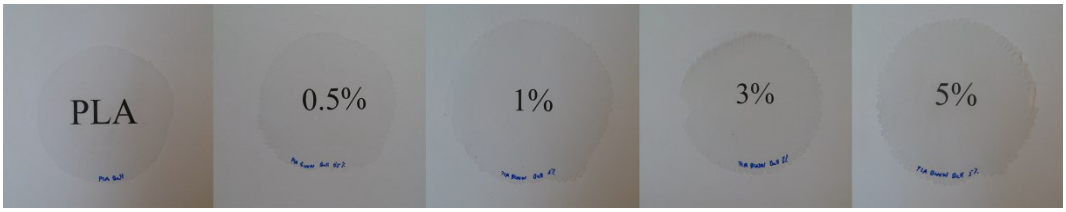

Figure 3A. Contact transparency pictures of films containing different BCNC contents in comparison with the pure PLA film obtained by means of ball milling and compression moulding.

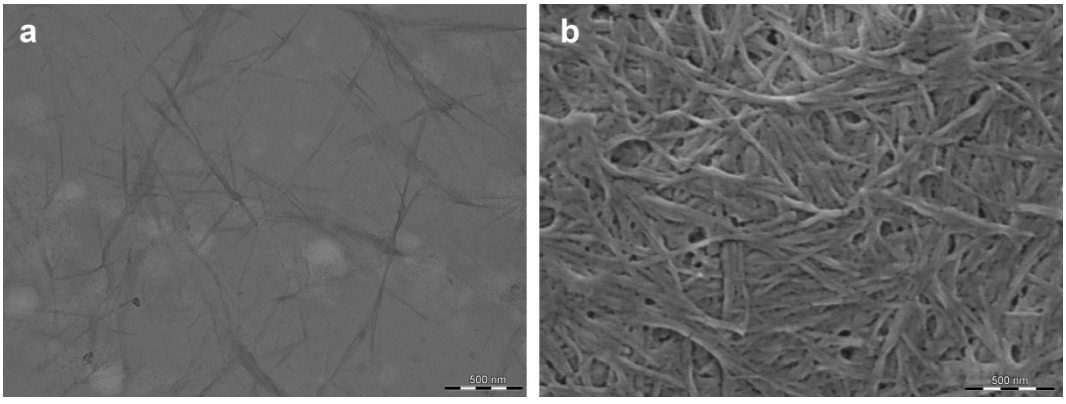

Figure 4A. TEM micrograph of BCNW in aqueous suspension obtained from partially hydrated BCNW (a) and SEM micrograph of freeze-dried BCNW (b).

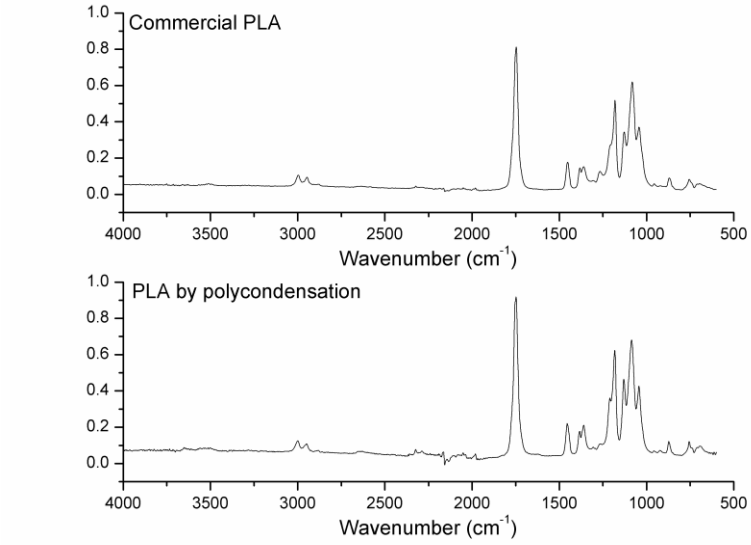

Figure 5A. FTIR spectra of commercial PLA and PLA synthesized by polycondensation.

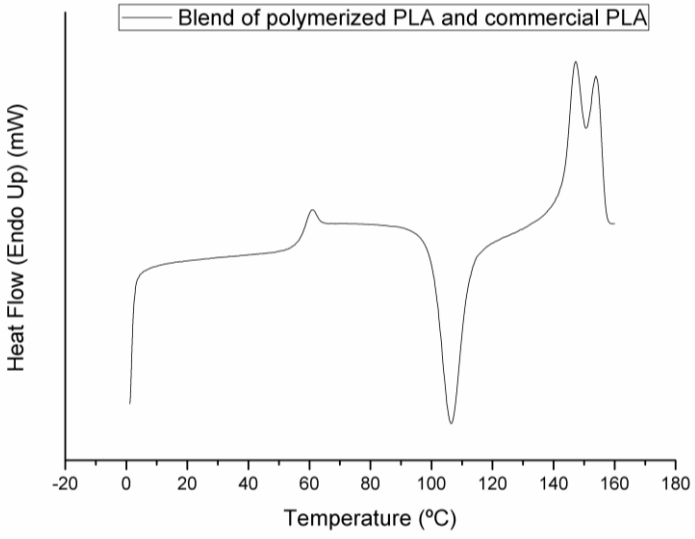

Figure 6A. Differential scanning calorimetry for a blend of commercial PLA and polymerized PLA.

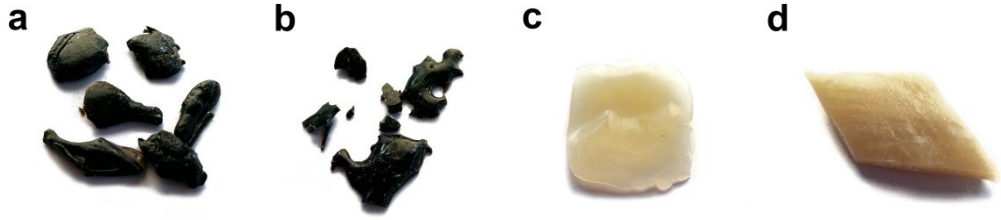

Figure 7A. Different PLA-based polymerized material in the presence of BCNW. Complete polymerization with the addition of BCNW at the beginning (a) and after the oligomerization stage (b). Two different lactic acid oligomers containing BCNW (masterbatches) (c, d).

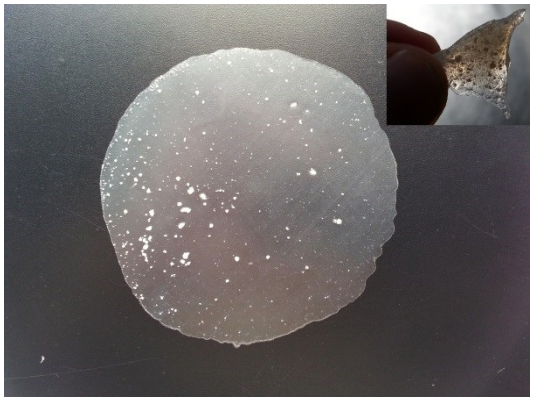

Figure 8A. Film of PLA –BCNW using the OLLA-BCNW masterbatch purified with chloroform through purification process 2. Inset image corresponding to the material just after the blending.

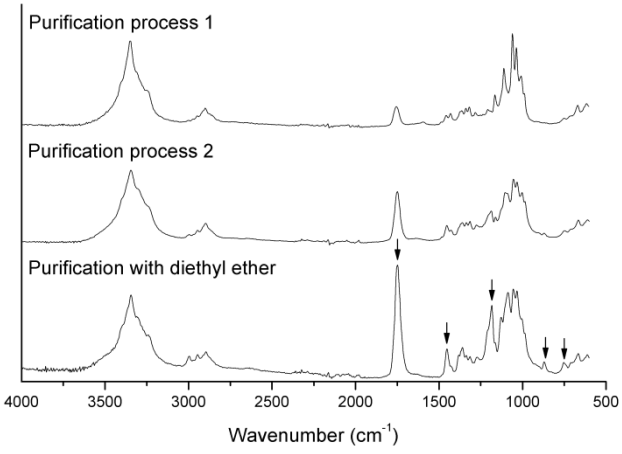

Figure 9A. FTIR spectra of OLLA-BCNW masterbatches purified with different purification processes. Arrows indicate characteristics spectral bands of OLLA.

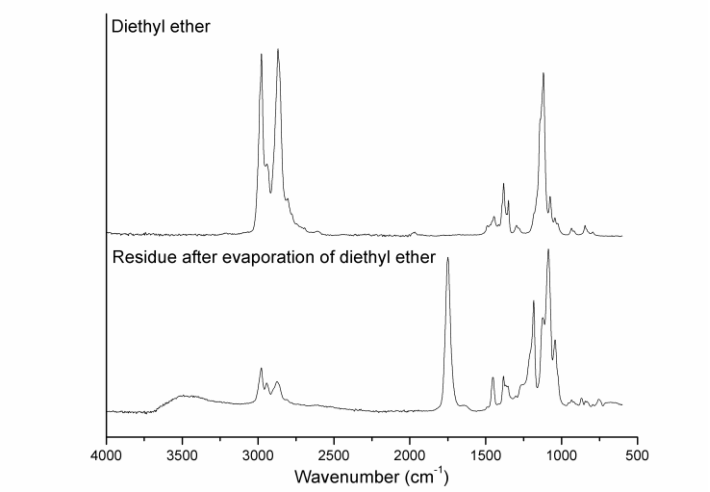

Figure 10A. FTIR of pure diethyl ether and the residue after evaporation of the used diethyl ether in the purification process.

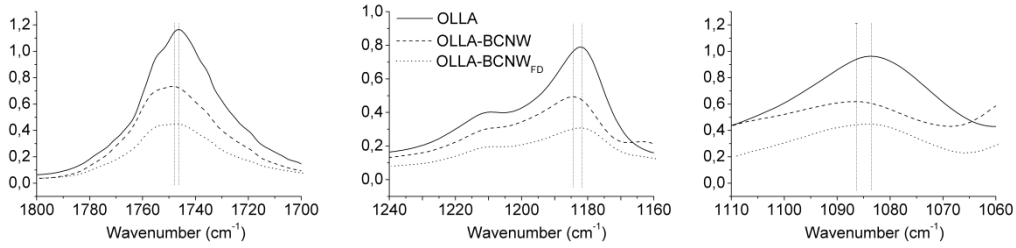

Figure 11A. FTIR spectra of lactic acid oligomers (OLLA) and OLLA-BCNW masterbatches using partially hydrated BCNW (OLLA-BCNW) and freeze-dried BCNW (OLLA-$BCNW_{FD}$).

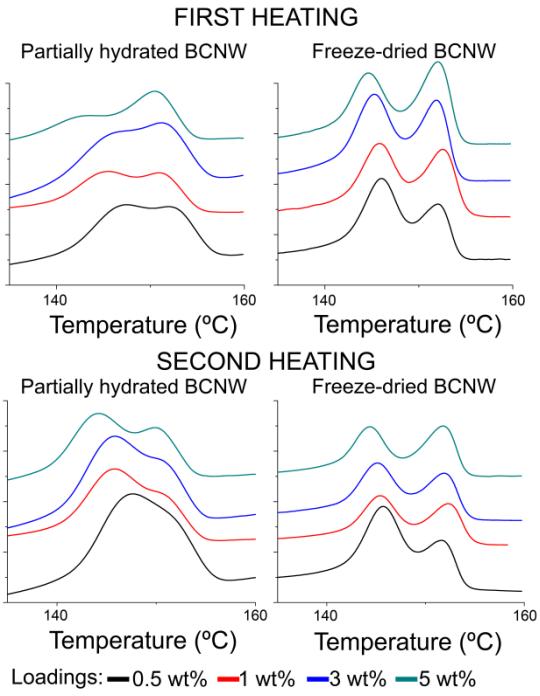

Figure 12A. Differential Scanning Calorimetry of PLA-BCNW materials using masterbatches with partially hydrated BCNW and freeze-dried BCNW.

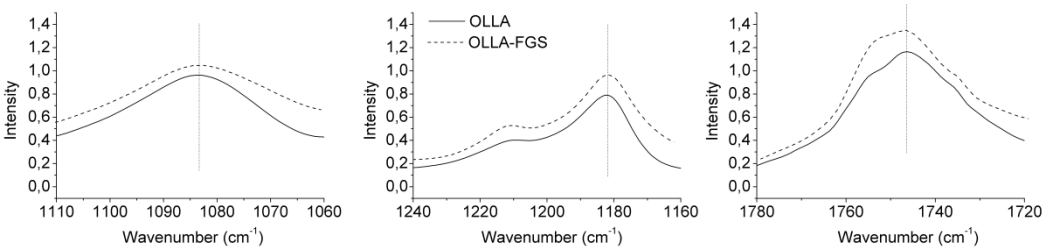

Figure 13A. FTIR spectra of lactic acid oligomers (OLLA) and OLLA-FGS masterbatches.

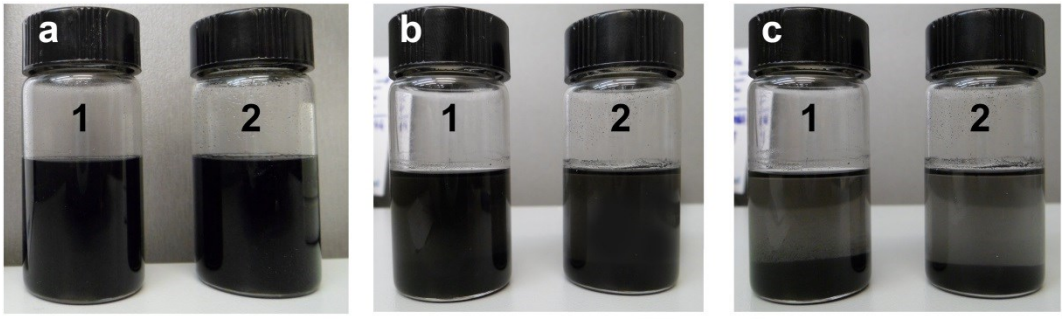

Figure 14A. Suspension of OLLA-FGS masterbatch (1) and physical mixture of OLLA and FGS (2) in chloroform. Pictures recorded immediately after the stirring was stopped (a), 24 h later (b) and 48 h later (c).

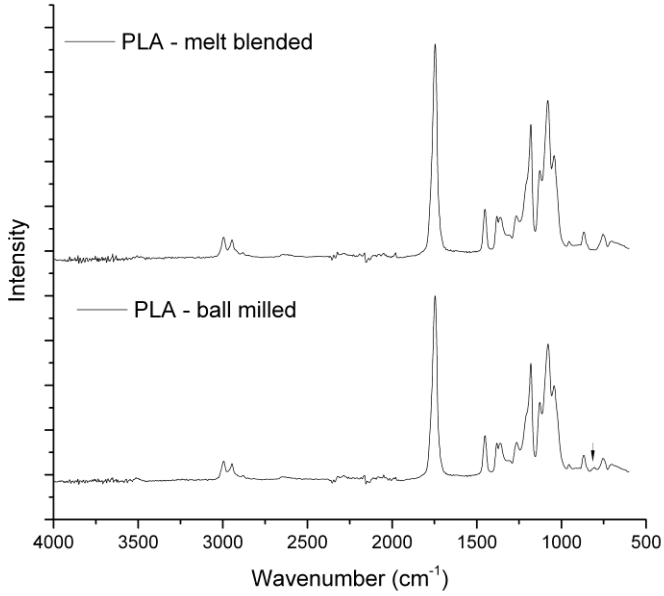

Figure 15A: FTIR spectra of PLA processed by melt blending and ball-milling.

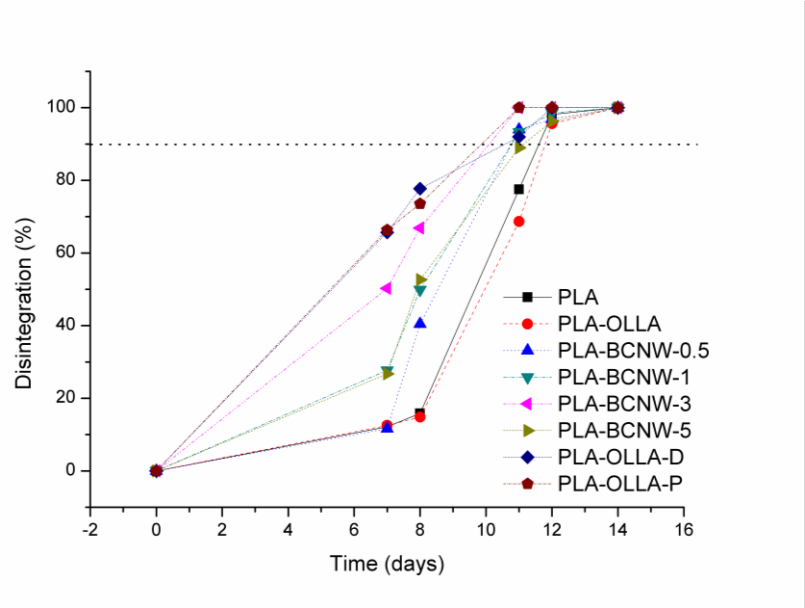

Figure 16A. Lost in weight as a result of the biodegradation process of PLA, PLA-BCNW nanocomposites and blends of PLA with 2.75 wt.% of OLLA (PLA-OLLA) and 25 wt.% of purified and unpurified OLLA (PLA-OLLA-P and PLA-OLLA-D) in composting conditions for up to 14 days.

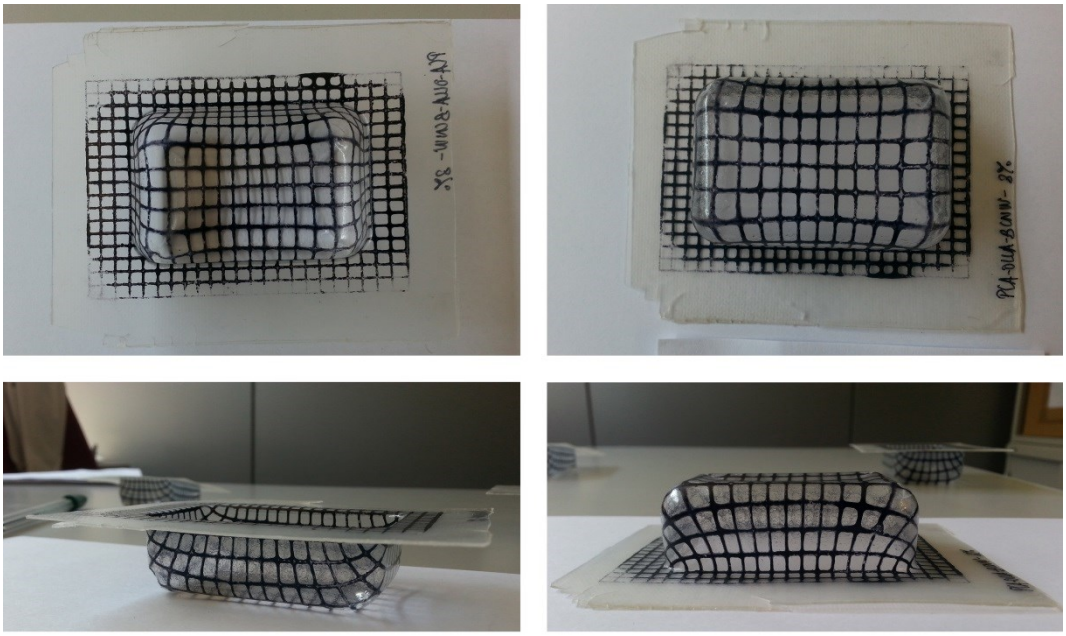

Figure 17A. Thermoformed trays performed from PLA-BCNW nanocomposites with 3 wt% loading.

ANNEX B

List of publications

J Mater Sci (2014) 49:2975–2986
DOI 10.1007/s10853-013-7929-x

An effect of lactic acid oligomers on the barrier properties of polylactide

J. Ambrosio-Martín · M. J. Fabra · A. Lopez-Rubio · J. M. Lagaron

Received: 24 September 2013 / Accepted: 28 November 2013 / Published online: 22 January 2014

Abstract Oligomers of lactic acid (LA) at different concentrations were melt-mixed with a polymeric matrix of high molecular weight polylactide (PLA) to improve their barrier properties. Purified and unpurified LA oligomers, obtained by a melt polycondensation reaction, were blended with PLA in order to study how the purification process affected the final film properties. In all the developed blend compositions, significant improvements in the permeability to both water and oxygen were observed in comparison with pure PLA, achieving permeability reductions of up to 54 %. This behaviour was ascribed to an antiplasticization phenomenon of the barrier properties related to the occupancy of the so-called Langmuir-free volume sites by the oligomer molecules. The results also showed that the permeability of these materials was greatly influenced by the presence of moisture, especially in the blends with unpurified oligomers. This behaviour was mainly ascribed to the higher content of the hydroxyl groups present in the latter materials, which led to an observable water sorption and hence to an increase in free volume for permeation.

J. Ambrosio-Martín · M. J. Fabra · A. Lopez-Rubio · J. M. Lagaron (✉)
Novel Materials and Nanotechnology Group, IATA, CSIC, Av. Agustín Escardino 7, 46980 Paterna, Valencia, Spain
e-mail: lagaron@iata.csic.es

J. Ambrosio-Martín
e-mail: jesus.ambromar@iata.csic.es

M. J. Fabra
e-mail: mjfabra@iata.csic.es

A. Lopez-Rubio
e-mail: amparo.lopez@iata.csic.es

Introduction

Biopolymer materials are attracting a great interest to counteract the environmental drawbacks related to the extremely slow degradation rate of many commonly used petroleum-based polymers and also to explore alternatives to petroleum to constitute polymer-based materials [1, 2].

Polylactides (PLA) are one of the most widely studied thermoplastic sustainable biopolymers family for monolayer and multilayer packaging applications. It derives from different sources, such as corn starch, tapioca products or sugarcanes, and can be obtained through different polymerization processes, such as polycondensation or ring opening polymerization. At the same time, it is one of the most interesting families of biodegradable materials because it has become commercially available, being produced on an industrial scale by several companies around the world [3] and presenting an interesting balance of properties. In the food packaging field, PLA has particular interest due to its excellent transparency and relatively good water resistance. Plasticizers can be added to PLA to reduce its relatively high stiffness, although they lead to a decrease in the oxygen barrier and also in transparency [4, 5]. Therefore, the main performance drawbacks of PLA are mainly associated to its low thermal resistance, excessive brittleness and insufficient barrier to oxygen and water compared to other benchmark packaging polymers like polyethylene terephthalate (PET) [6]. It is, thus, of great interest to enhance the properties of this material because of its degradable, renewable and eco-friendly properties while maintaining its inherent good properties such as transparency and biodegradability [7].

In order to overcome the low barrier properties of PLA, many studies concerning mass transfer phenomena have been done. These studies primarily focused on the

Cellulose (2015) 22:1201–1226
DOI 10.1007/s10570-014-0523-9

ORIGINAL PAPER

Melt polycondensation to improve the dispersion of bacterial cellulose into polylactide via melt compounding: enhanced barrier and mechanical properties

J. Ambrosio-Martín · M. J. Fabra · A. Lopez-Rubio · J. M. Lagaron

Received: 18 June 2014 / Accepted: 8 December 2014 / Published online: 28 January 2015

Abstract Nanocomposites of polylactide (PLA) and bacterial cellulose nanowhiskers (BCNW) with improved properties were obtained through melt compounding. Prior to melt processing, and with the aim of improving BCNW dispersion, lactic acid oligomers (OLLA) were in situ polymerized in the presence of the nanofiller (both freeze-dried and partially hydrated). This in situ polymerization reaction enhanced the compatibilization between hydrophilic cellulose and hydrophobic PLA, even leading to chemical grafting of the OLLA onto the surface of BCNW, when this was used in a partially hydrated form. The optimized dispersion attained through this pre-incorporation strategy was confirmed by comparison with materials obtained through direct melt compounding of PLA with BCNW. Differential scanning calorimetry experiments showed that although cellulose content had not effect on melting temperatures, the degree of crystallinity was significantly affected. Addition of grafted BCNW also resulted in improved mechanical properties increasing the elastic modulus and tensile strength up to 52 and 31 %, respectively, mainly ascribed to the promotion of filler–filler and filler–matrix interactions. Moreover, the developed nanocomposites showed improvements in the water and oxygen barrier properties (measured at 80 % RH), respectively, which make them attractive for food packaging applications. This could be explained by well-dispersed nanocrystals acting as blocking agents within the polymeric matrix, reducing the diffusion through the nanocomposite films and, hence, the water and oxygen permeability. Therefore, this work offers a new route for incorporating well dispersed nanocellulose within a hydrophobic PLA matrix, overcoming the dispersion problems that this entails, especially when working with melt compounding methods.

Keywords Bacterial cellulose · Cellulose nanowhiskers · Melt compounding · Lactic acid oligomers · Polylactide · In situ polymerization

Electronic supplementary material The online version of this article (doi:10.1007/s10570-014-0523-9) contains supplementary material, which is available to authorized users.

J. Ambrosio-Martín · M. J. Fabra · A. Lopez-Rubio · J. M. Lagaron (✉)
Novel Materials and Nanotechnology Group, IATA, CSIC, Av. Agustín Escardino 7, 46980 Paterna, Valencia, Spain
e-mail: lagaron@iata.csic.es

J. Ambrosio-Martín
e-mail: jesus.ambromar@iata.csic.es

M. J. Fabra
e-mail: mjfabra@iata.csic.es

A. Lopez-Rubio
e-mail: amparo.lopez@iata.csic.es

Introduction

Environmental concerns derived from the massive use of petroleum-based plastics, as well as possible future

Journal of Applied Polymer Science

Assessment of Ball Milling Methodology to Develop Polylactide-Bacterial Cellulose Nanocrystals Nanocomposites

Jesús Ambrosio-Martín,[1] Amparo Lopez-Rubio,[1] María José Fabra,[1] Giuliana Gorrasi,[2] Roberto Pantani,[2] Jose María Lagaron[1]

[1]Novel Materials and Nanotechnology Group, IATA, CSIC, Av. Agustín Escardino 7, 46980 Paterna (Valencia), Spain
[2]Department of Industrial Engineering, University of Salerno, Via Giovanni Paolo II 132, 84084 Fisciano Salerno, Italy
Correspondence to: J. M. Lagarón (E-mail: lagaron@iata.csic.es)

ABSTRACT: In this work, ball milling is evaluated as a methodology to develop polylactide (PLA)-bacterial cellulose nanocrystals (BCNC) nanocomposites. This technique, widely used for clay-based nanocomposites, is effective in breaking up to a very large extent the freeze-dried nanocellulose aggregates, giving raise to transparent films similar to the neat PLA films. Incorporation of the nanofiller through this methodology enhances the polymer crystallinity index. An increase in the onset degradation temperature and a significant reinforcing effect in terms of an increase in the storage modulus and in the tan delta peak are also observed. Improved barrier to oxygen at high relative humidity (80%) is also noticed, reaching the best performance at the lowest BCNC loading (0.5 wt %). These improvements are related to the relatively good nanocellulose dispersion and distribution attained for low loadings of the nanofiller. Thus, the ball milling methodology appears as a feasible processing methodology for developing PLA-BCNC nanocomposites. © 2014 Wiley Periodicals, Inc. J. Appl. Polym. Sci. **2015**, *132*, 41605.

KEYWORDS: biopolymers & renewable polymers; composites; films; nanoparticles; nanowires and nanocrystals; packaging

Received 4 August 2014; accepted 10 October 2014
DOI: 10.1002/app.41605

INTRODUCTION

The development of fully renewable biopolymer nanocomposites to replace synthetic polymers for different applications has been the subject of numerous studies during the last years. Nanocellulose [also referred to as cellulose nanocrystals (CNC) or cellulose nanowhiskers] represents one of the most interesting fillers for these applications due to its broad availability, low cost, and to the possibility of obtaining different morphological features depending on the cellulose source. In this sense, while CNC extracted from vegetal resources such as cotton or wood typically have a length of 100–300 nm and width of 5–20 nm,[1–3] those obtained from tunicin and bacterial cellulose (BCNC) may have several micrometres in length and a width of 5–50 nm.[4–6] CNC are usually obtained through hydrolysis with strong acids such as sulphuric acid or hydrochloric acid, which produce a preferential digestion of the amorphous domains of the material and cleavage of the nanofibril bundles.[7] One of the main difficulties associated with the use of unmodified CNC as reinforcing agents is their high hydrophilicity, which makes it difficult to disperse them in non-polar media. This is especially relevant when trying to implement the physical properties of biopolyesters using nanocellulose. Among the biopolyesters, polylactide (PLA) obtained from the fermentation of corn starch[8] is one of the most attractive materials due to its high transparency and ease of processability and thus has found commercial applications in food packaging and medicine. However, PLA also presents a number of drawbacks such as low thermal resistance, excessive brittleness, and relatively low barrier to oxygen and water vapor as compared to other packaging materials such as polyethylene terephthalate. The other great challenge when trying to develop PLA-based nanocomposites reinforced with CNC is to attain proper nanofiller dispersion through the use of industrial processing techniques, such as melt compounding methods, due to the above mentioned different nature between hydrophobic PLA and hydrophilic CNC. It has been observed that direct melt mixing of the freeze-dried nanocellulose with the polymer or biopolymer matrix provides materials with big nanocellulose agglomerates and thus insufficient physical properties.[9] Several strategies have been recently developed to improve nanocellulose dispersion in PLA matrices obtained through melt compounding, based on pre-incorporation of the nanofiller either in electrospun fibres[9] or in lactic acid oligomers.[10] Chemical modification of the nanofiller has also been investigated, and although improved adhesion with the PLA matrix was observed, good nanofiller dispersion was only obtained for low nanocellulose loadings.[11] Moreover, chemical

Journal of Applied Polymer Science

On the use of ball milling to develop PHBV-graphene nanocomposites (I)—Morphology, thermal properties, and thermal stability

Jesús Ambrosio-Martín,[1] Giuliana Gorrasi,[2] Amparo Lopez-Rubio,[1] María José Fabra,[1] Luís Cabedo Mas,[3] Miguel Angel López-Manchado,[4] Jose María Lagaron[1]

[1]Novel Materials and Nanotechnology Group, IATA, CSIC, Av. Agustín Escardino 7, Paterna 46980 (Valencia), Spain
[2]Department of Industrial Engineering University of Salerno, Via Giovanni Paolo II 132, Fisciano 84084 Salerno, Italy
[3]ESID, Universitat Jaume I, Avda. Vicent Sos Baynat s/n, Castellón 12071, Spain
[4]Institute of Polymer Science and Technology, (CSIC), Juan de la Cierva, 3, Madrid 28006, Spain
Correspondence to: G. Gorrasi (E-mail: ggorrasi@unisa.it) and J. María Lagaron (E-mail: lagaron@iata.csic.es)

ABSTRACT: In the first part of this work, novel nanocomposites based on poly (3-hydroxybutyrate co-3-hydroxyvalerate) (PHBV) and functionalized graphene nanosheets (FGS) were prepared through ball milling. As revealed by morphological characterization, this blending methodology was able to allow proper nanofiller dispersion and distribution into the matrix. Thermal properties were studied under non-isothermal and isothermal conditions and the addition of FGS into PHBV matrix, although no changes in crystallization mechanism were observed, it modified the crystallization kinetics leading to increased crystallinity. Thermal stability analysis revealed that FGS affected the mechanism of oxidative thermal degradation and had no effect on thermal degradation by pyrolysis. Furthermore, an analysis of isothermal degradation kinetics showed that FGS speeded up the degradation rate. The Sestak-Berggren model was used as a model to explain the isothermal degradation behavior of the obtained materials in good agreement with the experimental data. © 2015 Wiley Periodicals, Inc. J. Appl. Polym. Sci. **2015**, *132*, 42101.

KEYWORDS: biodegradable; biomaterials; biopolymers and renewable polymers; composites; graphene and fullerenes; nanotubes

Received 4 December 2014; accepted 11 November 2015
DOI: 10.1002/app.42101

INTRODUCTION

The massive use of petroleum-based polymers has resulted in environmental concerns derived not only from waste management issues, but also from their low degradation rates. As a result, there is a growing interest in the development of renewable and biodegradable materials to partially replace the oil-based ones. Alternatives such as polyhydroxyalkanoates (PHAs) have sparked great interest due to their biodegradable, biocompatible and renewable features. PHAs can be produced in different ways, i.e., chemically or biologically through fermentation from feedstock. This family comprises mainly the homopolymer, polyhydroxybutyrate (PHB), which has been extensively studied since it presents mechanical properties similar to those of conventional petroleum-based polymers, relatively good thermal properties and high stiffness due to its high crystallinity degree.[1] However, although high crystallinity is useful for some applications, the high stiffness limits its usage in other commercial applications. Moreover, another drawback of this polymer is its low thermal stability, making it unstable during melt processing and also limiting its applicability.[2] Several strategies have been developed to overcome these drawbacks, including blending with other polymers, such as poly (vinyl alcohol) (PVA),[3] polypropylene glycol (PPG),[4] and poly-ε-caprolactone (PCL)[5] or modification of the homopolymer by incorporation of different monomer types during the fermentation process. Copolymerization with hydroxyvalerate (HV) results in poly(3-hydroxybutyrate-co-3-hydroxyvalerate) (PHBV) which has improved mechanical and thermal properties, since incorporation of HV reduces the crystallinity, thus decreasing stiffness and brittleness, and also reducing the melting point without decreasing the thermal stability of the material, although greater improvements in this parameter are still needed.[1,6] However, reduction in crystallinity is widely known to affect the barrier properties of materials to low molecular weight substances, which is a key property of materials intended to be used in packaging applications.[7,8] Because of that, PHBV copolymers still present several drawbacks including high cost, relative brittleness and thermal instability, which had hampered the widespread usage of this family of polymers. As a strategy to improve biopolymer performance, many studies have focussed

JOURNAL OF Applied Polymer SCIENCE

On the use of ball milling to develop poly(3-hydroxybutyrate-co-3-hydroxyvalerate)-graphene nanocomposites (II)—Mechanical, barrier, and electrical properties

Jesús Ambrosio-Martín,[1] Giuliana Gorrasi,[2] Amparo Lopez-Rubio,[1] María José Fabra,[1] Luís Cabedo Mas,[3] Miguel Angel López-Manchado,[4] Jose María Lagaron[1]

[1]Novel Materials and Nanotechnology Group, IATA, CSIC, Av. Agustín Escardino 7 46980 Paterna (Valencia), Spain
[2]Department of Industrial Engineering University of Salerno, Via Giovanni Paolo II 132 84084 Fisciano Salerno, Italy
[3]ESID, Universitat Jaume I, Avda. Vicent Sos Baynat s/n 12071 Castellón, Spain
[4]Institute of Polymer Science and Technology, (CSIC), Juan de la Cierva, 3 28006 Madrid, Spain
Correspondence to: G. Gorrasi (E-mail: ggorrasi@unisa.it) and J. M. Lagaron (E-mail: lagaron@iata.csic.es)

ABSTRACT: In this work, poly (3-hydroxybutyrate-co-3-hydroxyvalerate) (PHBV) nanocomposites containing functionalized graphene sheets (FGS) were prepared by means of high-energy ball milling. The crystalline structure, oxygen barrier, mechanical and electrical properties, and biodegradability of the developed nanocomposites were analyzed and correlated with the amount of FGS incorporated and with their morphology, which was reported in a previous study. Addition of FGS into the PHBV matrix did not affect the crystal morphology of the material but led to somewhat enhanced crystallinity. The good dispersion and distribution of the nanofiller within the polymeric matrix, revealed in the first part of this study, was thought to be crucial for the mechanical reinforcing effect of FGS and also resulted in enhanced gas barrier properties at high relative humidity. Additionally, the conducting behavior of the nanocomposites, as interpreted by the percolation theory, displayed a very low percolation threshold set at ~0.3 vol % of FGS, while the materials exhibited an overall significantly enhanced conductivity. © 2015 Wiley Periodicals, Inc. J. Appl. Polym. Sci. **2015**, *132*, 42217.

KEYWORDS: biopolymers & renewable polymers; blends; graphene and fullerenes

Received 24 February 2015; accepted 11 March 2015
DOI: 10.1002/app.42217

INTRODUCTION

Great efforts have been focused on the development of environmentally friendly biodegradable polymers in the last decades because of the nonrenewable and nonbiodegradable character of the petroleum-based synthetic polymers, particularly in the packaging area, where a huge amount of plastic waste is generated on a daily basis. Polyhydroxyalkanoates (PHAs) are one of the most studied families of thermoplastic biodegradable polymers not only because of their environmentally friendly properties such as biodegradability, biocompatibility, and renewable character but also because these materials have mechanical properties similar to those of conventional petroleum-based polymers, relatively good thermal properties, melt compounding processability and high stiffness because of its high crystallinity degree.[1] Specifically, poly(3-hydroxybutyrate-co-3-hydroxyvalerate) (PHBV), the copolymers which belong to the PHAs family, have been extensively studied and quickly identified as good candidates to replace fossil-based commodity polymers. However, several properties of these biopolymers, including the mechanical, thermal and barrier properties need to be balanced or improved in order to extend their field of application.[1,2] Among the strategies used to balance these physical properties, the use of organic and inorganic nanofillers as reinforcing agents have been extensively used. For instance, inorganic nanofillers such as carbon nanotubes[3] and nanoclays[4–6] have been used. In the case of organic fillers, cellulose nanocrystals[1,7–9] have been the most widely used material for this purpose.

In last years, graphene, a two-dimensional material consisting of a single layer of carbon atoms packed in a hexagonal lattice, has gained much attention because of its remarkable physical properties such as mechanical, thermal, and electrical properties. Because of that, graphene materials are expected to be used in a variety of applications including sensors, batteries, supercapacitors, active and intelligent packaging devices and hydrogen storage systems.[10]

Out of all the processes for the production of graphene, e.g. mechanical exfoliation, chemical exfoliation, chemical vapor